DESIGN,SYNTHESIS AND EVALUATION OF SOME PYRAZOLE DERIVATIVES AS ANTITUBERCULAR AGENTS

A Thesis submitted to Gujarat Technological University

for the Award of

Doctor of Philosophy

in

Pharmacy

by

Ms. Nayee Kinjal Kanubhai

Enrollment No. 199999901517

under supervision of

Dr. Beenkumar R. Prajapati

Assistant Professor (M. Pharm, Ph. D)
Department of Pharmaceutical Chemistry
L.M. College of Pharmacy, Ahmedabad- 380009
Gujarat, India

GUJARAT TECHNOLOGICAL UNIVERSITY
AHMEDABAD

[September-2026]

DECLARATION

I declare that the thesis entitled **"DESIGN,SYNTHESIS AND EVALUATION OF SOME PYRAZOLE DERIVATIVES AS ANTITUBERCULAR AGENTS"** submitted by me for the degree of Doctor of Philosophy is the record of research work carried out by me during the period from June 2020 to June 2026 under the supervision of Dr. Beenkumar R. Prajapati and this has not formed the basis for the award of any degree, diploma, associateship, fellowship, titles in this or any other University or other institution of higher learning.

I further declare that the material obtained from other sources has been duly acknowledged in the thesis. I shall be solely responsible for any plagiarism or other irregularities, if noticed in the thesis.

Signature of the Research Scholar: Nayee Date: 10/09/2026

Name of Research Scholar: Ms. Nayee Kinjal Kanubhai

Place: Ahmedabad

CERTIFICATE

I certify that the work incorporated in the thesis **"DESIGN,SYNTHESIS AND EVALUATION OF SOME PYRAZOLE DERIVATIVES AS ANTITUBERCULAR AGENTS"** submitted by **Ms. Nayee Kinjal Kanubhai** was carried out by the candidate under my supervision/guidance. To the best of my knowledge:

(i) the candidate has not submitted the same research work to any other institution for any degree/diploma, Associateship, Fellowship or other similar titles (ii) the thesis submitted is a record of original research work done by the Research Scholar during the period of study under my supervision, and (iii) the thesis represents independent research work on the part of the Research Scholar.

Signature of the Research Supervisor: BRprajapati Date: 10/9/2026

Name of Supervisor: Dr. Beenkumar R. Prajapati

Place: L. M. College of Pharmacy, Ahmedabad

Course-work Completion Certificate

This is to certify that Ms. Nayee Kinjal Kanubhai enrolment no.199999901517 is enrolled for PhD program in the branch Pharmacy of Gujarat Technological University, Ahmedabad.

(Please tick the relevant option(s))

☐ He/She has been exempted from the course-work (successfully completed during M.Phil Course)

☐ He/She has been exempted from Research Methodology Course only (successfully completedduring M.Phil Course)

☑ He/She has successfully completed the PhD course work for the partial requirement for the award of PhD Degree. His/ Her performance in the course work is as follows-

Grade Obtained in Research Methodology PHD2001	Grade Obtained in Research and Publication Ethics [PHD2002]	Grade Obtained in Self-Study Course [PHD2003]
AB	AB	AB

Supervisor's Sign _____

(Dr. Beenkumar R. Prajapati)

Originality Report Certificate

It is certified that PhD Thesis titled **"DESIGN,SYNTHESIS AND EVALUATION OF SOME PYRAZOLE DERIVATIVES AS ANTITUBERCULAR AGENTS"** by Ms. Nayee Kinjal Kanubhai has been examined by us.

We undertake the following:

a. Thesis has significant new work / knowledge as compared already published or are under consideration to be published elsewhere. No sentence, equation, diagram, table, paragraph or section has been copied verbatim from previous work unless it is placed under quotation marks and duly referenced.

b. The work presented is original and own work of the author (i.e. there is no plagiarism). No ideas, processes, results or words of others have been presented as Author own work.

c. There is no fabrication of data or results which have been compiled / analyzed.

d. There is no falsification by manipulating research materials, equipment or processes, or changing or omitting data or results such that the research is not accurately represented in the research record.

e. The thesis has been checked using **Turnitin software** (copy of originality report attached) and found within limits as per GTU Plagiarism Policy and instructions issued from time to time (i.e. permitted similarity index <=10%).

Signature of the Research Scholar: Nayee Date: 10/09/2026

Name of the Research Scholar: Ms. Nayee Kinjal Kanubhai

Signature of the Research Supervisor: Prajapati Date: 10/9/2026

Name of the Research Supervisor: Dr. Beenkumar R. Prajapati

Place: L. M. College of Pharmacy, Ahmedabad

Kinjal Nayee

Thesis

Quick Submit

Quick Submit

Gujarat Technological University

Document Details

Submission ID
trn:oid:::1:3602722878

Submission Date
Jun 28, 2026, 9:03 AM GMT+5:30

Download Date
Jun 28, 2026, 9:12 AM GMT+5:30

File Name
Kinjal_thesis_-_26-06-2026_New.docx

File Size
11.1 MB

194 Pages

29,930 Words

177,224 Characters

7% Overall Similarity

The combined total of all matches, including overlapping sources, for each database.

Filtered from the Report

- Bibliography
- Quoted Text
- Cited Text
- Small Matches (less than 8 words)

Exclusions

- 1 Excluded Source

Match Groups

173 Not Cited or Quoted 7%
Matches with neither in-text citation nor quotation marks

0 Missing Quotations 0%
Matches that are still very similar to source material

0 Missing Citation 0%
Matches that have quotation marks, but no in-text citation

0 Cited and Quoted 0%
Matches with in-text citation present, but no quotation marks

Top Sources

5% Internet sources
6% Publications
4% Submitted works (Student Papers)

Integrity Flags

1 Integrity Flag for Review

Replaced Characters
81 suspect characters on 37 pages
Letters are swapped with similar characters from another alphabet.

Our system's algorithms look deeply at a document for any inconsistencies that would set it apart from a normal submission. If we notice something strange, we flag it for you to review.

A Flag is not necessarily an indicator of a problem. However, we'd recommend you focus your attention there for further review.

Match Groups

- **173** Not Cited or Quoted 7%
  Matches with neither in-text citation nor quotation marks
- **0** Missing Quotations 0%
  Matches that are still very similar to source material
- **0** Missing Citation 0%
  Matches that have quotation marks, but no in-text citation
- **0** Cited and Quoted 0%
  Matches with in-text citation present, but no quotation marks

Top Sources

5% Internet sources
6% Publications
4% Submitted works (Student Papers)

Top Sources

The sources with the highest number of matches within the submission. Overlapping sources will not be displayed.

1	Internet	patents.justia.com 1%
2	Internet	www.freepatentsonline.com 1%
3	Publication	Lan, Chunling Blue. "1,5,7-Triazabicyclo[4.4.0]dec-5-ene (TBD): Development of Sy... <1%
4	Student papers	Universidad de Alcalá <1%
5	Student papers	National Institute of Technology Warangal <1%
6	Publication	Chauhan, Monica. "Design and Synthesis of Some Novel Anti-Tubercular Agents", ... <1%
7	Publication	Vivek P. Chavda, Mahesh T. Chhabria, Divya M. Teli. "Recent Advancements in Tub... <1%
8	Student papers	University of Birmingham <1%
9	Internet	patents.glgoo.top <1%
10	Publication	Olga Balabon, Eleni Pitta, Maciej K. Rogacki, Eugenia Meiler et al. " Optimization o... <1%

11 Student papers
Indian Institute of Science Education and Research <1%

12 Publication
Maciej K. Rogacki, Eleni Pitta, Olga Balabon, Sophie Huss et al. "Identification and... <1%

13 Publication
Sarvan Maddipatla, Puja Kumari Agnivesh, Bulti Bakchi, Srinivas Nanduri, Nitin P... <1%

14 Publication
Yang, Shiyi. "Selective Activation of C–O and C–S Bonds by Highly Reactive Air-And... <1%

15 Publication
Bendale, Hersh. "Design, Synthesis and Biological Evaluation of Novel Taxane Bas... <1%

16 Publication
Huanyu Shi, Haotian Tang, Yan Li, Xinlong Shen et al. "Structure-guided discovery... <1%

17 Publication
Iara Lisboa de Matos. "Biotransformação de derivados de flavonoides empregand... <1%

18 Publication
Mikhail Tsymliakov, Maria Hanl, Jana Enns, Shiyang Zhai et al. "Rapid two-step m... <1%

19 Publication
Marcio Hayashi. "Novas metodologias empregando ilídeos de enxofre frente a es... <1%

20 Publication
Fridianto, Kevin Timothy. "Development of Cationic Dioxonaphthoimidazoles as P... <1%

21 Publication
Vahdani, Aria. "I. Design & Optimization of Organic Chromophores for Applicatio... <1%

22 Student papers
University of Warwick <1%

23 Publication
Shandesh Bhattarai, Edivan Carvalho Vieira, Mahendra Rai. "Bioactive Compound... <1%

24 Publication
N. V. R. Naidu, N. L. Ramesh, A. Jagannatha Reddy, Nagaraju Kottam et al. "Applie... <1%

Ph.D. Thesis Non-Exclusive License to

GUJARAT TECHNOLOGICAL

UNIVERSITY

In consideration of being a Research Scholar at Gujarat Technological University, and in the interests of the facilitation of research at the University and elsewhere, I, Ms. Nayee Kinjal Kanubhai having (Enrollment No.) 199999901517 hereby grant a non-exclusive, royalty free and perpetual license to the University on the following terms:

a. The University is permitted to archive, reproduce and distribute my thesis, in whole or in part, and/or my abstract, in whole or in part (referred to collectively as the "Work") anywhere in the world, for non-commercial purposes, in all forms of media;
b. The University is permitted to authorize, sub-lease, sub-contract or procure any of the acts mentioned in paragraph (a);
c. The University is authorized to submit the Work at any National / International Library, under the authority of their "Thesis Non-Exclusive License";
d. The Universal Copyright Notice (©) shall appear on all copies made under the authority of this license;
e. I undertake to submit my thesis, through my University, to any Library and Archives. Any abstract submitted with the thesis will be considered to form part of the thesis.
f. I represent that my thesis is my original work, does not infringe any rights of others, including privacy rights, and that I have the right to make the grant conferred by this non-exclusive license.
g. If third party copyrighted material was included in my thesis for which, under the terms of the Copyright Act, written permission from the copyright owners is required, I have obtained such permission from the copyright owners to do the acts mentioned in paragraph (a) above for the full term of copyright protection.
h. I understand that the responsibility for the matter as mentioned in the paragraph (g) rests with the authors / me solely. In no case shall GTU have any liability for any acts / omissions / errors / copyright infringement from the publication of the said thesis or otherwise.
i. I retain copyright ownership and moral rights in my thesis, and may deal with the copyright in my thesis, in any way consistent with rights granted by me to my University in this non-exclusive license.
j. GTU logo shall not be used /printed in the book (in any manner whatsoever) being published or any promotional or marketing materials or any such similar documents.
k. The following statement shall be included appropriately and displayed prominently in the book or any material being published anywhere: "The content of the published work

is part of the thesis submitted in partial fulfilment for the award of the degree of Ph.D. in Design,Synthesis and Evaluation of some Pyrazole Derivatives as Antitubercular Agents of the Gujarat Technological University".

l. I further promise to inform any person to whom I may hereafter assign or license my copyright in my thesis of the rights granted by me to my University in this nonexclusive license. I shall keep GTU indemnified from any and all claims from the Publisher(s) or any third parties at all times resulting or arising from the publishing or use or intended use of the book / such similar document or its contents.

m. I am aware of and agree to accept the conditions and regulations of Ph.D. including all policy matters related to authorship and plagiarism.

Date: 10/09/2026

Place: Ahmedabad

Signature of the Research Scholar

Recommendation of the Research Supervisor: .....

Recommendation of the Co-Supervisor (if any): .....

Signature of the Research Supervisor

Signature of the Co-Supervisor (if any)

Thesis Approval Form

The viva-voce of the PhD Thesis submitted by Ms. Nayee Kinjal Kanubhai (Enrollment No. 199999901517) entitled **"DESIGN,SYNTHESIS AND EVALUATION OF SOME PYRAZOLE DERIVATIVES AS ANTITUBERCULAR AGENTS"** was conducted on 10th September 2026 at Gujarat Technological University.

(Please tick any one of the following option)

☑ The performance of the candidate was satisfactory. We recommend that he/she be awarded the PhD degree.

☐ Any further modifications in research work recommended by the panel after 3 months from the date of first viva-voce upon request of the Supervisor or request of Independent Research Scholar after which viva-voce can be re-conducted by the same panel again.

(briefly specify the modifications suggested by the panel)

☐ The performance of the candidate was unsatisfactory. We recommend that he/she should not be awarded the PhD degree.

(The panel must give justifications for rejecting the research work)

Dr. Beenkumar R. Prajapati

Name and Signature of Supervisor with Seal

Dr. Amit Shard

1) (External Examiner 1) Name and Signature

Dr. Hardik Bhatt

2) (External Examiner 2) Name and Signature

ABSTRACT

Tuberculosis (TB) is a contagious airborne infectious disease caused by *Mycobacterium tuberculosis*. Each year millions of people continue to fall sick with TB. Development of drug resistance has narrowed down the conventional antituberculer therapeutic regimen. To address the growing problem of resistance there is an urgent requirement for a new class of antitubercular drugs with unique mechanisms of action to combat *M. tuberculosis*. In this study we have selected two targets Enoyl-ACP reductase (InhA) and Decaprenylphosphoryl-β-d-ribose 2′-epimerase (DprE1). Based on molecular docking study we have designed and synthesized series of acid chloride substituted pyrazole compounds (6a-o) as InhA inhibitors and amino substituted 6-methyl-1-phenyl-1*H*-pyrazolo[3,4-d]pyrimidin-4-ol compounds (7a-o) as DprE1 inhibitors. Structural elucidation of synthesized compounds were performed through IR, MASS, 1H NMR and 13C NMR spectroscopy. Synthesized compounds (6a-o) and (7a-o) were subjected to i*n-vitro* antimycobacterial activity against the *M. tuberculosis* (H37Rv) strain via the microplate alamar blue assay method and antioxidant activity using the DPPH assay method. The results demonstrated that the synthesized compounds effectively inhibited *M. tuberculosis* H37Rv, displaying promising anti-tubercular potential. Among them, compounds 6g, 6h, 6i, 6j, 6m, 7e, 7g, 7j and 7k exhibited promising antitubercular activity. In terms of antioxidant potential, compounds 6b, 6d, 7b, 7d and 7e exhibited good antioxidant activity, with 6m again emerging as the most effective. Cytotoxicity of the most active compounds 6i, 6m, 7g and 7j were checked on HepG2 cell line using the MTT assay. The docking results showed significant binding affinity between the synthesized compounds (6a-o), (7a-o) and the target enzyme InhA and DprE1. Stability of the interactions of most potent compounds 6m and 7g were assessed by a standard 100 ns dynamic simulation study. Pharmacokinetics properties of the synthesized compounds were checked using Swiss ADME and pkCSM. All these results indicate that the synthesized compounds could prove to be potential leads for further development of new potent antitubercular agents.

Keywords: Tuberculosis, InhA, DprE1, Pyrazole, Antitubercular, Docking, MD simulation, cytotoxicity

ACKNOWLEDGEMENT

Research always requires inspiration, motivation and dedication, especially when things are not going straight forward as per the plan. I owe my gratitude to all those people who have made this possible and because of whom my Ph. D experience has been one that I will cherish forever.

First and foremost I would like to thank ***God,*** *the almighty for providing me this opportunity and granting me the capability to proceed successfully. It's my fortune to be grateful to my parents,* ***Mr. Kanubhai Nayee*** *and* ***Mrs. Shobhanaben Nayee*** *for their effort, unconditional trust and endless support in every situation. Of course there is an earnest appreciation goes to my brother,* ***Dhruv*** *who has been such a supportive and caring younger sibling to grow up with.*

I would like to express my sincere gratitude to my project guide, ***Dr. Beenkumar R Prajapati,*** *Assistant Professor, Department of Pharmaceutical Chemistry, L.M. College of Pharmacy, who has supported me throughout my project with his patience, continuous encouragement, goodwill, enthusiasm and immense knowledge. I am also thankful to him for review my reports, commenting on my views and helping me understand and enrich my ideas. His invaluable mentorship, insightful feedback and continuous belief in my abilities have been instrumental in shaping this thesis. I attribute the level of my Ph. D degree to his encouragement and efforts.*

It takes an immense pleasure to mention ***Dr. Mahesh T. Chhabria, Principal L.M. College of Pharmacy, Pharmaceutical chemistry department*** *for providing me this opportunity, facilities, resources and technical support for the successful execution of this dissertation.*

I am also grateful to the Ph.D. Scholar's ***Ms. Sulekha, Ms. Radhika,*** *Dept. of Pharmaceutical Chemistry, L.M. College of Pharmacy, for her active participation in various ways to complete my project work. I am also grateful to Professor* ***Dr. Divyeshkumar Doshi, Dr. Haribhai Rabari****,* ***Dr. Dharmistha Parmar, Dr. Dipen Sureja****, and* ***Dr.Vanita Lasan****, Dept. of Pharmaceutical Chemistry, L.M. College of Pharmacy, for encouragement and support for this research work.*

I thank Dr Himani Dhotre (Previous CEO, Dishman Carbogens Amcis Limited) and all the staff of Dishman Carbogens Amcis Limited for helping me to achieve my dreams. I would also like to thanks my colleague ***Dr. Patrick Fernandes*** *and* ***Dr. Komal Pandya*** *for all fun, entertaining moment, motivation and constant support.*

I would like to give special thanks to ***Mr. Hansal Kumar Ph. D Scholar BHU IIT*** *for his valuable support during my Ph. D work.*

I would also like to thanks ***L. M. College of Pharmacy, AIC-LMCP foundation ,Oxygen Healthcare Pvt. Ltd.,*** *for spectral analysis, software support and* ***Maratha Mandal's NGH Institute of Dental Sciences & Research Centre, Belgaum*** *for Biological Screening.*

I am truly grateful to the honorable Doctoral Progress Committee (DPC) members of my dissertation, ***Dr. C. N. Patel*** *, Dean, Principal, Shri Sarvajanik Pharmacy College Mehsana, and* ***Dr.Dinesh Thakkar****, Associate Professor, A.R. College of Pharmacy & G. H. Patel Institute of Pharmacy, Anand for their time, expertise, valuable feedback and evaluation of this research work. Their constructive criticism and thoughtful suggestions have greatly enriched the quality of this thesis.*

I also thank ***Gujarat Technological University (GTU)*** *for holding my hands and making the PhD journey possible as a Part Time Research Scholar - GTU.*

I would also like to thank: LMCP admin staff – ***Bhagyashree, Yamini ben, Kruti, Neel bhai and Darshanbhai****; LMCP non-teaching staff –* ***Yogeshbhai, Amiben, Shagunbhai, Dharmeshbhai, Sunilbhai, Rajukaka, Bharatkaka, Prakashkaka, Mukeshbhai, Vinukaka, Sabajitkaka and Kishorbhai*** *for being on toes whenever needed.*

Last but not the least, I would like to thanks L.M. College of Pharmacy. I am undeniably proud to be associated with the college.

I am heartly thankful to all of them who have directly or indirectly supported me to complete my research work.

Kinjal Nayee

Table of Contents

List of Abbreviation

ADMET	Absorption, Distribution, Metabolism, Excretion, and Toxicity
AIDS	Acquired Immunodeficiency Syndrome
AUC0–24	Area Under the Curve from zero to 24 hours
BCE	Before Common Era
BCG	Bacillus Calmette–Guerin
BPaL	Bedaquiline, Pretomanid, and Linezolid
COVID	Corona Virus Disease
COX-2	cyclooxygenase-2
DMEM	Dulbecco's Modified Eagle Medium
DMSO	Dimethyl sulfoxide
DNA	Deoxyribonucleic acid
DPPH	2,2-diphenyl-1-picrylhydrazyl
DprE1	Decaprenylphosphoryl-β-D-ribose 2′-epimerase
EBA	Early bactericidal activity
ELISA	Enzyme-Linked Immunosorbent Assay
FBS	Fetal Bovine Serum
HCV	Hepatitis C Virus
HIV	Human Immunodeficiency Virus
HPZM/HPM	Isoniazid: Rifapentine: Pyrazinamide: Moxifloxacin/ Isoniazid: Rifapentine: Moxifloxacin
HRZE	Isoniazid (H), Rifampicin (R), Pyrazinamide (Z), and Ethambutol (E)
IFN	Interferon
IGRA	Interferon-Gamma Release Assay
INH	Isoniazid
InhA	Enoyl acyl carrier protein reductase
MABA	Micro plate Alamar Blue assay
MDR-TB	Multi drug resistant tuberculosis
MIC	Minimum inhibitory concentration
Mtb	Mycobacterium tuberculosis
MTT	3-(4,5-dimethylthiazol-2-yl)-2,5-diphenyltetrazolium bromide
NADH	Nicotinamide-adenine dinucleotide
NPT	Number of particles, Pressure, and Temperature
NVT	**N**umber of particles (N), **V**olume (V), and **T**emperature (T)
PCR	Polymerase Chain Reaction
PG	Peptidoglycan
RNA	Ribonucleic acid
SMART4TB	Supporting, Mobilizing, and Accelerating Research for Tuberculosis Elimination
TB	Tuberculosis
TDR-TB	Totally drug resistant tuberculosis
TLC	Thin layer chromatography
TNF	Tumor Necrosis Factor
tRNA	Transfer Ribonucleic Acid
TST	Tuberculin Skin Test
UNITE4TB	Academia and Industry United Innovation and Treatment for Tuberculosis
WHO	World Health Organization
XDR-TB	Extensively Drug-Resistant Tuberculosis

List of Figures

List of Tables

Annexure

1. SSIP grant certificate
2. Antitubercular activity certificate
3. Antioxidant activity certificate
4. DPC (Doctoral Progress Committee) review comments
5. List of publications
6. Poster presentation and other seminar participation certificate

CHAPTER-1

INTRODUCTION

CHAPTER- 1

1. INTRODUCTION

1.1. Tuberculosis

Tuberculosis is as old humanity itself. Only by working together can we turn the tide against this ancient killer.

-Tedros Adhanam Ghebreyesus

Tuberculosis is an infectious disease caused by the bacterium *Mycobacterium tuberculosis*. While the infection primarily targets the respiratory system, it can travel through the bloodstream to affect other vital organs, including the kidneys, spine, and brain.

Signs of tuberculosis have been found in human skeletal remains dating back more than 4,000 years. Evidence of tuberculosis like disease has been identified in ancient Egyptian mummies. Ancient civilizations in Egypt, India, and China described chronic lung illnesses that may have been tuberculosis. Around 460–370 BCE, Hippocrates described a disease called "phthisis" (consumption), characterized by weight loss, fever, and coughing. It was one of the most common causes of death in ancient Greece. During the middle ages, swollen lymph nodes in the neck caused by TB were known as "scrofula" and were sometimes called the "King's Evil" because people believed royal touch could cure it. The famous scientist Robert Koch was able to isolate the tubercle bacillus. Using the Methylene blue staining recommended by Paul Ehrlich, he identified, isolated and cultivated the bacillus in animal serum. Finally he reproduced the disease by inoculating the bacillus into laboratory animals. Robert Koch presented this extraordinary result to the Society of Physiology in Berlin on 24th March 1882, determining a milestone in the fight against TB (Barberis et al., 2017).

Tuberculosis is one of the top 10 causes of death worldwide and the leading cause of death from a single infectious agent. Globally in 2024, 10.7 million people fell ill with tuberculosis and 1.23 million died from the disease. The TB incidence rate was 131 (95% UI: 122–141) and the case fatality rate was 11.5%. Most of the people who develop TB disease each year are in 30 high TB burden countries: they accounted for 87% of the global total in 2024. The top eight (67% of the worldwide total) were India (25%), Indonesia (10%), the Philippines (6.8%), China (6.5%), Pakistan (6.3%), Nigeria (4.8%), the Democratic Republic of the Congo (3.9%) and Bangladesh (3.6%). Multidrug-resistant TB (MDR-TB) remains a public health crisis and a health security threat. Only about 2 in 5 people with drug-resistant TB

accessed treatment in 2024. Globally, the number of people falling ill with TB (incident cases) decreased in 2024 for the first time since 2020, following 3 consecutive years of increases (2021–2023) due to COVID-related disruptions to TB diagnosis and treatment. (World Health Organization, 2025).

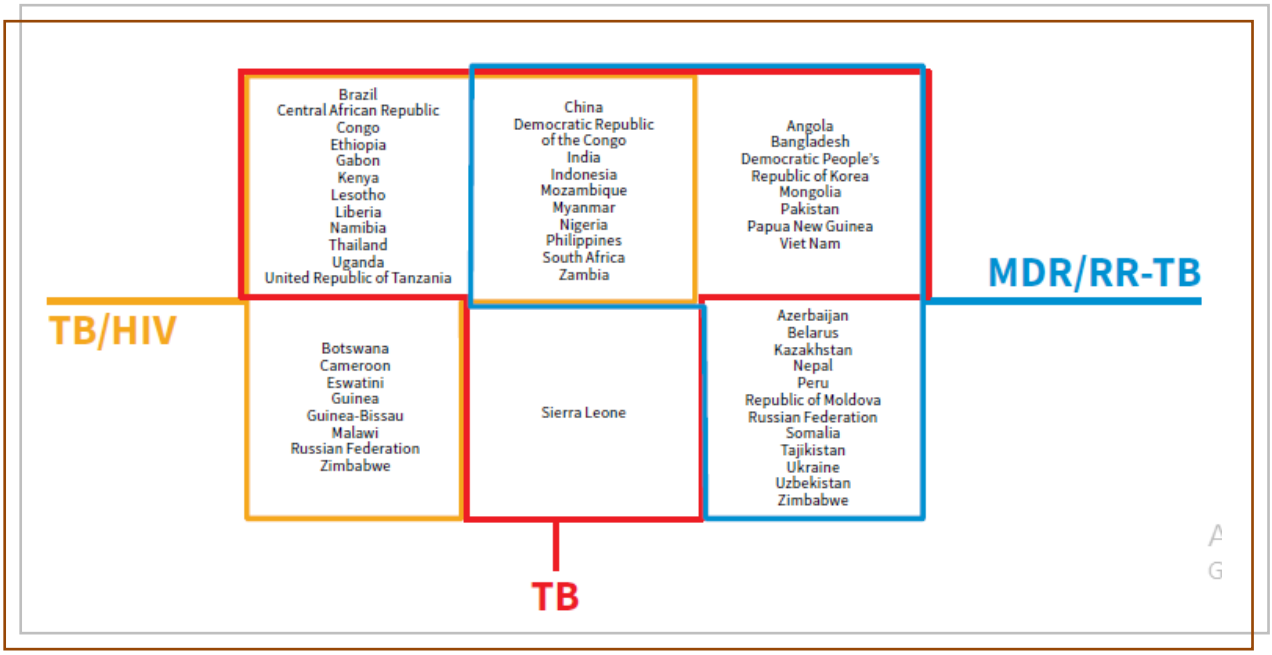

Fig.1: The three global lists of high-burden countries for TB, HIV-associated TB and MDR/RR-TB

Drug-resistant tuberculosis continues to be a major challenge, with the number of cases not being diagnosed or treated. Additionally, drug-resistant tuberculosis, concurrent epidemic of HIV-TB co-infections, and insufficient treatment facilities make this disease more complicated (Kebbahalli et al., 2025). The combination therapy for tuberculosis, developed over 40 years ago, includes Isoniazid, Pyrazinamide, Rifampicin, and Ethambutol, a four-drug combination. These therapies possess drawbacks, including extended treatment durations, drug interactions, unwanted adverse reactions, and poor patient compliance (Chakraborty & Rhee, 2015). Various side effects exist with the administration of first-line anti-tubercular drugs, including hepatitis, kidney failure, skin reactions, blood disorders, and gastrointestinal discomfort.

1.2. Mycobacterium

Mycobacteria are rod-shaped bacteria of the family Mycobacteriaceae (order Actinomycetales), the most important species of which, *M. tuberculosis* and *M. leprae,* cause tuberculosis and leprosy, respectively, in humans. *M. bovis* causes tuberculosis in cattle and in humans. Some mycobacteria are saprophytes (i.e., they live on decaying organic matter), and others are obligate parasites. Most are found in soil and water in a free-living form or in diseased tissue of animals (Kieser & Rubin, 2014).

❖ Properties of Mycobacterium

- Gram-positive
- Acid fast stain
- Catalase positive
- They may be arranged singly or in groups
- Non-motile, non-spore forming rod-shaped bacteria (0.2–0.6 mm wide and 1.0–10 mm long).

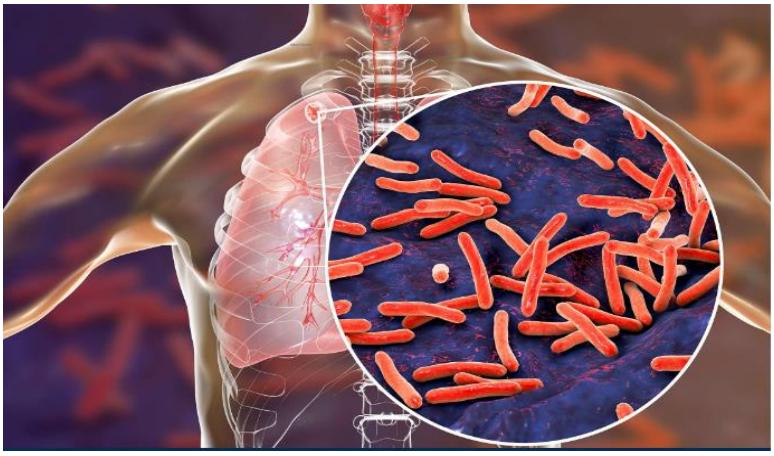

Fig.2: Species of *Mycobacterium tuberculosis* (Bender, 2019)

Mycobacteria can be divided into three groups:

1. *Mycobacterium tuberculosis* complex – causative pathogen of tuberculosis
2. Nontuberculous mycobacteria (NTM)
3. *Mycobacterium leprae* – causative pathogen of leprosy

1. Mycobacterium tuberculosis complex

Mycobacterium tuberculosis complex (MTBC) refers to a group of mycobacteria encompassing nine members of closely related species that causes tuberculosis in animals and humans. Among the nine members, *Mycobacterium tuberculosis* remains the main causative agent for human tuberculosis that results in high mortality and morbidity globally (Percival & Williams, 2014). The mycobacterium tuberculosis complex (MTBC) is a group of Mycobacteria that comprises of

- *Mycobacterium tuberculosis*
- *Mycobacterium africanum*
- *Mycobacterium bovis*
- *Mycobacterium canettii*
- *Mycobacterium microti*
- *Mycobacterium pinnipedii*
- *Mycobacterium caprae*
- *Mycobacterium orygis*
- *Mycobacterium mungi*

2. Nontuberculous mycobacteria (NTM)

Nontuberculous mycobacteria (NTM) are emerging pathogens responsible for a growing spectrum of diseases, particularly in individuals with underlying lung disorders or immune suppression. NTM are categorized based on growth rate and pigment formation into slowly growing mycobacteria and rapidly growing mycobacteria (Roshdi & Reza, 2025). The Runyon classification further subdivides NTM into four groups:

- Type I (photochromogens)
- Type II (scotochromogens)
- Type III (nonchromogens)
- Type IV (rapid growers)

3. Mycobacterium leprae

Mycobacterium leprae, slow-growing, acid-fast causative organism of leprosy (Hansen's) disease, is known to be the first bacterial pathogen to be identified as the cause of a human

infectious disease. The uniqueness of this bacterium is its ability to invade the Schwann cell of the peripheral nervous system (Rockefeller, 2001).

1.2.1. Cell wall of *Mycobacterium tuberculosis*

The mycobacterial cell wall is a complex structure that is an essential for cell growth, resistance to antibiotics and virulence. It is composed of three distinct macromolecules. They are surrounded by a non-covalently linked outer capsule of proteins and polysaccharides.

1. Peptidoglycan (PG)
2. Arabinogalactan (AG)
3. Mycolic acid

1. Peptidoglycan(PG): The peptidoglycan layer surrounds the plasma membrane and comprises long polymers of the repeating disaccharide N-acetyl glucosamine-N-acetyl muramic acid (NAG–NAM) that are linked via peptide bridges. Its mesh like arrangement confers rigidity to the cell, prevents osmotic lysis and responsible for cellular shape (Lederer, 1971)(Brennan, 2003)(Alzaidi, 2018).

2. Arabinogalactan(AG) : Arabinogalactan layer surrounded by the peptidoglycan layer. It is a biopolymer consisting of arabinose and galactose monosaccharides. It is a heteropolysaccharide that is covalently tethered 10%-12% of the muramic acid residues of PG via phosphodiester bond. Arabinogalactan, whose outer ends are esterified with high molecular weight fatty acids called mycolic acids (Lederer, 1971)(Brennan, 2003)(Alzaidi, 2018).

3. Mycolic acid

Mycolic acids, the major building blocks of mycobacterial cell envelope, are long α-chain branched, ß-hydroxylated fatty acids which upon pyrolysis are cleaved into a meroaldehyde main chain also called meromycolic chain and a meroacid or shorter α branch. They consist of 60 to 90 carbon atoms depending on mycobacterial species and various chemical functions like cyclopropane rings and oxygenated groups. Mtb mycolic acids are of three main types: alpha, methoxy and keto, where α is the most apolar with 74 to 80 carbon atoms and generally two double bonds or two cis cyclopropyl groups located in the meromycolic chain. The other two subtypes contain supplementary oxygen functions namely methoxy and keto

groups located in the distal part of the meromycolic chain and have 84 to 88 carbon atoms (Lederer, 1971)(Brennan, 2003)(Alzaidi, 2018).

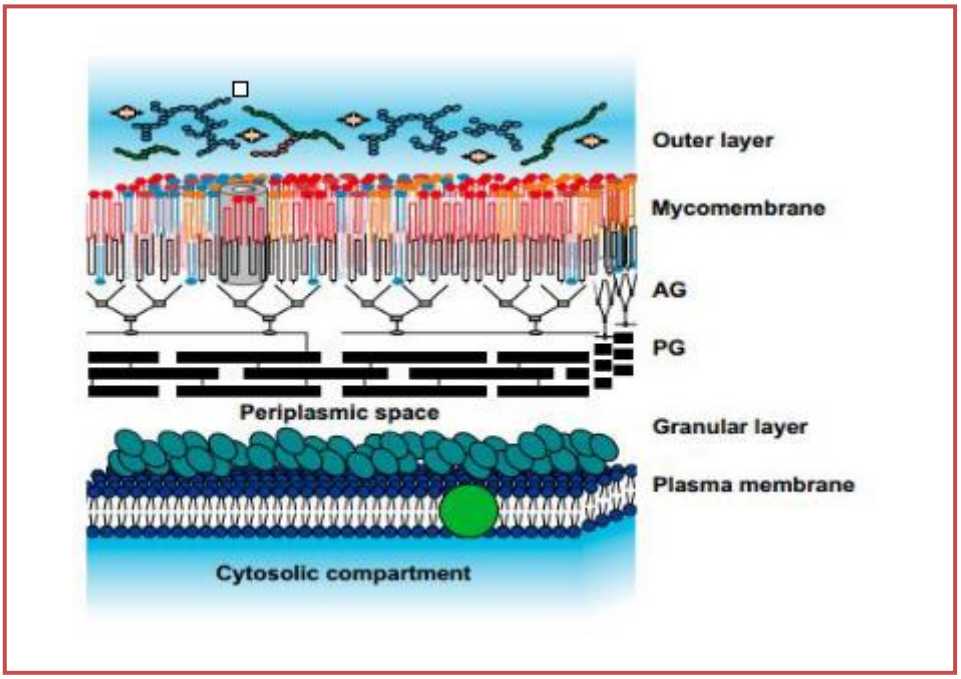

Fig. 3: Cell wall of *Mycobacterium tuberculosis* (Alzaidi, 2018)

1.2.2. Pathogenesis of Tuberculosis

The steps include in TB pathogensis are – exposure, infection, disease and death. Pulmonary TB occurs in the lung and comprises almost 85% of all TB cases. The upper lung lobes are more frequently affected by tuberculosis than the lower ones. The disease progression can be divided into following five stages.

Stage 1

Droplet nuclei are inhaled and are generated by talking, coughing and sneezing. Once nuclei are inhaled, the bacteria are non-specifically taken up by alveolar macrophages. The macrophages will not be activated, therefore unable to destroy the intracellular organism. The large droplet nuclei reaches upper respiratory tract and the small droplet nuclei reaches air sacs of the lung (alveoli) where infection begins. Disease onset when droplet nuclei reaches the alveoli. Bacteria multiplies within the inactivated macrophages until macrophages burst. Other macrophages diffuse from peripheral blood, phagocytose TB and are inactivated, rendering them unable to destroy TB.

Stage 2

Lymphocytes, specifically T-cells recognize TB antigen. This results in T-cell activation and the release of cytokines, including interferon (IFN). The release of IFN causes the activation of macrophages, which can release lytic enzymes and reactive intermediates that facilitates immune pathology. Tubercle forms, which contains a semi-solid or "cheesy" consistency. Although many activated macrophages surround the tubercles, many other macrophages are inactivated or poorly activated. The growing tubercle may invade a bronchus, causing an infection which may spread to other parts of the lungs. Tubercle may also invade artery or other blood supply. Spreading of TB may cause milliary tuberculosis, which can cause secondary lesions. Secondary lesions occur in bones, joints, lymph nodes, genitourinary system and peritoneum.

Stage 3

The caseous centers of the tubercles liquefy and the organism begins to rapidly multiply extracellularly. After time, the large antigen load cause the walls of nearby bronchi to become necrotic and rupture. This results in cavity formation and allows TB to spread rapidly into other airways and to other parts of the lung (Knechel, 2009).

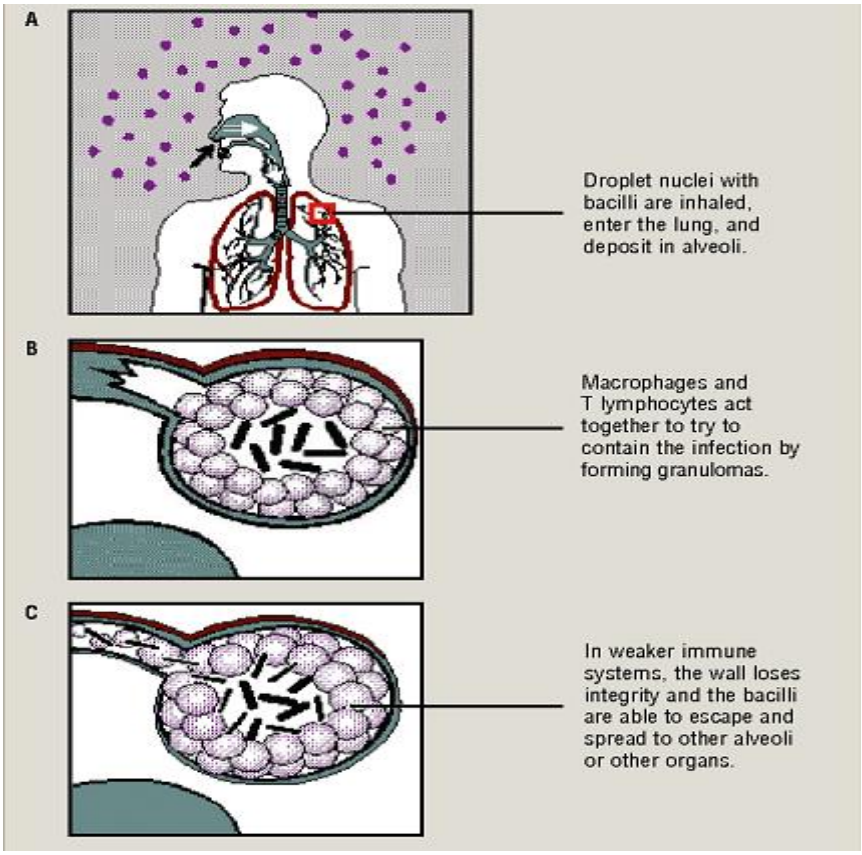

Fig. 4: Pathophysiology of *Mycobacterium tuberculosis* (Knechel, 2009)

1.3. Risk Factors of Tuberculosis

- HIV
- Silicosis
- Cancer
- Diabetes
- Malnutrition
- Alcoholism
- Gastrectomy
- Age
- Certain medications, such as corticosteroids and Infliximab (an anti-αTNF monoclonal antibody)

1.3.1. Transmission of *Mycobacterium Tuberculosis*

A person with laryngeal or pulmonary tuberculosis may cough, sneeze, talk, sing, or produce other small airborne droplets that are 97% of the time called "droplet nuclei" that are responsible for spreading *Mycobacterium tuberculosis*. These dangerous bacteria will remain inhaled and be phagocytosed (a process that encloses and gets rid of infections and other foreign objects) in the pulmonary alveoli. The main infection could not show any symptoms. Infectious particles can be inhaled by another person after they have been aerosolized and have been dispersed by circulation of air throughout a room or structure. Considering how tiny they are, droplet nuclei can float in the air for a long time. Sneezing generates the majority of droplet nuclei, which can spread to others up to 10 feet away. Most of the larger droplets that are inhaled with droplets of air end up in the upper respiratory tract, such as the nose and throat, where infections are less likely to spread. The respiratory system becomes infected when *M. tuberculosis* reaches the lungs, but extrapulmonary tuberculosis can also develop in other organs such as the lymphatics, pleura, bones and joints, or meninges. Inhaled infectious droplets settle throughout the airways.

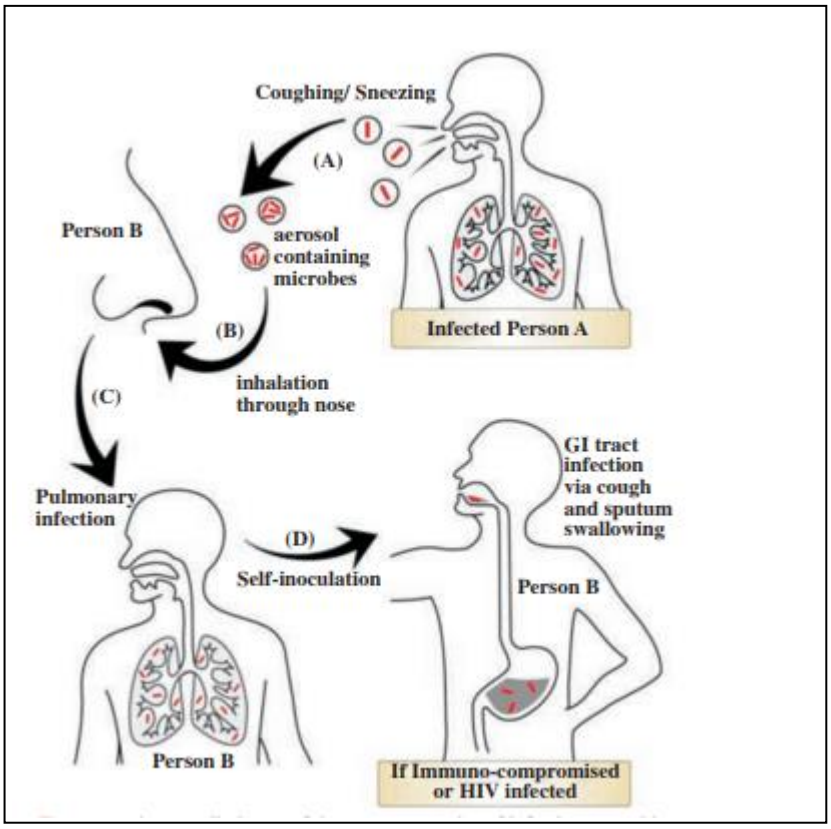

Fig.5: Spreading of *Mycobacterium tuberculosis* (Bhunia et al., 2015)

1.3.2. Tuberculosis and HIV co-infection

HIV-associated tuberculosis (HIV-TB) is associated with disproportionate mortality: approximately 24% of the 660,000 individuals with TB and HIV died, compared to 11% of those without HIV dying from TB in 2023. HIV is a key driver of ongoing high TB incidence in many countries, particularly in the World Health Organization Africa region, and TB is the leading cause of hospitalization in people with HIV (PWH) globally. Significant developments have occurred recently concerning the prevention, screening, diagnosis, and management of HIV-TB. Antiretroviral therapy and novel regimens for TB preventive therapy are now known to decrease TB incidence and improve survival(Sossen et al., 2025).

1.4. Sign and symptoms of tuberculosis

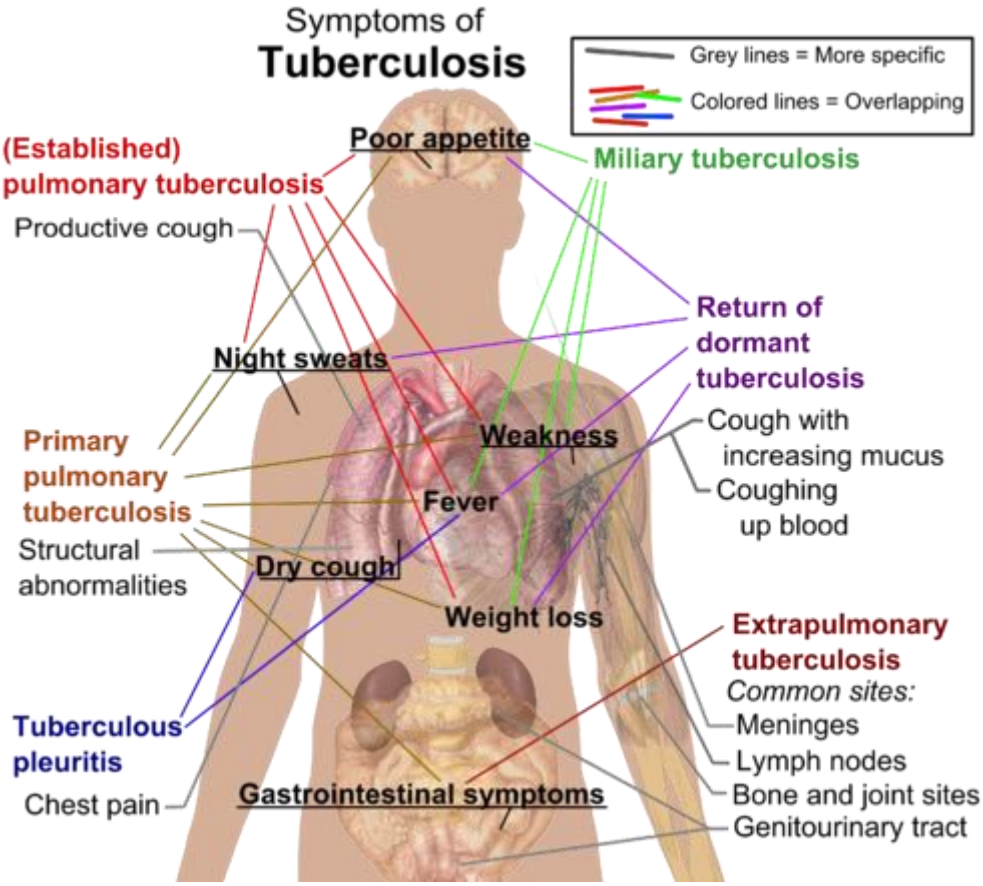

Fig.6: Sign and symptoms of tuberculosis

1.5. Types of Tuberculosis

Tuberculosis can be comprehensively grouped into two main types. One is pulmonary tuberculosis and the other is extrapulmonary tuberculosis. Pulmonary TB affects lungs and remains more prevalent. When the disease is transmitted from the lungs to different parts of the body, which happens in around 15-20% of the instances of active TB, then it is referred to as extrapulmonary tuberculosis. In this case, central nervous system, lymphatic system, kidneys, bone, and genitourinary framework are the frequently infected regions.

TB infections are classified based on where the bacteria are active in the body and how they respond to standard antibiotic regimens (Noraffandy Yahaya & Nur Fazila i Salleh, 2020).

1.5.1. Latent TB Infection

In latent TB, the bacteria remain dormant inside the body. Individuals with latent TB exhibit no clinical symptoms and cannot transmit the infection to others.

However, if the host's immune system becomes compromised, the infection can transition into active disease. Early therapeutic intervention is critical to stop this progression.

1.5.2. Active Pulmonary TB Disease

Active TB occurs when the bacteria multiply and cause symptoms. Pulmonary TB affects the lungs and is the most common form. It is highly contagious and spreads from person to person through microscopic airborne particles.

1.5.3. Extrapulmonary Tuberculosis

When the infection spreads outside the lungs, it is classified as extrapulmonary tuberculosis. This form can affect the lymph nodes, skeletal structures, joints, kidneys, and central nervous system.

- **Spinal TB (Pott's Disease):** Targets the vertebrae, causing persistent back pain and structural spinal stiffness.
- **Renal TB:** Attacks the kidneys, frequently resulting in blood in the urine (hematuria).
- **Meningeal TB:** Infects the membranes surrounding the brain, causing severe headaches and neck stiffness.
- **Lymph Node TB (Scrofula):** Leads to noticeable localized swelling, most commonly in the lymph nodes of the neck.

1.5.4. Drug-Resistant TB (DR-TB)

Drug-resistant TB develops when the bacteria mutate and no longer respond to standard antibiotic protocols.

- **Multi-Drug Resistant TB (MDR-TB):** Resistant to at least isoniazid and rifampicin, the two most powerful first-line TB medications.
- **Extensively Drug-Resistant TB (XDR-TB):** Resistant to isoniazid, rifampicin, and several second-line alternatives, making treatment exceptionally difficult.

1.6. Diagnosis of Tuberculosis

Diagnosis of tuberculosis is mainly depends on clinical features, histopathology, demonstration of acid fast bacilli (AFB) and isolation of mycobacterium tuberculosis from the clinical specimens.

1.6.1. Radiological Method

Chest X-ray

The chest radiograph is useful technique for diagnosis of TB disease. Chest abnormalities can suggest pulmonary TB disease. A posterior-anterior radiograph of the chest is the standard view used for the detection of chest abnormalities. Chest radiographs may be used to exclude TB disease in an HIV-negative person who has a positive TST reaction or IGRA and who has no symptoms or signs of TB disease.

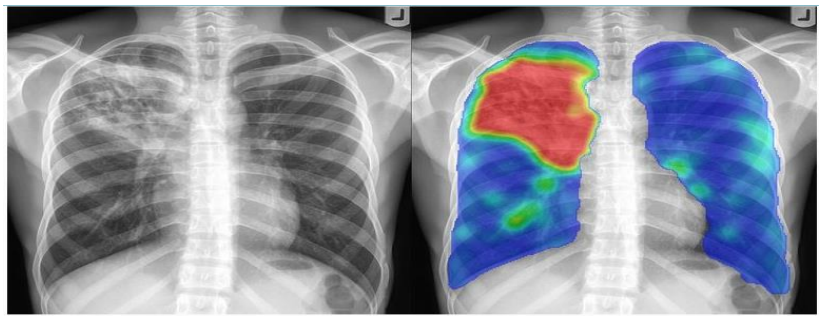

Fig.7: Chest X-ray analysis (Murphy, 2020)

1.6.2. Microscopy sputum smear

Microscopic examination of specially stained smears to detect acid-fast organisms such as *Mycobacterium tuberculosis* and nontuberculous mycobacteria. Acid fastness is a physical property that gives a bacterium the ability to resist decolorization by acids during staining procedures. Two techniques are used for the microbial examination (Mugenyi et al., 2024).

- Light-emitting diode fluorescence microscopy (LED-FM)
- Bright field microscopy

1.6.3. Culture method

Culture test involves studying bacteria by growing the bacteria on different substances. This is to find out if particular bacteria are present. In the case of the TB culture test the test is to see if the TB bacteria *Mycobacterium tuberculosis*, are present.

1.6.4. Drug sensitivity testing (DST)

These testing methods are based on the reduction of a coloured indicator added to liquid culture medium in a micro-titer plate after *M. tuberculosis* has been pre-incubated for several days *In-vitro* to different antibiotics and different drug concentrations.

1.6.5. Molecular drug resistance testing methods

It uses a hemi-nested PCR to amplify the Rifampin resistance-determining region (RRDR) of the *M. tuberculosis rpo*B gene. GeneXpert MTB/RIF® technique is used.

1.6.6. Latent TB infection detection

Indirectly measure TB infection by detecting memory T-cell response signifying the presence of host sensitization to *M. tuberculosis* antigens. Below techniques are used(Mugenyi et al., 2024).

- QuantiFERO-TB
- Gold Plus (QFT-Plus)
- WANTAI TB-IGRA
- SPOT®TBLISPOT-based
- IGRA(ELISPOT base)

1.6.7. The tuberculin skin test/ Mantoux test

The standard recommended tuberculin test is the Mantoux test, which is administered by injecting a 0.1 mL of liquid containing 5 TU (tuberculin units) PPD (purified protein derivative) into the top layers of skin of the forearm. Skin tests should be read 48-72 hours after the injection. The basis of the reading of the skin test is the presence or absence and the amount of induration (localized swelling). A negative test does not always mean that a person is free of tuberculosis.

1.7. Treatment of Tuberculosis

1.7.1. First line anti-tubercular agents

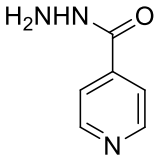

Isoniazid **(1)**

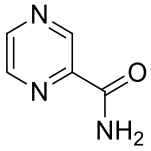

Pyrazinamide **(2)**

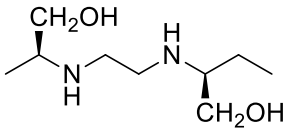

Ethambutol **(3)**

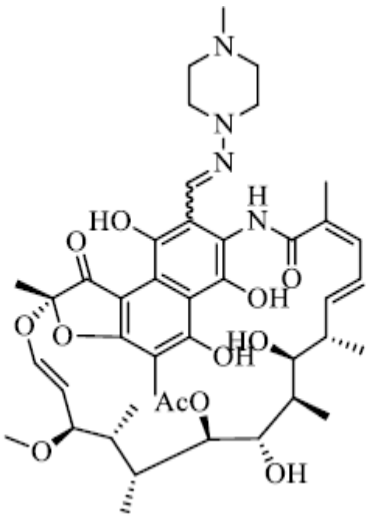

Rifampicin **(4)**

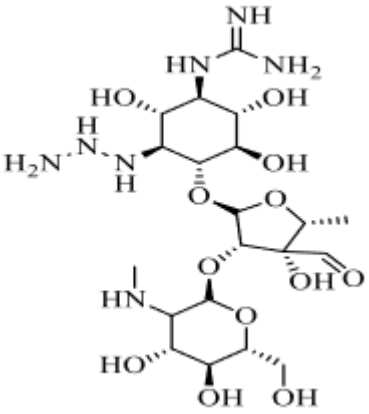

Streptomycin **(5)**

1.7.2. Second line anti-tubercular agents

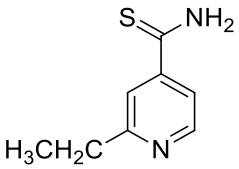

Ethionamide **(6)**

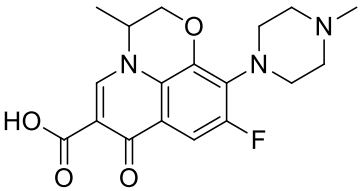

Ofloxacin **(7)**

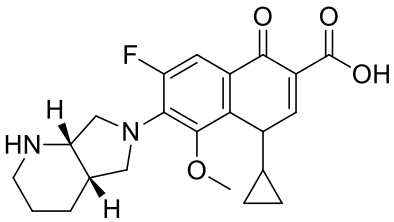

Moxifloxacin **(8)**

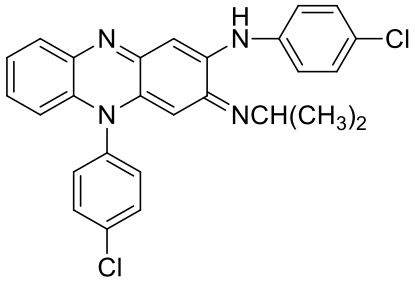

Clofazimine **(9)**

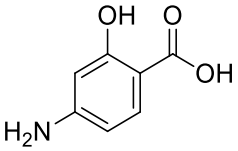

p-Aminosalicylic acid **(10)**

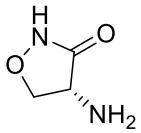

D-Cycloserine **(11)**

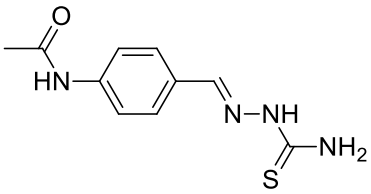

Thiacetazone **(12)**

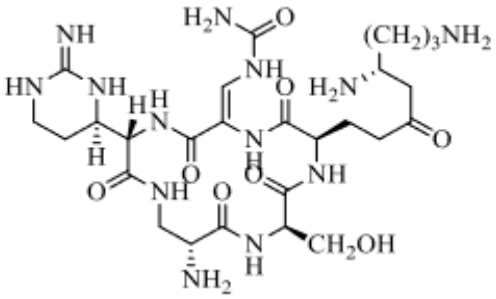

Capreomycin **(13)**

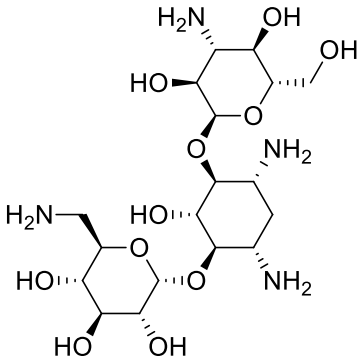

Kanamycin **(14)**

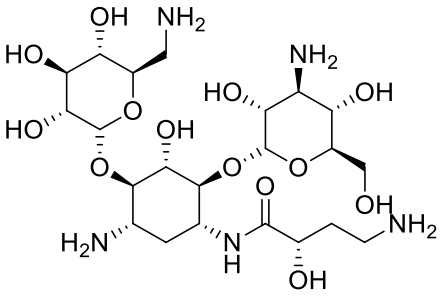

Amikacin **(15)**

1.7.3. Global new anti-tubercular drugs pipeline

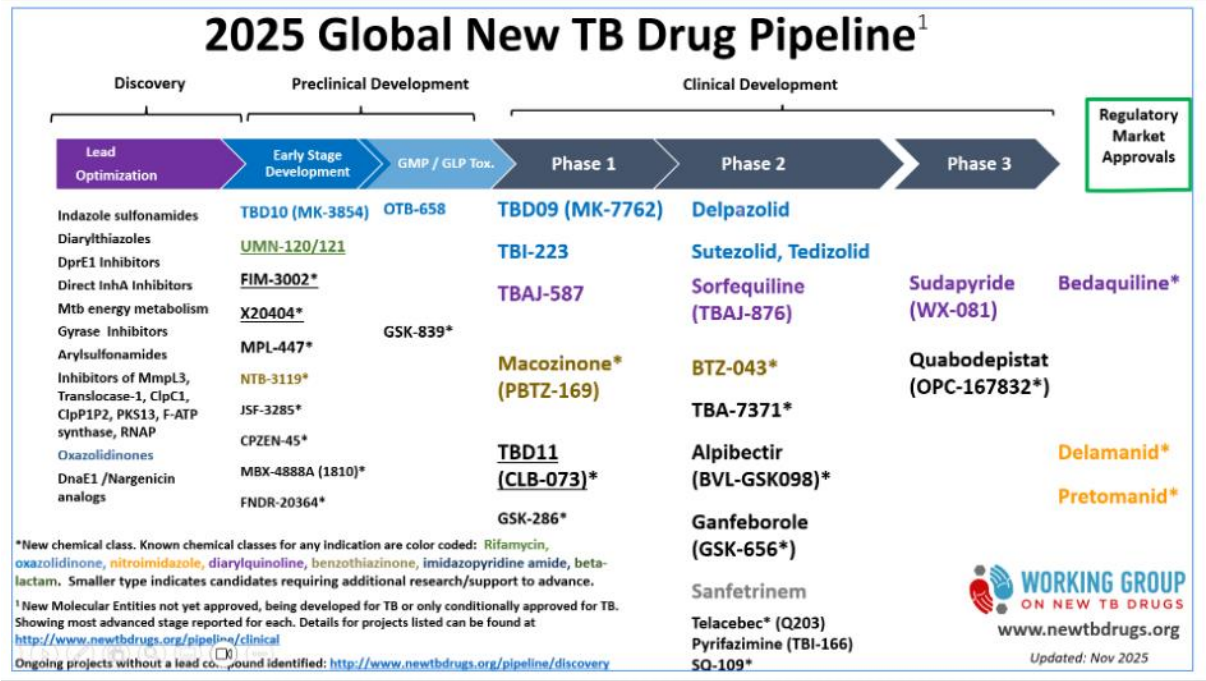

Fig. 8: Global Antitubercular drug pipeline (World Health Organization, 2025)

1.8. Anti-tubercular drugs and their targets (Laghari et al., 2016)

Tabel-1: Anti-tubercular drugs and their targets

Drugs	**Target**	**Mechanism**
Isoniazid	Enoyl acyl carrier protein reductase	Inhibition of biosynthesis of mycolic acids
Rifampicin	Subunit of DNA dependent RNA polymerase	Inhibition of RNA synthesis
Pyrazinamide	S1 component of 30s ribosomal subunit	Inhibit translation and trans - translation
Ethambutol	Arabinosyl transferases	Inhibit arabinogalactan biosynthesis
Streptomycin	S12 and 16S rRNA components of 30S ribosomal subunit	Inhibit protein synthesis
Kanamycin	30S ribosomal subunit	Inhibit protein synthesis
Amikacin	30S ribosomal subunit	Inhibit protein synthesis
Capreomycin	inhibiting bacterial protein synthesis by binding to the 70S ribosomal subunit	Inhibit protein synthesis
Para amino salicylic acid	Dihydropteroate synthase	Inhibit folate biosynthesis
Cycloserine	D-alanine racemase and ligase	Inhibit peptidoglycan synthesis
Fluoroquinolones (Moxifloxacin& Gatifloxacin)	DNA gyrase and topoisomerase IV	Inhibit DNA supercoiling

1.9. Anti-tubercular drugs and their mechanism (Capela et al., 2023)(Shetye et al., 2020)

Table-2: Anti-tubercular drugs and their mechanism

Chemical class and drugs	Structure	Mechanism of action
Diarylquinolines Analogue Bedaquiline TMC207 (Sirturo)	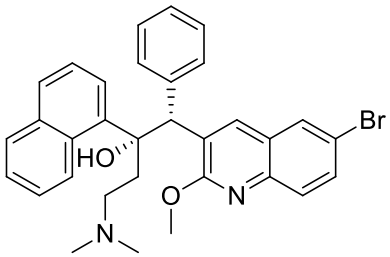 **(16)**	Inhibits energy production by targeting ATP
Nitroimidazole Analogues Delamanid (OPC-67683, Deltyba) PA-824	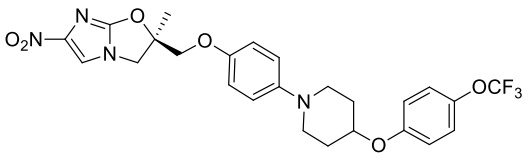 **(17)** 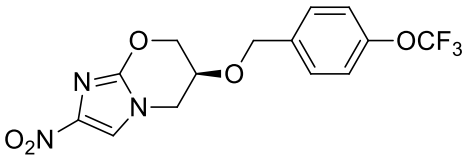 **(18)**	Destabilizes the bacterial cell membrane by blocking the synthesis of mycolic acids; poisons the bacterial cell by releasing nitric oxide when metabolized
Oxazolidininone Analogue Linezolid	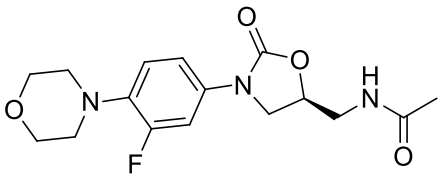 **(19)**	Protein synthesis inhibition (translation) by inhibiting the initiation step at the ribosome

PNU 100480 (Sutezolid) AZD5847	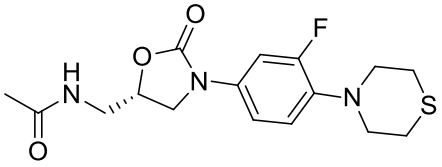 **(20)** 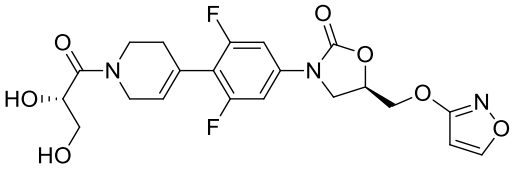 **(21)**	
Ethylene diamines SQ 109	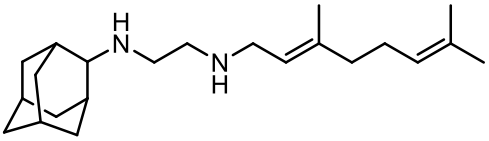 **(22)**	Cell wall biosynthesis inhibition. possibly by targeting the MmpL3 protein
Benzothiazinones BTZ 043 CPZEN-45	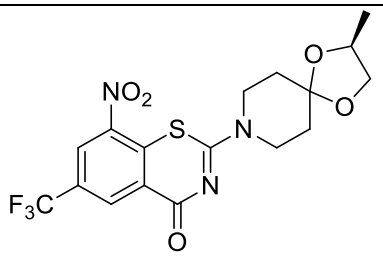 **(23)** 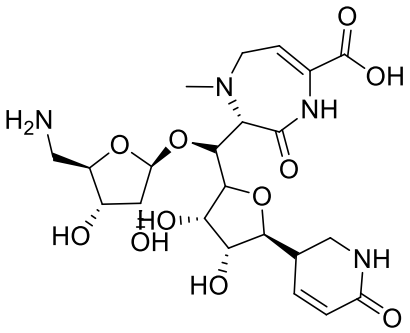 **(24)**	Peptidoglycan biosynthesis Peptidoglycan biosynthesis

Imidazopyridine Q2O3	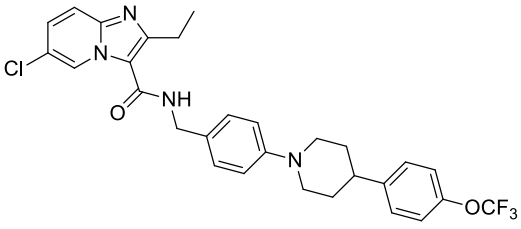 **(25)**	Targets the respiratory cytochrome bc1 complex, inhibiting the synthesis and homeostasis of adenosine triphosphate (ATP)
Quinolones Gatifloxacin	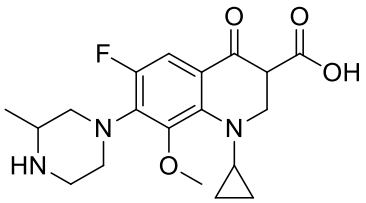 **(26)**	DNA synthesis inhibition (inhibition of gyrase)
DC-159a	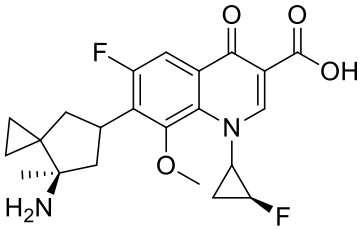 **(27)**	
Rifampicin Analogue Rifapentine	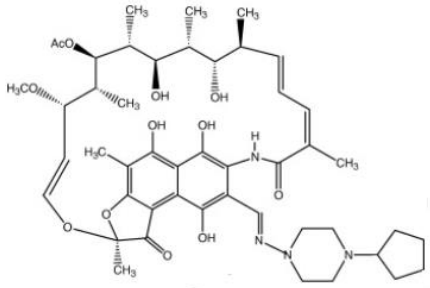 **(28)**	Inhibition of bacterial RNA synthesis (β-subunit of the DNA dependent RNA polymerase

1.10. Enoyl acyl carrier protein reductase (InhA)

The association of multifunctional FAS-I system (fatty acid synthase type I) originate from eukaryotes provides a good opportunity for its selective inhibition, but it is relatively different from the individual enzymes of the bacterial fatty acid synthase type II system (FAS-II). The striking antimicrobial drug targets, FAS-II pathway has gained much attention in the modern era for developing INH based new chemical entities. NADH-dependent enoyl acyl carrier protein (ENR) reductase encoded by mycobacterium gene InhA is the key catalyst involved in mycolic acid biosynthesis in FAS-II pathway. Earlier reports have recognized that InhA is the primary target for INH, a leading drug used for the treatment of tuberculosis for over 40 years. Reports have suggested that the formed INH-NADH adduct by the action of KatG (catalase-peroxide enzyme) on INH to form an acyl radical, which in turn covalently binds to NADH, acts as an effective inhibitor of InhA (Dixit et al., 2017).

The enoyl-ACP reductase encoded by the mycobacterium gene InhA is an essential enzyme in the biosynthesis of mycolic acid, the single most abundant component of the mycobacterium tuberculosis cell wall. This enzyme is required by this organism for cell wall synthesis, and inhibition of this enzyme results in death of the bacterial cell (Tallorin et al., 2016).

InhA is the target for the frontline antimycobacterial drug isoniazid (fig.9), a prodrug that is activated by the mycobacterial catalase-peroxidase enzyme KatG, to form a reactive species that acylates the nicotinamide moiety of NADH. Investigations into the mechanisms of resistance to isoniazid have revealed that KatG mutations are the primary cause, as without the oxidation of isoniazid to the active species, the necessary acylation of the nicotinamide cannot occur therefore, compounds that can directly inhibit InhA without the need for activation by KatG present a very promising opportunity to combat MDR-TB, XDR-TB and TDR-TB (Šink et al., 2015).

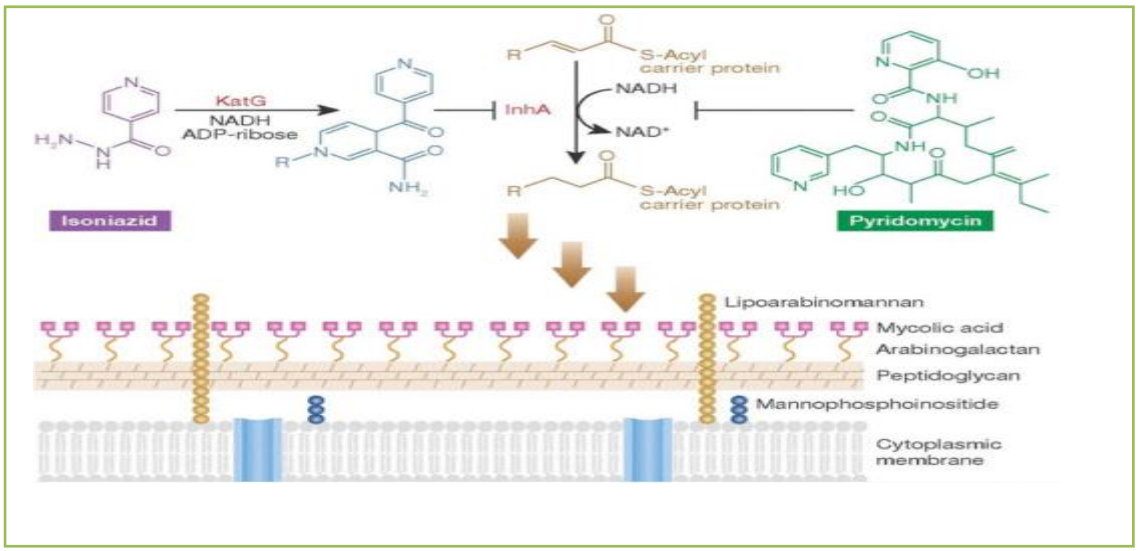

Fig.9: Inhibition of mycolic acid by enoyl acyl carrier protein reductase(InhA) enzyme (Wright, 2012)

1.11. Decaprenylphosphoryl-beta-D-ribose 2'-epimerase

Decaprenylphosphoryl-β-D-ribose-2′-epimerase (DprE1), a crucial enzyme in the process of arabinogalactan and lipoarabinomannan biosynthesis. Decaprenylphosphoryl-β-d-ribose 2′epimerase (DprE1) is one of the enzyme that catalyzes the biosynthetic pathway for the production of the two crucial heteropolysaccharide structure of Mtb cell envelope, arabinogalactan (AG) and lipoarabinomannan (LAM). LAM and AG consist of a typical sugar moiety, d-arab- inofuranose (d-Araf). Decaprenylphosphoryl-d-arabinose (DPA) is the sole donor of d-Araf. The metabolic pathway involved in the synthesis of DPA comprises the conversion of the sugar moiety, ribose, to arabinose. DprE1 enzyme catalyzes the oxidation of decaprenylphosphoryl-d-ribose (DPR) to form the intermediate, decaprenylphosphoryl-2′-keto-ribose (DPX) with the reduction of FAD cofactor to FADH2. Subsequently, the intermediate DPX is reduced to DPA by using NADH-dependent deceprenylphosphoryl-2-keto-ribose reductase (DprE2). The reduced form of the FAD cofactor, $FADH_2$, has to be oxidized through an electron acceptor like menaquinone or molecular oxygen to assist the new epimerization cycle, depicted in Fig.10. Also, this epimerization step takes place in the periplasmic localization of the Mtb cell wall, elucidating the vulnerable character of DprE1 by developing an enormous number of inhibitors with diverse heterocyclic ring scaffolds. According to their mechanism of inhibition, these inhibitors are classified as covalent inhibitors, which inhibit the DprE1 enzyme irreversibly by making a covalent adduct with Cys387 amino acid, and non-covalent inhibitors, which work as competitive inhibitors (Dash et al., 2024)(Chikhale et al., 2018).

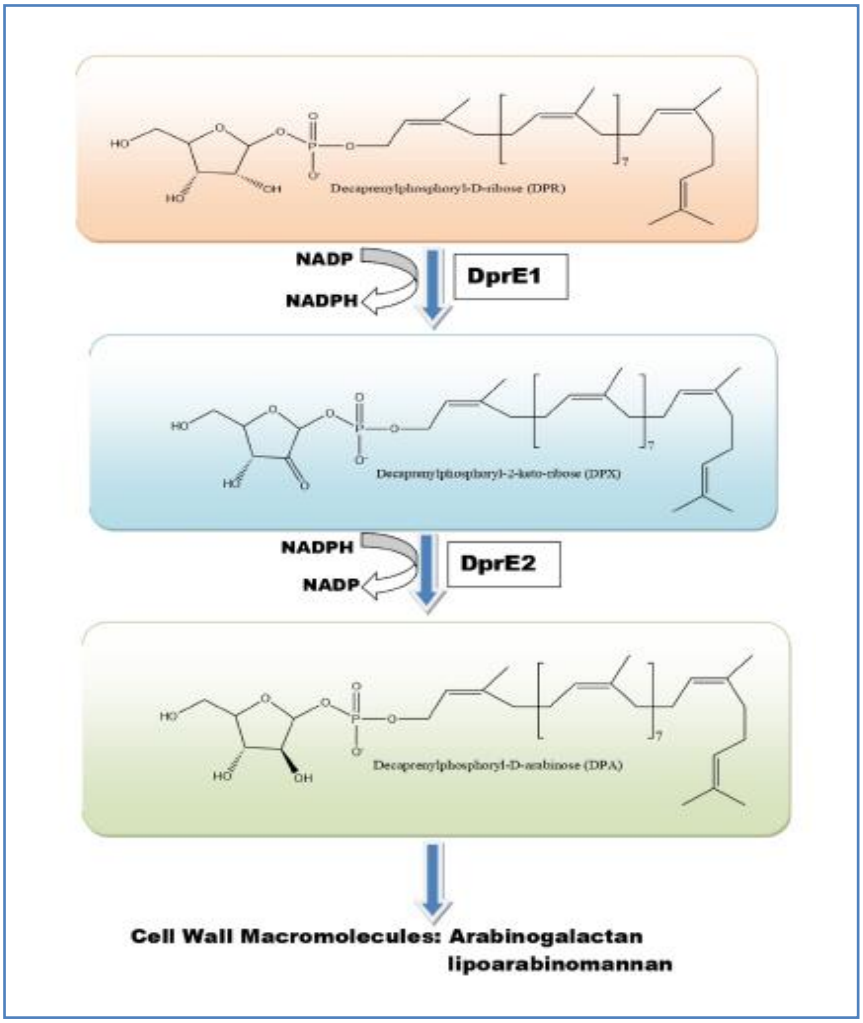

Fig. 10: Graphical representation of inhibition of cell wall synthesis by DprE1

1.12. Tuberculosis vaccine

Tuberculosis (TB) elimination requires vaccines capable of preventing pulmonary disease and transmission. BCG protects against severe childhood TB but inadequately prevents transmission. Throughout the history of public health, few medical interventions have had an impact comparable to vaccination. Vaccines have prevented millions of deaths, dramatically reduced the burden of infectious diseases and eventually led to their global eradication. Beyond their direct protective effects, vaccination programs illustrate how scientific innovation, when combined with sustained political commitment and societal engagement, can fundamentally alter the trajectory of human disease.

TB is presenting new challenges as a global health problem, especially with new threats of HIV co-infection and multidrug-resistant and extensively drug-resistant strains of *Mycobacterium tuberculosis*. The current TB vaccine, *Mycobacterium bovis* bacillus

Calmette–Guerin (BCG), is the most widely used vaccine worldwide but its efficacy against pulmonary TB in adults in many high-burden countries is limited. Different vaccine strategies will probably be required for the various needs that exist within a population in which some individuals have been previously immunized with BCG, co-infected with HIV or latently infected with *M. tuberculosis*. In the last 15 years, new strategies to improve or replace BCG in the laboratory have led to several promising vaccine candidates that are actively being evaluated in human clinical trials (Ly, 2008).

Despite the continued global burden of TB, bacille Calmette–Guérin (BCG) remains the only licensed TB vaccine and has been in use for more than a century. Developed in 1921 from an attenuated strain of the cow pathogen *Mycobacterium bovis*, BCG has been widely implemented in national immunization programme, particularly in high-burden settings, because of its proven efficacy in preventing severe forms of TB in infants and young children, including TB meningitis and miliary disease. In contrast, protection against pulmonary TB – the main driver of transmission – has been highly variable across studies and geographic regions. BCG is not a single, uniform vaccine but a group of related substrains that diverged during serial *In-vitro* passage. Genomic analyses have revealed deletions, duplications, and regulatory differences that influence antigen expression, innate immune activation, and immunogenicity, potentially contributing to heterogeneity in vaccine efficacy (Martín et al., 2026).

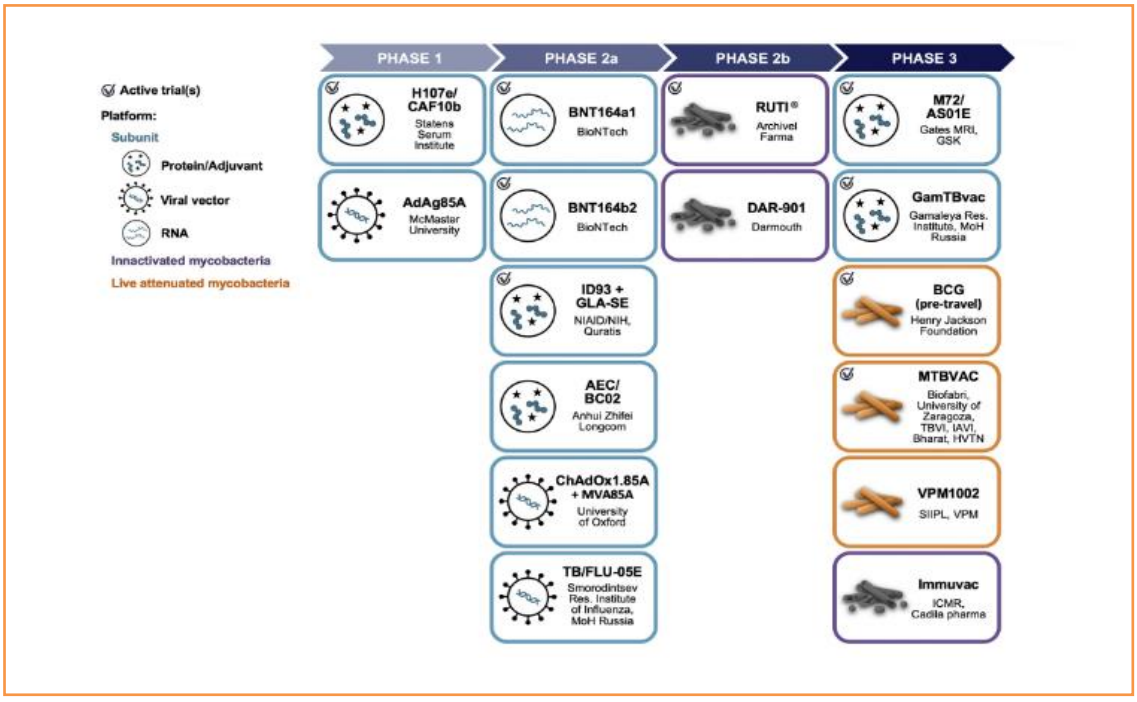

Fig. 11: Anti-tubercular vaccine pipeline

1.13. Current Tuberculosis Paradigm

Tuberculosis has been treated as a biologically homogenous disease, when emerging evidence suggests that people with tuberculosis are likely to have distinct phenotypes and immunological endotypes. This concept transformed cancer therapeutics through the establishment of The Cancer Genome Atlas, which led to the development of endotype-specific therapies and improved clinical outcomes. In tuberculosis, both intrinsic and extrinsic drivers are thought to drive the development of distinct host immune endotypes. Intrinsic drivers include deficiencies in key immune pathways such as interleukin (IL)-12/interferon (IFN)-ɣ or TNF signalling, or immune exhaustion, whilst extrinsic drivers such as diabetes mellitus, smoking or poor air quality, infecting strain and bacillary load may also shape the immune response. As our understanding of tuberculosis dynamic immunopathology evolves, it may be necessary to develop or repurpose drugs that target the host, rather than the pathogen, and tailor these host-directed therapies based on the host endotype, an approach that is already being trialled in sepsis. There is also pressing need to move away from traditional microbiologic and radiographic biomarkers alone, which inadequately capture a treatment regimen's sterilizing capacity or immunomodulatory benefits such as in reducing tissue fibrosis or preserving lung function, outcomes that are increasingly recognized as important in the long-term health of survivors. A proposed framework of precision medicine for tuberculosis includes incorporating therapeutic drug monitoring, endotype guided immunomodulatory therapy, and the use of multiplex biomarkers to guide length of treatment decisions or drug selection. Embedding these elements within adaptive trial designs may help identify responder subsets, refine combination regimens, and thereby realize the full potential of any regimen. Alongside these ambitions, given the increased complexity of what is proposed, it will be essential to incorporate implementation science from the outset to ensure that any findings can be translated effectively within the context of resource-limited tuberculosis programmes.

The landscape of tuberculosis research has been transformed by the emergence of adaptive trial design, platform trials, and collaborative research consortia, which enable the simultaneous and efficient evaluation of candidate drugs, and treatment strategies within a flexible trial infrastructure. Initiatives such as the Tuberculosis Trials Consortium (TBTC), UNITE4TB and SMART4TB exemplify this approach, fostering global collaboration and accelerating the generation of high-quality evidence. By harmonizing protocols and pooling expertise, these consortia address critical gaps in TB treatment ultimately aiming to eliminate the disease globally (Cross, 2025).

The work done in past two decades is ushering in a new era in tuberculosis treatment, that we hope will deliver shorter, safer and more person-centred treatments for tuberculosis. It is important to recognize that beyond therapeutics, there are advances being made in vaccine development, host-directed therapies, and renewed interest in novel biomarker to improve diagnostics, predict treatment response, and enable personalize treatments. However, scientific progress alone will not end the tuberculosis epidemic. To fully realize the potential of these breakthroughs, there must be a coordinated effort to address the challenges of equitable drug availability, provide person-centred treatment support beyond directly observed therapy, strengthening health system capacity, and advancing the science of implementation. Only through this comprehensive, integrated approach can we accelerate progress towards eliminating tuberculosis.

1.14. New anti-tubercular drugs under clinical trial (Cross, 2025)

1. TBAJ-876: It is a next-generation diarylquinoline antibiotic, structurally similar to Bedaquiline, but specifically engineered to improve potency and safety. It has demonstrated increased *In-vitro* activity, including against strains with Rv0678 mutations. Additionally, TBAJ-876 shows a reduced propensity for QT interval prolongation compared to Bedaquiline. The multiarm, pan-Phase 2 trial, NC-009 has evaluated the optimal dose of TBAJ-876 in combination with Pretomanid and Linezolid during the intensive phase of treatment (the first 8 weeks). It compares the bactericidal activity and safety of this regimen against the standard BPaL regimen and conventional HRZE therapy across five countries. Results are not yet in the public domain (NCT06058299).

2. Sudapyridine (WX-081):

Sudapyridine (WX-081) is a novel diarylpyridine compound structurally related to Bedaquiline, developed by substituting the quinolone moiety with a pyridine group. This modification retains potent antimycobacterial activity while potentially improving the drug's safety profile, particularly regarding cardiotoxicity. In both *In-vitro* and *In-vivo* studies, Sudapyridine has demonstrated mycobactericidal activity equivalent to Bedaquiline. Following encouraging Phase1and Phase2 studies. Sudapyridine has advanced to a Phase 3 trial for the treatment of Rifampicin-resistant disease (NCT05824871). If its efficacy and safety are confirmed in Phase 3, Sudapyridine could offer a valuable alternative for an all-oral regimen, particularly for those with baseline QT prolongation, or those receiving other

QT-prolonging drugs.

3. DprE1 inhibitors:

Among more promising new drug classes against tuberculosis are the inhibitors of DprE1 (decaprenyl- phosphoryl-β-D-ribose 2-epimerase subunit 1, an enzyme required for the biosynthesis of essential mycobacterial cell wall components, lipoarabinomannan and arabinogalactan. Several DprE1inhibitors; Quabodepistat(OPC-167832),BTZ043, and TBA-7371 are currently in Phase 2 trials, with additional candidates progressing through earlier stage development.

BTZ-043, one of the earliest DprE1 inhibitors to enter human trials demonstrated excellent penetration and accumulation in necrotic lesions, areas where many antibiotics struggle to reach therapeutic concentrations, compromising treatment efficacy.

TBA-7371 has completed a Phase1 single/ multiple ascending dose study in healthy volunteers (NCT03199339) to establish safety, tolerability, pharmacokinetics and drug interactions with Midazolam and Bupropion as well as an EBA trial in drug susceptible tuberculosis (NCT04176250).

4. GSK-656 (Gabfeborole):

Another promising candidate in tuberculosis drug development is GSK-656 (Gabfeborole), the first class benzoxaborole compound which selectively inhibits aminoacyl-tRNA synthetases, an essential enzyme involved in protein synthesis in Mtb. In a Phase 2a EBA trial, the molecule exhibited dose dependent bactericidal activity with an acceptable pharmacokinetic and safety profile. A Phase 2a EBA trial testing GSK-656 as a two drug combination with Bedaquiline/ Delamanid or with standard of care treatment (HRZE - Isoniazid, Rifampicin, Pyrazinamide and Ethambutol) in drug-sensitive disease (NCT05382312), whilst the European Union-backed UNITE4TB consortium is testing in a Phase 2b trial combinations of BTZ-043, GSK-656, Bedaquiline, Delamanid, Moxifloxacin, Linezolid and Pyrazinamide over a 4-month period for drug-sensitive TB through a platform trial across Europe, Asia, Africa and South America.

5. Telacebec (Q203):

It is a novel antimycobacterial agent that targets mycobacterial cytochrome bc1aa3, an enzyme in the mycobacterial respiratory chain. In response, Mtb can reroute respiration through the less energetically efficient cytochrome bd oxidase, which renders Telacebec's activity bacteriostatic rather than bactericidal. Nevertheless, in a Phase 2 EBA trial, daily Telacebec doses of 100– 300mg were found to be safe, well tolerated, and demonstrated a dose dependent reduction in sputum mycobacterial load.

6. Oxazolidinone Drug:

Delpazolid and Sutezolid Oxazolidinone class drugs. In EBA trial, Delpazolid was evaluated in a Phase 2b DECODE trial, which assessed multiple dosing schedules in combination with Bedaquiline, Delamanid and Moxifloxacin for drug-susceptible tuberculosis. In this 76 participant study, the 1200mg dose of Delpazolid dose achieved the highest additive efficacy alongside the other medications. The higher dose of 800 mg twice-daily resulted in two drug related serious adverse events (gastritis and anaemia) both occurring in participants with relatively high Delpazolid exposure, as measured by AUC0–24. Larger, later-phase trials can be expected given the promising results.

Sutezolid, predicted to have a lower risk of mitochondrial toxicity compared to linezolid, and demonstrating encouraging early bactericidal activity, was tested in a Phase 2b trial which assessed multiple dosing regimens in combination with Bedaquiline, Delamanid, and Moxifloxacin. The 600mg twice-daily arm showed the most significant change in clearance of Mtb from sputum, and outperformed the comparator arm without Sutezolid and a historical comparison of HRZE.

There was no peripheral neuropathy reported after the 12 week treatment, a single grade 4 neutropenia determined to benign ethnic neutropenia rather than drug related, a single grade 4 drug induced liver injury, and no cases of QT prolongation where the interval was above 480 milliseconds (CROI 2023 Conference). A Phase 2b/c trial combining Quabodepistat and Sutezolid with Bedaquiline and either Delamanid or Pretomanid for drug-resistant TB was terminated, with the comment that the trial's objective of identifying a new regimen capable of curing TB in 3 months or less was not achieved (NCT05971602).

1.15. Current new TB treatment

The standard for tuberculosis (TB) treatment has shifted dramatically, offering shorter, all-oral regimens instead of the traditional 6-to-18-month courses. For drug-resistant TB, the 6-month BPaLM regimen is now the global and national standard, while drug-susceptible TB can often be cured in 4 months using HPZM/HPM(Lopes, 2025).

1. Drug-Resistant TB (MDR/RR-TB)

For multidrug-resistant or rifampicin-resistant TB, the WHO and the National TB Elimination Programme (NTEP) prioritize shorter, highly effective regimens:

- The **BPaLM** Regimen: A 6-month oral combination of **B**edaquiline, **P**retomanid, **L**inezolid, and **M**oxifloxacin.
- The **BPaL** Regimen: Similar to BPaLM but excludes moxifloxacin; primarily used if resistance requires it.

2. Drug-Susceptible TB (DS-TB)

For newly diagnosed, non-resistant TB, the standard 6-month treatment has been streamlined for faster recovery:

- **The 4 Month Regimen:** Known as 2HPZM/2HPM, this shorter course replaces older drugs with a powerful combination of Isoniazid, Rifapentine, Pyrazinamide, and Moxifloxacin.

1.16. DOTS (**Directly Observed Treatment Short Course)**

National TB treatment guidelines strongly recommend using a patient centered case management approach including directly observed therapy **DOT** when treating persons with active TB disease. DOT is especially critical for patients with drug resistant TB, HIV-infected patients, and those on intermittent treatment regimens (Davies, 2003).

- **What is DOTS?**

DOTS means that a trained health care worker or other designated individual (excluding a family member) provides the prescribed TB drugs and watches the patient swallow every dose.

Why use DOT?

- DOT helps patients finish TB therapy as quickly as possible, without unnecessary gaps.
- DOT helps prevent TB from spreading to others.
- DOT decreases the risk of drug-resistance resulting from erratic or incomplete treatment.
- DOT decreases the chances of treatment failure and relapse.

- **Five Elements of DOTS**
  1. Political commitment and sustained financing
  2. Case-detection through quality assured methodologies
  3. Standardized treatment with supervision
  4. Effective drug supply
  5. Monitoring/Evaluation system, and impact measurement

1.17. Research and Innovation to end Tuberculosis

Artificial Intelligence

Artificial Intelligence (AI) is the simulation of human cognitive function using computer systems. AI techniques include machine learning that employs multiple algorithms to identify complex nonlinear relationships within large datasets, deep learning where multiple layers of processing are used to progressively extract higher level features, and generative AI that can create new content. AI has revolutionized healthcare and can be applied to improve disease screening and diagnosis, optimize treatment regimens and advance precision medicine, support drug and vaccine development, optimize health systems management, support disease surveillance and refine disease risk predictions, assist clinical care and improve patient education.

AI is providing a transformative role in TB control. In 2022, the WHO launched an operational research package to generate data on treatment decision algorithms for pulmonary TB in children. This operational research seeks to provide external validation of two decision algorithms designed to help clinicians determine whether to commence treatment. Computer-aided detection (CAD) software is being utilized to automate the interpretation of digital X-ray images and is now recommended as an alternative to human interpretation in WHO screening guidelines. WHO recommend the use of CAD for screening and triage when

interpreting plain X-ray s from patients ≥15 years old. CAD has the potential to improve access to screening as it can operate in both portable and ultra-portable X-ray machines, but it has the disadvantage of requiring calibration with local data due to heterogeneity in the accuracy of threshold scores and can only be applied to frontal X-ray images for adults. AI provides an opportunity to increase the efficacy of resources which in many high TB burden countries are constrained. The application of this technology to patients on directly observed therapy (DOT) has been successful in reducing the time and cost burden on both patients and healthcare workers. The application of AI to monitor treatment efficacy and predict prognosis is being explored. AI is successfully predicting treatment duration, adverse reactions, drug resistance, and treatment outcomes which paves the way for personalized care and improved treatment outcomes (Gilmour & Alene, 2024).

Advances in geographic information systems (GIS)

A geographic information system (GIS) is a computer based platform for capturing, storing, checking, and displaying data related to locations on Earth's surface. With the advancements in Information Technology, the scope of GIS has been redefined and expanded. Health GISs are integrated systems containing tools for managing, inquiring, analyzing, and presenting referenced health data. Mapping through GIS can significantly enhance the assessment of environmental health risks, enabling more effective analysis and understanding of the patterns and relationships in health related data (Saraswathi et al., 2025).

A geography-based screening and treatment approach that evaluates the clusters of TB cases and their characteristics can serve as an effective method for control of tuberculosis cases.

1.18. Challenges against tuberculosis

1. Elucidate the biological mechanisms of mycobacterial persistence and latency.
2. Discover and develop new drugs that have novel mechanisms of action and are effective against persistent bacilli.
3. Develop and validate animal models that reliably predict human treatment duration.
4. Develop and validate biomarkers and surrogate endpoints that predict efficacy and thereby shorten clinical trial duration.
5. Develop new preclinical approaches to identifying optimized drug combinations and new clinical and regulatory approaches to testing drug combinations in phase 2 and 3 clinical trials.
6. Enhance capacity to conduct clinical trials in high-burden countries.

1.19. Docking (Raval & Ganatra, 2022)

Docking is a method which predicts the preferred orientation of one molecule to a second when bound to each other to form a stable complex. Knowledge of the preferred orientation in turn may be used to predict the strength of association or binding affinity between two molecules using, for example, scoring functions. Molecular docking is a computer simulation procedure to predict the conformation of a receptor-ligand complex, where the receptor is usually a protein or a nucleic acid molecule (DNA or RNA) and the ligand is either a small molecule or another protein.

It can also be defined as a simulation process where a ligand position is estimated in a predicted or pre-defined binding site.

- It is the accurate method for predicting the biological activity of particular ligand.
- By using docking studies, fewer compounds need to be synthesized and assayed, and a higher number of compounds assayed are found to be active.

1.19.1. Types of Docking

Rigid Docking (Lock and Key)

In rigid docking, the internal geometry of both the receptor and ligand are treated as rigid.

Flexible Docking (Induced fit)

An enumeration on the rotations of one of the molecules (usually smaller one) is performed. Every rotation the energy is calculated; later the most optimum pose is selected.

Docking can be between...

Prtein-Ligand

Protein-protein

Protein-Nucleotide

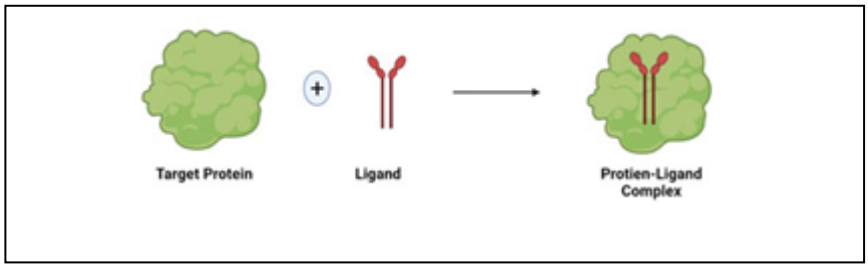

Fig.12: Molecular Docking

1.19.2. Types of Interaction

Electrostatic forces - Forces with electrostatic origin are due to the charges residing in the matter.

Electrodynamics forces - The most widely known is probably the van der waals interaction.

Steric forces – These are caused by entropy. For example, in cases where entropy is limited, there may be forces to minimize the free energy system.

Solvent related forces – These are due to structural change of the solvent. These structural changes are generated, when ions, colloids, proteins etc, are added into the structure of solvent. The most commonly are hydrogen bond and hydrophobic interaction.

1.19.3. Key Steps in Docking

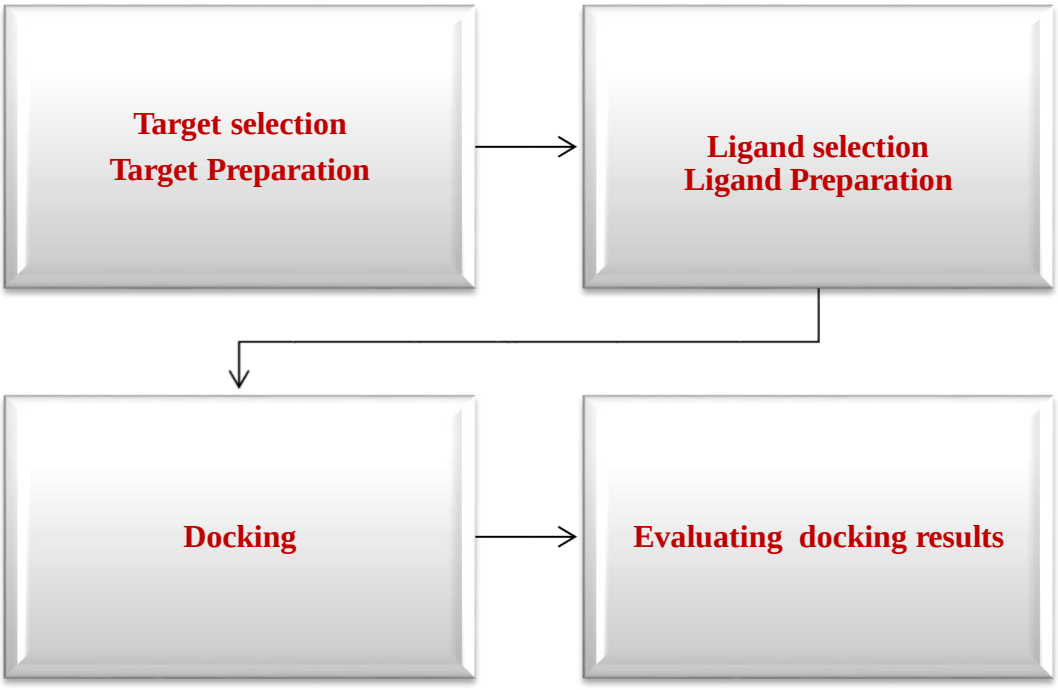

Fig. 13: Docking workflow

❖ **Receptor selection and preparation**

Building the Receptor

- The 3D structure of the receptor should be considered which can be downloaded from PDB.
- The available structure should be processed.
- The receptor should be biologically active and stable.

Identification of the Active Site

- The active site within the receptor should be identified.
- The receptor may have many active sites but the one of the interest should be selected.

Ligand selection and preparation

Ligand can be obtained from various databases like ZINK, PubChem or can be sketched using tools like ChemSketch.

Docking

The ligand is docked onto the receptor and the interactions are checked. The scoring function generates score, depending on which the best fit ligand is selected.

CHAPTER-2

REVIEW OF LITERATURE

CHAPTER-2

2. REVIEW OF LITERATURE

2. 1. Pyrazole

The term Pyrazole was given by Ludwig Knorr in 1883. Pyrazole refers to the class of simple aromatic ring organic compounds of the heterocyclic series characterized by a 5-membered ring structure composed of three carbon atoms and two nitrogen atoms in adjacent positions. Being so composed and having pharmacological effects on humans, they are classified as alkaloids, although they are rare in nature. In 1959, the first natural pyrazole, 1-pyrazolyl-alanine, was isolated from seeds of watermelons (Alam et al., 2015).

2.1. 1. Physical and Chemical Properties

Pyrazole is a π-excessive heterocycle and contains two nitrogen atoms; pyrrole type and pyridine type, at positions 1 and 2. Pyrazole exists in three partially reduced forms. Pyrazole is a colourless solid with m.p. 69-70°C, boiling point of pyrazole (186-188°C) is due to intermolecular hydrogen bonding, Pyrazole exist in two identical and non-separable tautomers due to rapid interconversion of tautomers. Pyrazole ring structure contains three carbon atoms along with two nitrogen atoms present in adjacent positions. The lone pair of first N-atom participates in delocalization with π-electrons while the other lone pair present on the second N-atom is non-Huckel lone pair and due to that lone-pair pyrazole shows lewis basicity with PKb 11.5. The pyrazole is represented by the following structure (M. Kumar & Panday, 2022).

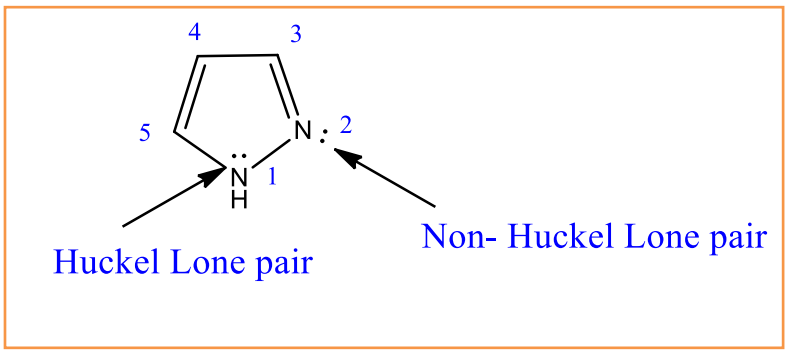

Fig.14: Structure of Pyrazole

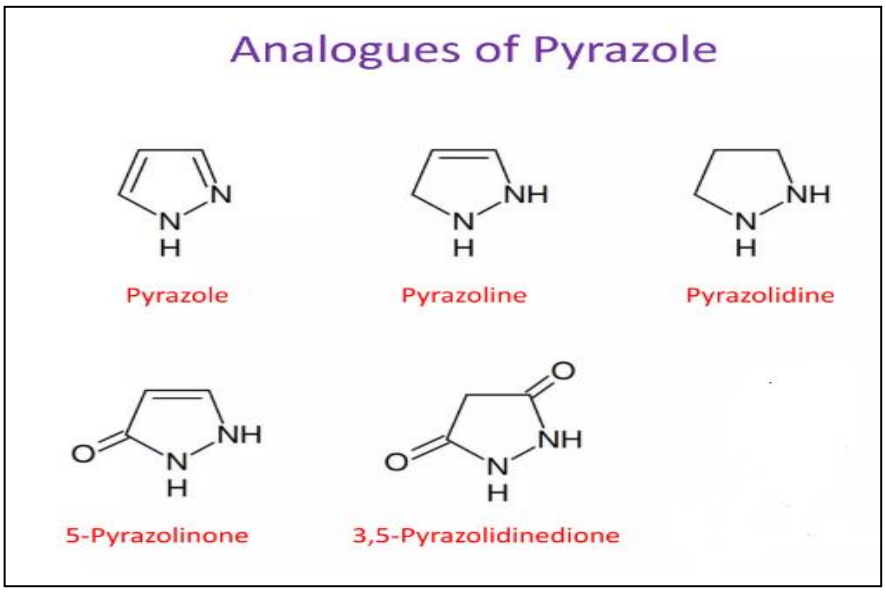

Fig.15: Pyrazole analogue

Pyrazole skeletons comprise various ranges of pharmacological activities such as analgesic, antipyretic, anticancer, antiviral, anti-inflammatory, antioxidants, antimicrobial, anti-diabetic, anti-convulsant, anti-arrhythmic. Pyrazole is a multipurpose effective molecule which is biologically active. Several synthetic routes are accorded to the development of pyrazole containing reactions to afford a novel molecule which is an enormous opportunity in the field of medicinal chemistry.

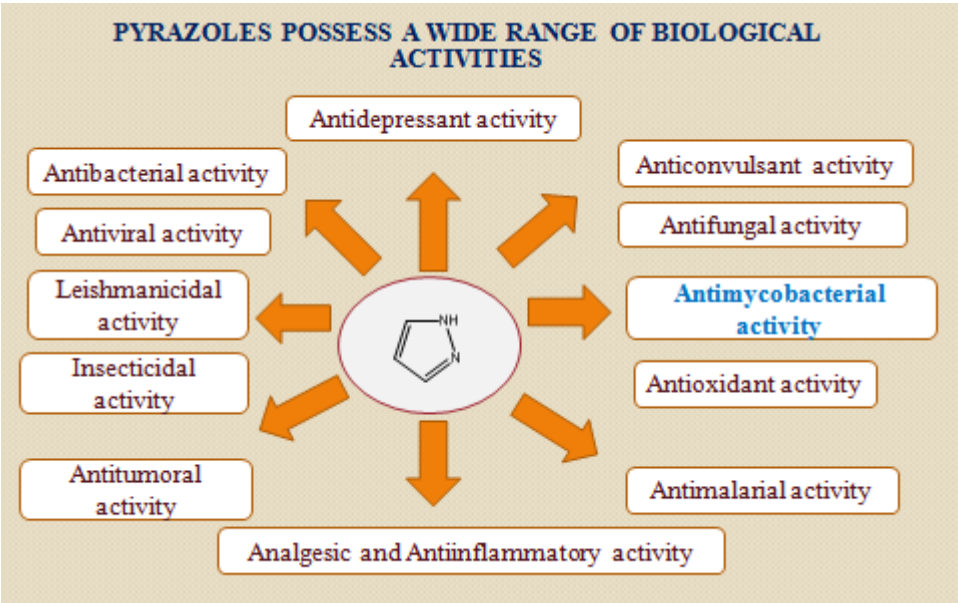

Fig.16: Various biological activities of Pyrazole heterocycle

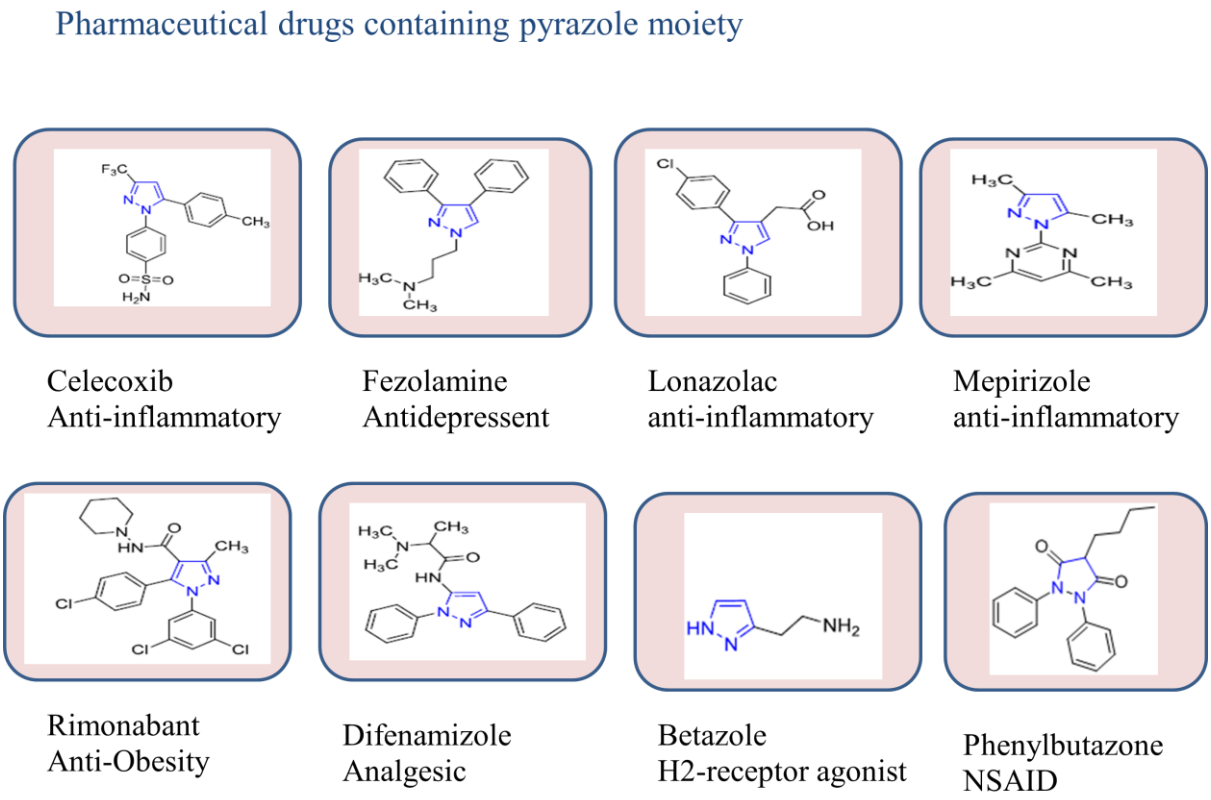

Fig.17: Pyrazole heterocycle containing marketed drugs

2.2. FDA approved pyrazole drug in 2022 to 2026

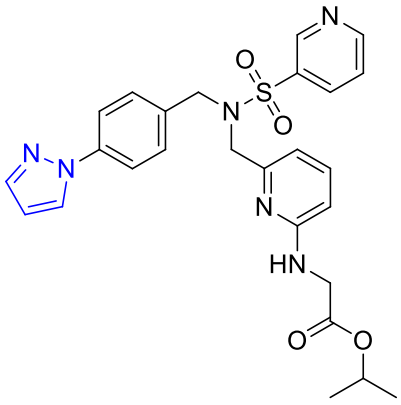

Omidenepag Isopropyl

(Glaucoma)

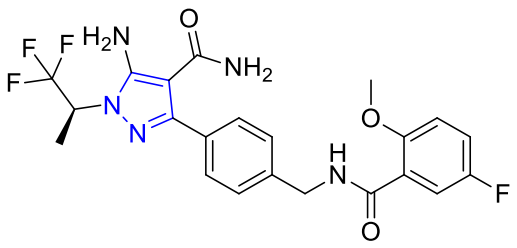

Pirtobrutinib

(Anticancer)

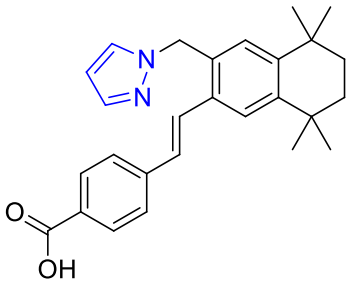

Palovarotene
(Heterotopic ossification and Fibrodysplasia ossificans progressiva)

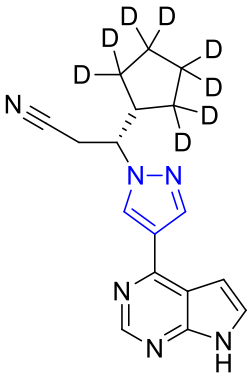

Deuruxolitinib (Severe alopecia areata)

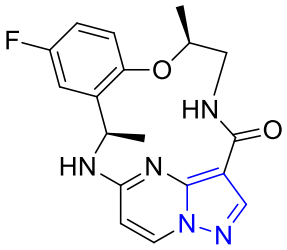

Repotrectinib (Anticancer)

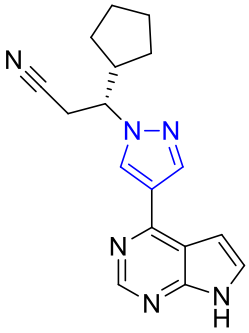

Ruxolitinib (Anticancer)

2.3. Chemistry of Pyrazolo[1,5-*a*]pyrimidines

Heterocycles hold a key place in organic and medicinal chemistry as they act as a bridge between life sciences and biochemical investigations. Aza heterocycles are essential scaffolds for generating wide range of chemical libraries for applications to obtain desired therapeutic/pharmacological activity. Among all the aza-heterocycles, Pyrazolo[1,5-*a*]pyrimidine is one such essential drug-like nucleus bearing enormous biologically applicability in drug discovery.

Pyrazolo[1,5-*a*]pyrimidine containing compounds are an important and strategic N-heterocycle family because of their proven applicability and synthetic versatility in preparing relevant chemicals in biological, pharmaceutical, photophysical, material science, and industrial fields. In this way, pyrazolo[1,5-*a*]pyrimidine synthesis and functionalization are highly desirable. Various research groups continue to focus on preparing this class of compounds, diversely substituted, to discover new and better applications. As a result, a deep and systematic study of the chemistry and properties of pyrazolo[1,5-*a*]pyrimidines is

necessary to understand their behaviour in various fields.

The heterocyclic fusion of pyrimidine and pyrazole rings resulted in formation of pyrazolo-pyrimidines, the structural analogs of biogenic purine class. Pyrazolopyrimidines and related fused heterocycles are of interest as potential bioactive molecules. (E.Rashad, 2014).

2.4. Synthesis of Pyrazole heterocycle containing compounds

2.4.1. From Tosylhydrazone

The pyrazole derivatives **(30)** are synthesized by 1,3-cycloaddition of the corresponding tosylhydrazones of the carbonyl compounds **(29)**, using a base in dry media (Grandi et al., 2007).

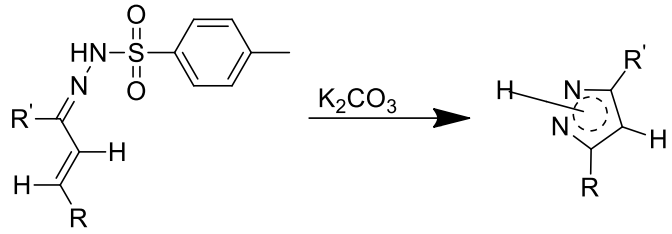

R= C_6H_5, R' = CH_3 (**29**) (**30**)

2.4.2. From Acetophenone (Microwave Synthesis)

The series of heterocycles, 1-(4-substitutedphenyl)-3-phenyl-1*H*-pyrazole-4-carbaldehyde **(34)** was synthesized by the reaction of acetophenone **(31)** with substituted phenyl hydrazine **(32)** in the presence of Vilsmeier-Haack reagent (Panneer et al., 2014).

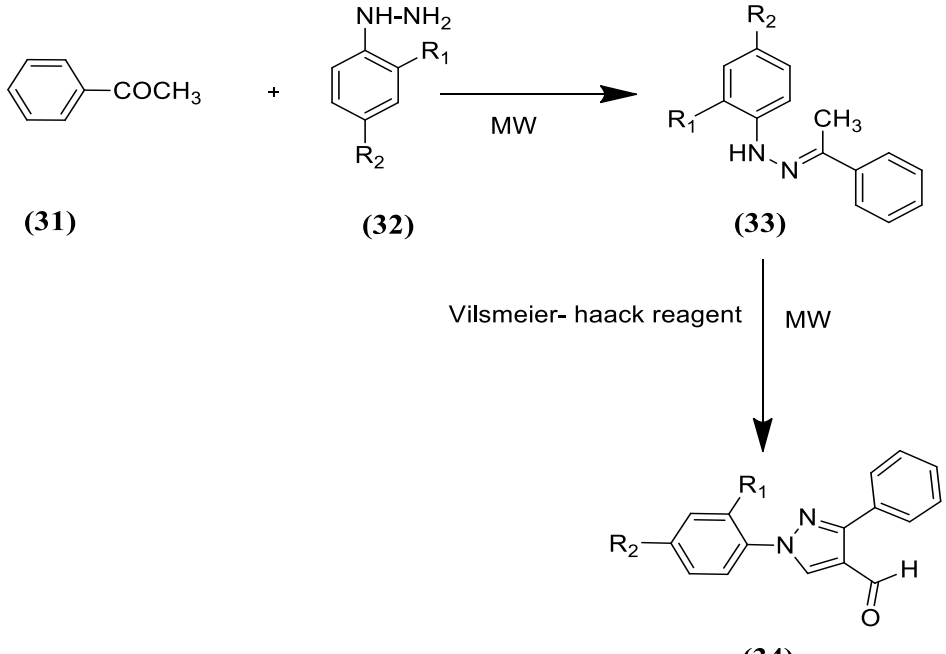

(31) **(32)** **(33)** **(34)**

R_1, R_2 = H, CH_3

2.4.3. From formyl glycol

Enantiomerically pure 4-substituted pyrazoles **(36)** synthesized from 2-formyl glycols**(35)** and arylhydrazines under solvent-free conditions (Yadav et al., 2004).

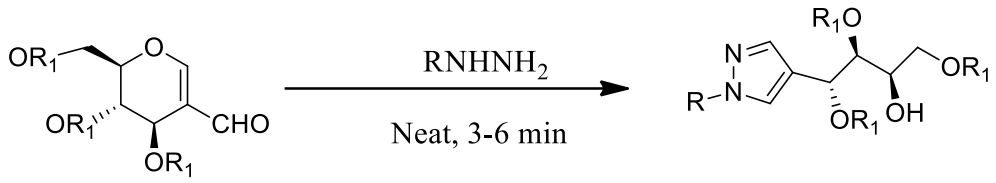

(35) **(36)**

R^1 = Me, Et, Bn

R= H, Ph, 2-EtC_6H_4, 3,4- ClC_6H_4, 4-MeOC_6H_4

2.4.4. From 1, 3-Diketoesters

Claisen condensation of ketone enolates **(37)** with diethyl oxalate **(38)** is the most general method used to prepare 1, 3-diketoesters **(39)** which constitute the building blocks of most of the pyrazole-3(5)-carboxylic acid derivatives **(40)** reported in the literature. Some of these compounds display important pharmacological activities (Fustero et al., 2011).

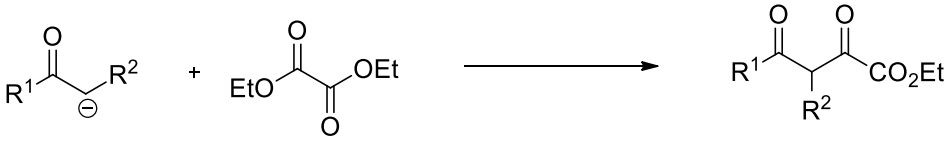

(37) **(38)** **(39)**

R^1 = Alkyl, (Het)Aryl
R^2= H, Alkyl, Het (Aryl), heteroatom
R= H, Alkyl, (Het) aryl

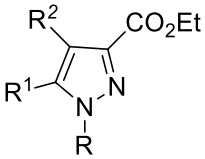

(40)

2.4.5. From α-epoxyketone

3,5-diaryl-1*H*-pyrazole derivatives **(43)** have been synthesized from α-epoxyketone **(41)** and semicarbazide hydrochloride**(42)** in presence of ethanol (Nikpour & Beigvand, 2008).

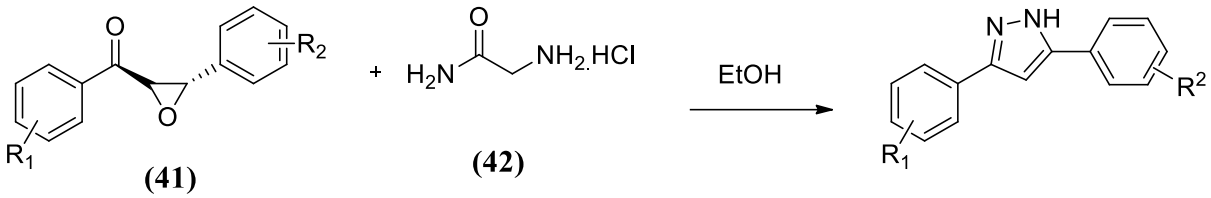

(41) **(42)** **(43)**

R^1= H, 4-Cl, 4-Me, 4-MeO
R^2= H, 2-Cl, 4-Cl, 4-Me, 4-MeO, $3NO_2$

2.4.6. From alkynyl ketones

Microwave irradiation of mixtures of alkynyl ketones**(44)** and arylhydrazines at 120 ^{0}C for 2 min afforded mixtures of 1,3- and 1,5- diarylpyrazoles **(45)** and **(46)** respectively, in high yields but, in general, with low regioselectivity (Fustero et al., 2011).

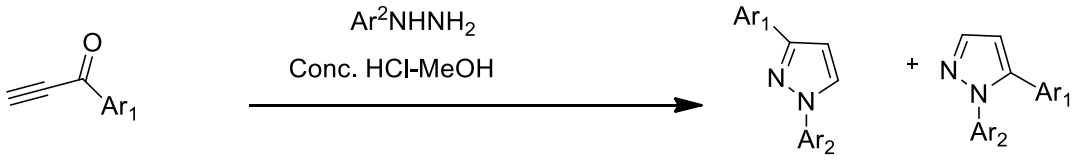

(44) **(45)** **(46)**

Ar^1= Ph, 4-MeO/ClC_6H_4
Ar^2= Ph, 4-Me/$O_2NC_6H_4$

2.4.7. From Weinreb amides

Persson and Nielsen developed an efficient approach to pyrazole-3-carboxylates from Weinreb amides, hydrazines, and ethyl propynoate (Persson & Nielsen, 2006).Weinreb amides **(48)** were reacted with the sodium acetylide of ethyl propynoate in an acyl substitution_conjugate addition sequence to furnish (E)-β-ethoxycarbonyl-N-methoxy-N-methyl-β-enaminones **(49)**, which regioselectively condensed with methyl and phenylhydrazines in a microwave assisted reaction to afford target pyrazoles **(50).**

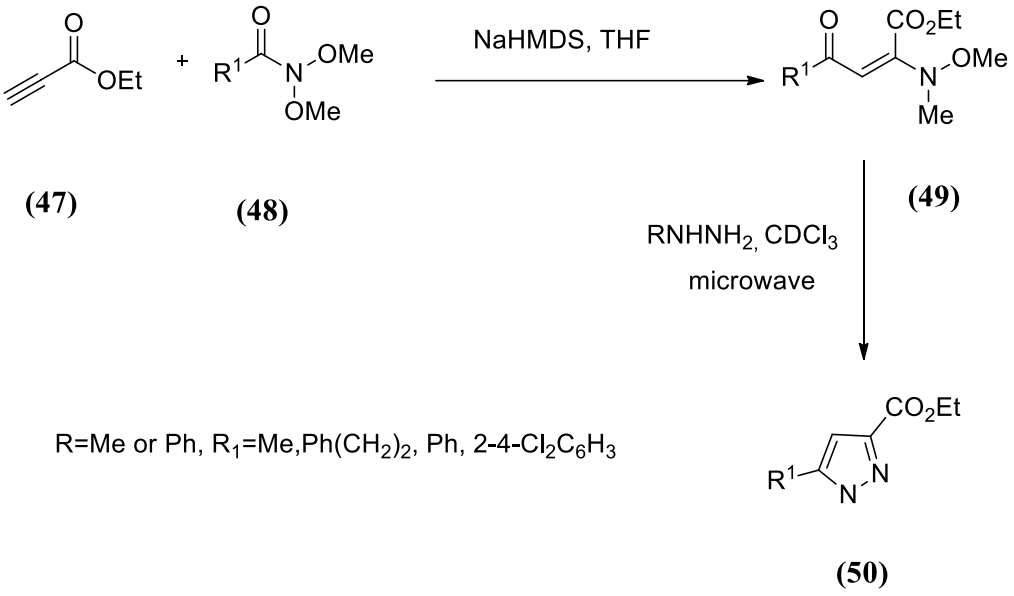

(47) **(48)** **(49)** **(50)**

2.4.8. From β-alkoxyvinyl trichloromethyl ketones

β-alkoxyvinyl trichloromethyl ketones **(51)** with hydrazine hydrochloride in EtOH, or phenylhydrazine in MeOH or EtOH, afforded alkoxycarbonylpyrazole derivatives **(52)** in good yields (Alex et al., 2005).

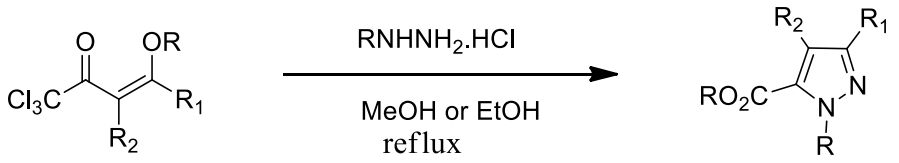

(51) **(52)**

R=Me, Et
R_1= H, Me, Ph, 2-furyl,2-thienyl
R_2= H, Me, R_1,R_2= -$(CH_2)_4$
R= H,Ph

2.4.9. From 5-tribuylstannyl-4-fluoropyrazole

4-fluoropyrazole derivatives **(56)** syntehsized from 5-tribuylstannyl-4-fluoropyrazole (X = Bu_3Sn) **(54)** and 4-fluoro-5-trimethylsilylpyrazole (X = Me_3Si) **(55).** Precursors obtained as the only products through a 1,3-dipolar cycloaddition of diazomethane and in situ prepared fluoro(tributylstannyl/trimethylsilyl) acetylenes(Fustero et al., 2011).

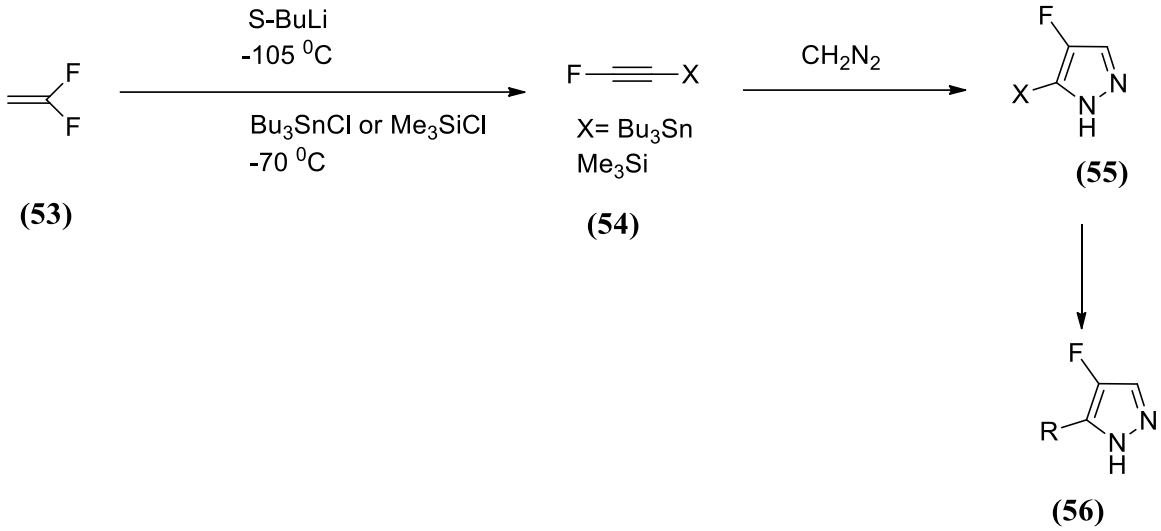

2.4.10. From α-bromocinnamaldehyde

Tetrasubstituted pyrazoles **(59)** were obtained in high yield through the regioselective 1,3-dipolar cycloaddition of α-bromocinnamaldehyde **(57)** to C-aryl-N-phenyl nitrile imines **(58)** at room temperature (Dadiboyena et al., 2010).

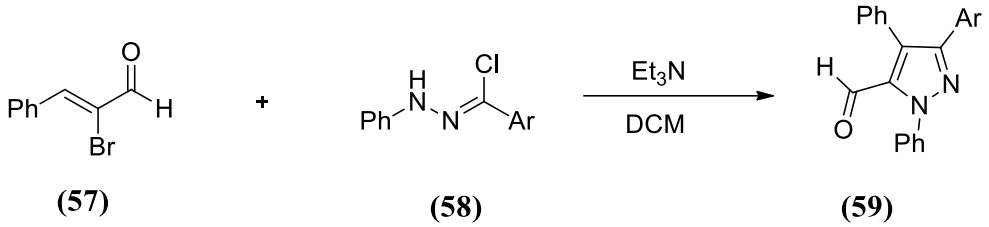

Ar= Ph, 4-Cl, $MeOC_6H_4$, 3-$O_2NC_6H_4$, ,2,6-ClC_6H_3

2.5. Therapeutic importance of Pyrazole

2.5.1. Analgesic and anti-inflammatory activity

Hassan *et al*. synthesized celecoxib analogs with benzofuran moieties and evaluated them for COX-2 inhibitory activity (Hassan et al., 2014). The compounds showed the highest anti-inflammatory activity, with IC_{50} values of 0.40 µM and 0.36 µM, respectively, compared to celecoxib.

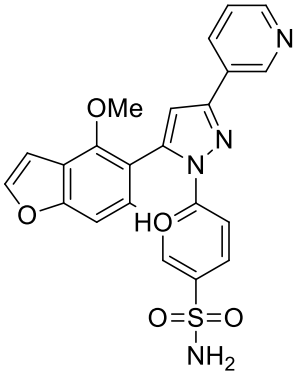

(60) IC_{50}= 0.40 µM

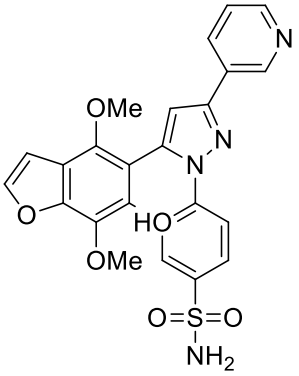

(61) IC_{50}= 0.36 µM

2.5.2. Pyrazole as Antifungal Agent

Pathak RB *et al.* (Pathak et al., 2012) synthesized and evaluated of 3-(4-chlorophenyl)-4-substituted pyrazole derivative with MIC value 1.6µg/mL.

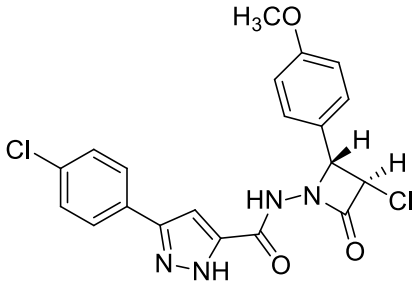

(62)

2.5.3. Pyrazole as apoptosis inducing agents

Arthur *et al.* (Shaw et al., 2010) have screened 3, 5-diaryl pyrazole derivatives and check growth inhibition on carcinoma cells. Best inhibition was observed with compounds bearing a 1,10-biphenyl moiety exhibited the most potent activity against OVCA, SW620, H460 and AGS cells with GI50 values of 0.67, 0.89, 0.73 and 0.79, µM respectively.

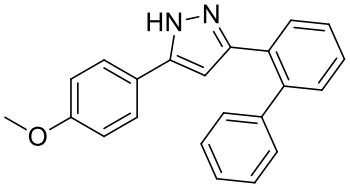

(63)

2.5.4. Pyrazole as antitumor agents

Insuasty B. *et al.* (Insuasty et al., 2010) synthesized pyrazolic analogues of chalcones and 3-aryl-4-(3-aryl-4,5-dihydro-1*H*-pyrazol-5-yl)-1-phenyl-1*H*-pyrazole showed remarkable activity mainly against leukemia (K-562 and SR), renal cancer (UO-31) and non-small cell lung cancer (HOP-92) cell lines, with the most important GI_{50} values ranging from 0.04 to 11.4 µM, from the *In-vitro* assays.

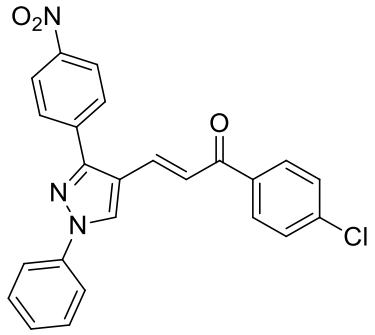

(64)

2.5.5. Pyrazole as anti malarial agents

Bekhit A. *et al.* (Bekhit et al., 2012) have investigated pyrazole derivatives for antimalarial activity. Compound **(65)** was reported to be the most active with IC_{50} of 0.033 µM when tested *In- vitro* model against chloroquine resistant (RKL9) strain of *P. falciparum.*

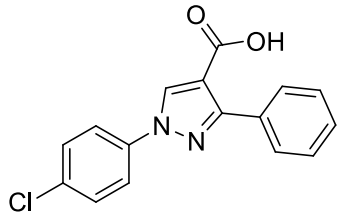

(65)

2.5.6. Pyrazole as antiviral agents

Dawood *et al.* (Dawood et al., 2015) synthesized pyrazoles with 1, 3-bisthiazole groups and investigated their antiviral profile. The most potent compound **(66)**, is a HCV inhibitor comparable to the reference drug.

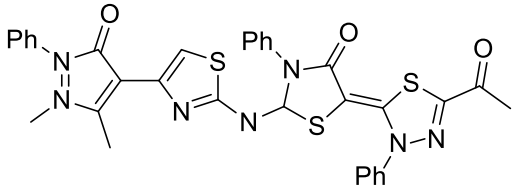

(66)

2.5.7. Pyrazole as anti-diabetic

Ines Dhouib *et al.* (Dhouib et al., 2023) synthesized 3,4-dimethylpyrano [2,3-c]pyrazol-6(2*H*)-one derivative **(67)** and evaluated against α-glucosidase. IC_{50} value is 0.1 ± 0.005 mg/mL.

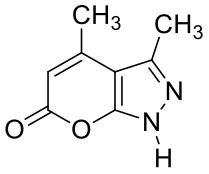

(67)

- In this study we have selected two targets, enoyl acyl carrier protein reductase (InhA) and (Decaprenylphosphoryl-beta-D-ribose 2'-epimerase (DprE1).

2.6. Anti-tubercular activity of Pyrazole

Because of its wide range of biological activity, pyrazole scaffold offers tremendous potential for medicinal chemistry and is of interest to researcher. It has been discovered that pyrazole heterocycle have interesting antitubercular activity. Taking this into account, Prafulla and his co-worker synthesized a series of fused benzimidazole with pyrazole derivatives and assessed them using the alamar blue assay for *In vitro* anti-TB activity against the *M. tuberculosis* H37Rv strain. Three compounds of this series had interesting activity. Compounds **68a**, **68b**, **68c** and **68d** were found to be the most potent MIC=6.25 µg/mL and their activity is similar to the reference drug Streptomycin (MIC=6.25 µg/ mL) (Sabale et al., 2018) .

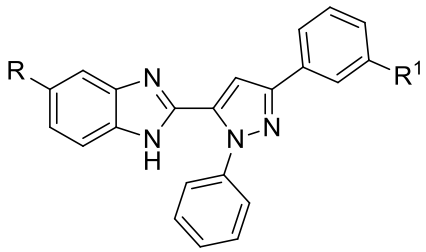

(68a-d)

Comp.	R	R^1	MIC in µg/mL
68a	$-NO_2$	-H	6.25
68b	$-NO_2$	$-OCH_3$	12.5
68c	$-CH_3$	-H	6.25
68d	$-OCH_3$	$-OCH_3$	6.25
Streptomycin			6.25

Yokokawa *et al.* have synthesized tetrahydropyrazolopyrimidine carboxamide derivative **(69)** as potent and orally active anti-tubercular agents MIC- 0.15µM (Yokokawa et al., 2013).

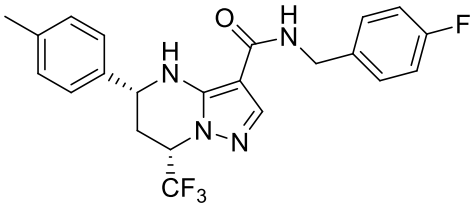

(69)

Ahsan *et al.* have synthesized novel 3-substituted-N-aryl-6,7-dimethoxy-3a,4-dihydro-3*H*-indeno[1,2-c]pyrazole-2-carboxamide analogue. MIC=0.78µg/mL (Ahsan et al., 2011).

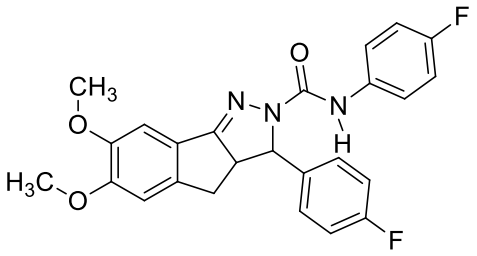

(70)

Daniele *et al.* have synthesized pyrazole derivatives and evaluated as inhibitors of *M. tuberculosis*. MIC is 4 µg/mL (Castagnolo et al., 2009).

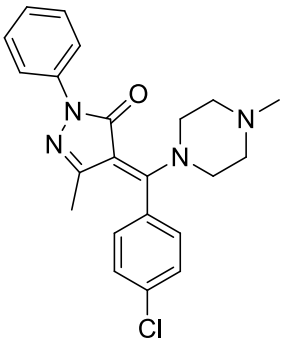

(71)

Ramiyan M. and Ramiyan V. *et al.* have reported pyrazole derivatives as anti TB agents with MIC- 0.76 µg/mL (Manikannan et al., 2010).

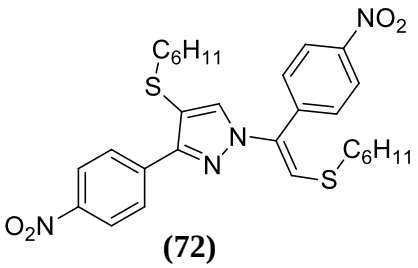

(72)

S. G. Alegaon , K. R. Alagawadi *et al.* synthesized and evaluated novel 3,5-diaryl-4,5-dihydro-1*H*-pyrazole derivatives for their *In-vitro* anti-tubercular activity against *Mycobacterium tuberculosis* H37Rv (Alegaon, Shankar G., Kallanagouda R. Alagawadi, 2014).

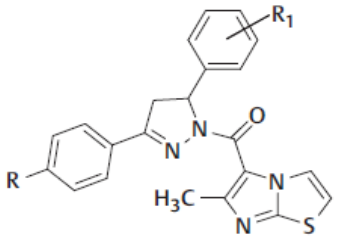

(73a-d)

Compounds	R	R_1	MIC (µg/mL)
73a	$-CH_3$	4-Chloro	0.39
73b	-Cl	2- Chloro	6.25
73c	$-CH_3$	2- Chloro	6.25
73d	-Br	2,4-Didhloro	6.25

Sameer Shaikh *et al.* synthesized new 1, 3-diphenyl pyrazole derivatives using molecular hybridization approach and evaluated for their antitubercular and cytotoxic activity (Shaikh et al., 2017).

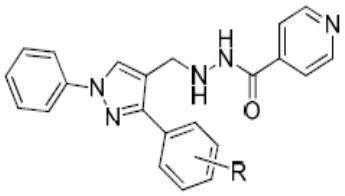

(74a-c)

Compounds	R	MIC (µM)
74a	4-F	16.06
74b	4-Br	13.91
74c	$4\text{-}OCH_3$	31.15

Prashant Aragade *et al.* synthesized series of 3-[3-(substituted phenyl)-1-isonicotinoyl-1*H*-pyrazol-5-yl]-2*H*-chromen-2-one was found to be the most active against *M. tuberculosis* (Aragade & Palkar, 2013).

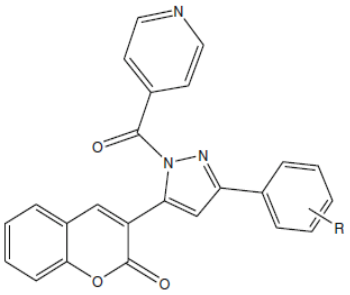

(75a-d)

Compounds	R	MIC (µg/mL)
75a	4-F	16.06
75b	4-Cl	1.25
75c	2,4- $(Cl)_2$	1.25
75d	3-NO_2	1.25

Xu z gao *et al*. reported 3-substituted-N-aryl-6,7-dimethoxy-3a,4-dihydro-3*H* indeno[1,2 c]pyrazole 2-carboxamide analogues displayed equal potency against both MTB H37Rv and INH resistant MTB, which was as active as INH (MIC: 0.78 µM) against MTB H37Rv, and 16 times more potent than INH (MIC:12.5 µM) against INH resistant MTB (Xu et al., 2017)**.**

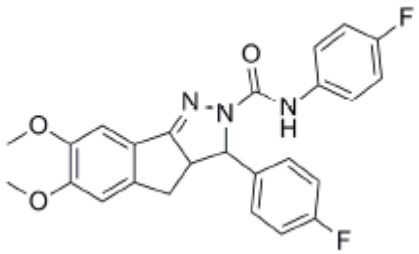

(76)

TB47, a new drug candidate targeting QcrB in the electron transport chain, has shown a unique synergistic activity with Clofazimine and forms a highly sterilizing combination (Yu et al., 2021).

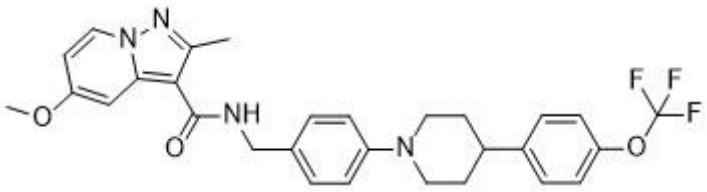

(77)

2.7. Pyrazole as enoyl acyl carrier protein reductase (InhA) inhibitor

María Martínez-Hoyos *et al.* reported GSK693 is a promising InhA direct inhibitor. Mtb MIC= 0.2 µM (Martínez-Hoyos et al., 2016).

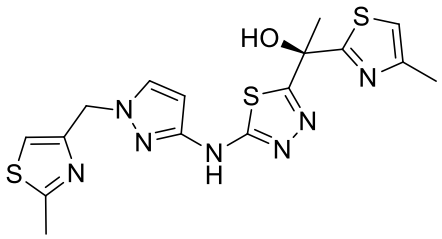

(78)

Mayur K. Vekariya *et al.* performed docking study, synthesis and evaluation of morpholinopyrimidine based pyrazole derivatives. The molecular docking studies also revealed the good interaction of the active tubercular compounds with the active site of the target enzymes InhA. MIC - 6.25 µg/mL (Vekariya et al., 2018)

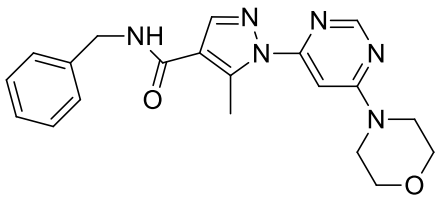

(79)

Sheshagiri R. Dixit *et al.* synthesized novel compounds 3-(4-(1*H*-pyrrol-1-yl)phenyl)-5-substituted phenyl-4,5-dihydro-1*H*-pyrazole-1-carbaldehydes as potent InhA inhibitor (Dixit et al., 2017).

.

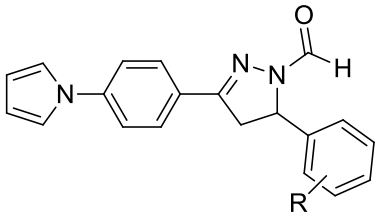

R=3-OCH_3 MIC= 6.25 µg/mL

2.4-di –OCH_3 MIC =3.125µg/mL **(80)**

Nayak N *et al*. have synthesized INH–pyrazole analogues as a potent anti-mycobacterial agents (Nayak et al., 2015).

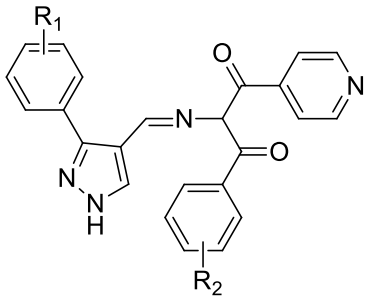

(81a-c)

Sr. No.	R_1	R_2	MIC (µg/mL)
81a	3-Cl	4-F	1.6
81b	3-Cl	4-Cl	1.6
81c	3-Cl	2-Cl	0.8

Lourdes Encinas, *et al.* reported compounds (**82a-f)** showed InhA inhibition at low concentrations combined with good activity against *M. tuberculosis* with MIC values in the range of 0.2−1 µM (Guardia et al., 2014).

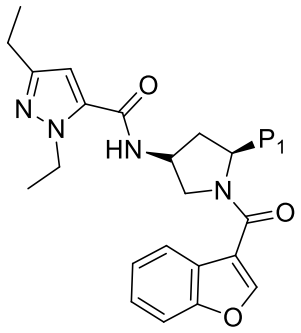

(82a-f)

Compounds	P_1
82a	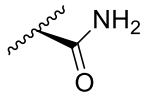
82b	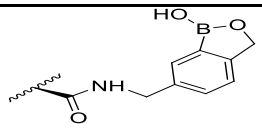
82c	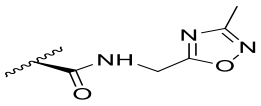
82d	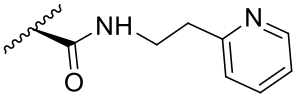
82e	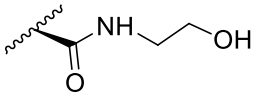
82f	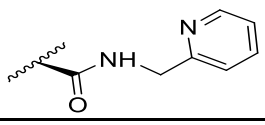

Jaimin D. Bhatt *et al.* synthesized a series of novel pyrazole linked triazolo-pyrimidine hybrids and evaluated for their anti-tuberculer activity against Mtb H37Rv strain. Some of the screened entities rendered promising antitubercular activity. MIC- 0.39 µg/mL (Bhatt et al., 2015).

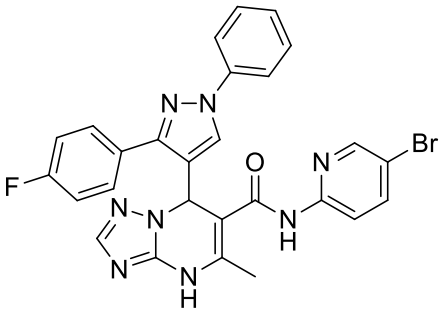

(83)

Shankar G. Alegaon *et al* synthesized series of 1, 3, 4-trisubstituted pyrazole derivatives and evaluated for their *Mycobacterium tuberculosis* (MTB) (H37Rv) inhibitory activity. Compounds **84b**, **84e** and **84f** showed most significant anti-mycobacterial activity with MIC 0.78 µg/mL(Alegaon et al., 2017).

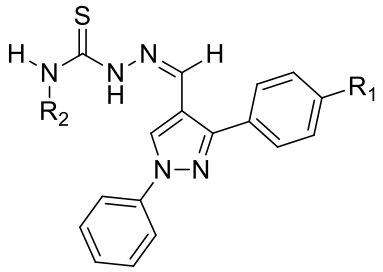

(84a-f)

Compounds	**R_1**	**R_2**
84a	-Cl	-H
84b	-Br	-H
84c	$-OCH_3$	-H
84d	-Cl	$-C_6H_5$
84e	-Br	$-C_6H_5$
84f	$-OCH_3$	$-C_6H_5$

Bachar Rébat Moulkrere *et al* synthesized and characterized Two series of heterocyclic compounds derived from 3-acetyl-4-hydroxy-6-methyl-2*H*-pyran-2-one (DHA) and 2-acetylbutyrolactone. The compounds were evaluated for their activities against *Mycobacterium tuberculosis*. MIC- 2.5 µg/mL and 5 µg/mL (Moulkrere et al., 2018).

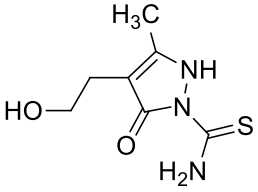

(85)

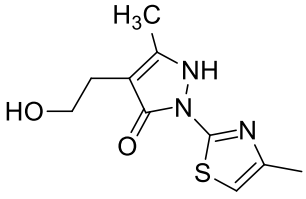

(86)

2.8. The chemical structures of novel DprE1 inhibitors under clinical development for Mtb treatment

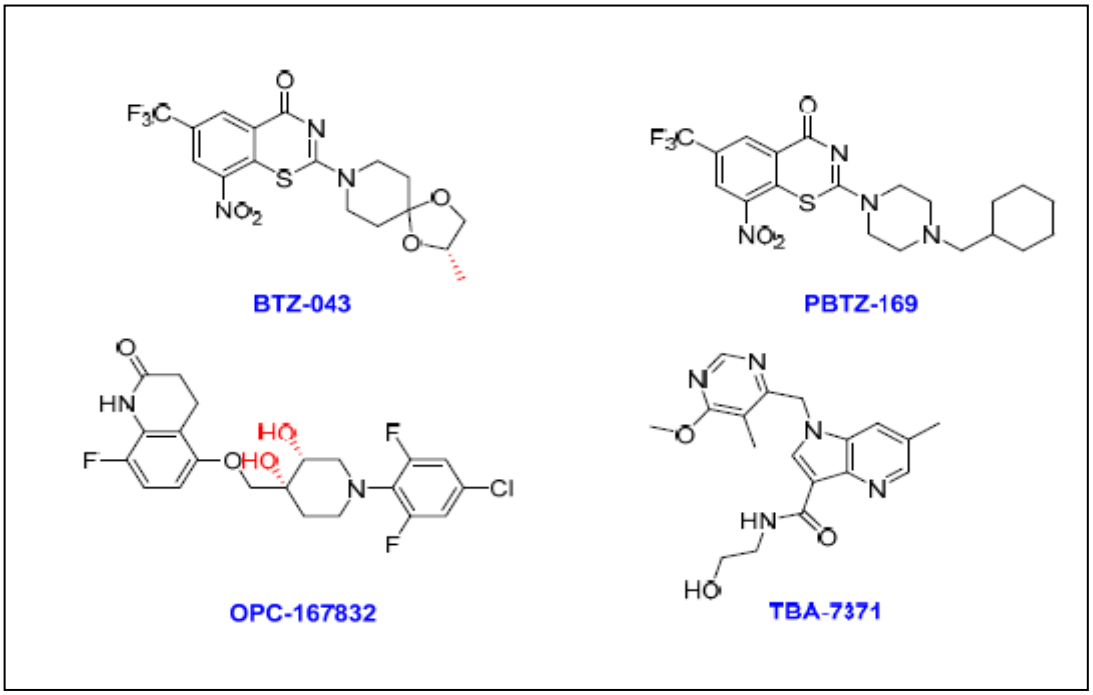

Fig.18: The chemical structures of novel DprE1 inhibitors under clinical development for Mtb treatment (Legoabe & Beteck, 2021)

2.9. Reported DprE1 inhibitors (Oh et al., 2021)

No.	Target	Scaffold	SAR plan from hit	Most advanced analogue	*In vivo* efficacy	Ref.
1.1	DprE1	4–Aminoquinolone piperidine amides	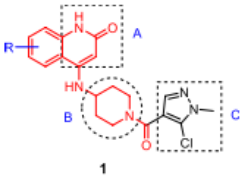 1	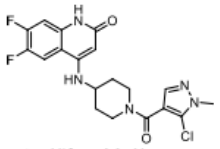 2 MIC_{80} = 0.8 μM IC_{50} = 6 nM (DprE1)	N/D[a]	(Naik et al., 2014)
1.2		Pyrazolopyridones	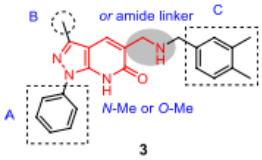 3	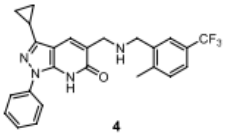 4 MIC_{80} = 0.1 μM (*Mtb*) IC_{50} = 5 nM (*Msm* DprE1)	N/D	(Panda et al., 201
1.3		2-Carboxy quinoxalines	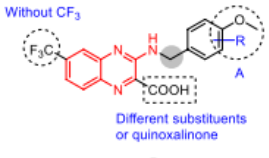 5	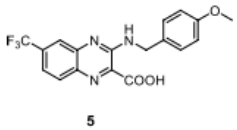 5 MIC_{99} = 3.1 μM (H37Rv) IC_{50} = 0.041 (DprE1)	N/D	(Neres et al., 2015
1.4		5-Hydroxy pyrimidinediones	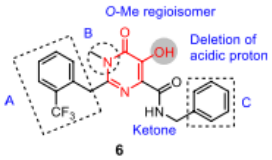 6	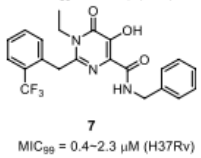 7 MIC_{99} = 0.4–2.3 μM (H37Rv)	N/D	(Oh et al., 2018)

Decaprenylphosphoryl-β-D-ribose 2′-epimerase (DprE1), a vital enzyme for cell wall synthesis, plays a crucial role in the formation of lipoarabinomannan and arabinogalactan. It was first reported as a druggable target on the basis of inhibitors discovered in high throughput screening of a drug library. Since then, inhibitors with different types of chemical scaffolds have been reported for their activity against this enzyme (Chikhale et al., 2018).

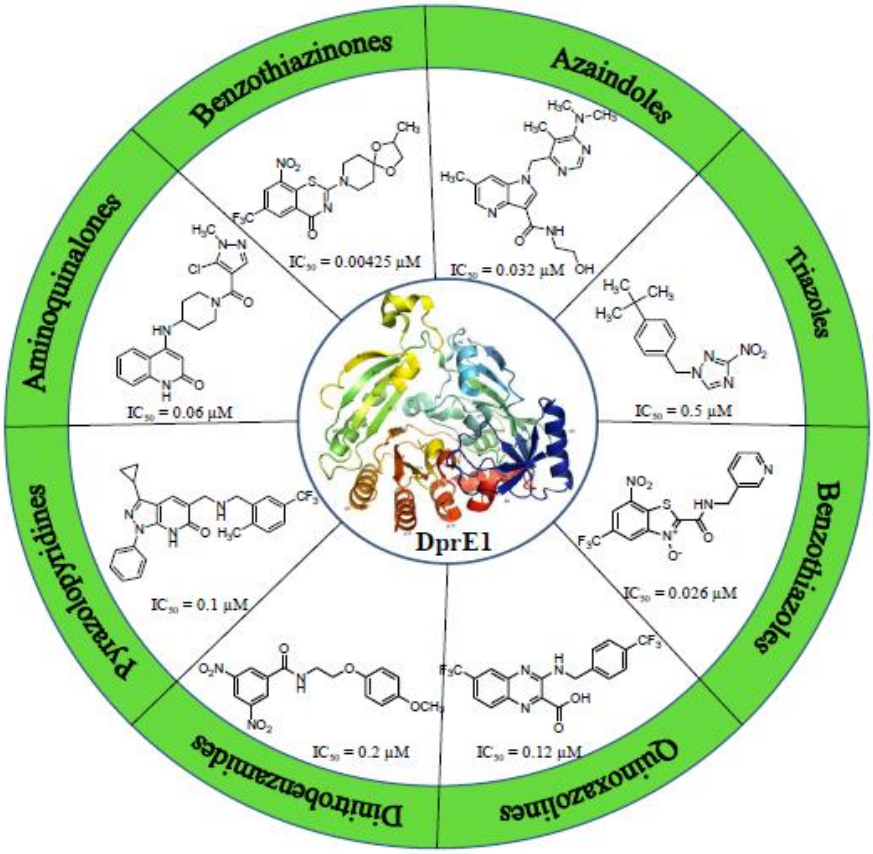

Fig.19: Various chemical scaffold have DprE1 inhibitory activity

2.10. Pyrazole as Decaprenyl phosphoryl-β-D-Ribose 2'-epimerase (DprE1) inhibitor

Panda *et al.* reported pyrazolo-pyridone class of inhibitors, active against DprE1 enzyme. Mtb MIC= 0.1µM, IC50 Msm DPrE1= 0.005 µM (Panda et al., 2014)

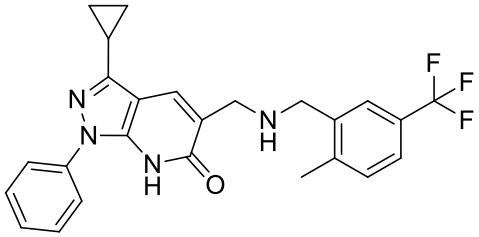

(87)

Maciej K. Rogacki *et al.* reported the discovery and profiling of a novel antimycobacterial inhibitors of the decaprenylphospho-β-D-ribofuranose 2-oxidase (DprE1). The series is characterized by enzymatic and whole-cell activity, low cytotoxicity, and physicochemical profile (Rogacki et al., 2018) DprE1 pIC50=<4.0, Mtb MIC= >125 µM.

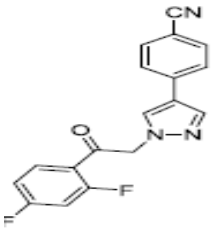

(88)

Maruti Naik *et al.* reported 4-aminoquinolone piperidine amides as a novel scaffold with potent cidality on *Mycobacterium tuberculosis* (Mtb) (Naik et al., 2014). Compounds with potent DprE1 inhibition (IC50 < 10 nM) along with potent cellular activity (MIC = 60 nM) against Mtb.

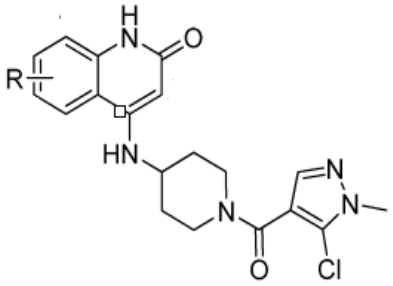

(89a-f)

Compounds	**R**	**DprE1 IC_{50} (µM)**	**Mtb MIC (µM)**
89a	6-F	0.005	1.6
89b	6,7-di-F	0.006	0.8
89c	7-F	0.007	3.1
89d	8-F	0.011	3.1
89e	7,8-di-F	0.009	1.6
89f	1-N-CH_3	0.14	25

Gautam Kumar *et al.* synthesized series of novel pyrazole–coumarin and evaluated for their antitubercular activity against the *Mycobacterium tuberculosis* H37Rv strain using the microplate alamar blue assay (G. Kumar, 2020).

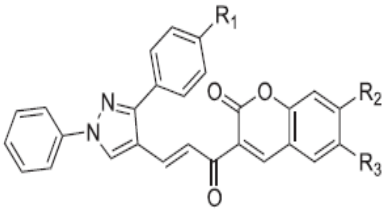

(90a-f)

Comp.	R_1	R_2	R_3	MIC µg/mL
90a	$-CH_3$	-H	-Br	6.25
90b	$-CH_3$	-H	-Cl	12.5
90c	$-CH_3$	$-OCH_3$	-H	3.125
90d	-OH	-H	-Cl	6.25
90e	-OH	$-CH_3$	-H	6.25
90f	-OH	-H	-H	3.125

Yanina V. Burgart *et al.* synthesized pyrazole derivatives which is active against DprE1. MIC is 0.36, 3.1,6.2 µg/mL (Burgart et al., 2020).

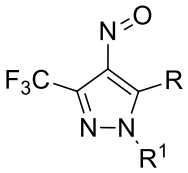

(91)

R^1=H, R=Ph (a), Thien-2-yl (b), Fur-2-yl (c), p-Tol

Lutete Peguy Khonde *et al.* reported 1,3-Diarylpyrazolyl acylsulfonamides as potent anti-tubercular agents targeting cell wall biosynthesis in *Mycobacterium tuberculosis*. MIC-4.7µM (Khonde et al., 2021).

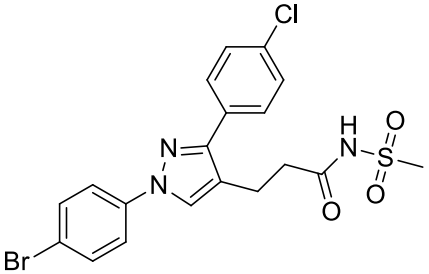

(92)

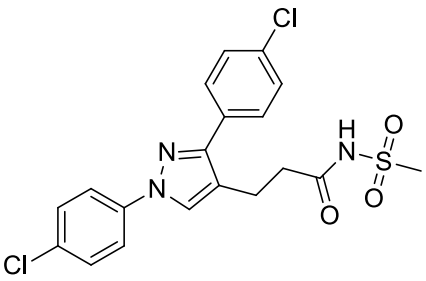

(93)

Kailash P. *et al.* synthesized series of novel pyrazole derivatives as a core nucleus clubbed with different unsaturated carbonyl group as a potent antitubercular agents (Parmar, 2015).

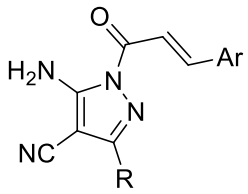

(94a-g)

Compounds	MIC µg/mL	R	Ar
94a	1	-NH-2,4-diCH_3-C_6H_4	C_6H_5
94b	3.25	-NH-3-Cl-C_6H_5	4-OCH_3-C_6H_4
94c	6.25	Piperidine	4-Cl-C_6H_4
94d	25	-NH-2,3-diCH_3-C_6H_4	C_6H_5
94e	25	-NH-4-F-C_6H_5	4-OCH_3-C_6H_5
94f	50	-NH-4-CH_3-C_6H_5	4-Cl-C_6H_5
94g	50	Piperidine	C_6H_5

K. Nayee *et al.* synthesized pyrazole derivatives and checked their antitubercular activity against H37Rv strain. Among the synthesized compounds **95a**, **95b** and **95c** showed similar activity of standard drug streptomycin with MIC 6.25µg/ mL (Nayee, 2017)

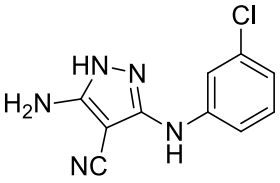

95a

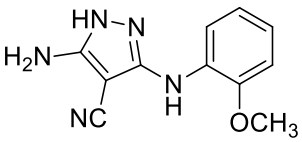

95b

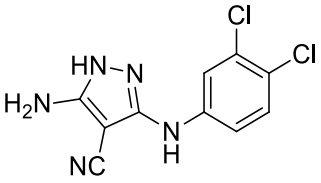

95c

2.11. Recent advances of anti-tubercular agents

Treatment for tuberculosis requires new agents with unique structures, targets, and mechanisms. **Manyi Xu *et al.*** performed phenotypic screening and identified a phenoxazinone scaffold questiomycin A **(96a)** with potent activity against *Mycobacterium tuberculosis* H_{37}Rv strain (MIC: 0.41 µg/mL) and broad-spectrum activity against drug-resistant clinical isolates (MIC: 0.16–0.31 µg/mL). Structural optimization of questiomycin A **(96a)** yielded lead **(96b)** with enhanced activity against drug-resistance MTB (MIC:

0.063–0.25 μg/mL) and good intracellular anti-mycobacterial activity. Preliminary mechanistic investigations revealed that (**96b)** disrupts mycobacterial envelope integrity by inhibiting Malonyl CoA-acyl carrier protein transacylase (encoded by FabD gene), an unexploited target in the essential mycolic acid biosynthesis pathway (Xu, 2026).

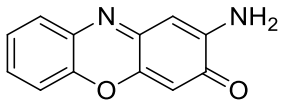

96a

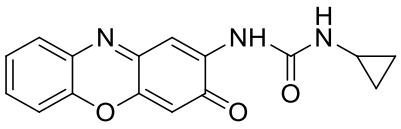

96b

Guoquan Wan *et al.* have designed and synthesized a series of novel nitroimidazole derivatives from Delemanid by introducing an aliphatic spirocyclic moiety. Most compounds demonstrated potent *In-vitro* anti-tubercular activity with negligible cytotoxicity. Compound **(97b)** exhibited superior activity against Mtb H37Ra over Delamanid (MIC values: 0.2 vs 1.0 ng/mL), and maintained robust efficacy against clinical drug-resistant strains (Wan, 2026).

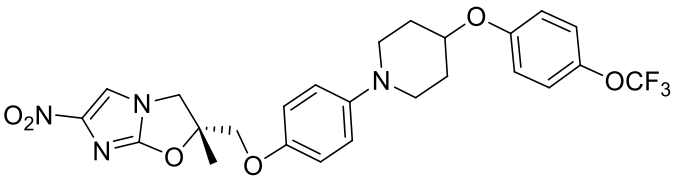

97a

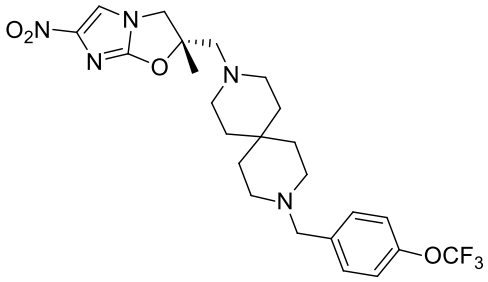

97b

Liu Yang *et al.* performed structure-based virtual screening and computationally guided design and identified a series of novel scaffold N-(1-(6-oxo-1,6-dihydropyrimidine)-pyrazole) acetamide derivatives with significant anti-mycobacterial activities. Among them, compounds **98a** and **98b** are capable of effectively suppressing the proliferation of Mtb with MIC values of 1.56 μM and 0.78 μM, comparable with isoniazid and much superior to the phase II candidate TBA-7371 (MIC = 12.5 μM) (Yang, 2024).

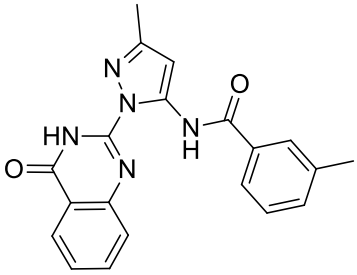

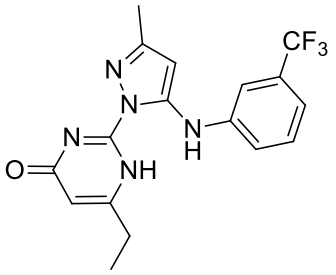

98a **98b**

Guoquan Wan *el al.* identified a novel 1,3-disubstituted pyrazole derivative, compounds **99a** and **99b**, which exhibited improved anti-tubercular activity, with MIC values of 5.34 and 5.04 μg/mL against H37Ra, respectively. Additionally, compounds **99a** and **99b** exhibited favourable safety profiles, showing no obvious toxicity to Vero, A549, and HepG2 cell lines (Wan G. G., 2025).

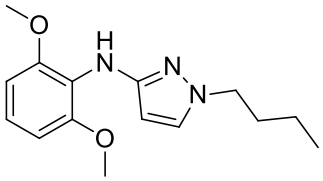

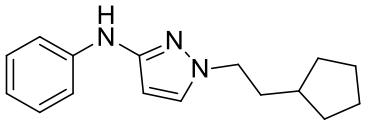

99a **99b**

Reham A. *et al.* designed, synthesized and evaluated pyrazole-linked benzothiazole hybrids compounds **100a, 100b,100c, 100d** and **100e** displayed promising anti-TB activity in comparison to the reference compound Isoniazid against the drug sensitive strain with (MIC: 1.74–3.68 μM/mL). Compounds **100a**, **100d** and **100e** showed strong inhibition of InhA in comparison to the reference compound, triclosan, with IC50 values of 6.4–7.9 μM (Mohamed-Ezzat, 2024).

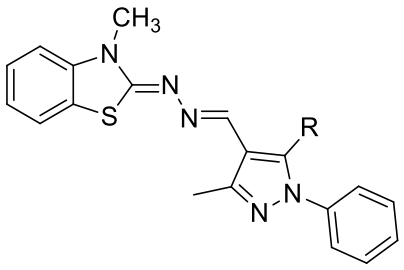

R	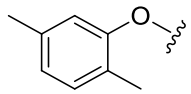	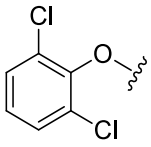	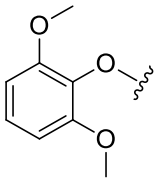	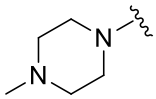	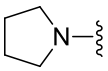	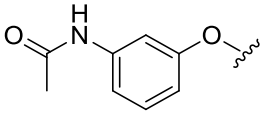
	100a	**100b**	**100c**	**100d**	**100e**	**100d**

Marwa M Shaaban *et al.* synthesized series of 3-(p-chlorophenyl)-1-phenylpyrazole derivatives tethered to substituted ureas and evaluated against *Mycobacterium tuberculosis* virulent cell line H37Rv, and assessed for their InhA inhibitory activities. The urea derivatives **101a** and **101b** exhibited the most promising anti-tubercular activity (MIC = 6.25 µg/mL) surpassing triclosan (MIC-20 µg/mL) with potential InhA inhibition (Shaaban, 2024).

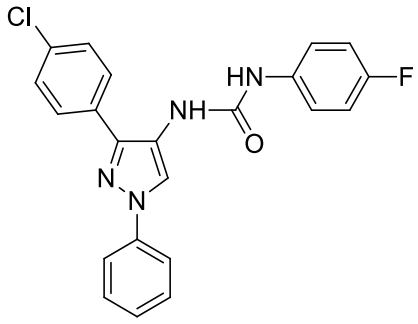

101a

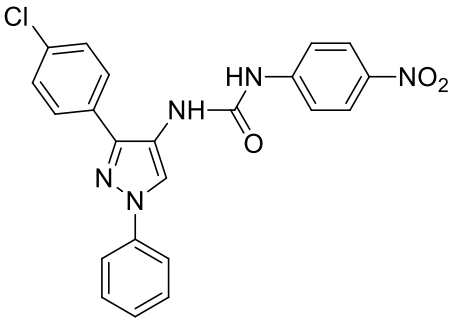

101b

CHAPTER-3

AIM OF WORK

CHAPTER- 3

3. AIM OF PRESENT WORK

Today the difficulties faced in managing TB are due to

1. The long duration treatment regimens.
2. The emergence of drug resistant Mtb strains.
3. Co-infection with HIV/AIDS.

Emergence of multi-drug resistant tuberculosis (MDR) and extensive drug resistant tuberculosis (XDR) have made controlling of this infectious disease more complicated and challenging. Research on the topic highlights the significance of enzymes participating in the biosynthesis of mycobacterial cell walls as promising targets for drug development against tuberculosis. InhA, and DprE1 enzymes are crucial in the production of mycolic acid, has surfaced as a valuable target for combating the proliferation of all mycobacterial species. Its suppression by various scaffolds highlights its promise as a central target for creating new anti-TB medications. Different scaffolds have been investigated for their effectiveness against InhA and DprE1 activity.

The azole groups containing heterocyclic compounds possess significant pharmacokinetic property, lipophilicity that influence the ability of drug to reach the target by trans-membrane diffusion and show promising activity against resistant TB by inhibiting the biosynthesis of Fatty acid. Pyrazole derivatives possesses a wide spectrum of activities including anticancer, anti-inflammatory, antimicrobial, antiviral and anti-tubercular. These observations gave motivation to search for potential pharmacologically active leads carrying pyrazole substituents. Pyrazole derivatives have been reported to inhibit the enoyl ACP reductase and Decaprenylphosphoryl-β-D-ribose 2′-epimerase(DprE1) which is the key enzyme responsible for the cell wall of mycobacteria.

Enoyl ACP reductase (inhA) responsible for the mycolic acid biosynthesis and Decaprenylphosphoryl-β-D-ribose 2′-epimerase (DprE1) responsible for the preparation of arabinogalactan, both are essential components in cell wall of mycobacteria. The *M. tuberculosis* cell wall has an intricate and unique structure composed of a thick peptidoglycan layer and an outer membrane made up mostly of various lipopolysaccharides and fatty acids with imbedded glycolipids and wax esters. Most of the anti-tubercular drugs are unable to cross cell wall due to thick layer of

mycolic acid. It is plan to synthesize pyrazole derivatives using molecular docking study. In 2017 at L.M. College of Pharmacy laboratory various pyrazole derivatives were synthesized after docking study. Higher docking score compounds were synthesized and checked their anti-tubercular activities by micro plate alamar blue assay (MABA) using H37Rv strain. Total 7 compounds (LMKN-1 to LMKN-7) were synthesized and evaluated their potency against *Mycobacterium tuberculosis* H37Rv strain. The standard drugs are Ciprofloxacin(MIC of 3.12 µg/ mL), Pyrazinamide (3.12 µg/ mL) and Streptomycin(6.25 µg/ mL). Potency of LMKN-4, LMKN-6 and LMKN-7 found to be similar with streptomycin.

In extention above one we have synthesized pyrazole derivatives which are inhibitors of Enoyl ACP Reductase (InhA) and Decaprenyl phosphoryl-β-D-Ribose 2'-epimerase (DprE1). All the synthesized compounds have been evaluated by micro plate Alamar Blue assay (MABA) using H37Rv strain.

Objective:

- To evaluate the suitability of the designed compounds as anti-TB agents by performing molecular modeling studies by assessing their binding affinity to the target protein, and check the stability of the enzyme-ligand complexes by performing molecular dynamics studies.

- To assess the suitability of the designed compounds as potential drug-like agents by theoretically evaluating their physico-chemical and pharmacokinetic parameters using SWISS ADME and pkCSM software.

- To synthesize the designed compounds and characterize them using spectral techniques

- To biologically evaluate the synthesized compounds for InhA and DprE1enzyme inhibitory and anti-TB activities.

Work plan of proposed research project work:-

1. Identification of target inhibitors: various pyrazole containg compounds were identified by literature which are inhibitor of InhA and DprE1.
2. Structure based molecular docking approach to identify critical feature based on ligand-protein interaction using co-crystal structures of enoyl acyl carrier protein reductase (InhA) and Decaprenylphosphoryl-β-D-ribose 2'-epimerase (DprE1).
4. Synthesis of designed molecules.
5. Characterization of synthesized compounds by physical characteristic like melting point and spectral characteristics like IR, MASS, ^{1}H NMR and ^{13}C NMR.
6. Pharmacological evaluation of synthesized compounds.
7. Checked drug likeness properties.
8. Performed molecular dynamic simulation for the ligand stability.

CHAPTER-4

RESULTS AND DISCUSSION

CHAPTER-4

4. RESULTS AND DISCUSSION

4.1. Designing strategy of enoyl acyl carrier protein reductase inhibitor (InhA)

To improve anti-tubercular activity, an efficient synthetic protocol for the pyrazole moiety has been established. Fig. 20 depicts commercially accessible anti-tubercular drugs with pyrazole and 1, 3, 4-oxadiazole motifs. The structure activity relationship (SAR) of various pharmacophore was taken into account in the design of targeted compounds **(6a-o);** Fig. 20). Modification in the side chain of the Isoniazid and Pyrazinamid drug by altering the amide functional group with substituted acid chloride functional group and introducing the five-member heterocyclic ring into the standard drug Isoniazid and Pyrazinamid, novel scaffolds **(6a-o)** were designed, synthesized and evaluated for the *In-vitro* antitubercular activity.

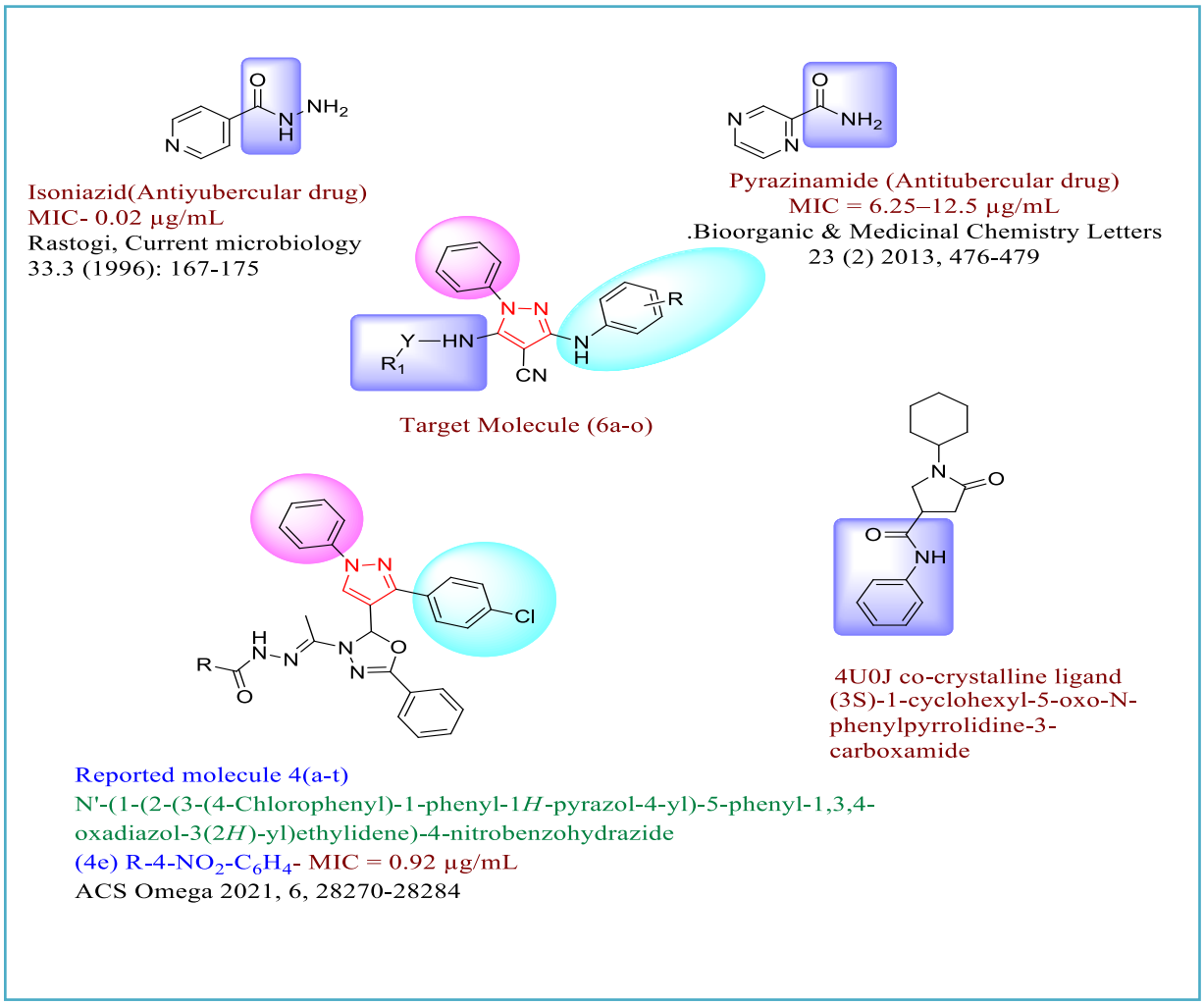

Fig.20: Design concept of InhA inhibitors (6a-o)

4.2. Designing strategy of Decaprenylphosphoryl-β-D-ribose 2'-epimerase (DprE1)

The Design Concept is based on PBTZ169 (Macozinone) and reported molecules. We have designed pyrazolo-pyrimidine derivatives. Phenyl-substituted pyrazole and hydroxyl pyrimidine nucleus were placed in region-1, while in the second region, amino group is introduced.

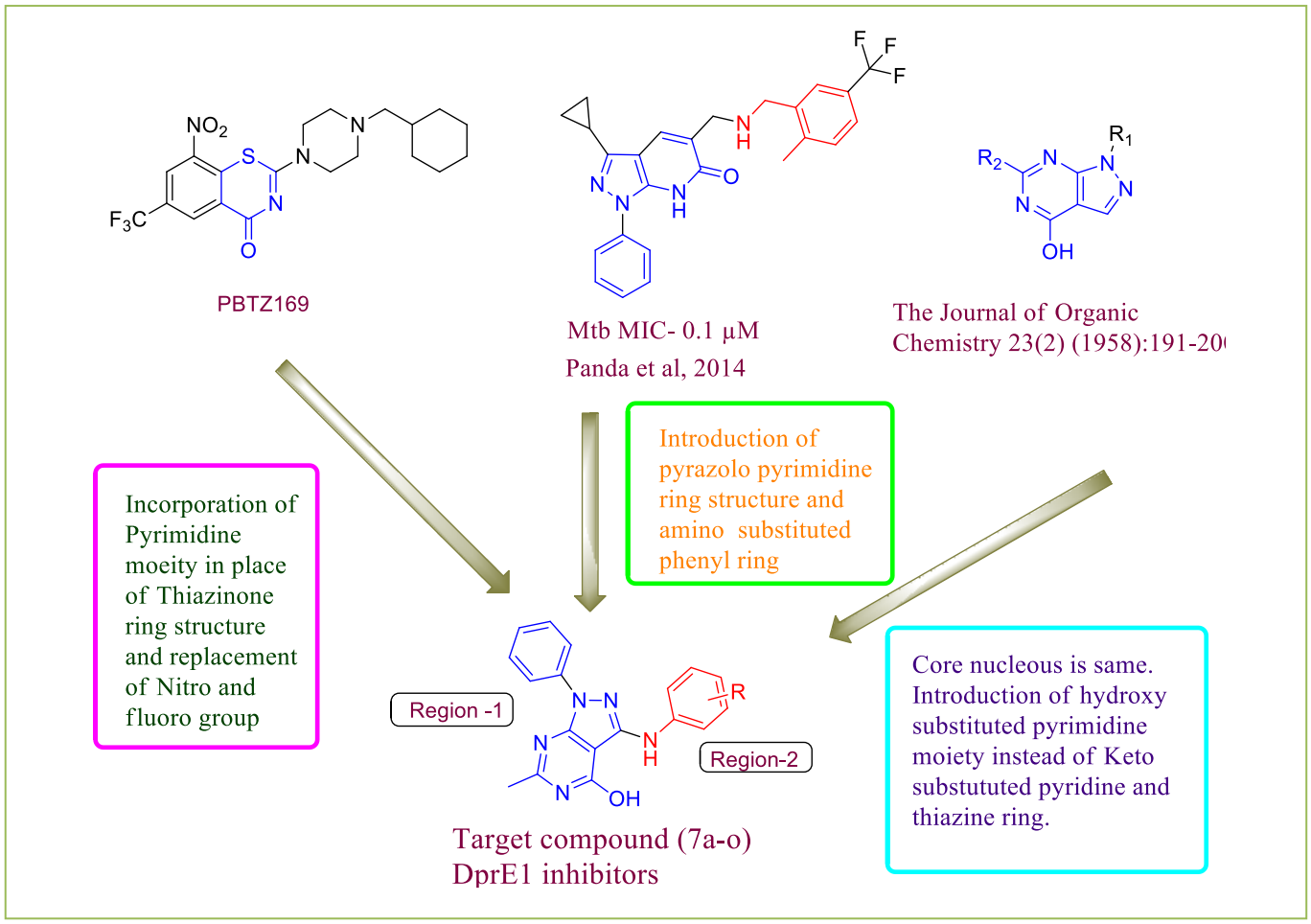

Fig.21: Design concept of DprE1 inhobitors (7a-o)

4.3. Docking

Molecular docking was employed to predict the binding interactions of molecules to the active site residues of the target enzyme. Molecular docking studies help researchers to identify the best match between ligands and proteins with the least amount of energy.

Structure Preparation for docking:

Enoyl ACP reductase (InhA)

- Crystal structure of 4U0J with bound inhibitor having resolution 1.62 Å were retrieved from Protein Data Bank.

Decaprenylphosphoryl-β-D-ribose 2′-epimerase (DprE1)

- Crystal structure of 4NCR with bound inhibitor having resolution 1.88 Å were retrieved from Protein Data Bank.

Molecular docking was executed by using Autodock Vina and Autodock tools 1.5.6 programs (Olson, 2009). BIOVIA Discovery Studio 2021 was employed to examine the 2D and 3D interactions of the ligand–receptor complex (Warude et al., 2023). Chem Office tool (ChemDraw 12.0) was used to draw the structures of the compounds with proper 2D orientation. Maximum of nine conformers were considered for each ligand during the docking process.

Enoyl acyl carrier protein reductase (InhA)

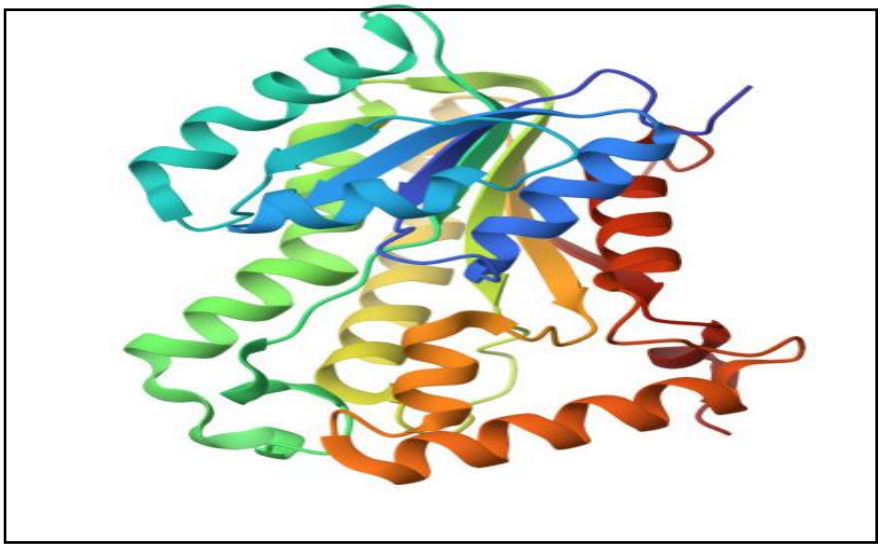

Fig.22 Crystal structure of 4U0J

Enoyl acyl carrier protein reductase (InhA) is a key enzyme involved in fatty acid synthesis, mainly mycolic acid (Fekadu et al., 2022). The molecular docking study of the synthesized compounds were carried out to evaluate their binding interactions against enoyl acyl carrier protein reductase (InhA) and compared with standard drugs Isoniazid and co-crystalline structure (3S)-1-Cyclohexyl-5-oxo-N-phenylpyrrolidine-3-carboxamide. In Table-3 summarized the binding affinities of the synthesized compounds along with their hydrogen bonding and amino acid interactions against enoyl acyl carrier protein reductase. The confirmation with lowest binding energy was displayed as the best binding energy. It has been shown that an amino acid can form different bonds with different parts of the ligand. Conventional hydrogen bond, van der Waals, carbon-hydrogen bond, pi-sigma, pi-alkyl, pi-pi stacked bonds were observed. Docking score of the synthesized compounds were found to have ranging from -8.0 to -10.2(kcal/mol) (Table -3). Among the docked ligands, compound **6e**, **6f**, **6g**, **6h**, **6i**, **6j**, **6k**, **6l** and **6m** reported lowest binding energy. The best results were obtained by compound **6e** (-10.1 kcal/mol), **6f** (-9.5 kcal/mol), **6g** (-9.1 kcal/mol), **6h** (-10.2 kcal/mol), **6i** (-9.9 kcal/mol), **6j** (-9.5 kcal/mol), **6k** (-9.7 kcal/mol), **6l** (-9.2 kcal/mol) and **6m** (-9.0 kcal/mol). All the compounds have higher binding affinity than standard drug Isoniazid (-5.8 kcal/mol) and co-crystalline ligand 4U0J(-8.6 kcal/mol).

The most potent compounds **6g, 6h, 6i, 6j** and **6m** which possess -9.1, -10.2, -9.9, 9.5 and -9.0 docking scores respectively. Compared to standard drug Isoniazid and co-crystalline ligand 4U0J, the most active compounds **6g, 6h, 6i, 6j and 6m** showed similar interactions with amino acid residues Gly-14, Ile122, Leu63,Asp64, Phe41, Val65, Ile95, Gly96, Ile21, Gly14, Ile16, Thr196, Leu63, Asp64, Sere94, Ser20, Phe97, Phe41, Val65 and Met147. The most active molecule **6m** showed two conventional hydrogen bonding interactions with Gly96 and Lys165 residues, Van der waals interaction with Ser20, Tyr158, Ser94, Met161, Met147, Ile194, Gly192, Ala191, Asp148 and Ile95, a pi-sigma and pi-alkyl interactions with Thr196, Leu218, Met 199, Ile21 and Pro193 residue and pi-pi stacked interactions with Phe149(Fig. 25**).** The compound **6i** Showed conventional hydrogen bonding interaction with Gly96, Lys165, Van der waals interactions with Ser20, Ser94, Ile95, Met147, Asp148, Ile215, Ile194, Ala191, Gly192 and other interaction(pi-alkyl,pi-pi stacked, pi-sigma) with Phe149, Ile21, Met161, Tyr158, Leu218, Met199, Pro193, Thr196 amino acid residues(Fig.24). The amino (-NH) group of the compound **6h** affords one conventional hydrogen bonding interactions with Gly14 and van der waals interactions with Lys118, Ile122, Leu63, Asp64, Ser94, Thr196, Ser20, Ile15, Gly96. The phenyl ring bound to the

nitrogen provides a pi-alkyl interaction with the Val65, Ile95, Ile16 and Pi-pi stacked interaction with Phe41, and Phe97 residues(Fig.23). In the case of co-crystalline ligand 4U0J, there are numerous types and numbers of interactions(Fig.26). Van der waals interactions with Met147, Thr196, Asp64, Leu63, Ser94, Ser20, Gly14, Ile16 and Phe97. One conventional hydrogen bond interactions with Gly96 residues, four pi-alkyl interactions with Ile21, Ile122, Val65 and Ile95 residues, a pi-pi stacked interaction with Phe41 residue. The hydrogen bond interaction and the van der Waals interactions give the compounds pharmacological importance, as hydrogen bonds strongly affect the pharmacological action of ligands. Isoniazid, which is used as a reference drug. It was also docked into the active pocket of the studied receptor, and its result is presented in Fig.27. In fact, Isoniazid affords three van der waals interactions with Asp64, Ser13 and Gly40. Three conventional hydrogen bond interactions with Leu63, Thr39, and Gly14 residues, three pi-alky interactions with Ile95, Val65 and Ile122 residues. One pi-stacked interaction with Phe41 residue. In conclusion, the most active compounds **6m, 6i, 6g**, **6h, 6j** have good binding energy than Isoniazid and co-crystalline ligand.

Table-3: Binding affinity and amino acid interactions of the compounds **(6a-o)** with 4U0J receptor.

Comp.	**Structure**	**Binding affinity (Kcal/mol)** **(Docking score)**	**Amino acid interactions**
6a	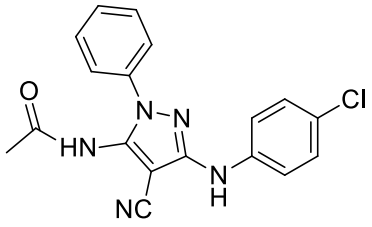	-8.5	Hydrogen bond interactions: Gly96, Tyr158, Ile95, Lys165,Gly14, Ser94,Ile16 Vander walls interactions: Val65, Phe97 Other Interactions: Met161, Phe41, Ile122

6b	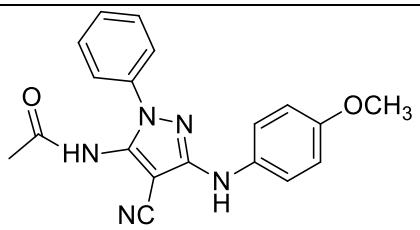	-8.4	Hydrogen bond interactions: Gly96, Val65, Phe97, Ile95, Ser94, Ile16 Vander walls interactions: Tyr158, Gly14, Phe97 Other Interactions: Met161, Ile122, Phe41
6c	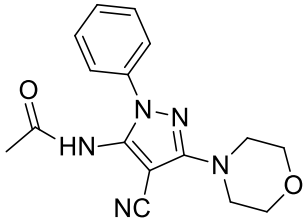	-8.0	Hydrogen bond interactions: Ser94,Gly96, Gly14, Ile95 Vander walls interactions: Ile21, Ala22, Ser20, Ile16, Phe97,Val65 Other Interactions: Ile122, Phe41
6d	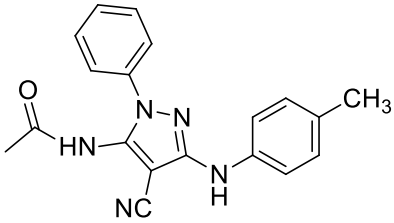	-8.6	Hydrogen bond interactions: Thr196,Met147, Ser94,Ile194, Asp148,Ala191, Gly192, Lys165 Vander walls interactions: Ser20, Gly96, Ile95 Other Interactions: Pro193, Tyr158, Met199, Ile21, Phe149

6e	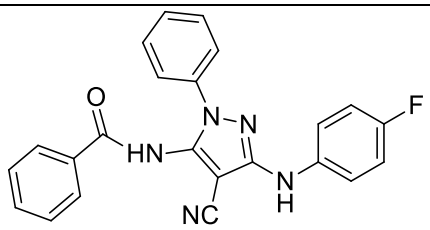	-10.1	Hydrogen bond interactions: Thr17, Gly96, Ser20, Ile95 Vander walls interactions: Leu197, Thr196, Ser94, Phe97, Asp64, Leu63 Other interactions: Ile16, Ile122, Val65, Phe41, Ala198, Ser19
6f	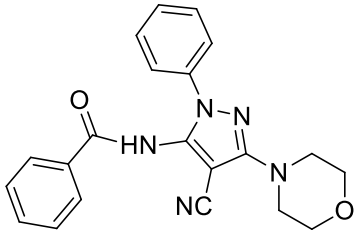	-9.5	Hydrogen bond interactions: Gly96, Thr196, Ile95 Vander walls interactions: Ser20, Ala198, Ser94, Phe97, Asp42, Asp64 Other interactions: Phe41, Ile16, Val65, Ile122
6g	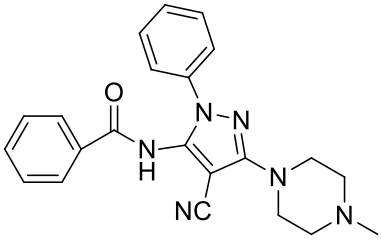	-9.1	Hydrogen bond interactions: Tyr158, Gly96 Vander walls interactions: Leu218, Pro193, Ile194, Gly192, Ile21, Asp148, Gly14, Ile16, Ala198, Thr196, Ile202 Other interactions: Phe149, Ile215, Ala191, Met199

6h	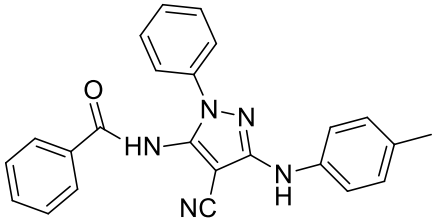	-10.2	Hydrogen bond interactions: Gly14 Vander walls interactions: Lys118, Ile122, Leu63, Asp64, Ser94, Thr196, Ser20, Ile15, Gly96 Other interactions: Phe97, Phe41, Val65, Ile95, Ile16
6i	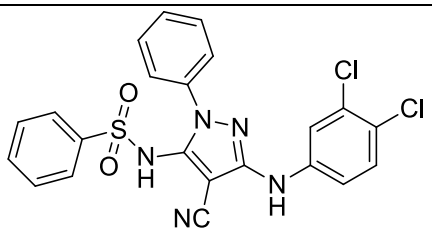	-.9.9	Hydrogen bond interactions: Gly96, Lys165 Vander walls interactions: Ser20, Ser94, Ile95, Met147, Asp148, Ile215, Ile194, Ala191, Gly192 Other interactions : Phe149, Ile21, Met161, Tyr158, Leu218, Met199, Pro193, Thr196
6j	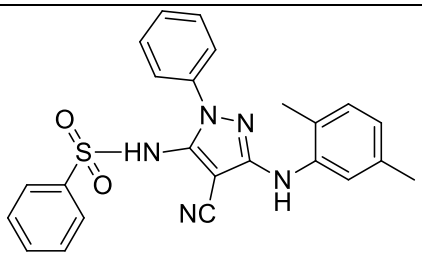	-9.5	Hydrogen bond interactions: Ser94, Lys165 Vander walls interactions: Pro193, Ile194, Gly192, Asp148, Met147, Ile21, Ser20, Ile16, Thr196, Gly96 Other interactions: Phe149, Tyr158, Ala198, Met199

6k	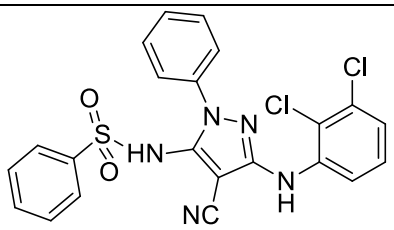	-9.7	Hydrogen bond interactions: Gly96, Thr196, Ile95 Vander walls interactions: Met199, Ser20, Ser94, Gly14, Asp64, Phe97 Other interactions: Phe41, Ile21, Ile16, Ala198, Val65, Ile122
6l	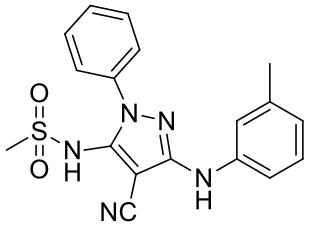	-9.2	Hydrogen bond interactions: Gly96, Lys196 Vander walls interactions: Ser20, Tyr158, Ser94, Met161, Met147, Ile95, Gly192, Asp148, Ala191, Ile194, Leu218 Other interactions: Phe149, Pro193, Met199, Ile21, Thr196
6m	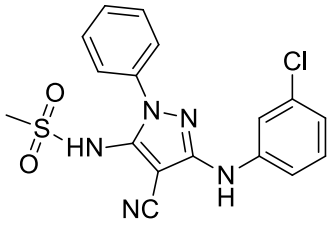	-9.0	Hydrogen bond interactions: Lys165, Gly96 Vander walls interactions: Ser20, Tyr158, Ser94, Met161,Met147, Ile194, Gly192, Ala191, Asp148, Ile95, Other interactions: Phe149, Leu218, Met199, Ile21, Pro193, Thr196

6n	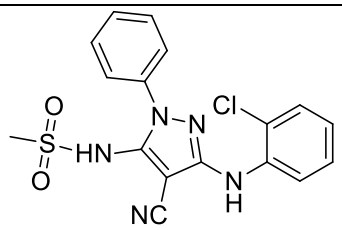	-8.7	Hydrogen bond interactions: Lys165, Gly96 Vander walls interactions: Tyr158,Ser20, Ser94, Met161,Met147, Pro193, Ile194, Ala191, Gly192, Asp148,Ile95 Other interactions: Phe149, Met199, Ile21, Thr196
6o	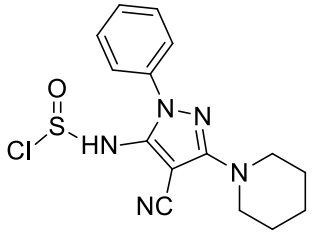	-8.0	Hydrogen bond interactions: Lys165 Vander walls interactions: Ser20, Ser94, Gly96, Met147, Ile95, Asp148, Tyr158, Pro193, Ile194 Other interactions: Phe149,Met199, Ile21, Thr196
4U0J Co-crystalline ligand	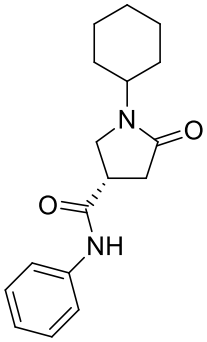	-8.6	Hydrogen bond interactions: Gly96 Vander walls interactions: Met147, Thr196, Asp64, Leu63, Ser94, Ser20, Gly14, Ile16, Phe97 Other interactions: Phe41, Ile21, Val65, Ile95, Ile122
Isoniazid	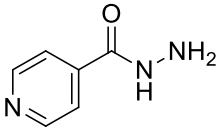	-5.8	Hydrogen bond interactions: Leu63, Thr39, Gly14

			Vander walls interactions: Asp64, Ser13, Gly40 Other interactions: Phe41, Ile95, Val65, Ile122

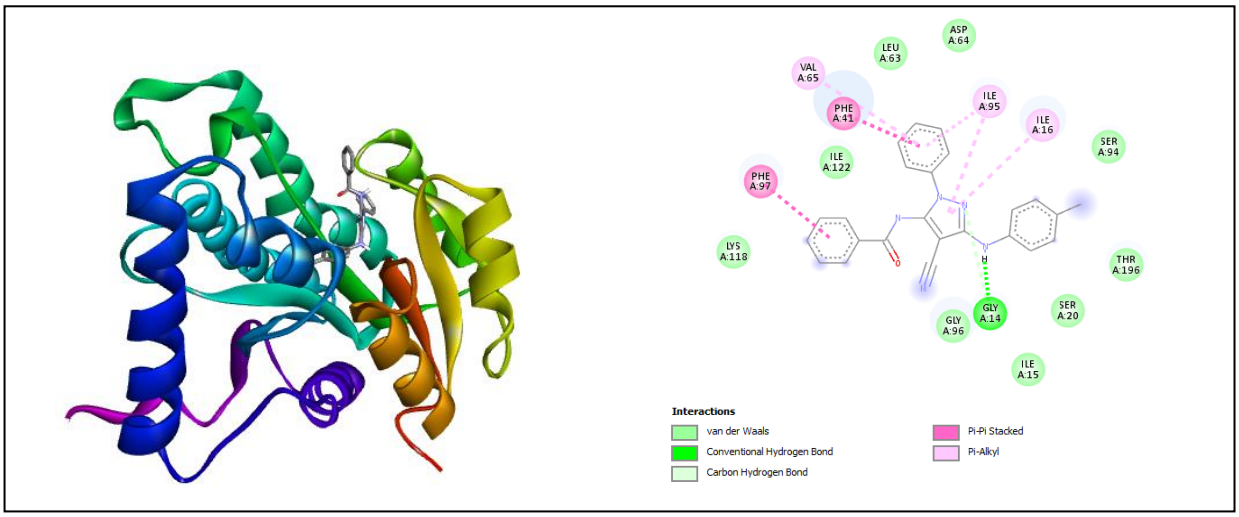

Fig.23**:**3D and 2D structure of the interaction of compound (**6h**) with protein (PDB ID-4U0J)

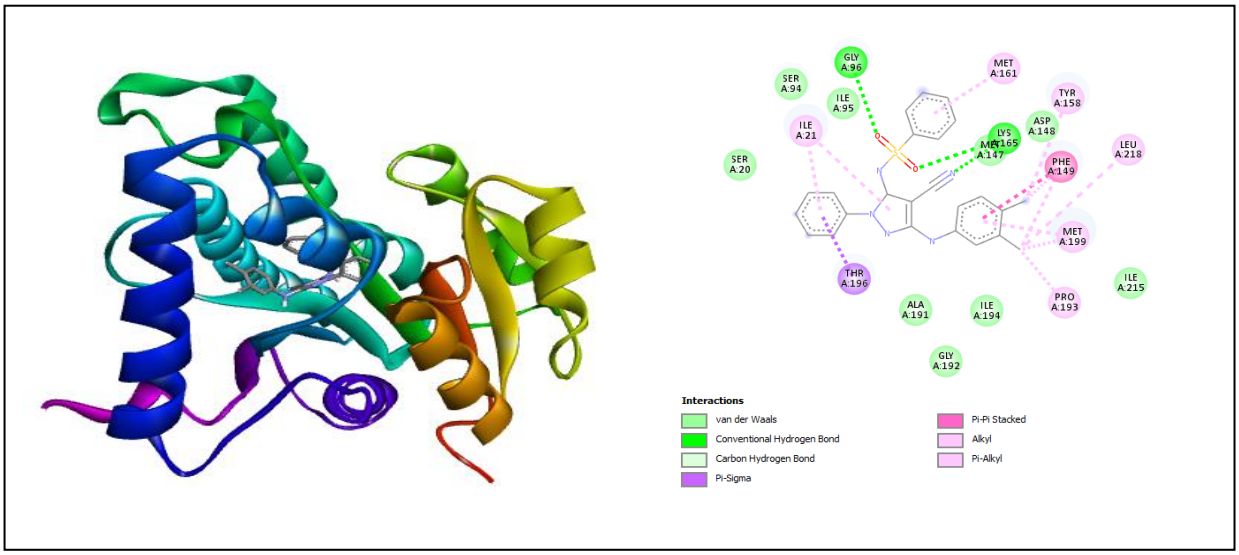

Fig.24: 3D and 2D structure of the interaction of compound (**6i**) with protein (PDB ID -4U0J)

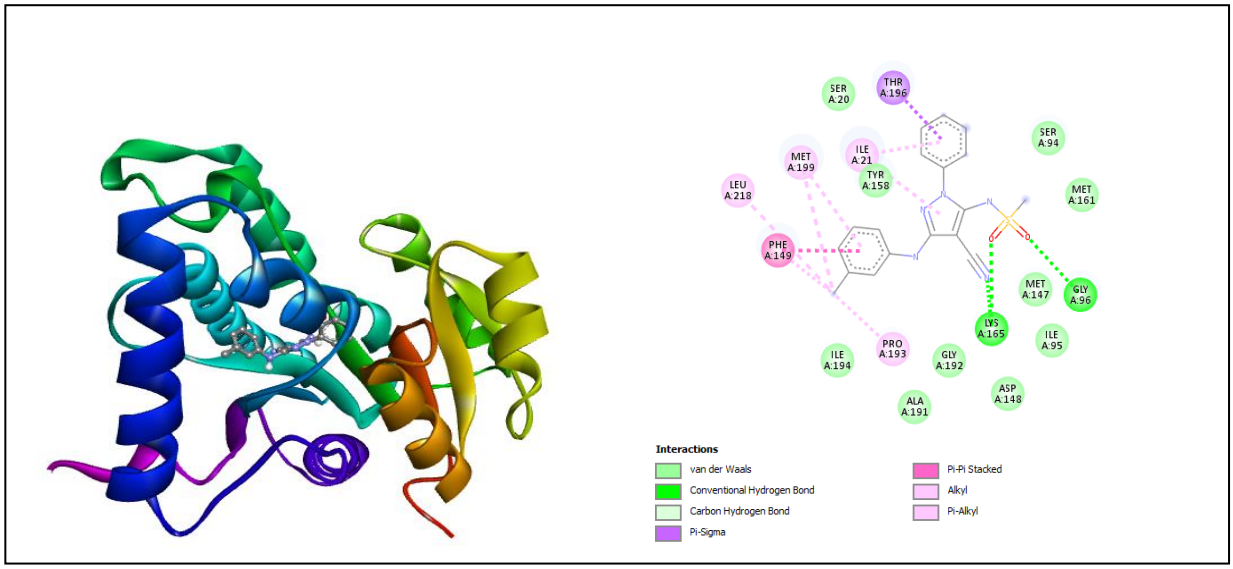

Fig.25:3D and 2D structure of the interaction of compound (**6m**) with protein (PDB ID-4U0J)

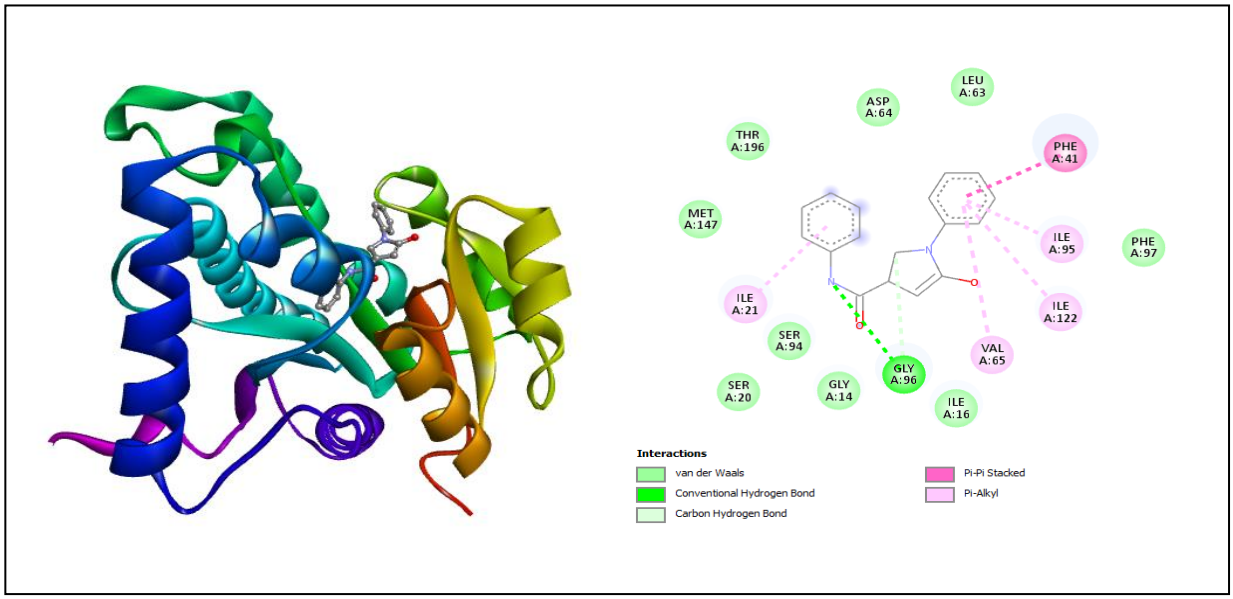

Fig.26: Docking image of Co-crystalline ligand with protein 4U0J

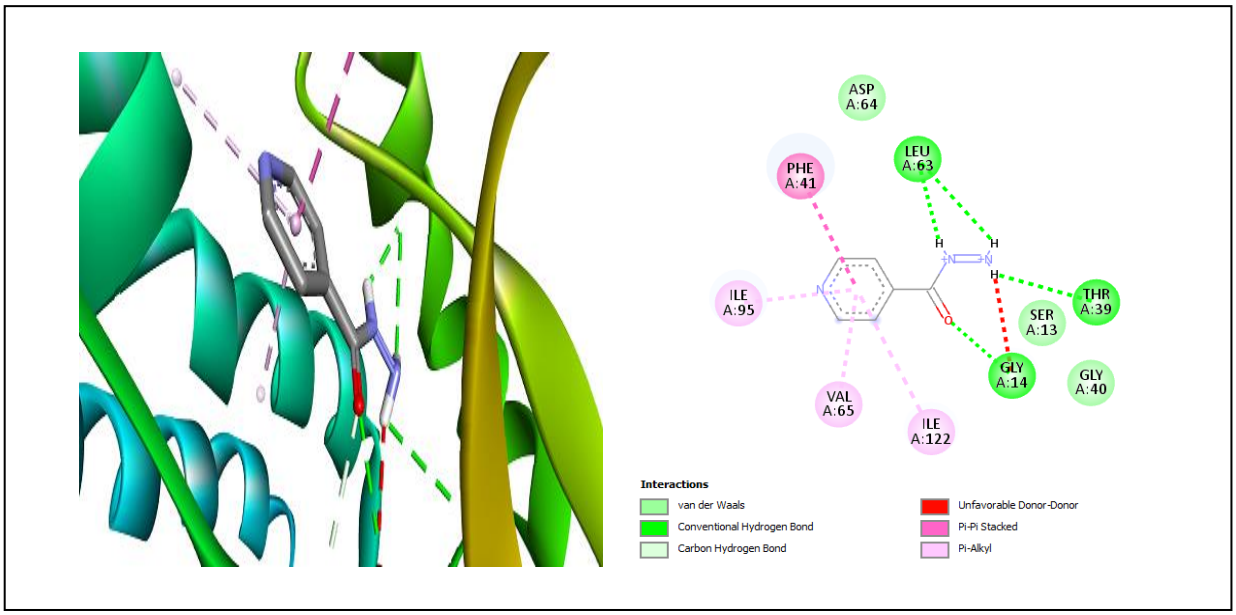

Fig.27: Docking Image of Isoniazid with protein 4U0J

Decaprenylphosphoryl-β-d-ribose 2′-Epimerase 1 (DprE1) inhibitors

DprE1 crystal structure was obtained from the Protein Data Bank (RSCB) using the PDB ID code 4NCR.

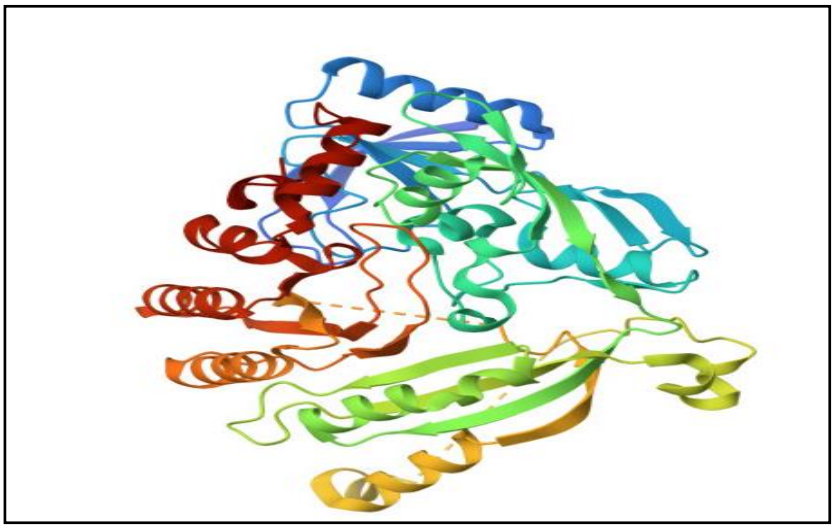

Fig.28: Crystal structure of 4NCR

The binding interactions of the DprE1 protein and synthesized compounds **(7a-o)** were determined and compared with the reference drug Isoniazid and co-crystalline ligand 2-(4-

(cyclohexylmethyl)piperazin-1-yl)-8-nitro-6-(trifluoromethyl)-4*H*-benzo[e][1,3]thiazin-4-one. Table-4 represents the docking results of the synthesized compounds **(7a-o)**.

Docking analysis, various bonding interactions with amino acid residues were observed, e.g., conventional hydrogen bonds, van der Waals, carbon-hydrogen, pi-sigma, pi-alkyl, and pi-pi stacked. The docking score (binding affinity) of the compounds **(7a-o)** exhibited a range of -7.4 to -8.6 (kcal/mol), as shown in Table-4. Compounds **7a**, **7b**, **7d**, **7e**, **7g**, **7h**, **7i**, **7j**, **7k**, and **7n** exhibited the lowest binding affinity. The compounds that showed good results were **7d** (-8.3 kcal/mol), **7g** (-8.5 kcal/mol), **7h** (-8.6 kcal/mol), **7i** (-8.4 kcal/mol), **7j** (-8.3 kcal/mol), and **7n** (-8.3 kcal/mol).

Anti-tubercular potent compounds **7e**, **7g**, **7j**, and **7k** have docking scores of -8.2, -8.5, -8.3, and -8.2, respectively. In comparison to the co-crystalline ligand 4NCR, the potent compounds **7e**, **7g**, **7j**, and **7k** exhibited similar interactions with the amino acid residues Phe267, Gln100, Leu265, Lys103, Glu263, Lys266, Leu106, and Pro107. Two conventional hydrogen bonding interactions of the most potent compound **7g** were found with amino acid residues Phe267 and Leu265, Van der Waals interactions with Leu106, Lys266, Gln100, Asp99, Glu263, Phe267, Leu265, and pi-alkyl interactions with Lys103 and Pro107 (Fig.30).

The compound **7e** exhibited interactions with Phe267, Leu265, Leu106, Gln100, Phe267, Leu265, Lys266, Lys103 and Pro107 amino acid residues (Fig.29). Compound **6j** exhibited interactions with Phe267 and Leu265, Leu106, Glu263, Gln100, Phe267, Leu265, Leu106, and Lys266. The nitrogen-linked phenyl ring has a pi-alkyl interaction with Lys103 and Pro107 (Fig.31). Compound **6k** exhibited interactions with Phe267 and Leu265, Leu106, Glu263, Gln100, Phe267, Leu265, Lys266, Lys103 and Pro107 (Fig.32).

For the 4NCR Co-crystalline ligand, various types of interactions with amino acid are exist. Van der Waals interactions with Glu263, Lys266, Leu106, Pro264, Ile80, Ala104, Gln100. Conventional hydrogen bonding interactions occur with Phe267, Gln100, and Leu265, along with pi-alkyl interactions involving Lys103 and Pro107 residues (Fig.33). The hydrogen bonding interaction and the Van der Waals interaction impart the compounds' pharmacological significance.

Table-4: Binding affinity and amino acid interactions of the compounds **(7a-o)** with 4NCR protein

Comp.	**Structure**	**Binding affinity Kcal/mol (Docking score)**	**Amino acid interactions**
7a	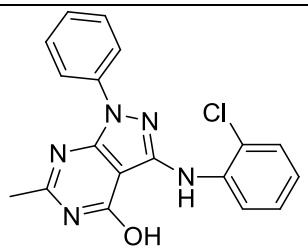	-8.2	Hydrogen Bond interactions: Phe267 Vander walls interactions: Leu265, Lys266, Leu106, Glu263, Ala104, Gln100, Phe267, Lys266, Leu106 Other Interactions: Lys103, Pro107,
7b	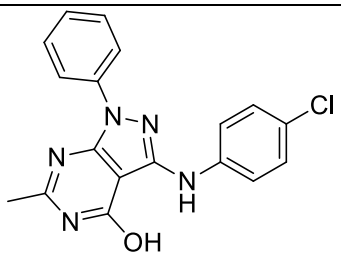	-8.2	Vander walls interactions: Lys266, Leu265, Leu106, Glu263, Gln100, Asp99, Phe267 Other Interactions: Phe267, Lys103, Pro107
7c	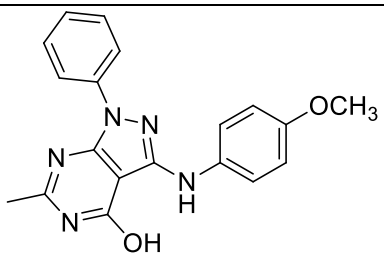	-8.1	Hydrogen bond interactions: Phe267, Lys266, Asp99 Vander walls interactions: Leu106, Leu265, Gln100, Glu263, Lys266, Phe267 Other Interactions: Lys103, Pro107
7d	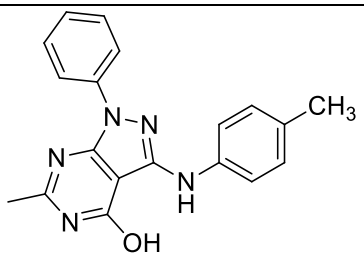	-8.3	Hydrogen bond interactions: Phe267, Leu265, Lys266 Vander walls interactions: Leu106, Glu263, Phe267, Leu106, Lys266, Leu265, Gln100, Asp99 Other interactions: Lys103, Pro107
7e	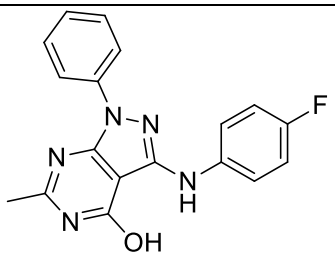	-8.2	Hydrogen bond interactions: Phe267, Leu265, Lys266 Vander walls interactions: Leu106, Gln100, Phe267, Leu265, Lys266

			Other interactions: Lys103, Pro107
7f	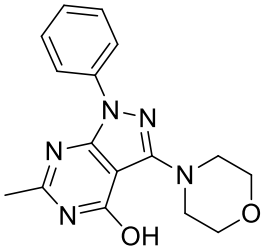	-7.4	Hydrogen bond interactions: Phe267 Vander walls interactions: Leu106, Leu265, Lys266, Glu263, Gln100, Ala104, Leu106, Phe267 Other interactions: Lys103, Pro107
7g	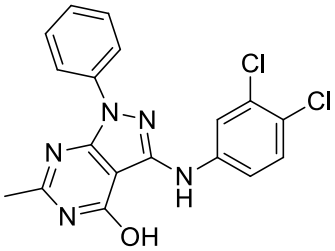	-8.5	Hydrogen bond interactions: Phe267, Leu265 Vander walls interactions: Leu106, Lys266, Gln100, Asp99, Glu263, Phe267, Leu265 Other interactions: Lys103, Pro107
7h	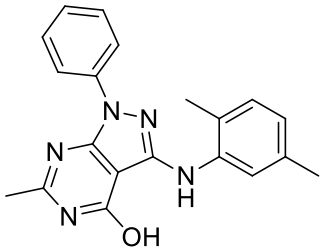	-8.6	Hydrogen bond interactions : Phe267 Vander walls interactions: Leu106, Leu265, Lys266, Ala104, Gln100, Glu263, Phe267, Leu106 Other interactions: Lys103, Pro107
7i	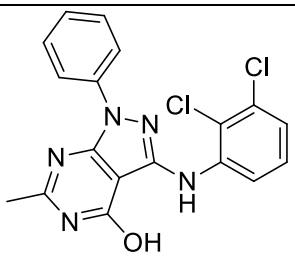	-8.4	Vander walls interactions: Leu106, Lys266, Ala104, Leu265, Gln100, Glu263, Pro107, Phe267 Other interactions: Lys103, Pro107, Phe267
7j	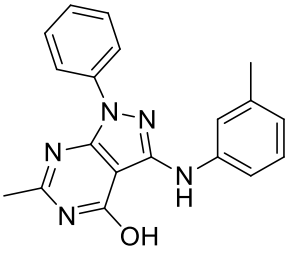	-8.3	Hydrogen bond interactions: Phe267, Leu265, Lys266 Vander walls interactions: Leu106, Glu263, Gln100, Phe267, Leu265, Leu106, Lys266 Other interactions: Lys103, Pro107

7k	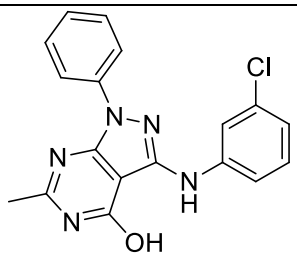	-8.2	Hydrogen bond interactions: Phe267, Leu265, Lys266 Vander walls interactions: Leu106, Glu263, Gln100, Phe267, Leu106, Leu265, Lys266 Other interactions: Lys103, Pro107
7l	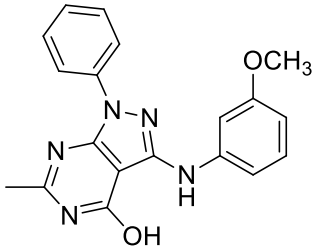	-8.0	Hydrogen bond interactions: Phe267, Leu265 Vander walls interactions: Lys266, Leu106, Glu263, Pro107, Phe267 Other interactions: Lys103, Pro107
7m	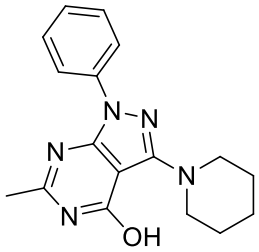	-7.7	Hydrogen bond interactions: Phe267, Leu265 Vander walls interactions: Phe267, Leu106, Lys266, Leu265, Leu106, Glu263, Gln100, Ala104 Other interactions: Lys103, Pro107
7n	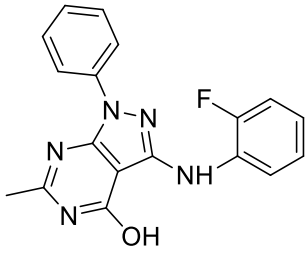	-8.3	Hydrogen bond interactions: Phe267 Vander walls interactions: Leu106, Lys266, Gln100, Leu265, Phe267 Other interactions: Lys103, Pro107, Leu265.Glu263
7o	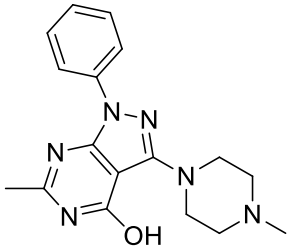	-7.7	Hydrogen bond interactions: Phe267, Glu263 Vander walls interactions: Phe267, Leu106, Leu265, Lys266, Gln100 Other interactions: Lys103, Pro107

4NCR Co-crystallin e ligand PBTZ169	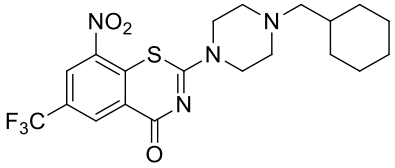	-8.1	Hydrogen bond interactions: Phe267, Gln100, Leu265, Lys103, Glu263 Vander walls interactions: Glu263, Lys266, Leu106, Pro264, Ile80, Ala104, Gln100 Other interactions: Lys103, Pro107, Ser262

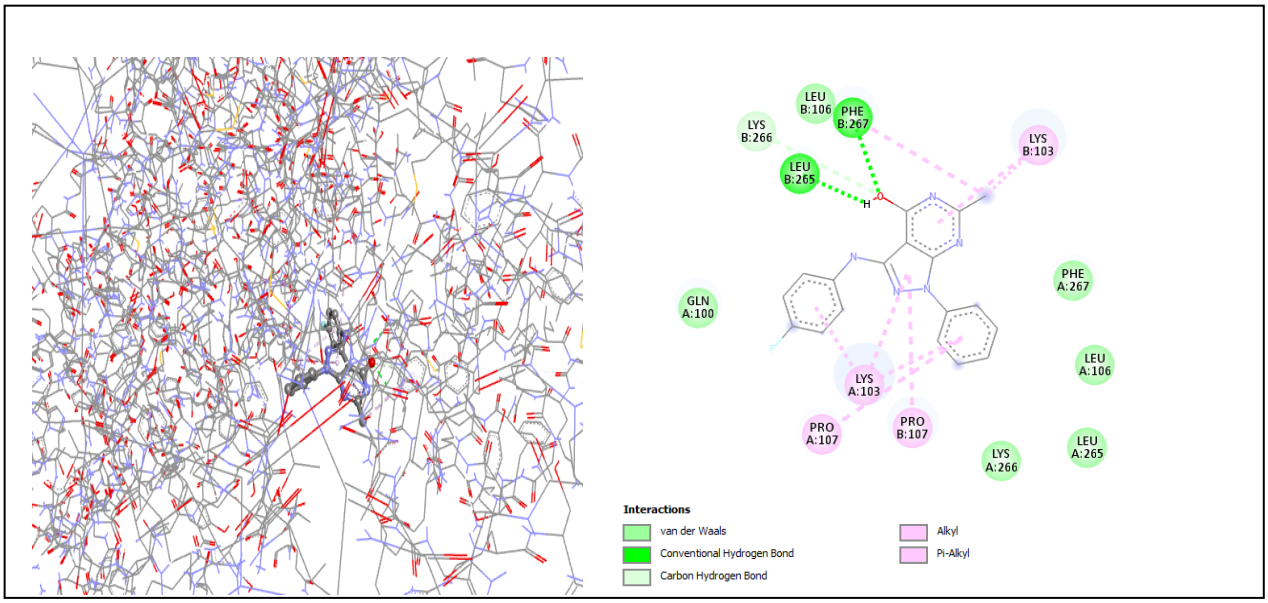

Fig.29: 3D and 2D structure of the interaction of docked compound **(7e)** with protein 4NCR

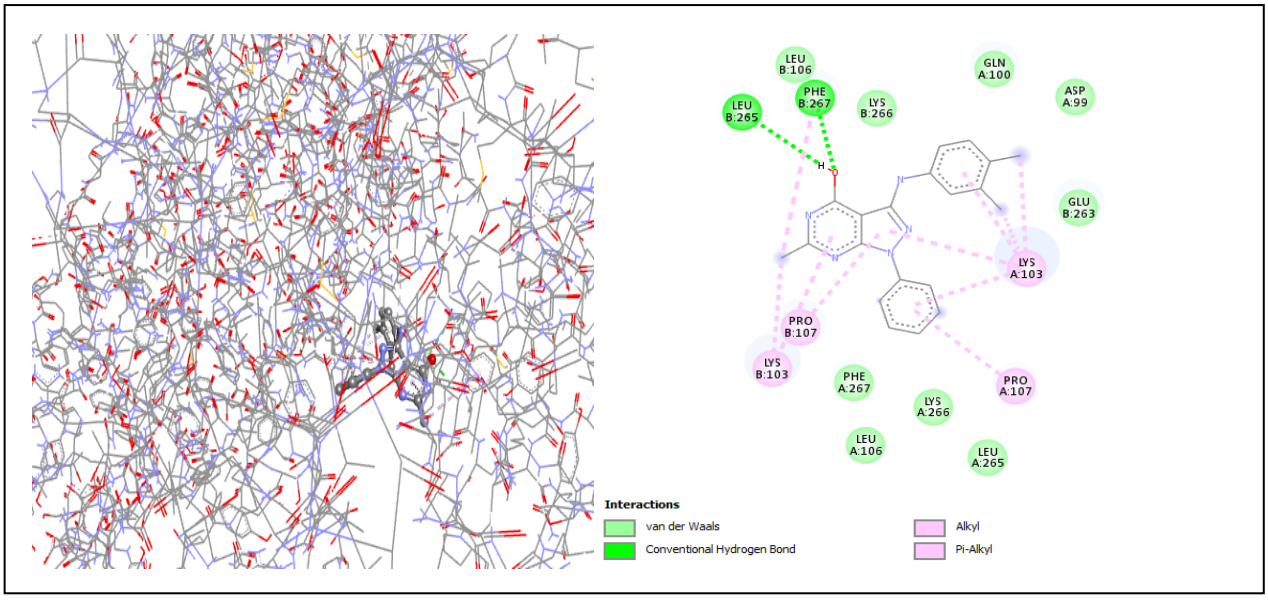

Fig.30: 3D and 2D structure of the interaction of docked compound **(7g)** with protein 4NCR

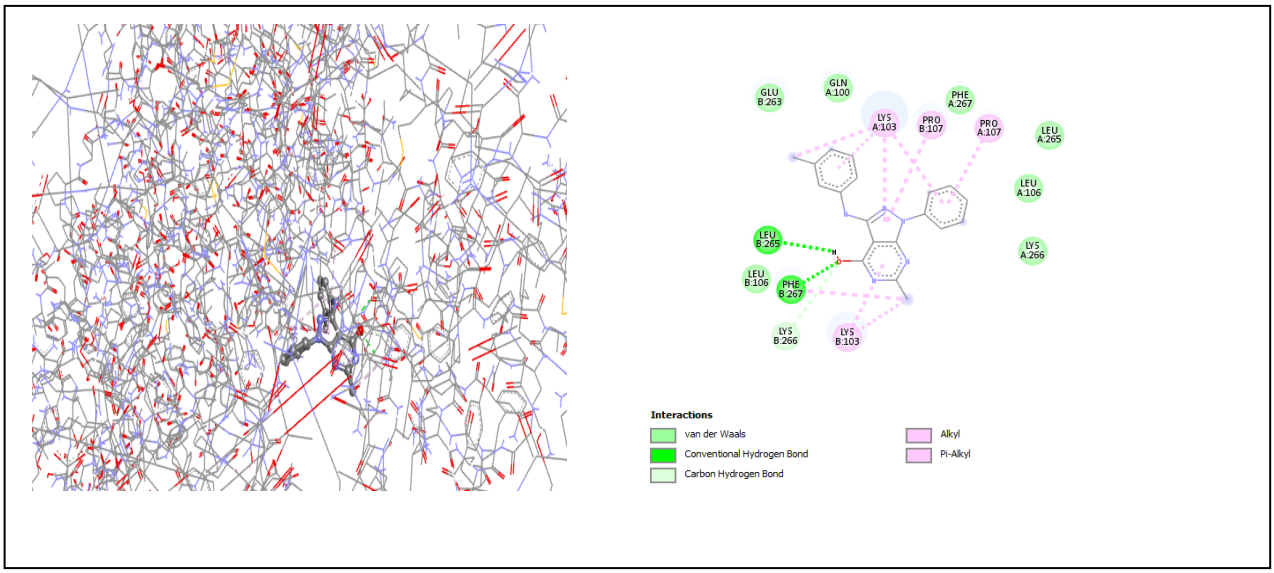

Fig.31: 3D and 2D structure of the interaction of docked compound **(7j)** with protein 4NCR

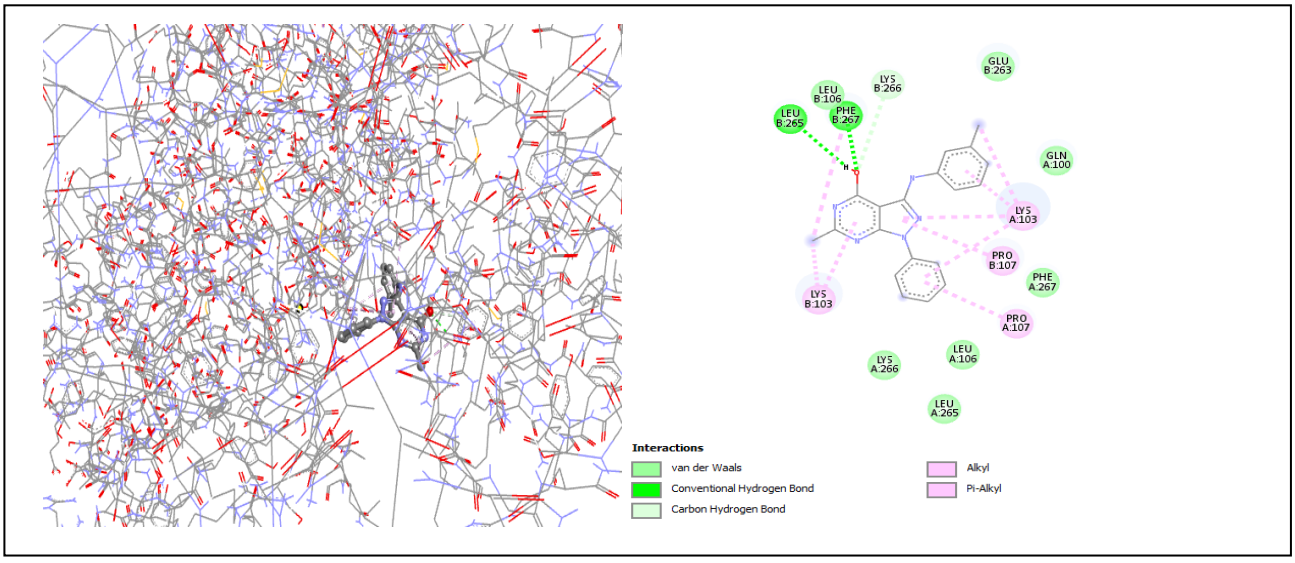

Fig.32: 3D and 2D structure of the interaction of docked compound **(7k)** with protein 4NCR

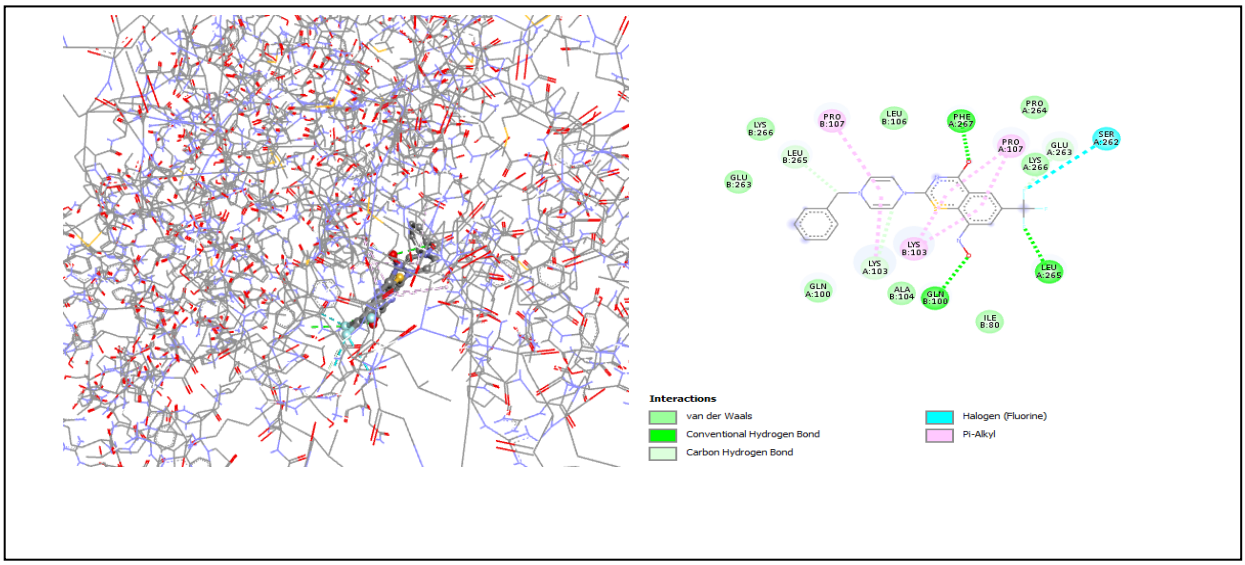

Fig.33: 3D and 2D structure of the interaction of Co-crystalline ligand PBTZ169 with protein 4NCR

4.4. Synthetic pathway

Designed compound have been synthesized by below synthetic scheme.

Reaction Scheme:

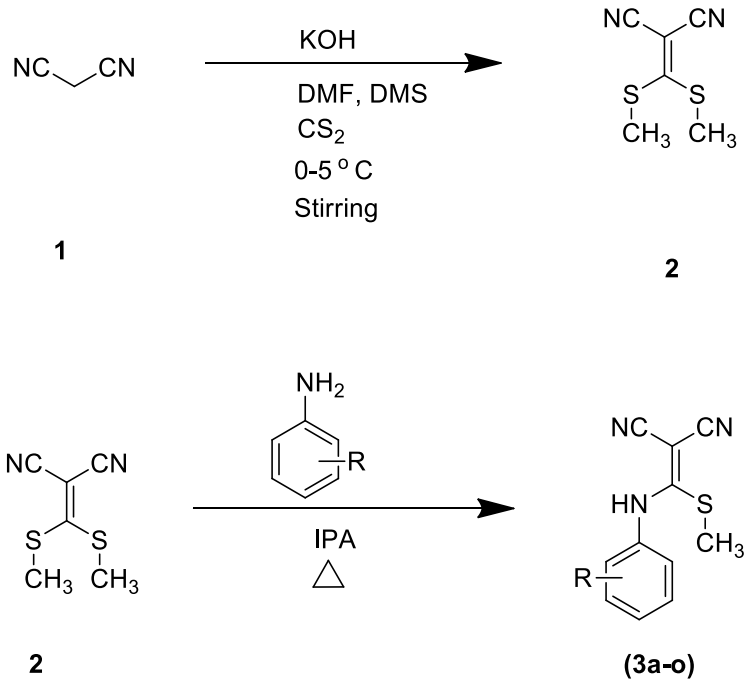

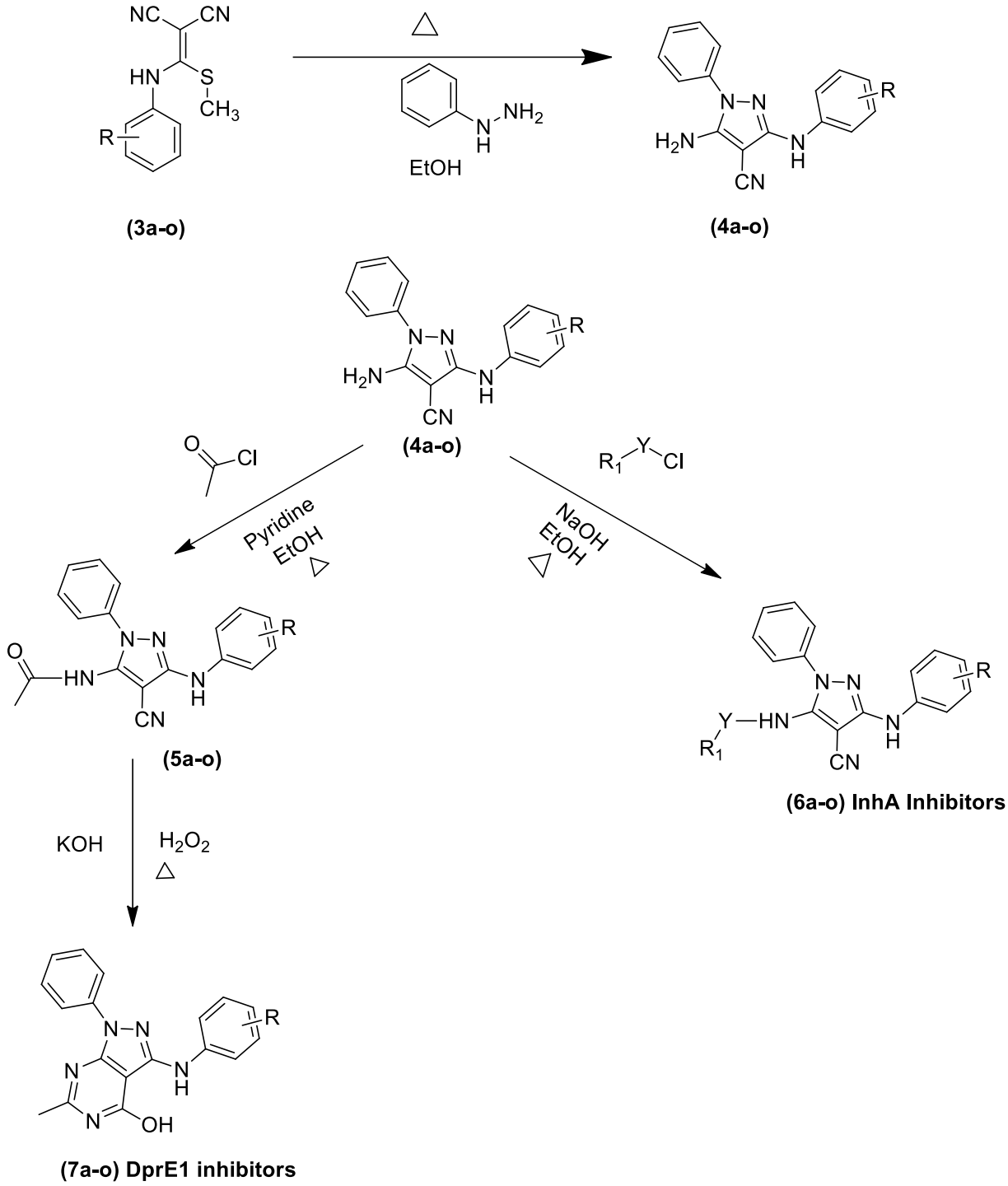

R= 4-OCH_3,, 4-Cl, 4-F, 3-Cl, 3,4- di-Cl, 3-OCH_3, 2,5-di-CH_3, 4-CH_3, 3-CH_3, 2-F, 2-Cl, 2,3 di-Cl , Morpholine, Piperidine, N-CH_3-Piperazine

R_1	Y
$-CH_3$	
$-C_6H_5$	
$-C_6H_5$	
$-CH_3$	
-Cl	

1) KOH, CS_2, DMF, DMS, stirring 0-5 ^{0}C, 2) substituted amine, IPA reflux 50-60 ^{0}C for 6-7 hr., 3)Phenyl hydrazine, Ethanol 70-80 ^{0}C, 4) Acetyl chloride, Pyridine, EtOH/ substituted acid chloride, NaOH, Ethanol 50-60 ^{0}C, 5)KOH, H_2O_2, 70-75 ^{0}C

4.4.1. Reaction Mechanism

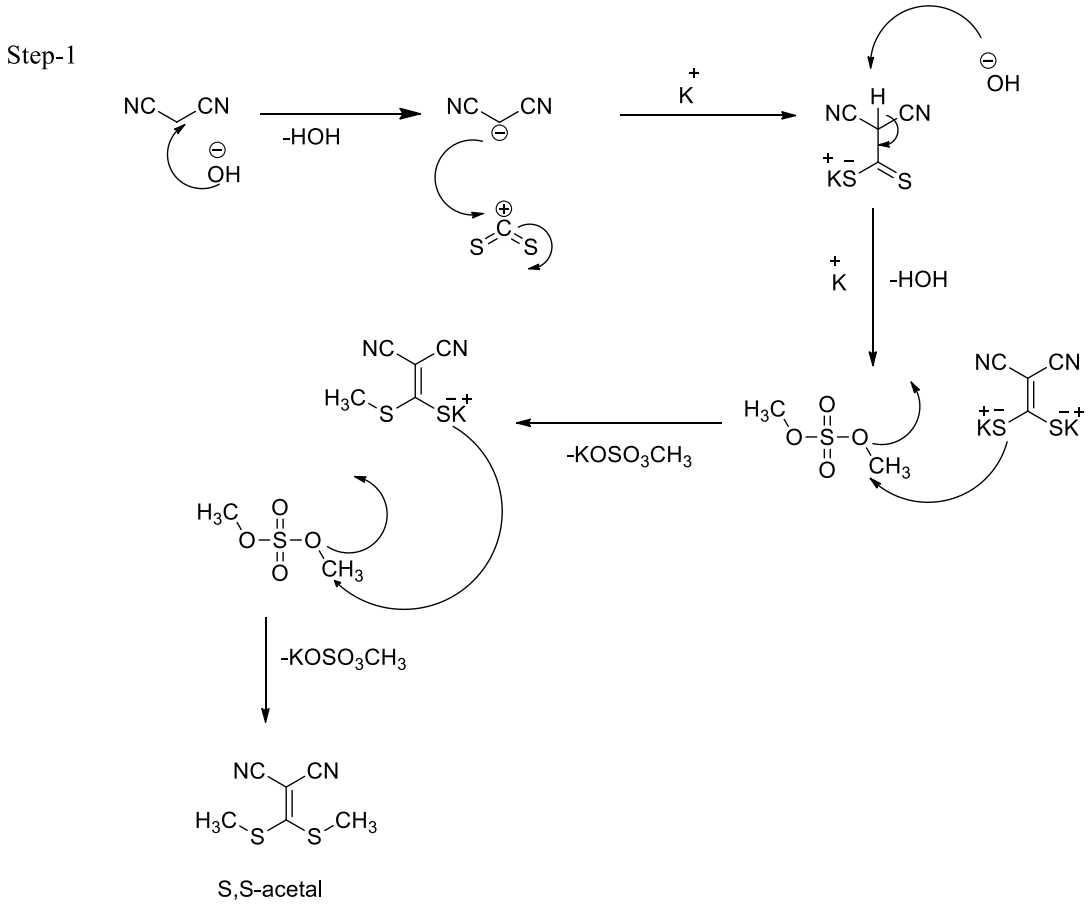

Step-2

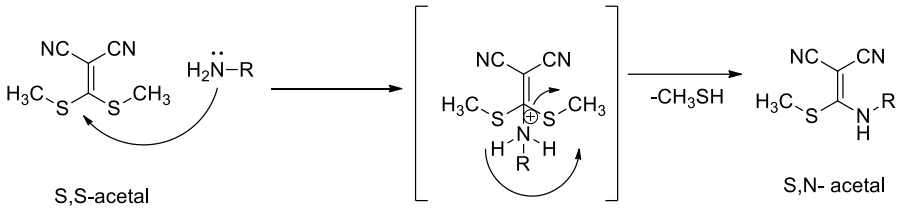

Step-3

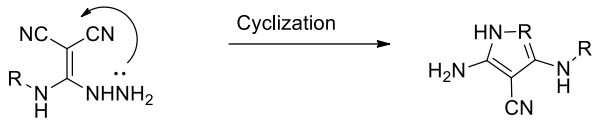

Step-4

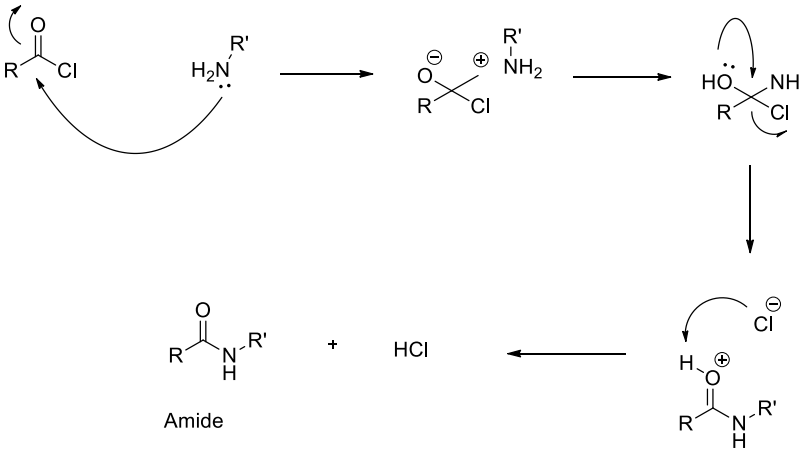

Step-5

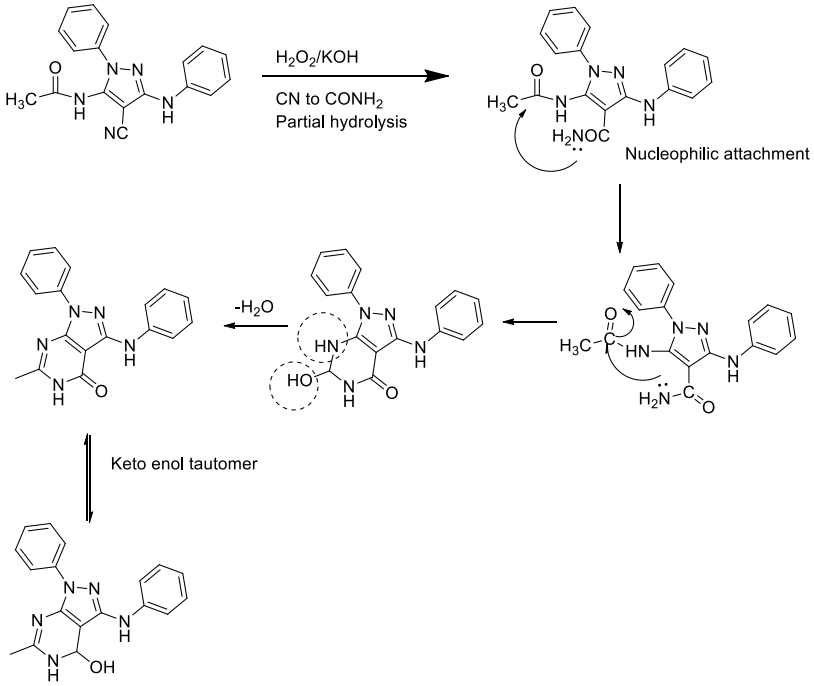

4.5. Synthetic approach

4.5.1. Synthesis of 2-(bis(methylthio)methylene)malononitrile (S,S-Acetal) (2)

One of the general method for the Preparation of ketenediothioacetal with an alkyl substitution the sulphur atom is through the alkylation of the dithiolate anion obtained by the base catalysed condensation of an active methylene compound with carbon disulfide. Alkylation with equivalent of an alkylating agent yielded symmetrical dithioacetal**(2)**

Scheme 1

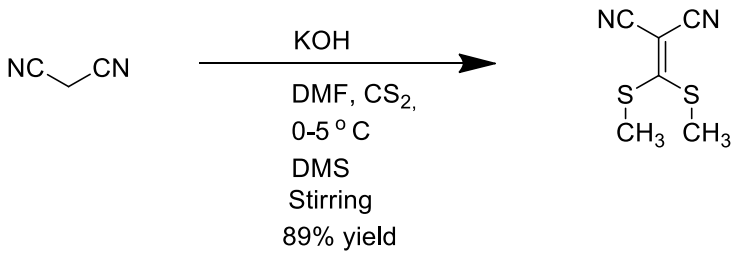

(1) **(2)**

4.5.2. Synthesis of of 2-((methylthio)(aminosubstituted)methylene)malononitrile (S,N actal) (3a-o)

Cynoketene S,N-acetal **(2)** was obtained by nucleophilic displacement of methylmercapto group of ketenedithioacetal in reflux condition using isopropyl alcohol as solvent.

Scheme 2

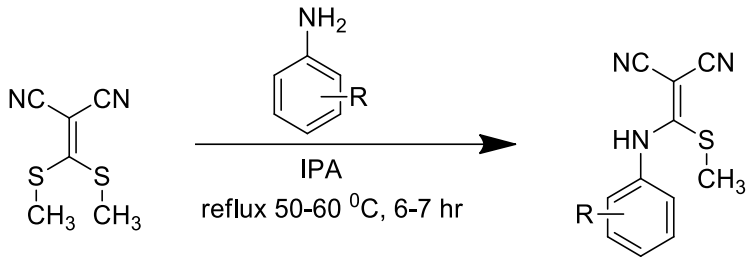

(2) **(3a-o)**

4.5.3. Synthesis of 5-amino-3-(amine substituted)-1-phenyl-1*H*-pyrazole-4-carbonitrile (4a-o)

Reaction of S, N-acetal of malononitrile with phenyl hydrazine in presence of ethanol, cyclized to 5-amino-3-(amine substituted)-1-phenyl-1*H*-pyrazole-4-carbonitrile**.**

Scheme 3

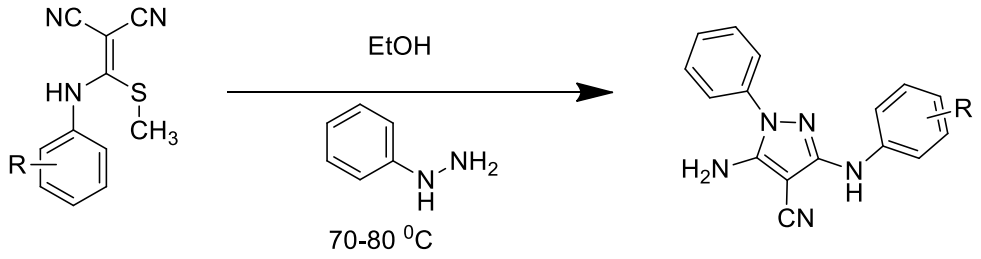

(3a-o) **(4a-o)**

4.5.4. Synthesis of N-(4-cyano-1-phenyl-(amino substituted)-1*H*-pyrazol-5-yl)acetamide **(5a-o)**

The nucleophilic substitution reaction between compounds (**4a-o)** and acetyl chloride to obtain Compounds (**5a-o).**

Scheme 4

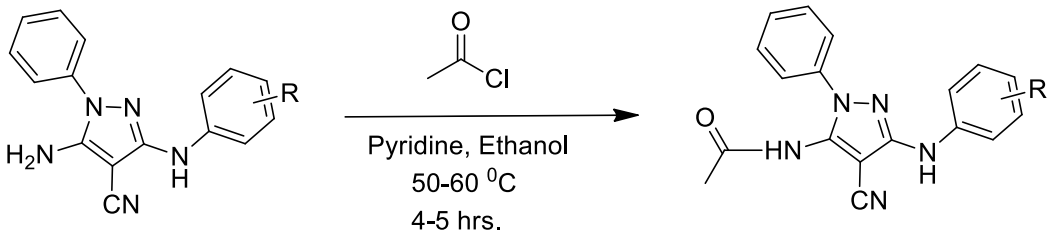

(4a-o) **(5a-o)**

(3a-o), (4a-o) and (5a-o) R= 4-Cl, 4-OCH_3, Morpholine, 4-CH_3, 4-F, Morpholine, N-methyl Piperazine, 4-CH_3, 3,4-di-Cl, 2,5-di CH_3, 2,3-di-Cl, 3-CH_3, 3-Cl, 2-Cl, Piperidine

4.5.5. Synthesis of acid chloride substituted pyrazole derivatives (6a-o)

Target compounds **(6a-o)** was achieved by the nucleophilic substitution reaction of 5-amino-1-phenyl-3-(amine substituted)-1*H*-pyrazole-4-carbonitrile **(4a-o)** with substituted acid chlorides.

Scheme 5

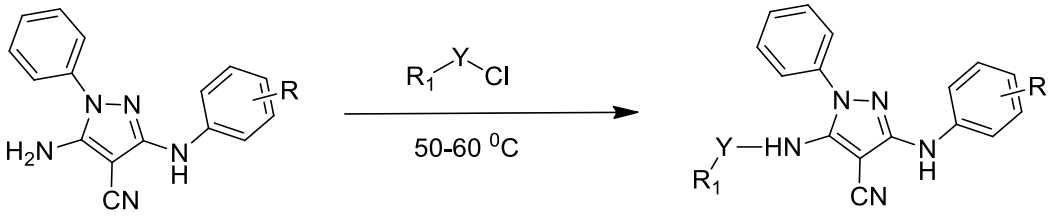

(4a-o) **(6a-o)**

6a. $R_{1=}$ -CH_3, Y= -C=O, **6b**. R_1= -CH_3 ,Y= -C=O, **6c**. $R_{1=}$ -CH_3, Y= -C=O, **6d**. R_1-CH_3, Y= -C=O, **6e**. R_1= - C_6H_5, Y= -C=O, **6f**. R_1= - C_6H_5, Y= -C=O, **6g**. R_1= - C_6H_5, Y= -C=O, **6h**. R_1= - C_6H_5, Y= -C=O, **6i**. R_1= -C_6H_5, Y- O=S=O, **6j**. R_1= -C_6H_5, Y- O=S=O, **6k**. R_1= -C_6H_5, Y- O=S=O, **6l**. R_1= -CH_3, Y- O=S=O, **6m**. R_1= -CH_3, Y- O=S=O, **6n**. R_1= -CH_3, Y- O=S=O, **6o**. R_1= -Cl, Y- -S=O

Reagents and solvents

(6a-6d): CH_3COCl, Pyridine, EtOH

(6e-6o): Substituted acid chloride (Benzoyl chloride, Benzene sulfonyl chloride, Methane sulfonyl chloride and Thionyl chloride), NaOH and EtOH

4.5.6. Synthesis of amino substituted 6-methyl-1-phenyl-1*H*-pyrazolo[3,4-d]pyrimidin-4-ol (7a-o)

Target compounds, amino-substituted 6-methyl-1-phenyl-1*H*-pyrazolo[3,4-d]pyrimidin-4-ol (**7a-o),** were achieved by the cyclization reaction of compounds (**5a-o)** in the presence of potassium hydroxide and hydrogen peroxide.

Scheme 6

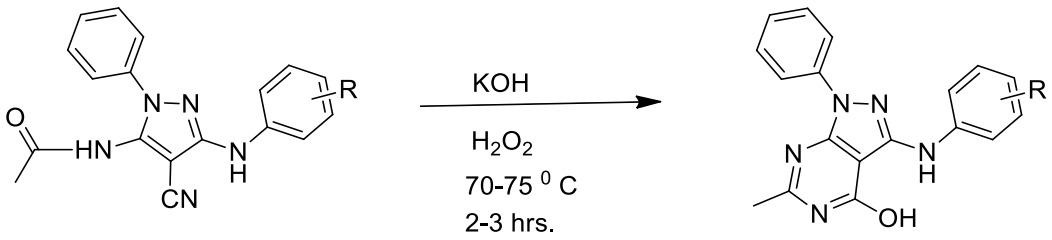

(5 a-o) **(7a-o)**

(5a-o) and (7a-7o) R= 4-Cl, 4-OCH_3, Morpholine, 4-CH_3, 4-F, Morpholine, N-methyl Piperazine, 4-CH_3, 3,4-di-Cl, 2, 5-di CH_3, 2,3-di-Cl, 3-CH_3, 3-Cl, 2-Cl, Piperidine

4.6. Physical and spectral characteristics

4.6.1. Physical characteristics

All the synthesized compounds are crystalline powder, soluble in ethyl acetate and ethanol.

4.6.2. Spectral characteristic

4.6.2.1. IR Spectra

IR spectroscopy of all the synthesized derivatives were carried out on FT-IR 8400s SHIMADZU spectrophotometere using KBr. Sharp absorption band around 2216-2212 cm^{-1} due to presence of cyano (-CN) group. The NH group showed peak around 3500-3300 cm^{-1}.

4.6.2.2. Mass Spectra

Mass spectroscopy of all the synthesized compounds were carried out in a Perkin-Elmer LC-MS PE Sciex API/65. All the compounds showed corresponding M, M+1 and M+2 peaks. Compounds with chloro group shown M+2 peak due to isotopic abundance.

4.7. Physical characteristics of synthesized compounds

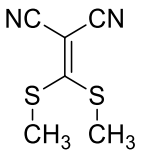

(2)

Table-5: Physical characteristics of 2-(bis(methylthio)methylene)malononitrile (S,S- acetal) **(2)**

Comp.	Molecular Formula	Molecular Weight (g/mol)	Melting Point (^{o} C)	% yield	R_f
2	$C_6H_6N_2S_2$	170.26	60- 64 ^{0}C (57-59 ^{0}C)*	89%	0.4

Mobile Phase: n-Hexane: Ethyl acetate (7:3)

Table-6: Physical characteristics of 2-((methylthio)(amino substituted)methylene) malononitrile (S,N- acetal) **(3a-o)**

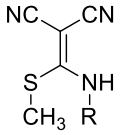

(3a-o)

Comp.	**R**	**Molecular Formula**	**Molecular weight (g/mol)**	**Melting Point (^{o}C)**	**% yield**	**R_f**
3a	4-Cl- C_6H_5	$C_{11}H_8ClN_3S$	249.72	142-145 (157 °C)*	82	0.42
3b	4-OCH_3-C_6H_5	$C_{12}H_{11}N_3OS$	245.30	146-148 (149-151 °C)*	87	0.25
3c	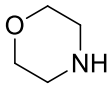	$C_9H_{11}N_3OS$	209.27	135-138 (140-141 °C)*	85	0.68
3d	4-CH_3-C_6H_5	$C_{12}H_{11}N_3S$	229.30	162-163(165-167)*	87	0.45
3e	4-F- C_6H_5	$C_{11}H_8FN_3S$	233.26	135-137	78	0.52
3f	3-Cl,4-Cl- C_6H_4	$C_{11}H_7Cl_2N_3S$	284.16	150-153	59	0.46
3g	2,5 di CH_3- C_6H_4	$C_{13}H_{13}N_3S$	243.33	150-155	65	0.42
3h	2-Cl,3-Cl- C_6H_4	$C_{11}H_7Cl_2N_3S$	284.16	140-142	75	0.45
3i	3-CH_3- C_6H_5	$C_{12}H_{11}N_3S$	229.30	116-119(109-111)*	52	0.58
3j	3-Cl- C_6H_5	$C_{11}H_8ClN_3S$	249.72	154-156 (150-152)*	59	0.35
3k	2-Cl- C_6H_5	$C_{11}H_8ClN_3S$	249.72	153-155(158-160)*	82	0.48
3l	3-OCH_3-C_6H_5	$C_{12}H_{11}N_3OS$	245.30	138-140(141-142)*	50	0.62
3m		$C_{10}H_{13}N_3S$	207.30	95-98 (93-95 °C)*	58	0.55
3n	2-F- C_6H_5	$C_{11}H_8FN_3S$	233.26	115-116	78	0.45
3o	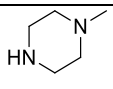	$C_{10}H_{14}N_4S$	222.31	113-114 (115-116 °C)*	49	0.56

Mobile Phase: n-Hexane: Ethyl acetate (7:3)

Table-7: Physical characteristics of 5-amino-3-(amine substituted)-1-phenyl-1*H*-pyrazole-4-carbonitrile **(4a-4o)**

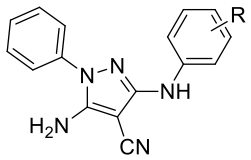

(4a-o)

Comp.	**R**	**Molecular Formula**	**Molecular weight (g/mol)**	**Melting Point (^{o} C)**	**% yield**	**R_f**
4a	4-Cl	$C_{16}H_{12}ClN_5$	309.75	140-142	87	0.62
4b	4-OCH_3	$C_{17}H_{15}N_5O$	305.33	172-175 (183-184)*	85	0.58
4c	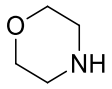	$C_{14}H_{15}N_5O$	269.30	117-119	90	0.76
4d	4-CH_3	$C_{17}H_{15}N_5$	289.33	165-167 (170-172 °C)*	85	0.64
4e	4-F	$C_{16}H_{12}FN_5$	293.30	146-148	84	0.73
4f	3-Cl,4-Cl	$C_{16}H_{11}Cl_2N_5$	344.20	160-162	75	0.71
4g	2,5 di-CH_3	$C_{18}H_{17}N_5$	303.36	95-100	70	0.64
4h	2-Cl,3-Cl	$C_{16}H_{11}Cl_2N_5$	344.20	129-132	86	0.70
4i	3-CH_3	$C_{17}H_{15}N_5$	289.33	125-130	76	0.71
4j	3-Cl	$C_{16}H_{12}ClN_5$	309.75	120-125	53	0.72
4k	2-Cl	$C_{16}H_{12}ClN_5$	309.75	182-185 (202-205)*	85	0.80
4l	3-OCH_3	$C_{17}H_{15}N_5O$	305.33	135-140	59	0.73
4m	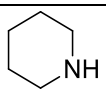	$C_{15}H_{17}N_5$	267.33	100-102	92	0.72
4n	2-F	$C_{16}H_{12}FN_5$	293.30	178-182 (183-186)*	87	0.61
4o	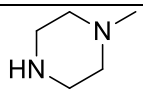	$C_{15}H_{18}N_6$	282.34	130-135	50	0.80

Mobile phase = n-Hexane: ethyl acetate 5:5

Table-8: Physical characteristics of N-(4-cyano-3-(amino substituted)-1-phenyl-1*H*-pyrazol-5-yl)acetamide **(5a-o)**

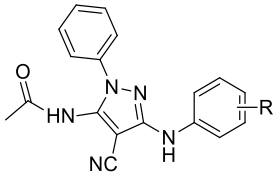

(5a-o)

Comp.	**R**	**Molecular Formula**	**Molecular Weight (g/mol)**	**Melting Point (^{o} C)**	**% yield**	**R_f**
5a	2-Cl	$C_{18}H_{14}ClN_5O$	351.09	112-115	86	0.70
5b	4-Cl	$C_{18}H_{14}ClN_5O$	351.09	162-165	80	0.70
5c	4-OCH_3	$C_{19}H_{17}N_5O_2$	347.37	110-112	82	0.71
5d	4-CH_3	$C_{19}H_{17}N_5O$	331.37	141-143	80	0.77
5e	4-F	$C_{18}H_{14}FN_5O$	335.34	85-90	76	0.75
5f	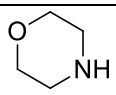	$C_{16}H_{17}N_5O_2$	311.34	137-139	84	0.81
5g	3-Cl,4-Cl	$C_{18}H_{13}Cl_2N_5O$	386.23	118-120	70	0.85
5h	2,5 di-CH_3	$C_{20}H_{19}N_5O$	345.40	115-117	74	0.65
5i	2-Cl,3-Cl	$C_{18}H_{13}Cl_2N_5O$	386.23	122-125	83	0.71
5j	3-CH_3	$C_{19}H_{17}N_5O$	331.37	190-195	72	0.64
5k	3-Cl	$C_{18}H_{14}ClN_5O$	351.09	129-132	50	0.68
5l	3-OCH_3	$C_{19}H_{17}N_5O_2$	347.37	120-122	60	0.86
5m	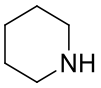	$C_{17}H_{19}N_5O$	309.37	124-127	89	0.68
5n	2-F	$C_{18}H_{14}FN_5O$	335.34	142-145	85	0.74
5o	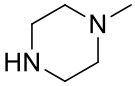	$C_{17}H_{20}N_6O$	324.38	130-134	60	0.51

Mobile phase = n-Hexane: ethyl acetate 5:5

Table-9: Physical characteristics of acid chloride substituted pyrazole derivatives/ InhA inhibitors **(6a-o)**

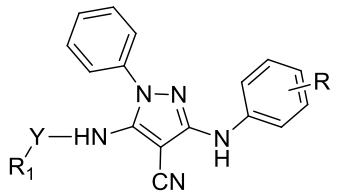

(6a-o)

Comp.	**R/Amine**	**R_1**	**Y**	**Molecular Formula**	**M.W. (g/mol)**	**Melting Point (^{o}C)**	**% yield**	**R_f**
6a	4-Cl	-CH_3		$C_{18}H_{14}ClN_5O$	351.09	162-165	80	0.70
6b	4-OCH_3	-CH_3		$C_{19}H_{17}N_5O_2$	347.37	110-112	82	0.71
6c	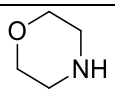	-CH_3		$C_{16}H_{17}N_5O_2$	311.34	137-139	89	0.75
6d	4-CH_3	-CH_3		$C_{19}H_{17}N_5O$	331.37	141-143	83	0.71
6e	4-F	-C_6H_5		$C_{23}H_{16}FN_5O$	397.40	168-172	90	0.76
6f	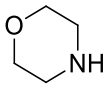	-C_6H_5		$C_{21}H_{19}N_5O_2$	373.41	175-180	78	0.83
6g	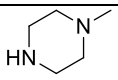	-C_6H_5		$C_{22}H_{22}N_6O$	386.45	190-195	52	0.70
6h	4-CH_3	-C_6H_5		$C_{24}H_{19}N_5O$	393.44	150-152	80	0.64
6i	3-Cl,4-Cl	-C_6H_5		$C_{22}H_{15}Cl_2N_5O_2S$	484.36	140-145	73	0.62
6j	2,5-di-CH_3	-C_6H_5		$C_{24}H_{21}N_5O_2S$	443.52	148-152	75	0.86

6k	2,3-di-Cl	-C_6H_5		$C_{22}H_{15}Cl_2N_5O_2S$	484.36	145-150	76	0.71
6l	3-CH_3	-CH_3		$C_{18}H_{17}N_5O_2S$	367.42	168-170	62	0.56
6m	3-Cl	-CH_3		$C_{17}H_{14}ClN_5O_2S$	387.84	172-174	53	0.66
6n	2-Cl	-CH_3		$C_{17}H_{14}ClN_5O_2S$	387.84	152-155	72	0.42
6o		-Cl		$C_{15}H_{16}ClN_5OS$	349.84	95-100	68	0.68

Mobile phase = n-Hexane: ethyl acetate 5:5

Table-10: Physical characteristics of amino substituted 6-methyl-1-phenyl-1*H*-pyrazolo[3,4-d]pyrimidin-4-ol/ DprE1 inhibitors **(7a-o)**

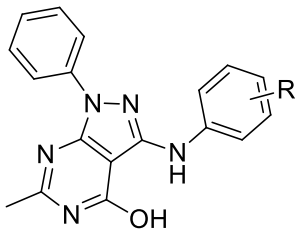

(7a-o)

Comp.	**R/Amine**	**Molecular Formula**	**Molecular Weight (g/mol)**	**Melting Point (° C)**	**% yield**	**R_f**
7a	2-Cl	$C_{18}H_{14}ClN_5O$	351.79	180-182	85	0.63
7b	4-Cl	$C_{18}H_{14}ClN_5O$	351.79	160-165	87	0.52
7c	4-OCH_3	$C_{19}H_{17}N_5O_2$	347.37	190-192	75	0.66
7d	4-CH_3	$C_{19}H1_7N_5O$	331.37	170-172	90	0.50
7e	4-F	$C_{18}H_{14}FN_5O$	335.34	145-148	86	0.40
7f	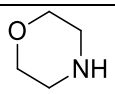	$C_{16}H_{17}N_5O_2$	311.34	155-160	84	0.75
7g	3,4-di Cl	$C_{18}H_{13}Cl_2N_5O$	386.23	164-167	74	0.66
7h	2,5-di CH_3	$C_{20}H_{19}N_5O$	345.40	148-150	79	0.50
7i	2,3-di-Cl	$C_{18}H_{13}Cl_2N_5O$	386.23	140-142	80	0.42
7j	3-CH_3	$C_{19}H_{17}N_5O$	331.37	97-102	64	0.67
7k	3-Cl	$C_{18}H_{14}ClN_5O$	351.79	175-180	56	0.45
7l	3-OCH_3	$C_{19}H_{17}N_5O_2$	347.37	168-172	52	0.63
7m	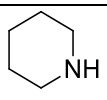	$C_{17}H_{19}N_5O$	309.37	240-245	79	0.55
7n	2-F	$C_{18}H_{14}FN_5O$	335.34	85-90	72	0.58
7o	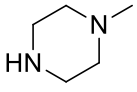	$C_{17}H_20N_6O$	324.38	138-142	75	0.64

Mobile phase = n-Hexane: ethyl acetate 5:5

Table-11: Spectral characteristics of acid chloride substituted pyrazole derivatives (InhA inhibitors **(6a-o)**

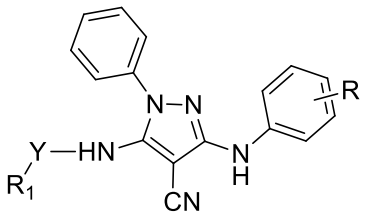

(6a-o)

Mass	**IR(cm^{-1})**	**^{1}H-NMR (δ, ppm)**	**^{13}C-NMR (δ, ppm)**
Compound-6a			
352.2, 353.4(M+2)	3240(NH str.), 1656(CO-NH str.), 2225(CN str.)	2.19 (s, 3H), 7.81-7.78 (m, 7H), 7.77 -7.65 (m, 1H), 7.55-7.53 (m, 1H), 7.42-7.37 (m, 2H)	169.46, 153.17,144.53, 139.67, 137.97, 129.26, 128.87, 127.51, 127.48, 124.06, 122.30, 114.13, 66.17, 24.00
Compound-6b			
348.2	3245(NH str.), 1670 (CO-NH str.), 2220 (CN str.), 1242 (Aromatic-CO)	2.19 (s, 3H), 8.12-8.10 (m, 2H), 7.81-7.77 (m, 2H),7.67-7.66 (m, 2H),7.42-7.39 (m, 1H), 7.00-6.96 (m, 2H), 3.80 (s, 3H)	169.46, 156.01, 153.13, 144.53, 137.97, 135.32, 129.26, 127.51, 124.06, 121.85, 114.80, 114.13, 66.17, 55.35, 24.00
Compound-6c			
311.4	3326(NH str.), 1628 (CO-NH str.), 2208 (CN str.)	2.27 (3H, s),7.80-7.77 (m, 2H), 7.70-7.68 (m, 2H), 7.42- 7.39 (m, 1H), 3.86-3.74 (m, 8H)	169.38, 159.79,144.81, 138.29, 129.27, 127.51, 124.00, 113.22, 67.78, 66.36, 48.26, 24.00
Compound-6d			
332.2	3332(NH str.), 1646 (CO-NH str.), 2209 (CN str.)	8.06-8.03 (m, 2H), 7.81-7.77 (m, 2H), 7.67-7.65 (m, 2H), 7.42 (tt, *J* = 7.1, 1.3 Hz, 1H), 7.24-7.22 (m, 2H), 2.35 (d, *J* = 0.9	169.46, 152.91, 144.53, 138.72, 137.97, 132.01, 129.26, 128.88, 127.51, 124.06, 120.90, 114.13, 66.18, 24.00, 20.73

		Hz, 3H)	
Compound-6e			
398.14	3340(NH str.), 1650 (CO-NH str.), 2215 (CN str.)	8.21-8.19 (m, 2H), 7.97-7.95 (m, 2H), 7.81-7.77 (m, 2H), 7.70 -7.65 (m, 2H), 7.52-7.46 (m, 1H), 7.46-7.39 (m, 3H), 7.20-7.16 (m, 2H)	166.42, 158.74, 156.77, 152.64, 145.07, 138.13, 137.88, 137.86, 133.38, 132.19, 129.26, 128.77, 128.49, 127.51, 124.00, 122.04, 121.97, 115.14, 114.96, 114.09, 67.36
Compound-6f			
374.15	1635 (CO-NH str.), 2218 (CN str.)	7.97 -7.96 (m, 1H), 7.81 -7.77 (m, 1H), 7.78(m, 2H) 7.70-7.68 (m, 1H), 7.52-7.39 (m, 5H), 3.85-3.74 (m, 8H)	166.46, 159.84, 144.92, 138.32, 133.38, 132.19, 129.27, 128.77, 128.49, 127.51, 123.97, 113.17, 70.00, 66.36, 48.26
Compound-6g			
387.20	1652(CO-NH str.), 2235 (CN str.)	7.97-7.96 (m, 1H), 7.81-7.77 (m, 2H), 7.70-7.68 (m, 2H), 7.52 -7.39 (m, 5H), 3.67-3.66 (m, 4H), 3.02-3.00 (m, 4H), 2.91 (s, 3H)	166.46, 159.75, 145.11, 138.34, 133.38, 132.19, 129.27, 128.77, 128.49, 127.51, 123.97, 113.17, 70.00, 54.27, 47.59, 45.01
Compound-6h			
393.14	3318(NH str.), 1682 (CO-NH str.), 2208 (CN str.)	8.07-8.01 (m, 2H), 7.97-7.96 (m, 2H), 7.81-7.77 (m, 2H), 7.67-7.66 (m, 1H), 7.52-7.39 (m, 5H), 7.23 (dt, *J* = 7.1, 0.8 Hz, 2H), 2.35 (s, 3H)	166.42, 152.75, 145.07, 138.72, 138.13, 133.36, 132.19, 132.01, 129.26, 128.88, 128.77, 128.49, 127.51, 124.00, 120.90, 114.09, 67.36, 20.73
Compound-6i			
484.4, 486.2 (M+2), 488.8 (M+4)	3325(NH str.), 1459 (SO_2-NH str.), 2208 (CN str.)	7.79-7.75 (m, 3H), 7.70 (dq, *J* = 7.7, 1.6 Hz, 2H), 7.56 (dq, *J* = 8.8, 1.6 Hz, 2H), 7.43-7.39 (m, 4H), 7.27-7.26 (m,	152.51, 142.11, 140.76, 138.38, 137.44, 133.74, 130.74, 129.74, 129.22, 129.20, 127.84, 127.52, 124.93, 124.04, 121.61,

		1H)	120.20, 113.84, 70.47
Compound-6j			
443.2	3494(NH str.), 1450 (SO_2-NH str.), 2210 (CN str.)	7.95 (tt, *J* = 7.3, 1.3 Hz, 1H), 7.79-7.76 (m, 3H), 7.70 (dq, *J* = 7.7, 1.6 Hz, 2H), 7.56 (dq, *J* = 8.8, 1.6 Hz, 2H), 7.43-7.39 (m, 3H), 7.01 (dq, *J* = 8.2, 1.0 Hz, 2H), 6.80 (ddd, *J* = 7.7, 2.3, 1.1 Hz, 1H), 2.28 (d, *J* = 1.1 Hz, 6H)	152.53, 142.11, 140.38, 138.38, 137.44, 136.66, 133.74, 130.43, 129.22, 129.20, 127.84, 127.66, 127.52, 124.04, 123.01, 120.97, 113.84, 70.45, 21.62, 17.64
Compound-6k			
484.30, 486.2 (M+2), 488.5 (M+4)	3350(NH str.), 1459 (SO_2-NH str.), 2208 (CN str.)	8.08 (dd, *J* = 7.9, 1.1 Hz, 1H), 7.96 (tt, *J* = 7.3, 1.3 Hz, 1H), 7.79-7.76 (m, 2H), 7.70 (dq, *J* = 7.7, 1.6 Hz, 2H), 7.58 -7.55 (m, 2H), 7.43-7.39 (m, 3H), 7.18 (d, *J* = 7.9 Hz, 1H), 7.08 (dd, *J* = 7.8, 1.2 Hz, 1H)	152.27, 142.17, 139.72, 138.38, 137.44, 134.10, 133.74, 129.22, 129.20, 129.03, 127.84, 127.52, 124.41, 124.04, 123.04, 120.03, 113.81, 70.43
Compound-6l			
368.12	3245(NH str.), 1345 (SO_2-NH str.), 2234 (CN str.)	7.79-7.76 (m, 2H), 7.70 (dq, *J* = 7.7, 1.6 Hz, 2H), 7.45-7.39 (m, 3H), 7.14 (d, *J* = 7.6 Hz, 1H), 6.84 (dddd, *J* = 8.2, 2.2, 1.4, 0.7 Hz, 1H), 3.03 (s, 3H), 2.36 (d, *J* = 0.7 Hz, 3H)	152.37, 141.63, 141.19, 138.63, 137.52, 129.22, 128.85, 127.52, 124.41, 124.07, 121.12, 118.27, 113.84, 68.41, 39.83, 21.45
Compound-6m			
387.7, 389.4(M+2)	3325(NH str.), 1312(SO_2-NH str.), 2219 (CN str.)	7.79 -7.76 (m, 2H), 7.70 (dq, *J* = 7.7, 1.6 Hz, 2H), 7.55 (t, *J* =	152.68, 142.18, 141.63, 137.52, 133.61, 129.24, 129.22, 127.52, 124.07,

		2.2 Hz, 1H), 7.41 (tt, *J* = 7.1, 1.4 Hz, 1H), 7.24 (d, *J* = 7.8 Hz, 1H), 7.13 (ddd, *J* = 7.7, 2.2, 1.2 Hz, 1H), 6.96 (ddd, *J* = 7.9, 2.1, 1.2 Hz, 1H), 3.03 (s, 3H)	123.37, 119.92, 119.50, 113.84, 68.41, 39.83
Compound-6n			
387.7, 389.4(M+2)	3322(NH str.), 1320(SO_2-NH str.), 2213 (CN str.)	8.19 (dd, *J* = 7.7, 1.4 Hz, 1H), 7.79-7.76 (m, 2H), 7.70 (dq, *J* = 7.7, 1.6 Hz, 2H), 7.54 (dd, *J* = 8.1, 1.4 Hz, 1H), 7.43-7.39 (m, 2H), 7.22-7.19 (m, 1H), 3.03 (s, 3H)	151.78, 141.63, 138.05, 137.52, 129.38, 129.22, 127.52, 127.38, 125.51, 124.88, 124.07, 123.01, 113.84, 68.37, 39.83
Compound-6o			
349.6	1434(SO-NH str.), 2241 (CN str.)	7.79-7.76 (m, 2H), 7.70 (dq, *J* = 7.7, 1.6 Hz, 2H), 3.64-3.62 (m, 4H), 1.73-1.69 (m, 4H), 1.56 (p, *J* = 5.8 Hz, 2H)	159.27, 147.08, 138.44, 129.23, 127.52, 124.06, 113.07, 68.76, 49.03, 26.26, 24.44

Table-12: Spectral characteristics of amino substituted 6-methyl-1-phenyl-1*H*-pyrazolo[3,4-d]pyrimidine-4-ol derivatives/ DprE1 inhibitors **(7a-o)**

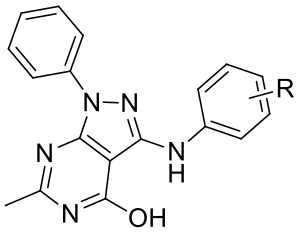

(7a-o)

Mass	**IR(cm^{-1})**	**^{1}H-NMR (δ, ppm)**	**^{13}C-NMR (δ, ppm)**
Compound-7a			
351.12, 353.3(M+2)	3435(-NH), 3342 (-OH), 2926 (C-H str.)	2.40 (3H, s), 8.20 (dd, *J* = 7.7, 1.4 Hz, 1H), 7.83-7.80 (m, 2H), 7.58 -7.53 (m, 2H), 7.54 (dd, *J* = 8.0, 1.4 Hz, 1H), 7.43-7.39 (m, 2H), 7.22 -7.19 (m, 1H)	166.23, 162.50, 153.42, 145.93, 138.38, 138.29, 129.38, 128.92, 127.39, 127.01, 125.56, 124.88, 123.01, 121.54, 93.93, 25.06
Compound-7b			
351.45, 353.25(M+2)	3438(-NH), 3345 (-OH), 2924 (C-H str.)	δ 2.40 (3H, s), 7.58-7.37 (5H, 7.42 (tdd, *J* = 7.8, 1.6,1.0 Hz), 7.80 (d, *J*= 8.4 Hz, 1H), 7.58-7.54(m, 2H), 7.42-7.37 (m, 2H)	166.23, 162.49, 153.38, 147.16, 139.95, 138.38, 128.87, 128.92, 127.48, 127.01, 122.29,121.54, 94.05, 25.06
Compound-7c			
347.15	3312 (-NH), 3352 (-OH), 2935 (C-H str.)	2.40 (3H, s), 3.80 (s, 2H), 6.96 (ddd, 2H), 8.12- 8.10 (m, 2H), 7.83- 7.80 (m, 2H), 7.58- 7.56 (m, 2H), 7.42-7.39 (m, 1H), 7.00-6.95 (m, 2H)	166.23, 162.49, 156.01, 153.38, 146.75, 138.38, 135.74, 128.92, 127.01, 121.85, 121.54, 114.81, 94.05, 55.35, 25.06
Compound-7d			
331.68	3362 (-NH), 3310	2.35 (d, *J* = 1.0 Hz,	166.23, 162.49, 153.38,

	(-OH), 2942 (C-H str.)	3H), 2.35(d, *J* = 1.0 Hz, 3H), 8.05- 8.03 (m, 2H), 7.83- 7.79 (m, 2H), 7.58- 7.56 (m, 2H), 7.41 (tt, *J* = 7.2, 1.3 Hz, 1H), 7.24-7.22 (m, 3H)	147.20, 139.28, 138.38, 132.01, 128.92, 128.89, 127.01, 121.54, 120.91, 94.05, 25.06, 20.73
Compound-7e			
335	3390 (-NH), 3415 (-OH), 2937 (C-H str.)	2.40 (3H, s), 8.21- 8.19 (m, 2H), 7.83- 7.79 (m, 2H), 7.58- 7.56 (m, 3H), 7.41 (tt, *J* = 7.2, 1.3 Hz, 1H), 7.20- 7.16 (m, 2H)	166.23, 162.49, 158.74, 156.77, 153.38, 146.78, 138.64, 138.62, 138.38, 128.92, 127.01, 122.02, 121.95, 121.54, 115.15, 114.97, 94.05, 25.06
Compound-7f			
311.47	3353 (-OH), 2952 (C-H str.)	2.40 (3H, s), 7.83-7.79 (m, 2H), 7.58- 7.56 (m, 2H), 3.84- 3.80 (m, 4H), 3.77 (dd, *J* = 5.7, 4.5 Hz, 4H)	164.99, 161.89, 155.38, 149.14, 138.77, 128.92, 127.01, 121.49, 95.96, 66.36, 48.28, 25.06)
Compound-7g			
386.1, M+2: 388.4, M+4: 390	3352 (-NH str.), 3443(O-H str.), 2926 (C-H str.)	2.40 (3H, s), 7.83-7.75 (m, 2H), 7.74 (d, *J* = 2.2 Hz, 1H), 7.58-7.56 (m, 2H), 7.42 -7.39 (m, 2H), 7.27-7.25 (m, 2H)	166.23, 162.49, 153.38, 146.47, 140.87, 138.38, 130.76, 129.76, 128.92, 127.01, 124.92, 121.61, 121.54, 120.22, 94.08, 25.06
Compound-7h			
346.16	3326 (-NH str.), 3264 (O-H str.), 2921(C-H str.)	2.40 (s, 3H), 2.28 (d, *J* = 1.1 Hz, 3H), 2.34 (s, 3H), 7.83-7.78 (m, 3H), 7.58- 7.56 (m, 2H), 7.42- 7.39 (m, 2H), 7.00 (dq, *J* = 8.3, 0.9 Hz, 1H), 6.81- 6.69 (m, 1H)	166.23, 162.49, 153.38, 145.76, 140.68, 138.38, 136.77, 130.40, 128.92, 127.64, 127.01, 123.01, 121.54, 120.92, 93.98, 25.06, 21.62, 17.67

Compound-7i			
386.30, M+2: 388.64, M+4: 390	3350 (-NH str.), 3410 (O-H str.), 2923 (C-H str.)	2.40 (3H, s), 8.06 (dd, *J* = 7.9, 1.1 Hz, 1H), 7.83-7.79 (m, 2H), 7.58- 7.56 (m, 2H), 7.41 (tt, *J* = 7.2, 1.3 Hz, 1H), 7.20 (d, *J* = 7.9 Hz, 2H), 7.08 (dd, *J* = 7.8, 1.2 Hz, 1H)	166.23, 162.50, 153.42, 146.09, 140.11, 138.38, 134.14, 129.03, 128.92, 127.01, 124.41, 123.00, 121.54, 120.03, 94.03, 25.06
Compound-7j			
332. 15	3359 (-NH str.), 3409 (O-H str.), 2921 (C-H str.)	2.40 (3H, s), 2.36 (m, 3H), 7.83-7.79 (m, 2H), 7.58- 7.56 (m, 2H), 7.45- 7.39 (m, 3H), 7.14 (d, *J* = 7.6 Hz, 1H), 6.84 (dddd, *J* = 8.2, 2.2, 1.4, 0.7 Hz, 1H)	166.23, 162.49, 153.38, 146.95, 141.44, 138.71, 138.38, 128.92, 128.88, 127.01, 124.39, 121.54, 121.12, 118.31, 94.05, 25.06, 21.45
Compound-7k			
352, 354 (M+2)	3412(-NH str.), 3323 (-OH str.), 2915(C-H str.)	2.40 (3H, s), 7.83-7.79 (m, 2H), 7.58- 7.54 (m, 3H), 7.41 (tt, *J* = 7.2, 1.3 Hz, 1H), 7.27 (d, *J* = 15.8 Hz, 1H), 7.13 (ddd, *J* = 7.7, 2.2, 1.2 Hz, 1H), 6.99 (ddd, *J* = 7.9, 2.1, 1.2 Hz, 1H)	166.23, 162.49, 153.38, 146.50, 142.27, 138.38, 133.61, 129.22, 128.92, 127.01, 123.34, 121.54, 119.97, 119.51, 94.08, 25.06
Compound-7l			
348.14	3367(-NH), 3417 (-OH), 2935 (C-H str.)	2.40 (3H, s), 3.82 (s, 3H) 7.83-7.79 (m, 2H), 7.58-7.56 (m, 2H), 7.42-7.38 (m, 2H), 7.22-7.17 (m, 2H), 6.53- 6.50 (m, 1H)	166.23, 162.49, 160.94, 153.38, 146.51, 142.79, 138.38, 130.03, 128.92, 127.01, 121.54, 114.64, 110.46, 105.96, 94.08, 55.59, 25.06
Compound-7m			

310.23	3400 (O-H str.), 2922 (C-H str.)	2.40 (3H, s), 1.58-1.54 (m, 4H), 1.73 -1.69 (m, 2H), 7.83-7.79 (m, 2H), 7.58-7.56 (m, 3H), 3.63-3.60 (m, 4H)	164.99, 161.99, 155.36, 148.96, 138.77, 128.92, 127.01, 121.49, 95.87, 49.09, 26.26, 25.06, 24.44
Compound-7n			
336.13	3342 (-NH str.), 3410 (-OH str.), 2940 (C-H str.)	2.40 (3H, s), 8.20 (ddd, *J* = 8.8, 3.7, 1.4 Hz, 1H), 7.83-7.79 (m, 2H), 7.57 (dq, *J* = 7.5, 1.2 Hz, 2H), 7.41 (tt, *J* = 7.2, 1.3 Hz, 1H), 7.29-7.26 (m, 1H), 7.17-7.08 (m, 2H)	166.23, 162.50, 155.65, 153.69, 153.42, 146.62, 146.56, 138.38, 129.54, 129.43, 128.92, 127.01, 125.46, 125.44, 123.97, 123.91, 122.33, 122.28, 121.54, 115.29, 115.12, 94.05, 25.06
Compound-7o			
325.02	3343(-OH str.), 2910 (C-H str.)	2.40 (3H, s), 2.91 (s, 3H), 3.68-3.66 (m, 4H), 3.02-2.91 (m, 4H), 7.83-7.79 (m, 2H), 7.58-7.56 (m, 3H)	164.99, 161.87, 155.31, 149.26, 138.77, 128.92, 127.01, 121.49, 96.05, 54.24, 47.62, 45.01, 25.06

4.8. Spectra of synthesized compounds

4.8.1. IR, Mass, ^{1}H and ^{13}C NMR of compound 6h

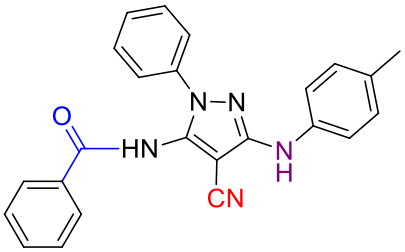

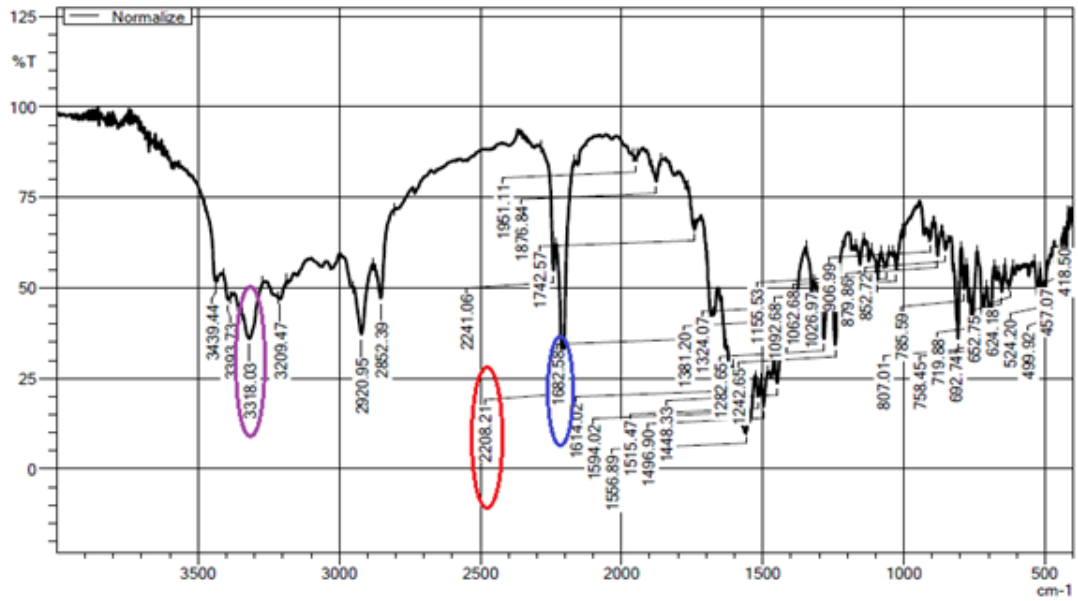

Fig.34: IR spectrum of compound **6h**

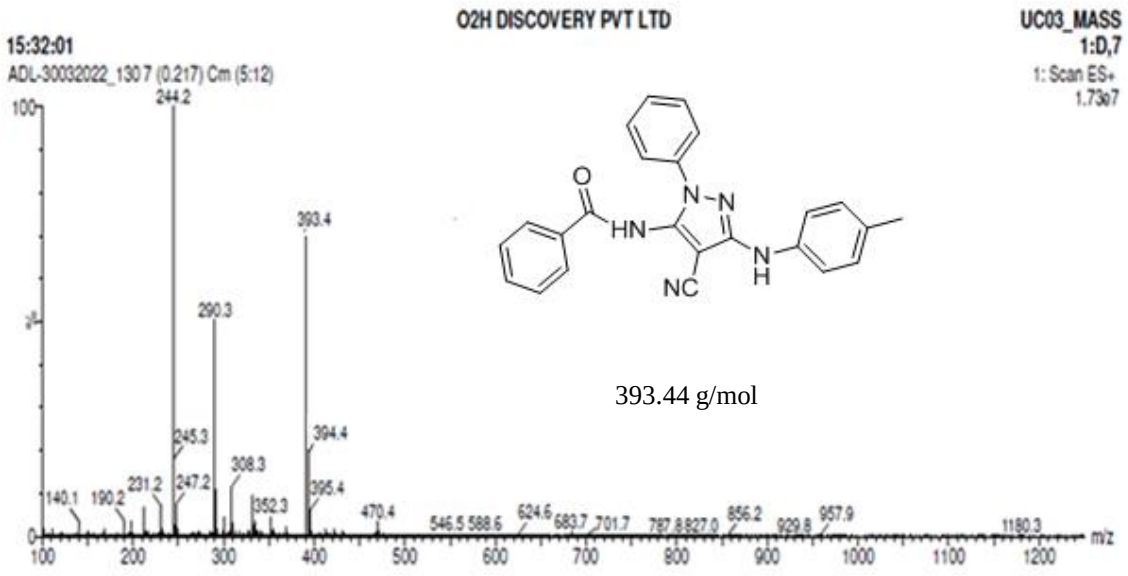

Fig.35: Mass spectrum of compound **6h**

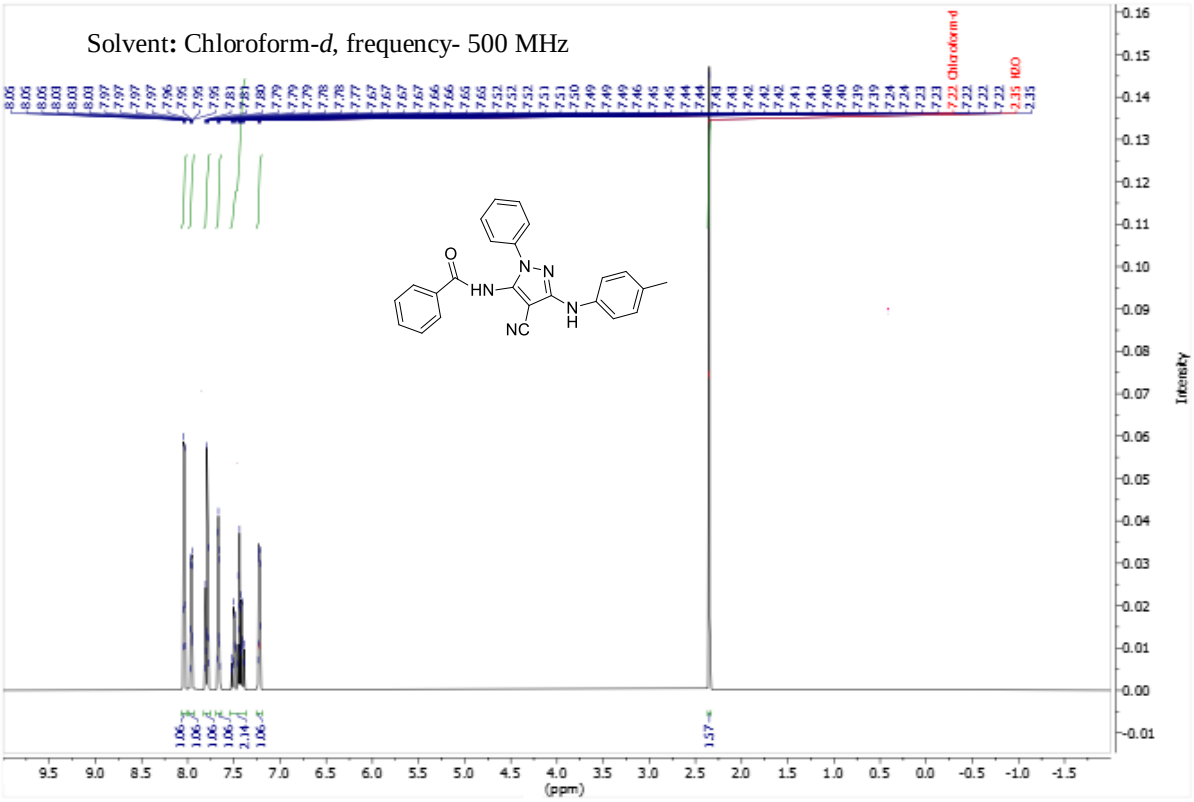

Fig.36: ^{1}HNMR spectrum of compound **6h**

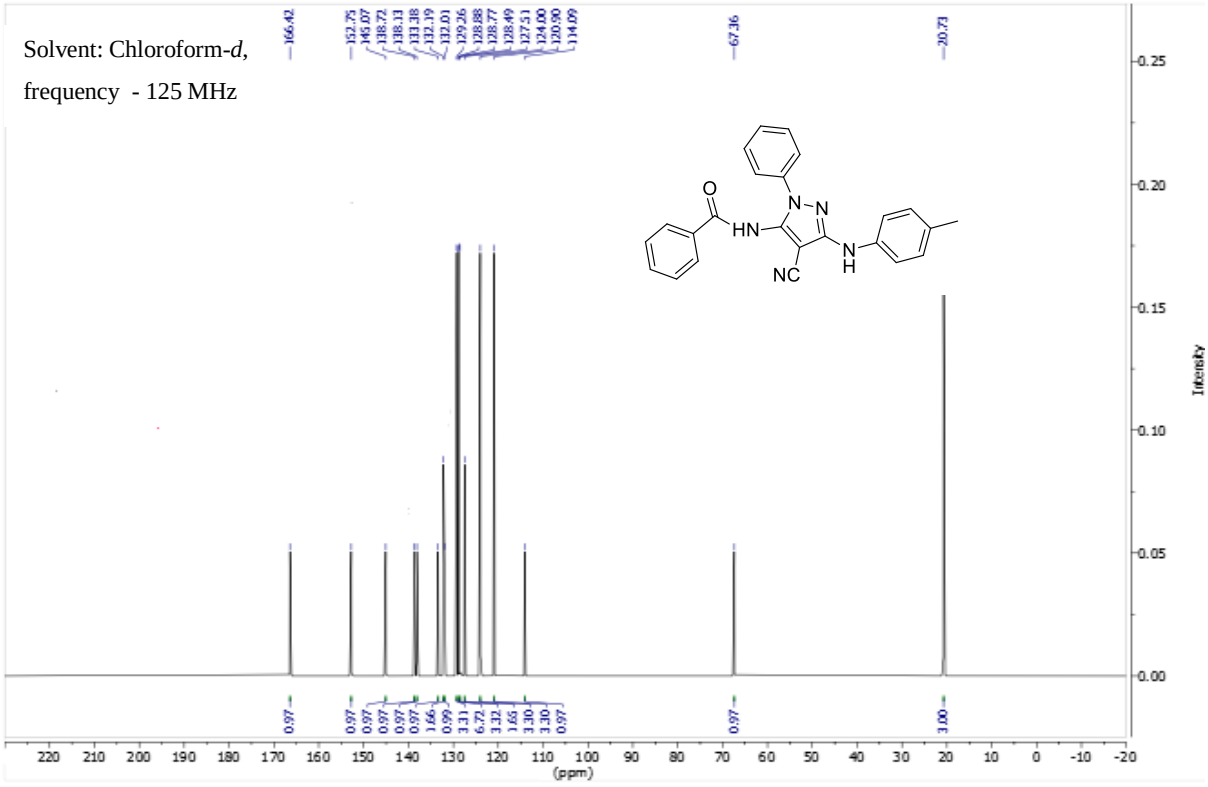

Fig.37: ^{13}C NMR spectrum of compound **6h**

4.8.2. IR, Mass, ^{1}H and ^{13}C NMR of compound 6m

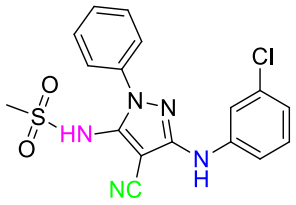

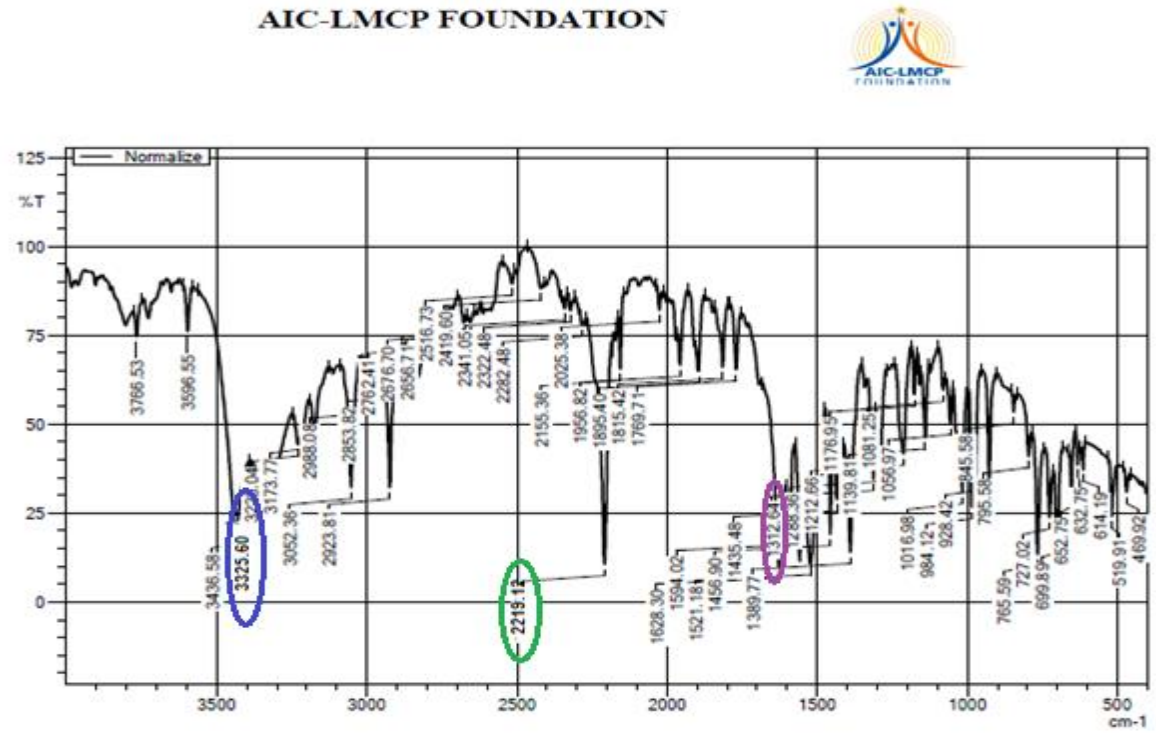

Fig.38: IR spectrum of compound **6m**

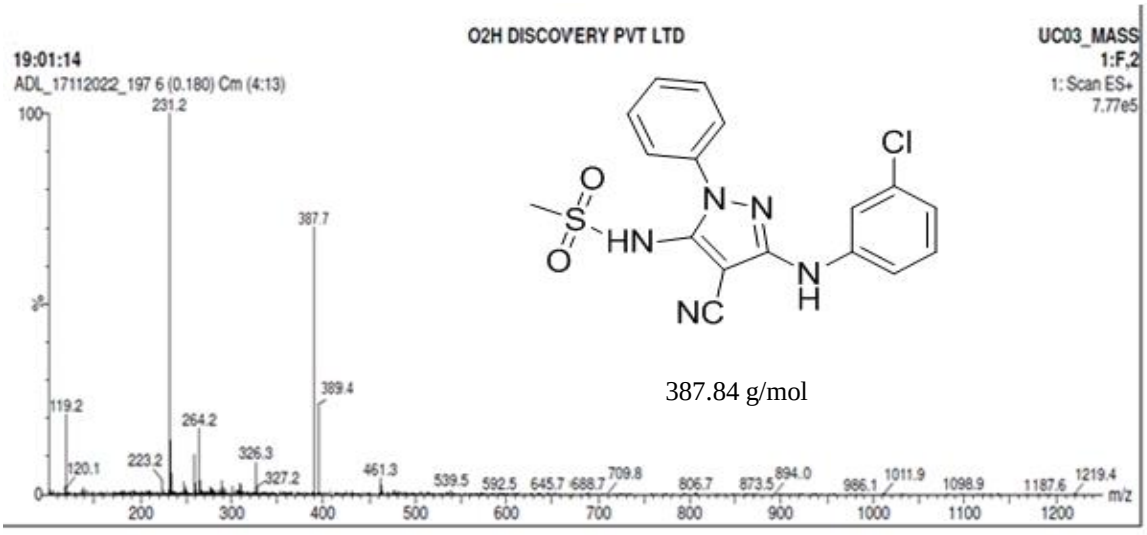

Fig.39: Mass spectrum of compound **6m**

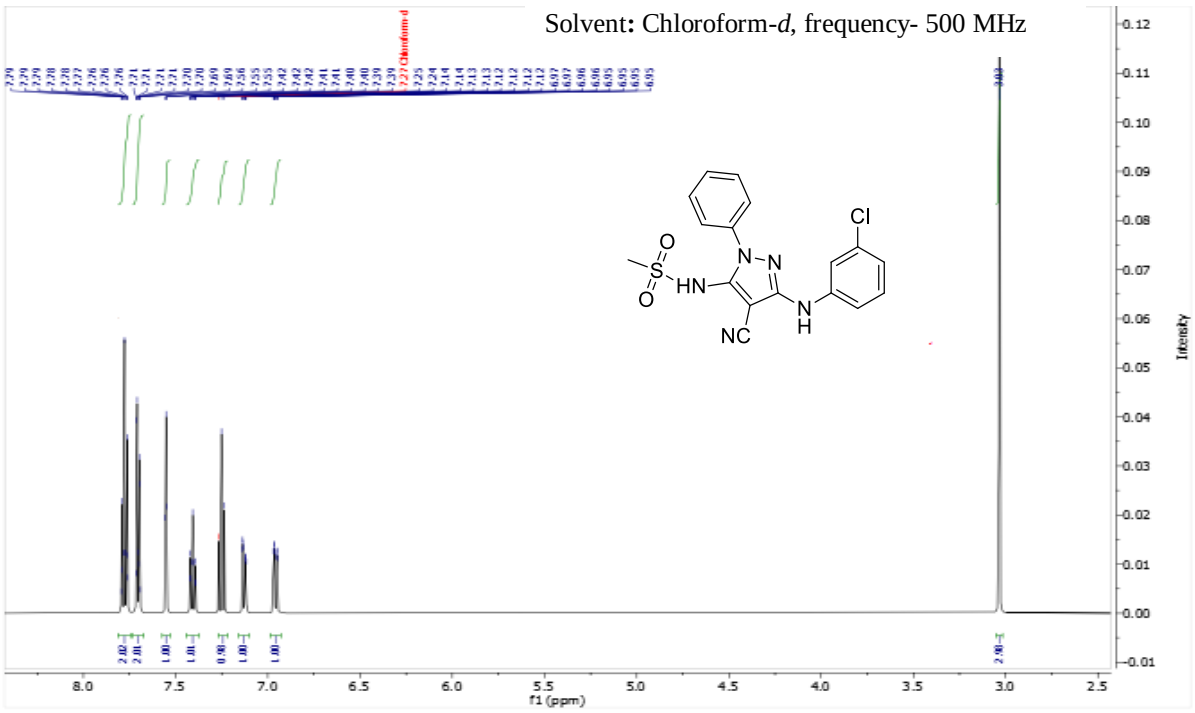

Fig.40: [1]HNMR spectrum of compound **6m**

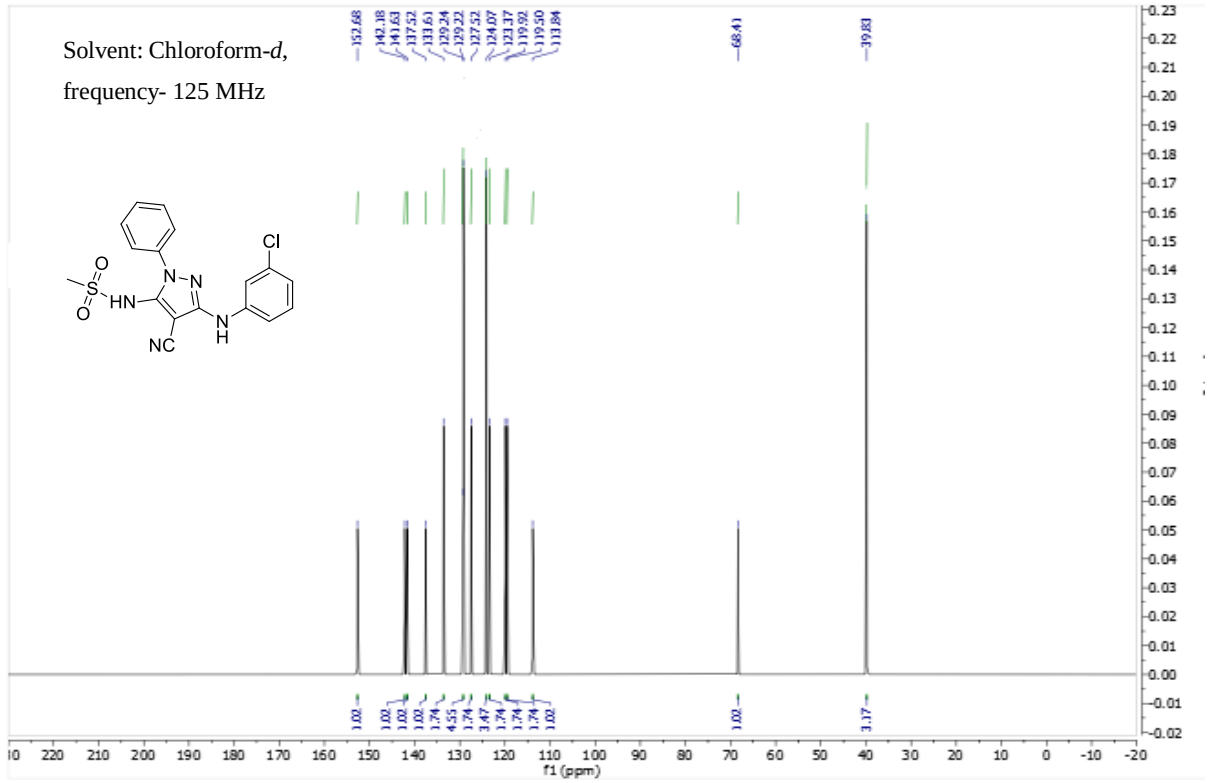

Fig.41: [13]C NMR spectrum of compound **6m**

4.8.3. IR, Mass, ^{1}H and ^{13}C NMR of compound 7g

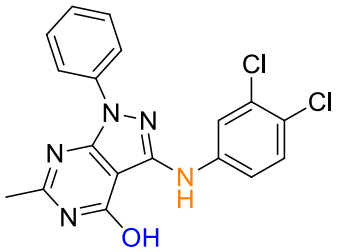

AIC-LMCP FOUNDATION

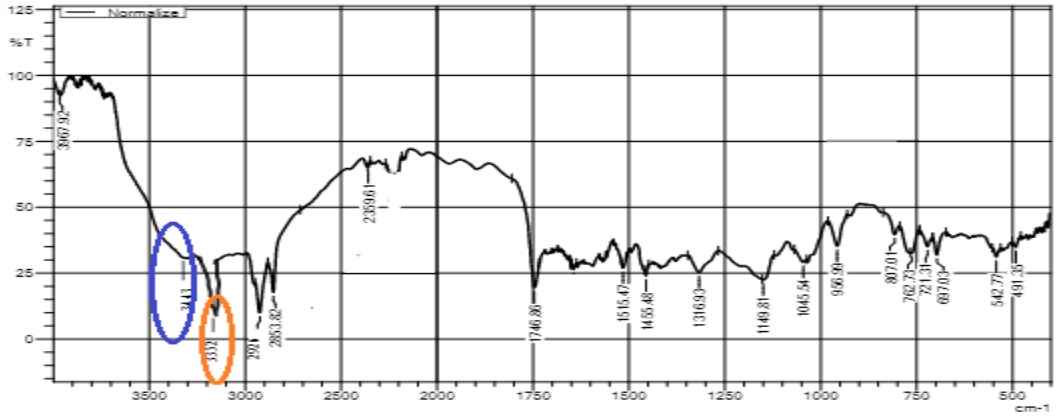

Fig.42: IR spectrum of compound **7g**

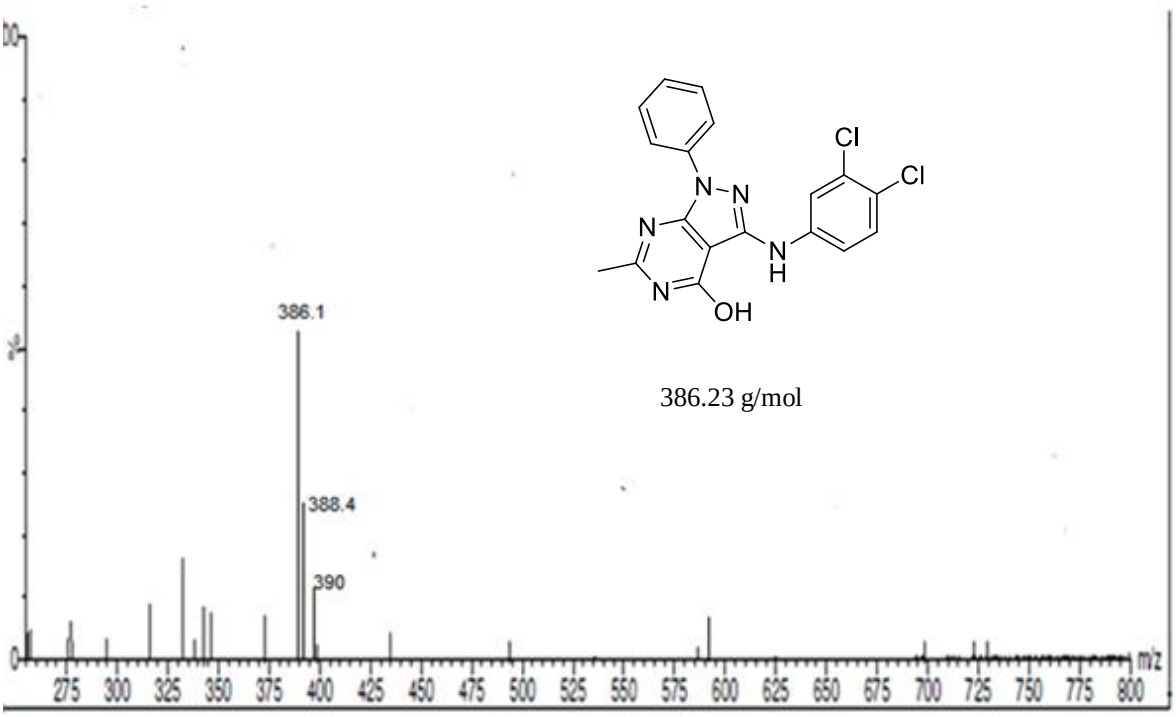

386.23 g/mol

Fig.43: Mass spectrum of compound **7g**

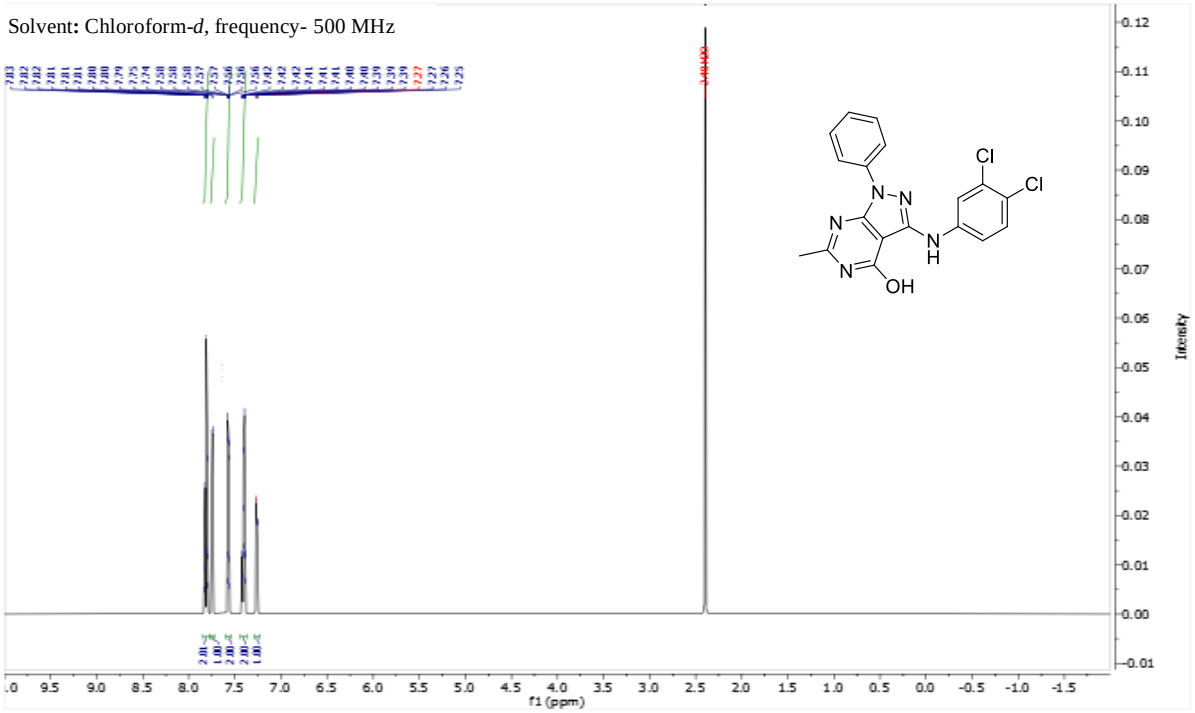

Fig.44: ^{1}HNMR spectrum of compound **7g**

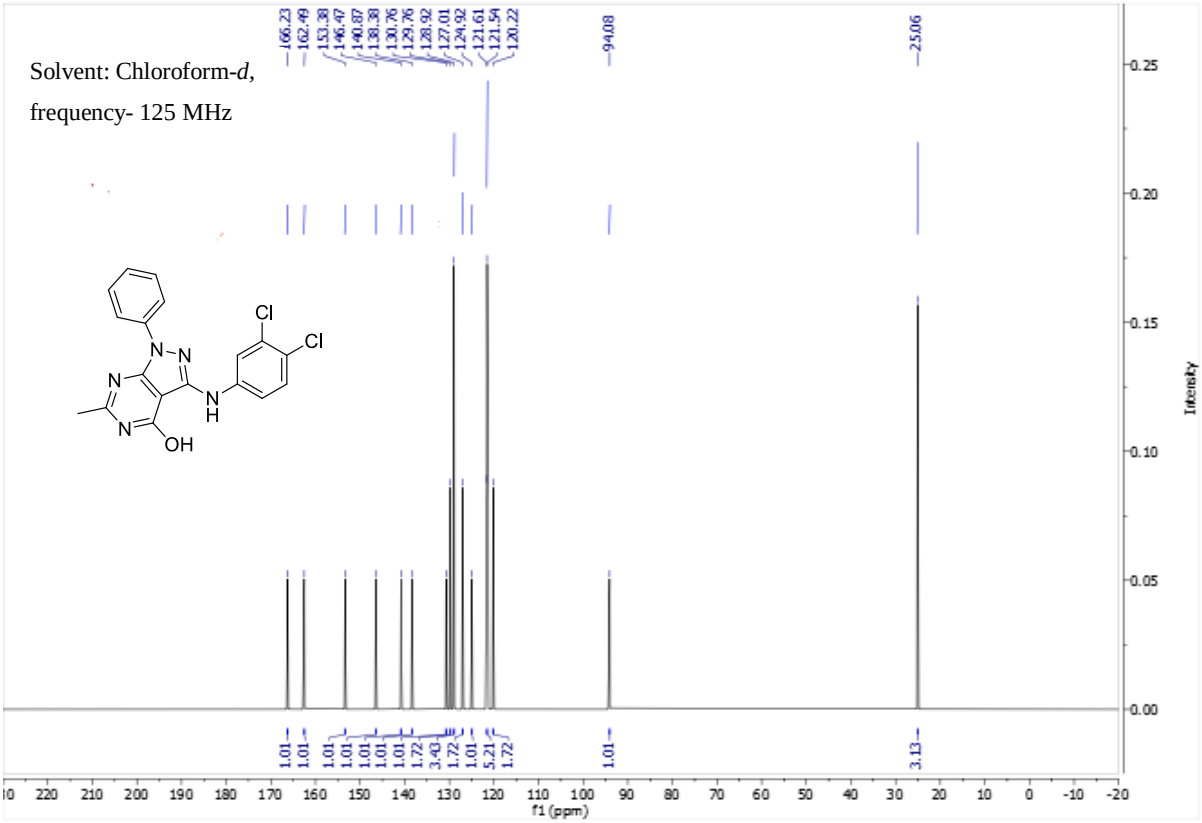

Fig.45: ^{13}C NMR spectrum of compound **7g**

4.8.4. IR, Mass, ^{1}H and ^{13}C NMR of Compound 7j

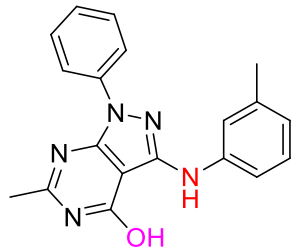

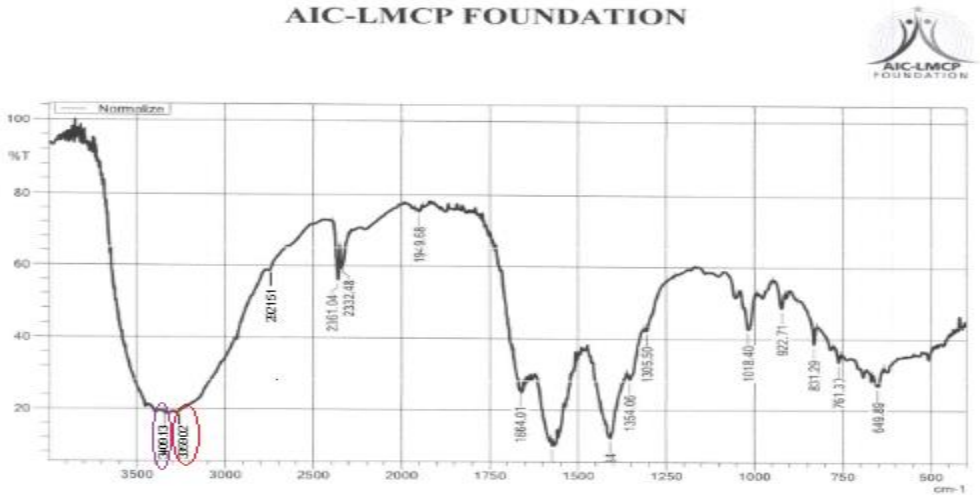

Fig.46: IR spectrum of compound **7j**

Mass spectra of compound 7j

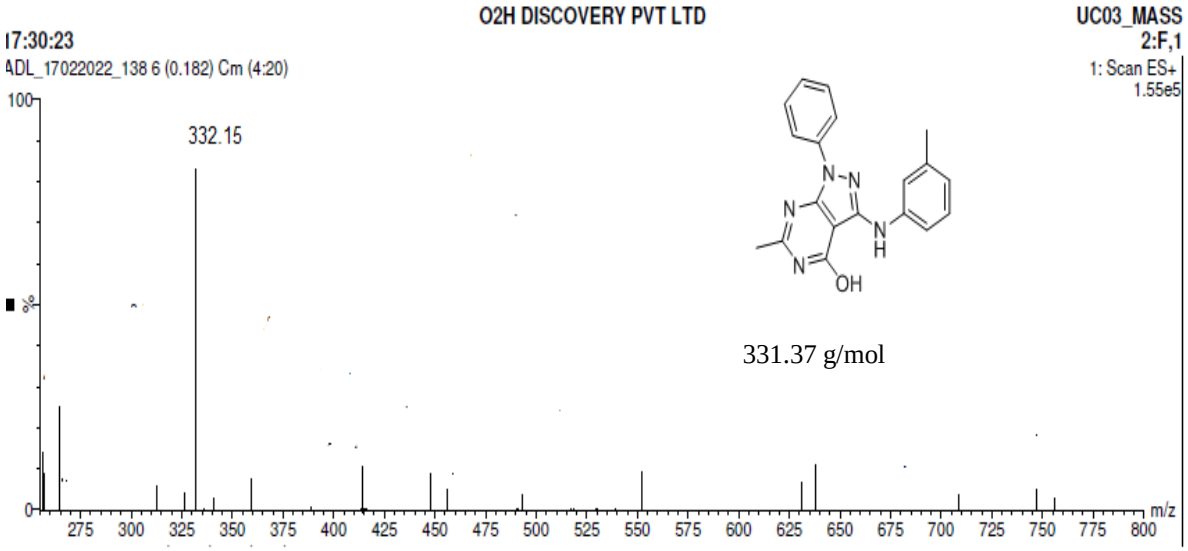

Fig.47: Mass spectrum of compound **7j**

[1]HNMR and [13]C NMR of compound 7j

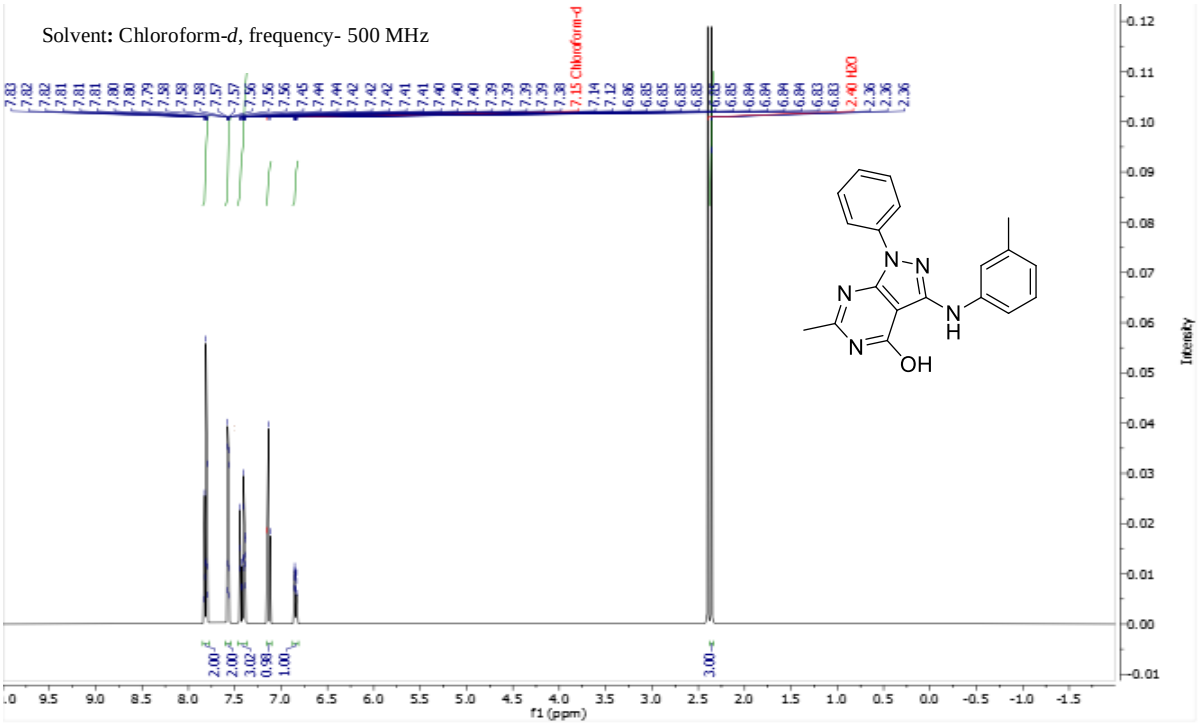

Fig.48: [1]HNMR spectrum of compound **7j**

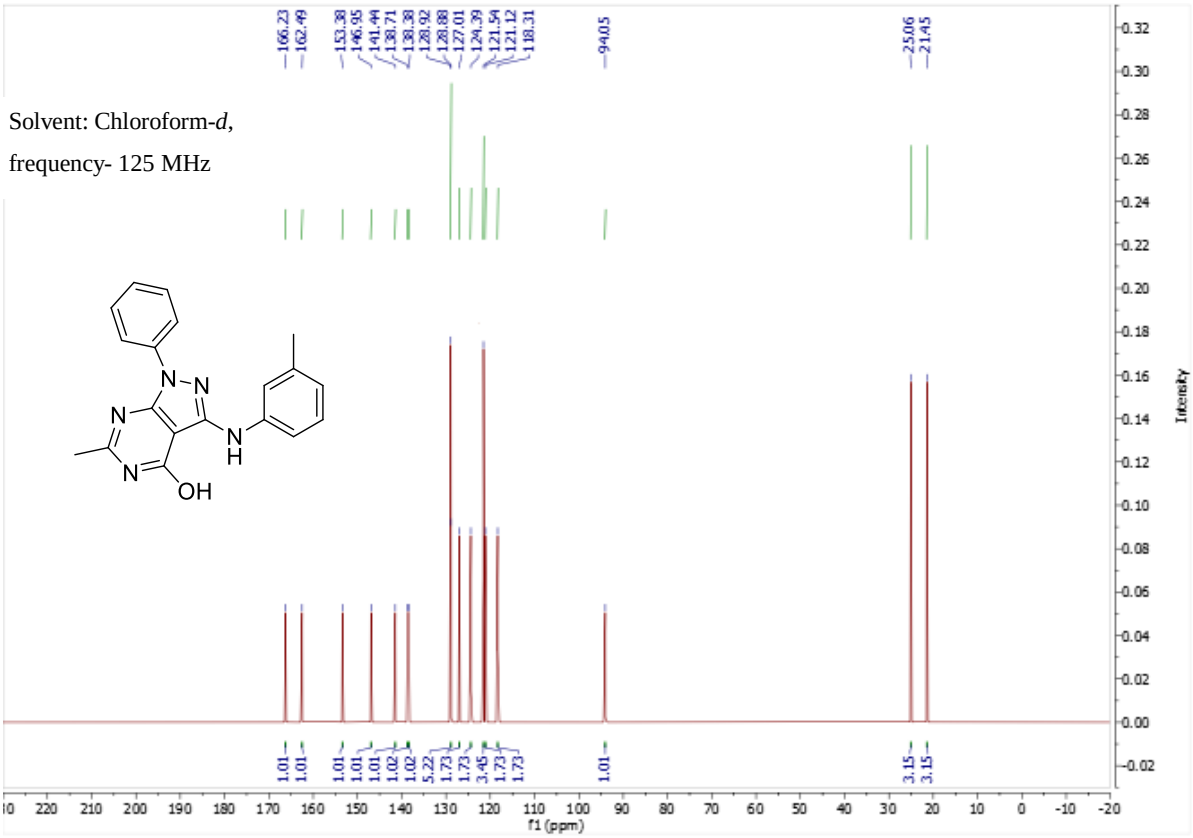

Fig.49: [13]C NMR spectrum of compound **7j**

4.9. Pharmacological screening

4.9.1. Microplate Almar Blue Assay

All the synthesized compounds were screened for their antimycobacterial activity by MABA (Micro-plate Almar Blue Assay) using H37Rv strain. This methodology is non-toxic, uses a thermally stable reagent and shows good correlation with propotional and BACTEC radiometric method.

4.9.1.1. Principle

Alamar blue is a reagent and accompanying assay used to quantify cellular metabolic activity. Taken at a single time point, it can be used to determine the concentration of viable cells in a sample. Taken at two or more time points of the same or similar samples, the assay can be used to measure cell growth kinetics the growth of a cell population over time.

The reagent solution contains the non-fluorescent blue coloured molecule resazurin which, when chemically reduced (a metabolic activity of cells), turns into the highly fluorescent pink-coloured resorufin. Both the colour change and the change in fluorescence allow for the direct measurement of cell metabolic activity via absorbance or fluorescence measurements in a plate reader (Brien et al., 2000).

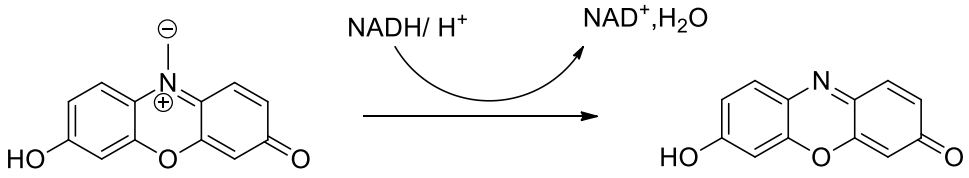

Resazurin (Blue) Resorufin (Pink)

4.9.2. Results of anti-tubercular activity

4.9.2.1. Anti-tubercular activity of standard drugs

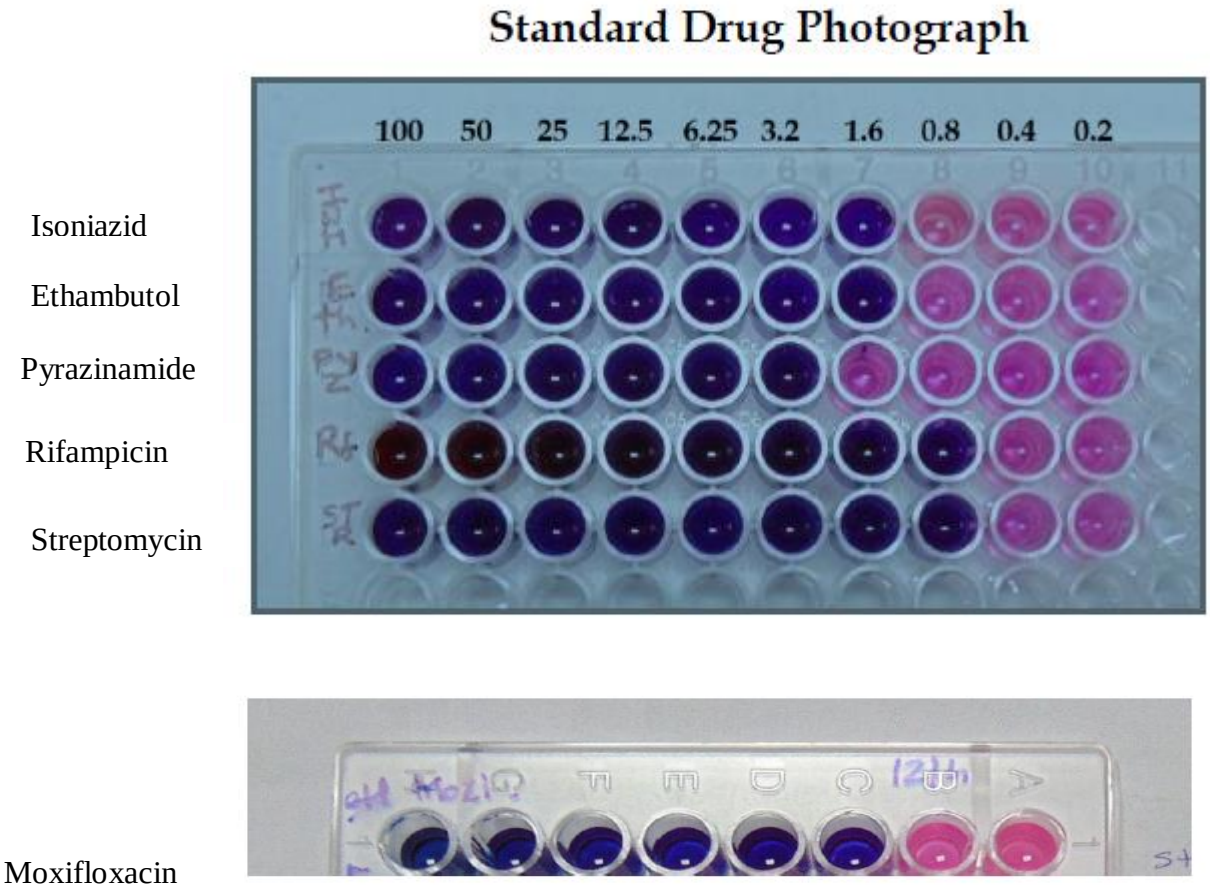

Fig.50: Biological activity of standard drugs

- Isoniazid – 1.6µg/mL
- Ethambutol – 1.6µg/mL
- Pyrazinamide- 3.125µg/mL
- Rifampicin – 0.8µg/mL
- Streptomycin- 0.8µg/mL
- Moxifloxacin- 0.8 µg/mL

4.9.2.2 Anti-tubercular activity of synthesized compounds

Anti-tubercular Activity of InhA inhibitors (Compounds 6a-o)

100 50 25 12.5 6.25 3.12 1.6 0.8

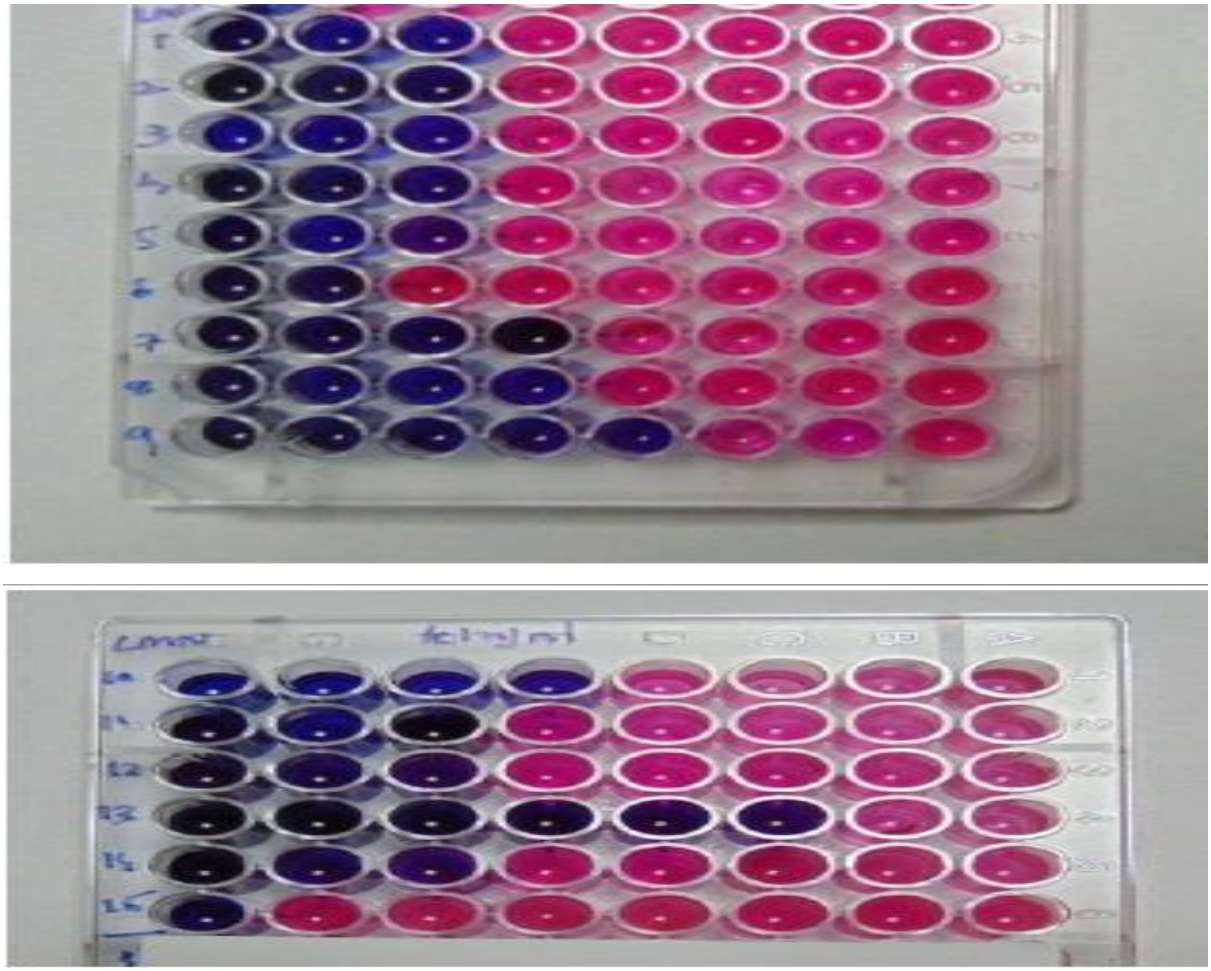

Fig.51: Antitubercular activity of compounds **(6a-o)**

Anti-tubercular Activity of DprE1 inhibitors(Compounds 7a-o)

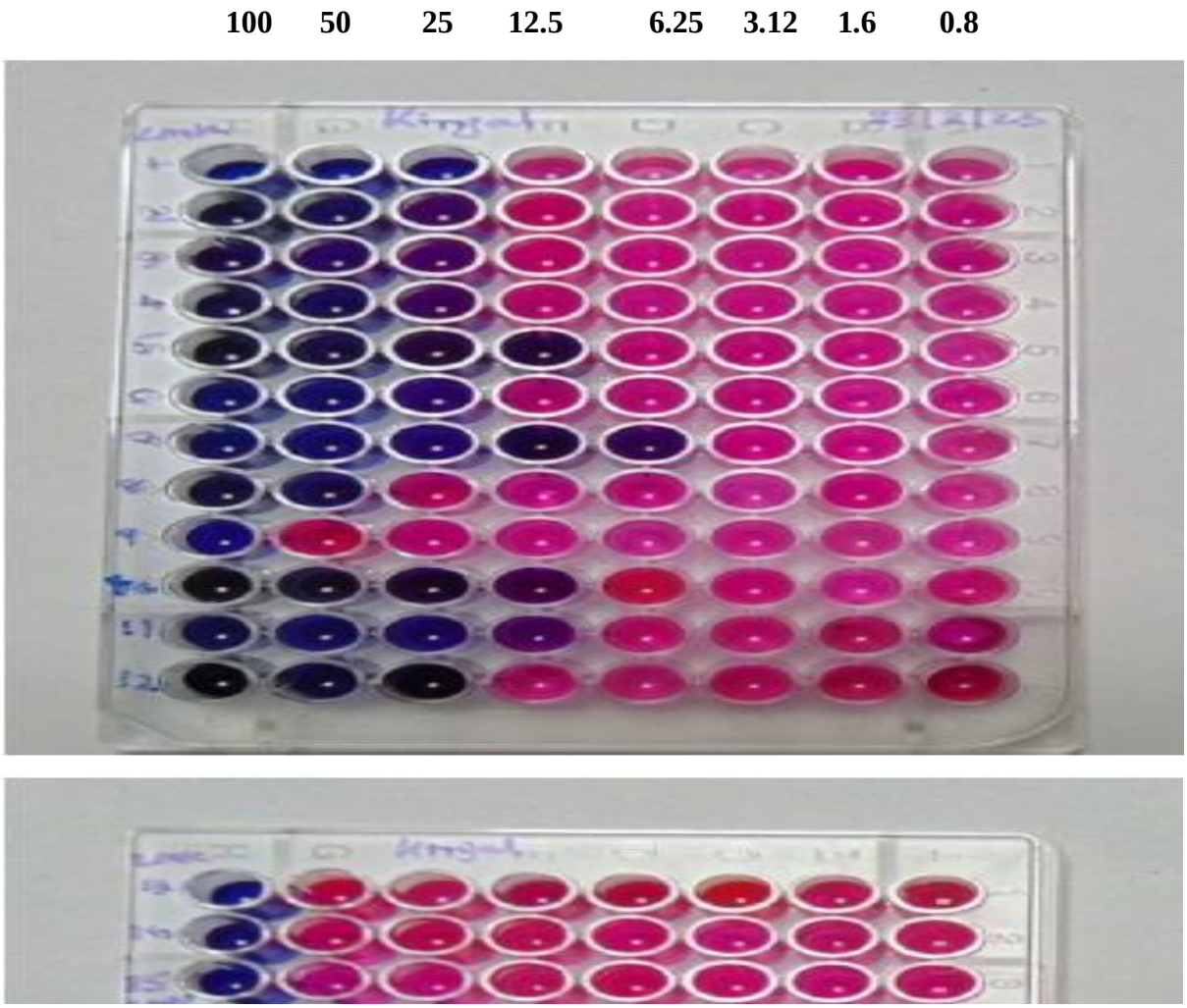

Fig.52: Antitubercular activity of compounds **(7a-o)**

Table-13: Anti-tubercular activity of synthesized compounds (6a-o) and (7a-o)

Compounds	**100 µg/mL**	**50 µg/mL**	**25 µg/mL**	**12.5 µg/mL**	**6.25 µg/mL**	**3.12 µg/mL**	**1.6 µg/mL**	**0.8 µg/mL**
6a	S	S	S	R	R	R	R	R
6b	S	S	S	R	R	R	R	R
6c	S	S	S	R	R	R	R	R
6d	S	S	S	R	R	R	R	R
6e	S	S	S	R	R	R	R	R
6f	S	S	R	R	R	R	R	R
6g	S	S	S	S	R	R	R	R
6h	S	S	S	S	R	R	R	R
6i	S	S	S	S	S	R	R	R
6j	S	S	S	S	R	R	R	R
6k	S	S	S	R	R	R	R	R
6l	S	S	S	R	R	R	R	R
6m	S	S	S	S	S	S	R	R
6n	S	S	S	R	R	R	R	R
6o	S	R	R	R	R	R	R	R
7a	S	S	S	R	R	R	R	R
7b	S	S	S	R	R	R	R	R
7c	S	S	S	R	R	R	R	R
7d	S	S	S	R	R	R	R	R
7e	S	S	S	S	R	R	R	R
7f	S	S	S	R	R	R	R	R
7g	S	S	S	S	S	R	R	R
7h	S	S	R	R	R	R	R	R
7i	S	R	R	R	R	R	R	R
7j	S	S	S	S	R	R	R	R
7k	S	S	S	S	R	R	R	R
7l	S	S	S	R	R	R	R	R
7m	S	R	R	R	R	R	R	R
7n	S	R	R	R	R	R	R	R
7o	S	R	R	R	R	R	R	R

S -Sensitive; R- Resistant

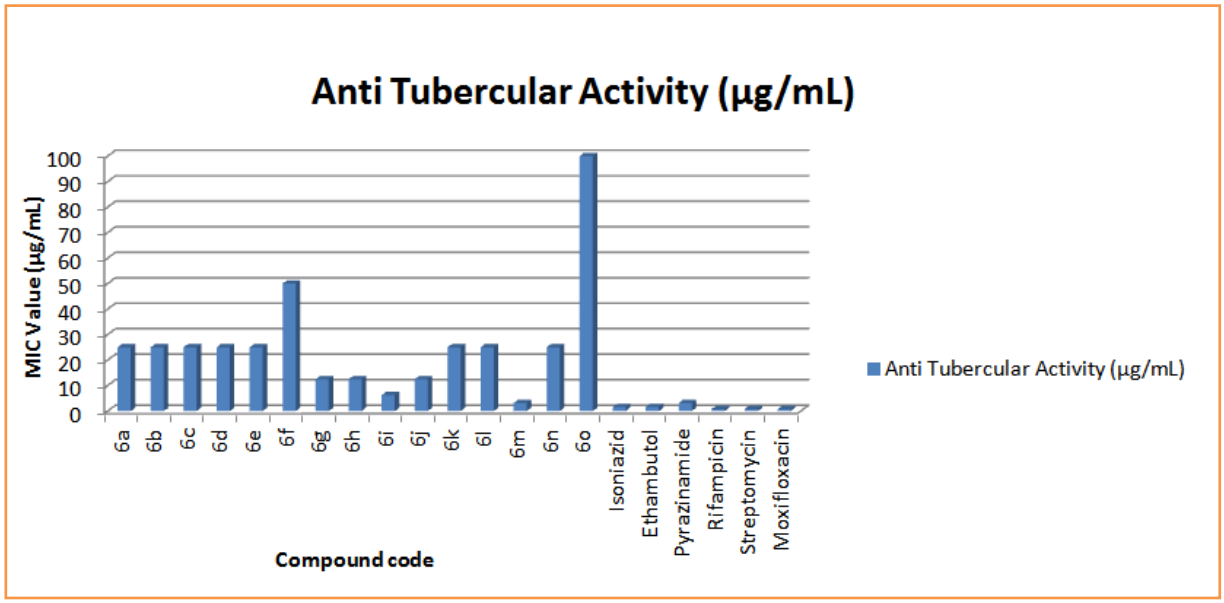

Fig.53: Graphical representation of anti-tubercular activity of InhA inhibitors **(6a-o)**

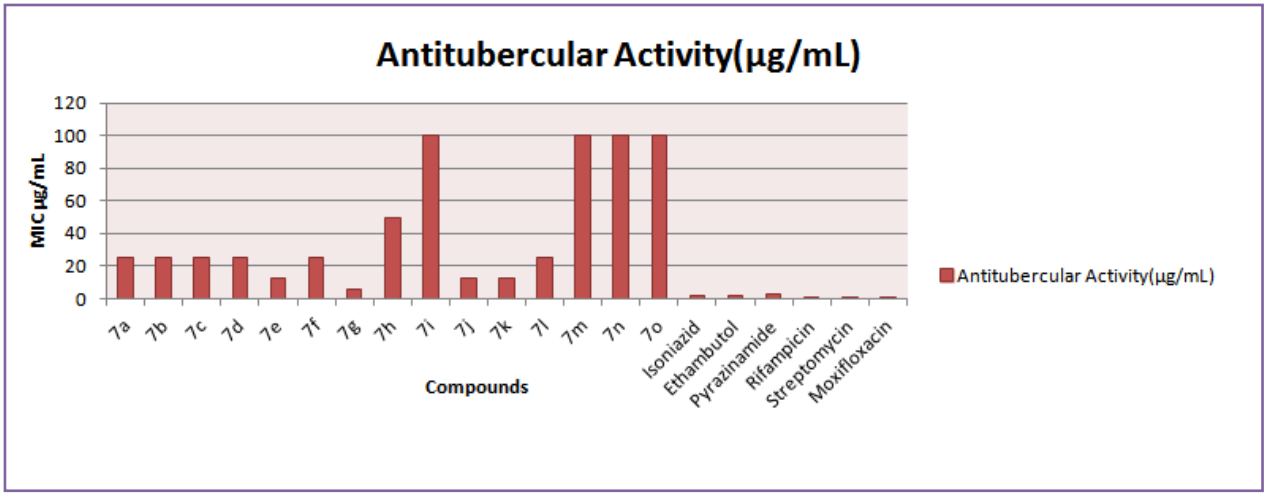

Fig.54: Graphical representation of anti-tubercular activity of DprE1inhibitors **(7a-o)**

Table -14: Anti-tubercular activities of synthesized compounds (6a-o), (7a-o) and standard drugs

Compounds	MIC (µg/mL) H37RV strain	Compounds	MIC (µg/mL) H37RV strain
6a	25	7a	25
6b	25	7b	25
6c	25	7c	25
6d	25	7d	25
6e	25	7e	12.5
6f	50	7f	25
6g	12.5	7g	6.25
6h	12.5	7h	50
6i	6.25	7i	100
6j	12.5	7j	12.5
6k	25	7k	12.5
6l	25	7l	25
6m	3.12	7m	100
6n	25	7n	100
6o	100	7o	100
Isoniazid	1.6	Isoniazid	1.6
Ethambutol	1.6	Ethambutol	1.6
Pyrazinamide	3.125	Pyrazinamide	3.125
Rifampicin	0.8	Rifampicin	0.8
Streptomycin	0.8	Streptomycin	0.8
Moxifloxacin	0.8	Moxifloxacin	0.8

4.10. Structure Activity Relationship (SAR)

The overall structure activity relationship is illustrated in Fig.55. Electron-withdrawing substitutions at R attached to pyrazole ring appears to be good anti-tubercular activity. Similarly, electron donating group at this place shown moderate anti-tubercular activity. Here, heteroaromatic rings like morpholine and piperidine at position R were found to have decrease the potency. On other side of pyrazole ring incorporation of acetyl chloride and thionyl chloride decreased the potency whereas benzoyl chloride, benzene sulfonyl chloride and methane sulfonyl chloride increase the antitubercular activity.

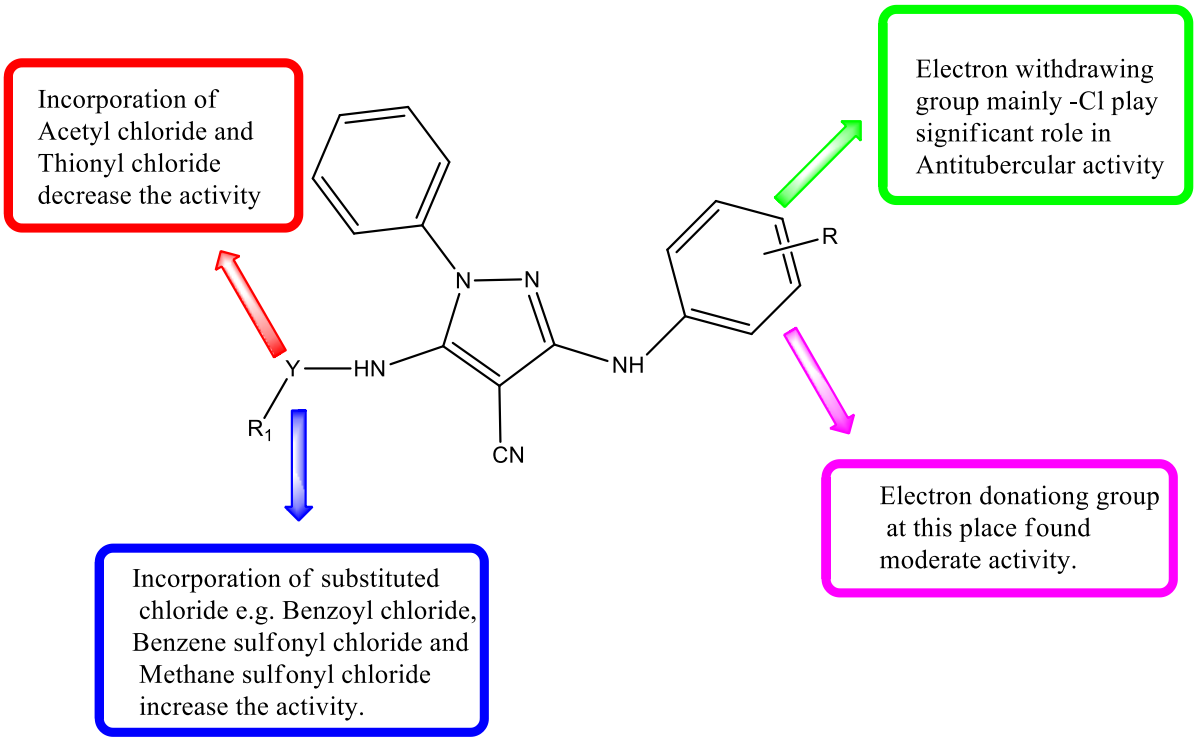

Fig.55: Structure activity relationship of compounds **(6a-o)**

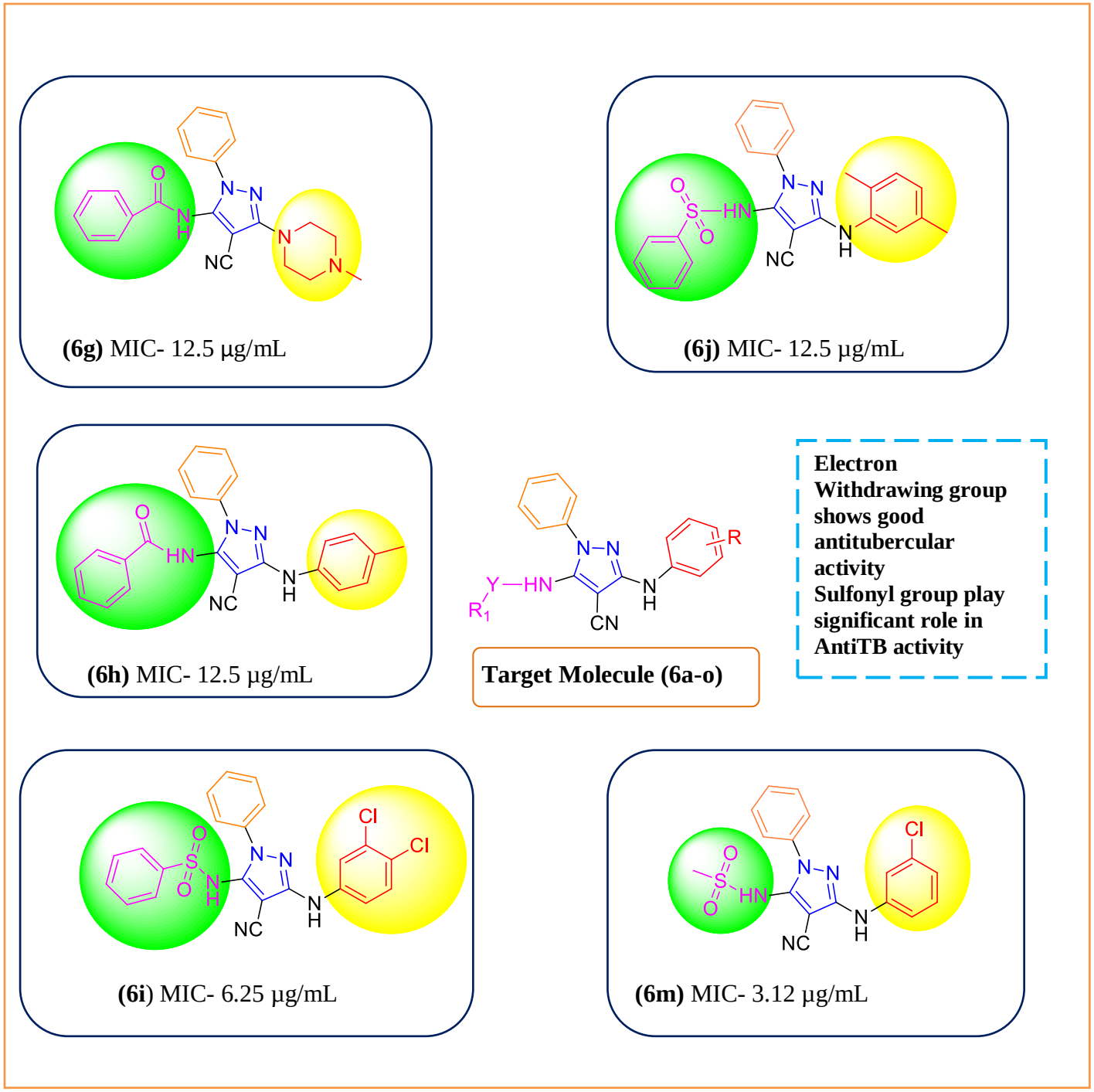

Fig.56: Schematic overview of most active compounds against *M. tuberculosis* H37Rv strain.

4.11. Rational for antioxidant activity and MTT assay

The inclusion of DPPH radical-scavenging data when studying anti-tuberculosis (anti-TB) compounds is mechanistically justified because oxidative stress plays a significant role in the primarily within macrophages, where it is exposed to reactive oxygen species (ROS) host–pathogen interaction during *Mycobacterium tuberculosis* infection. MTB resides generated as part of the host's innate immune response. Although the bacterium possesses robust antioxidant defences, excessive oxidative stress can contribute to host tissue damage, inflammation, and disease progression. Therefore, compounds with both anti-TB activity and antioxidant potential may offer dual therapeutic advantages.

The DPPH assay specifically measures the ability of a compound to donate hydrogen atoms or electrons to neutralize free radicals. This activity can reflect a compound's general antioxidant capacity, which is mechanistically relevant because certain anti-TB scaffolds exert their effects through redox modulation, ROS generation, or interference with MTB's own oxidative stress–management systems. Conversely, oxidative properties of a candidate molecule might contribute to antimicrobial potency but also raise concerns about cytotoxicity. Thus, characterizing antioxidant behaviour through DPPH helps predict redox-related pharmacological and toxicological profiles.

Additionally, some anti-TB agents, particularly natural products such as phenolics, flavonoids, or quinones, possess inherent redox-active groups. DPPH screening helps differentiate whether activity arises from direct antimycobacterial mechanisms or nonspecific radical-scavenging behaviour. It also informs structure-activity relationship (SAR) analyse by correlating functional groups responsible for redox behaviour with antimycobacterial potency.

Overall, DPPH data provide complementary mechanistic insight, supporting the rational design, optimization, and safety assessment of anti-TB compounds with potential redox-modulating effects. Furthermore, if the compounds are showing potent scavenging, then the compounds may be utilised for the anticancer purpose after performing its detailed cell line studies.

MTT assay in relation to anti-TB activity is that MTT measures cell viability/metabolic activity**,** which can be used to determine whether a test compound is cytotoxic to host cells and therefore whether it's apparent anti-TB effect is likely to be selective rather than simply due to general toxicity.

4.11.1. Antioxidant activity by DPPH assay method

The DPPH (2, 2-Diphenyl-1-picrylhydrazyl) technique is a standard laboratory test utilized to assess the antioxidant properties of plant extracts, food products, or pure substances. Antioxidant substances are commonly employed due to their capacity to release hydrogen or electrons to neutralize free radicals. The oxidative characteristics of a potential molecule may enhance antimicrobial effectiveness but also raise concerns about cytotoxic effects. Therefore, identifying antioxidant properties via the DPPH assay method helps to identify redox-related pharmacological and toxicological characteristics.

Furthermore, certain anti-tubercular drugs, especially natural compounds like flavonoids, phenolics, and quinones, contain intrinsic redox-active functionalities. DPPH assessment aids SAR studies by functional groups linking influencing to anti-tubercular effectiveness.

In conclusion, DPPH findings offer further mechanistic understanding and support the rational design of anti-tubercular agents that may have redox-modulating properties. Moreover, if the compounds demonstrate strong scavenging activity, they could be applied for anticancer purposes following comprehensive cell line investigations.

Free radicals are regarded as important for physiological processes. Radical interacts extensively with biomolecules found in living cells and can disrupt the cells usual physiological functions (Muluk et al., 2020). Consequently, antioxidant activities of the newly developed compounds **(6a-o)** and **(7a-o)** were evaluated through the DPPH method and compared with reference drugs ascorbic acid and curcumin.

Based on the findings from the DPPH test, according to the results obtained from the DPPH test, the best performing compounds were **6m** (43.01 %) and **6b** (25.90%). The moderate antioxidant activity 15.73 was shown by compound **6d** (Table-14). Compounds **7b** (19.37%) and **7d** (20.48%) exhibited good antioxidant activity, while compound **7e** (15.59%) demonstrated moderate antioxidant activity (Table-15). The percentage of inhibition indicates the free radical scavenging activity.

Table-15: DPPH scavenging activity (%) of synthesized compounds (6a-o)

Compounds	Compounds Concentration	DPPH Dye Concentration	%RSA (Radical Scavenging Activity)
6a	100 µM	100 µM	1.61
6b	100 µM	100 µM	25.90
6c	100 µM	100 µM	1.37
6d	100 µM	100 µM	15.73
6e	100 µM	100 µM	0.9
6f	100 µM	100 µM	3.47
6g	100 µM	100 µM	1.61
6h	100 µM	100 µM	1.20
6i	100 µM	100 µM	9.90
6j	100 µM	100 µM	1.60
6k	100 µM	100 µM	1.50
6l	100 µM	100 µM	1.60
6m	100 µM	100 µM	43.01
6n	100 µM	100 µM	5.89
6o	100 µM	100 µM	1.61
Ascorbic Acid	100 µM	100 µM	90.15
Curcumin	100 µM	100 µM	80.95

Table-16: DPPH scavenging activity (%) of synthesized compounds (7a-o)

Compounds	Compound Concentration	DPPH Dye Concentration	%RSA (Radical Scavenging Activity)
7a	100 µM	100 µM	12.69
7b	100 µM	100 µM	19.37
7c	100 µM	100 µM	4.01
7d	100 µM	100 µM	20.48
7e	100 µM	100 µM	15.59
7f	100 µM	100 µM	7.57
7g	100 µM	100 µM	6.90
7h	100 µM	100 µM	7.34
7i	100 µM	100 µM	12.91
7j	100 µM	100 µM	10.69
7k	100 µM	100 µM	7.10
7l	100 µM	100 µM	4.67
7m	100 µM	100 µM	2.00
7n	100 µM	100 µM	2.00
7o	100 µM	100 µM	2.00
Ascorbic Acid	100 µM	100 µM	90.15
Curcumin	100 µM	100 µM	80.95

4.12. Cytotoxicity by MTT assay

The potent abtitubercular compounds **6i**, **6m**, **7g** and **7j** were selected for cytotoxic activity through MTT assay on the HepG2 cell line. Table-17 and Table-18 represents the results of the cytotoxic study. The cytotoxicity values for compounds **6i** and **6m** are 125 ± 0.16 µM and 273.8 ± 0.05 µM**.** Compounds **7g** and **7j** were 71.63 ± 0.10 µM and 9.281 ± 0.20µM, respectively. Compounds **6i**, **6m** and **7g** demonstrated a relatively low toxicity profile against the HepG2 cell line.

Table-17: Cytotoxicity study on HepG2 cell line for compounds **6i** and **6m**

Comp.	**R**	**R_1**	**X**	**Anti-tubercular activity MIC (µg/mL)**	**Cytotoxicity IC_{50} µM**	**SI Index IC_{50}/MIC**
6i	3,4-di-Cl	$-C_6H_5$	O=S=O	6.25	125 ± 0.16	20
6m	3-Cl	$-CH_3$	O=S=O	3.12	273.8 ± 0.05	87.75

Table-18: Cytotoxicity study on HepG2 cell line for compounds **7g** and **7j**

Comp.	**R**	**Anti-tubercular activity MIC (µg/mL)**	**Cytotoxicity IC_{50} µM**	**SI Index IC_{50}/MIC**
7g	3,4-di-Cl	6.25	71.63 ± 0.10µM	11.46
7j	$3\text{-}CH_3$	12.5	9.281 ± 0.20µM	0.742

4.13. Molecular dynamic simulation

MD simulation enabled the exploration of dynamics of biomolecules, including protein-ligand complexes, across nm to µm timescales. Here in this study, the MD simulation was conducted to examine the ligand (**6m)** interactions with InhA enzyme (PDB ID- 4U0J) and **(7g)** interactions with the DprE1 enzyme (PDB ID: 4NCR) specifically over a duration of 100 ns. Molecular dynamics simulation, as it accounts for various binding conformations throughout the simulation process. MD simulations help in assessing interactions of protein and ligand at an atomic level. Enoyl acyl carrier protein reductase (InhA) and decaprenylphosphoryl-beta-D-ribose 2'-epimerase (DprE1) for 100ns to analyze the binding stability of protein-ligand complex. Structural alteration observed during the simulation process was evaluated through RMSD, RMSF, SASA, Rg, and hydrogen bond number (Nayee et al., 2026).

4.13.1. Root Mean Square Deviation (RMSD) analysis

RMSD offers to understand the alterations in the structure conformation during the simulation. RMSD captures the differences that exist between the original structure and the final structure of the simulation execution. Typically, a more compact deviation indicates that the structure is quite stable (Reuter & Martinez, 2011).

Fig. 57a illustrates the protein, ligand (**6m)** deviations, and the complex. The results indicate that (**6m)** exhibited a steep increase in deviation during the first 10 ns of the simulation, reflecting deviations from its docked pose. However, these deviations remained within 0.6 Å, indicating minimal structural alterations. At 15 ns, the RMSD of **6m** stabilized at approximately 0.5 Å, signifying the formation of stable interactions with the protein's active site residues and thus attaining convergence. This stability persisted until the end of the simulation, marking a successful simulation that effectively captured the binding modes of (**6m)**. Further changes in the order of 1-3 Å are acceptable for small and globular proteins and suggest no large conformational changes which are taking place (Pandey et al., 2022).

Fig. 58a demonstrated the deviations of protein, ligand **(7g),** and protein-ligand complex. Changes within the range of 1 to 3 Å are permissible for small and globular proteins, indicating that significant conformational alterations are not occurring (Pandey et al., 2022)(Nayee et al., 2026). Here, the compound exhibited similar deviations in the range of 1Å to 3Å indicating acceptable conformational changes.

4.13.2. Root mean square fluctuation (RMSF analysis)

In this study, the mean RMSF was approximately 0.1 nm (Fig.57b), with a maximum fluctuation observed at around 0.6 nm. The overall RMSF plot indicates reduced flexibility in the protein upon ligand (**6m)** binding. This reduction in flexibility may stabilize the protein structure and potentially hinder its ability to perform its intended biological activity, reflecting the ligand's inhibitory effects.

Analysis of RMSF indicates the dynamics of structural change of ligand and protein backbone and movement of specific atoms or atom groups in relation to the reference structure, averaged across all atoms. Both flexible and rigid residues in a protein play a crucial role in its biological function (Martínez, 2015). Here, the average RMSF value is around 0.1 nm (Fig.58b), exhibiting the highest variation of approximately 0.8 nm solely at the initial stage of the simulation. The overall RMSF graph shows decreased protein

flexibility upon ligand binding (**7g**). It could stabilize the protein structure and possibly restrict its capacity to carry out its biological function, suggesting inhibitory effects of the ligand.

4.13.3. Radius of gyration (Rg) analysis

The radius of gyration (Rg) values for (**6m)**, ranging from 1.18 to 1.18 nm (Fig.57c), suggest that the protein-ligand complex maintained a stable and compact conformation throughout the simulation. The radius of gyration of the compound (**7g)** varies from 2.2 to 2.3 nm (Fig. 58c), indicating that the complex of protein and ligand preserved a compact and stable structure during the simulation procedure. Stable radius of gyration values indicate slight changes in conformation, emphasizing the compactness and stability of the protein-ligand complex, essential for preserving functional integrity.

4.13.4. Solvent Accessible Surface Area (SASA) analysis

SASA assessment in MD simulation measures protein surface area that contacts solvents, indicating hydrophobic interactions between non-polar residues. These types of interactions protect the hydrophobic core from the nearby aqueous environment and stabilize the enzyme. It is essential for the inhibition of the enzyme (Khan et al., 2022). The SASA plot for (**6m)** revealed a mean SASA of approximately 135 nm^2 (Fig. 57d), which indicates a low level of surface exposure. This suggests that **6m** potentially interacts with key hydrophobic regions of the protein, facilitating stable binding. The graph of SASA for the compound (**7g)** showed an average SASA of around 215 nm^2 (Fig. 58d), suggesting a moderate degree of surface exposure. This indicates that the compound may engage with essential hydrophobic areas of the protein, promoting stable attachment. These interactions could be vital for the inhibitory activity of the ligand on the enzyme and stabilization of the protein-ligand complex.

4.13.5. Hydrogen bonding analysis

In MD simulation, analysis of hydrogen bonds reveals the frequency, lifespan, and geometry of non-covalent interactions, essential for assessing structural stability and dynamics. In the case of (**6m)**, the analysis revealed an average of nearly two hydrogen bonds throughout the 100ns trajectory. During the first 10ns, a smaller deviation (~0.6Å) was observed (Fig. 57a and 57e), indicating fewer hydrogen bonds at this stage, suggesting initial adjustments in ligand positioning within the binding site.

As the simulation progressed, (**6m)** formed stable hydrogen bonds with the active site residues of Mtb enoyl reductase, reinforcing its stable binding within the active site. This pattern highlights the importance of hydrogen bonding in maintaining the ligand conformation and its therapeutic potential.

The hydrogen bond distribution plot shows that most hydrogen bonds occur within a 0.2–0.3 nm range (Fig. 57f), indicating strong and stable interactions. This supports the stable binding of (**6m)** with the protein throughout the simulation**.**

The analysis of hydrogen bonds showed initial spikes in the number of hydrogen bonds, with 4-3 bonds between 0-20 ps, followed by 5-4 bonds from 40-60 ps. (Fig. 57e). This suggests that the ligand undergoes significant conformational adjustments and establishes multiple interactions with the protein in the early stages of the simulation. As the progress of the simulation, the number of hydrogen bonds reduced to 1-2, indicating that at the end of the simulation process, the ligand and protein have a stable binding conformation. This pattern reflects the ligand's transition from an initial adjustment phase to a more stable, energetically favourable binding mode. The plot of hydrogen bond distribution indicates that the majority of hydrogen bonds form within the range of 0.2–0.4. (Fig. 57f), suggesting interactions that are moderately stable.

The molecular dynamics simulation of compound (**7g)** with DprE1 revealed important insights concerning the stability of the complex. RMSD of compound (**7g)** displayed an acceptable level of deviations, indicating a stable binding interaction. RMSF suggested a decrease in the flexibility of the protein when binding occurred, indicating the possible inhibitory effect of the ligand. The Rg and SASA values show a stable and compact complex structure, with compound **(7g)** engaging with hydrophobic regions.

Finally, the analysis of hydrogen bond revealed stable protein- ligand binding interactions, especially in the 0.2–0.4 nm range. These findings indicate that compound (**7g)** establishes stable binding interactions with the protein, increasing therapeutic inhibitory activity (Nayee et al., 2026)

The MD simulation of compound (**6m)** with Mtb enoyl reductase with DprE1 revealed key findings regarding the binding stability of the complex. RMSD analysis showed compound **(6m)** had minimal deviations, signifying stable binding event. The RMSF analysis indicated a reduction in protein flexibility upon binding, reflecting the ligand's potential inhibitory effect.

The radius of gyration (Rg) values and SASA analysis indicated a compact and stable conformation of the complex, with compound **6m** and **7g** interacting with hydrophobic regions.

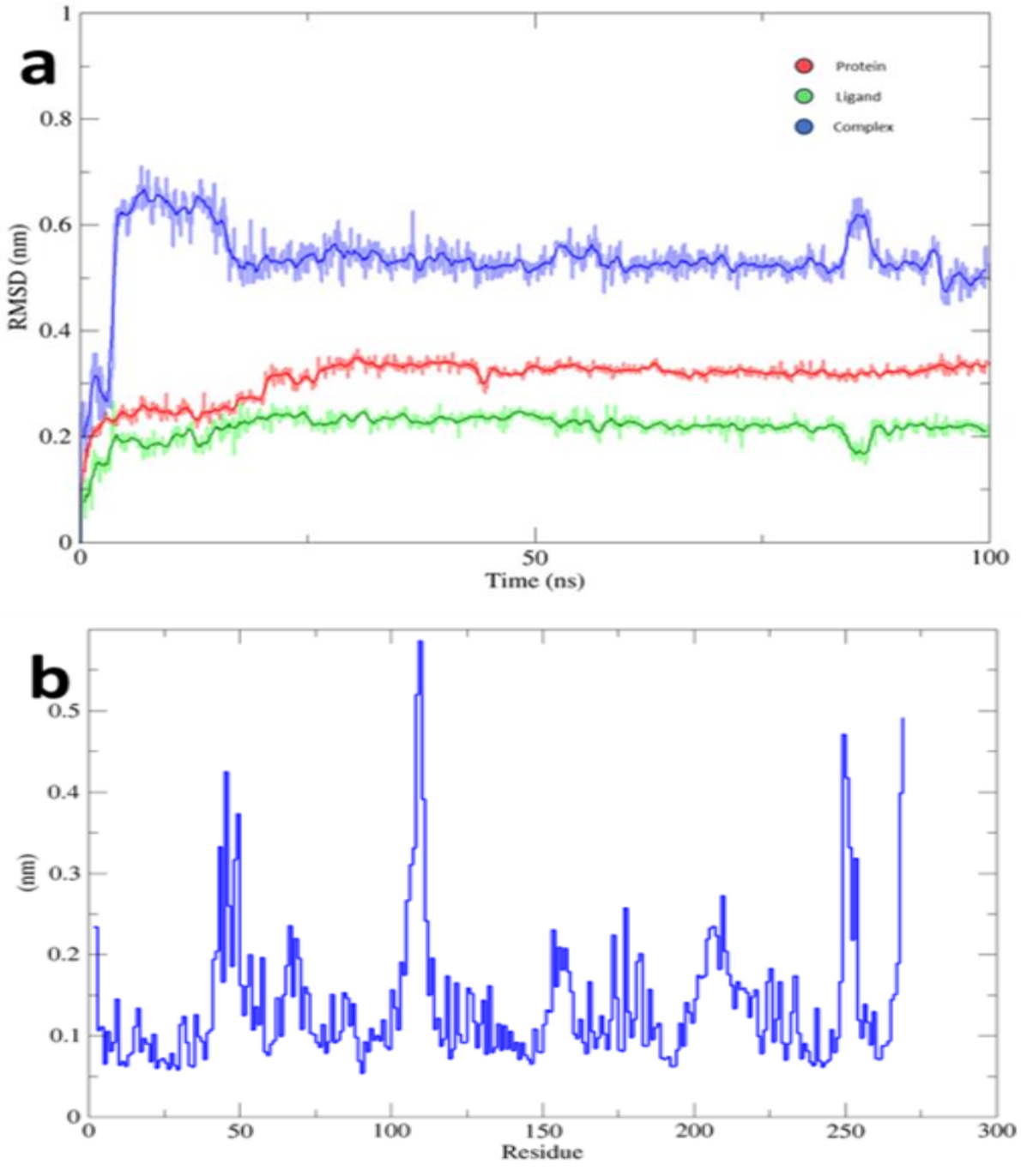

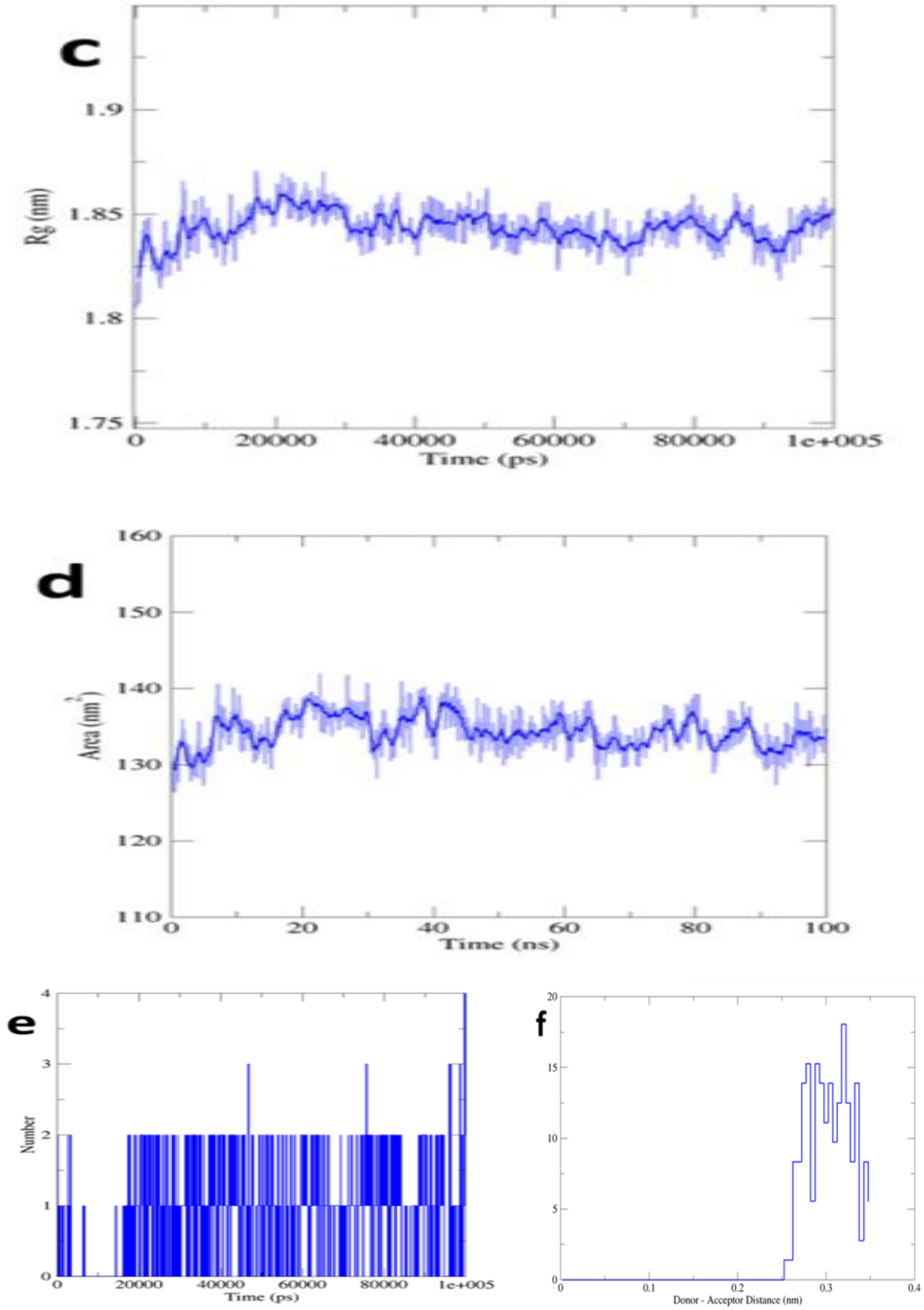

Fig. 57: MD analysis, a) RMSD, b)RMSF, c).Radius of gyration, d) SASA, e) Hydrogen bonding number and f) hydrogen bonding distance for compound **(6m)**

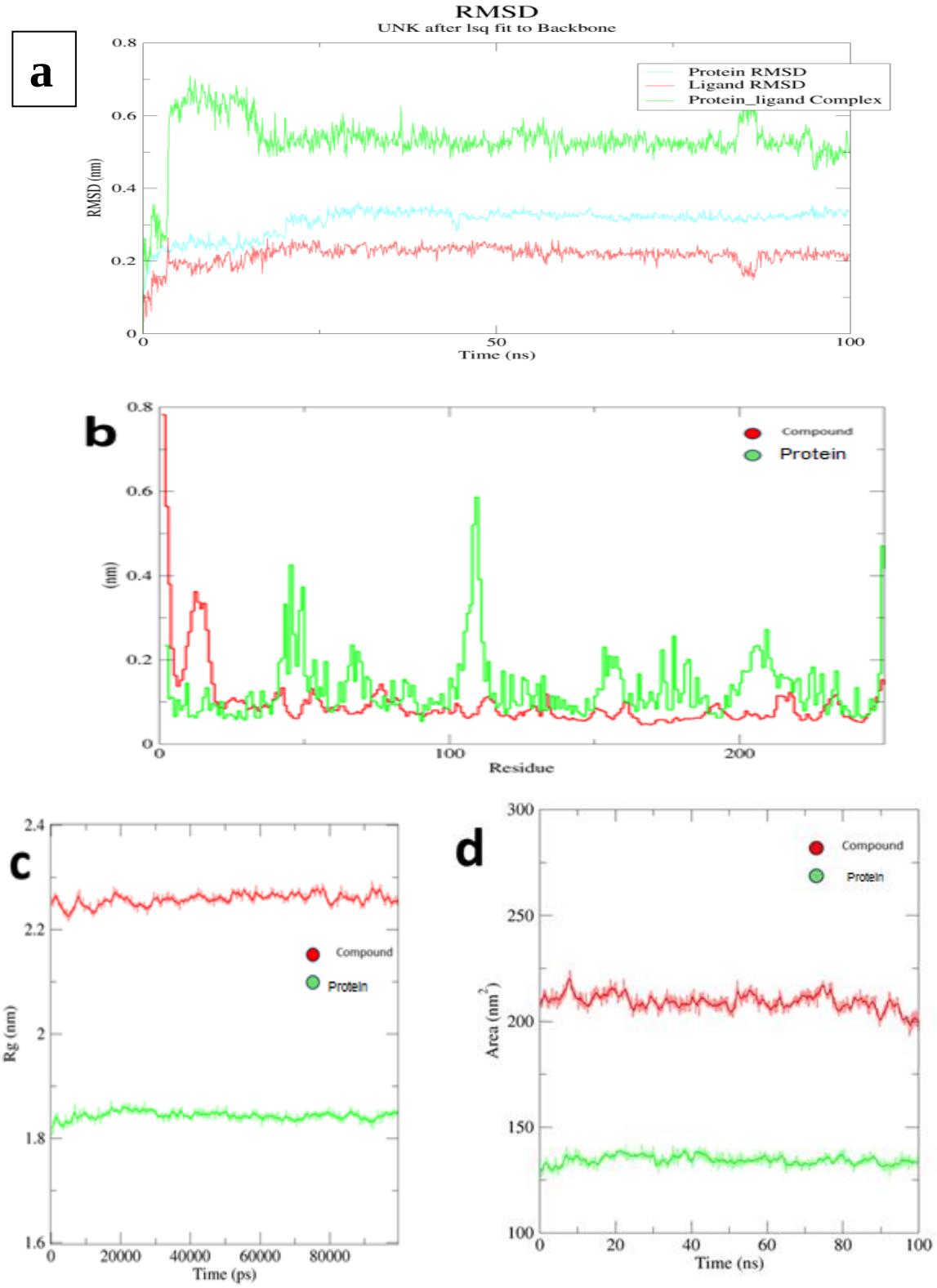
a
RMSD
UNK after lsq fit to Backbone
Protein RMSD
Ligand RMSD
Protein_ligand Complex
RMSD (nm)
Time (ns)
b
Compound
Protein
(nm)
Residue
c
Compound
Protein
Rg (nm)
Time (ps)
d
Compound
Protein
Area (nm²)
Time (ns)

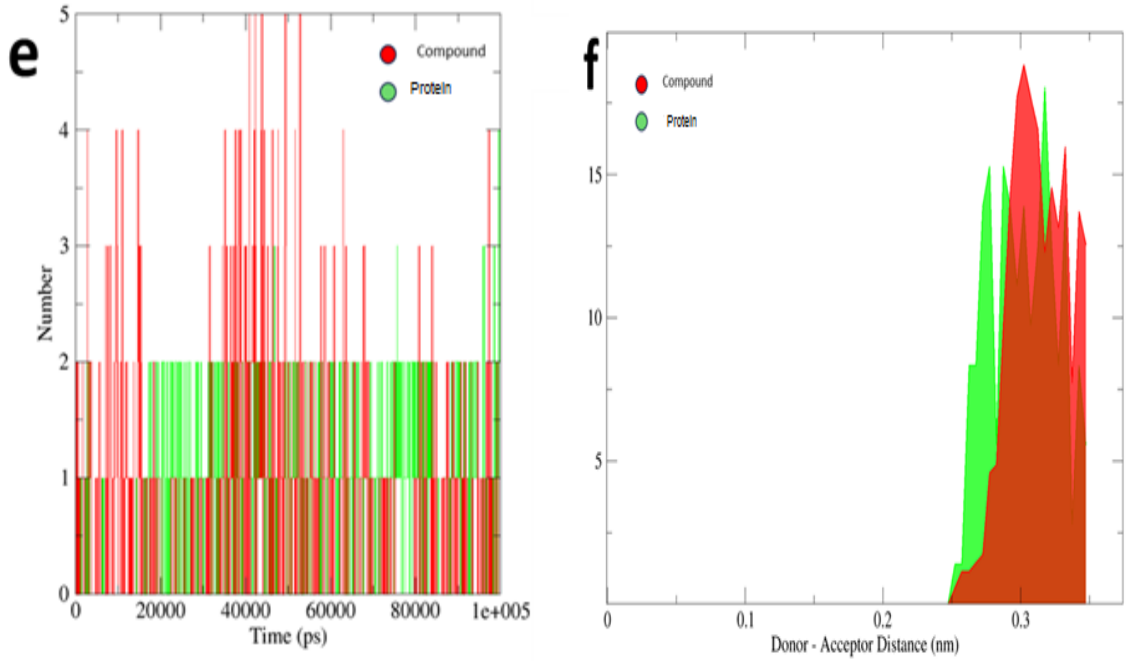

Fig.58: MD analysis, **a**. RMSD, **b**. RMSF, **c.** Radius of gyration, **d**. SASA, **e**. Hydrogen bonding number and **f**. hydrogen bonding distance for compound **(7g)**

4.14. ADMET properties

Using the pkCSM and Swiss ADME web tools, understand the ADMET parameters of compounds **(6a-o)** and **(7a-o)**. Molecular properties and drug likeness parameters are illustrated in Table-19 and Table-21. Lipinski's rule of five specifies thorough drug-like attributes, if logP <5, molecular weight <500, H-bond acceptors <10, and H-bond donors <5 (Khaldan et al., 2023). The rule of five indicates that a compound is expected to achieve bioavailability and permeability. Table-20 and Table 22 indicates the effective absorption and penetration of compounds **(6a-o)** and **(7a-o)**. The findings from the pharmacokinetic studies indicate that the compounds **(6a-o)** and **(7a-o)** are absorbed effectively, permeable, and exhibit drug-like characteristics. Additional assessment was conducted employing the bioavailability score (ABS) criteria (Martin, 2005). The bioavailability score is 0.55. Moreover, the synthetic probability was checked by a scale in the range of 1 (very easy) to 10 (extremely difficult).

Furthermore, the compounds have good intestinal absorption, ranging from 90.09% to 96.95%, more than 30% of the minimum values required. The permeability > 0.3 to <- 1 log BB and log PS > -2 indicates that the substance can penetrate the CNS (Martin, 2005)(Nayee

et al., 2026).

The data shown in Table-22 indicated that compounds **(7a-o)** demonstrated a strong likelihood to penetrate into the blood-brain barrier. Examining drug metabolism is important because it reveals how the changes of drugs are changed in the body by enzymatic processes. The metabolic processes of drugs are managed by CYP families 1A2, 2C19, 2C9, 2D6, and 3A4. On the other hand, the more persistent the drug is in the body, the lower the clearance value. Furthermore, the compounds **(6a-o)** and **(7a-o)** possess a degree of toxicity. Finally, the compounds exhibited acceptable ADMET characteristics. The Ames test has been utilized to determine if a molecule is mutagenic. Except for molecules **6c**, **6e**, **6h**, **6i**, **6j**, **6n** and **6o** all the molecules were found to be no toxic. Molecules **7c**, **7e**, **7f**, **7g**, **7h**, and **7l** were identified as non-toxic. Additionally, all the molecules examined were toxic to the liver. In terms of oral rat acute toxicity, compounds with smaller LD50 values are more lethal than compounds with larger LD50.

Table-19: Molecular properties descriptors and lead-likeness of the InhA inhibitors (6a-o)

Comp.	**Molecular Formula**	**Mol. wt. g/mol**	**HBA**	**HBD**	**mlogP**	**Synthetic accessibility**	**Bioavailability score**	**Lipinski violation**	**Drug likeness**
6a	$C_{18}H_{14}ClN_5O$	351.79	3	2	2.89	2.99	0.55	0	YES
6b	$C_{19}H_{17}N_5O_2$	347.37	4	2	1.69	3.08	0.55	0	YES
6c	$C_{16}H_{17}N_5O_2$	311.34	4	1	1.07	2.91	0.55	0	YES
6d	$C_{19}H_{17}N_5O$	331.37	3	2	2.62	3.05	0.55	0	YES
6e	$C_{23}H_{16}FN_5O$	397.40	4	2	3.94	3.18	0.55	0	YES
6f	$C_{21}H_{19}N_5O_2$	373.41	4	1	2.28	3.12	0.55	0	YES
6g	$C_{22}H_{22}N_6O$	386.45	4	1	2.49	3.23	0.55	0	YES
6h	$C_{24}H_{19}N_5O$	393.44	3	2	3.78	3.30	0.55	0	YES
6i	$C_{22}H_{15}Cl_2N_5O_2S$	484.36	4	2	3.85	3.60	0.55	0	YES
6j	$C_{24}H_{21}N_5O_2S$	443.52	4	2	2.91	3.79	0.55	0	YES
6k	$C_{22}H_{15}Cl_2N_5O_2S$	484.36	4	2	3.85	3.63	0.55	0	YES
6l	$C_{18}H_{17}N_5O_2S$	367.42	4	2	1.52	3.32	0.55	0	YES
6m	$C_{17}H_{14}ClN_5O_2S$	387.84	4	2	1.79	3.27	0.55	0	YES
6n	$C_{17}H_{14}ClN_5O_2S$	387.84	4	2	1.79	3.29	0.55	0	YES
6o	$C_{15}H_{16}ClN_5OS$	349.84	3	1	1.87	3.53	0.55	0	YES

Table-20: ADME Properties of Compounds (6a-o)

comp	Absorption	Distribution		Metabolism CYP Inhibitor					Excretion	Toxicity		
	Intestinal absorption (human)	log BB	logPS	CYP 1A2	CYP 2C19	CYP 2C9	CYP 2D6	CYP 3A4	Total Clearance	AMES	LD50	Hepatotoxicity
6a	90.015	-0.272	-1.905	YES	YES	YES	NO	YES	-0.129	NO	2.447	YES
6b	87.673	-0.126	-2.165	YES	YES	YES	NO	YES	0.185	NO	2.891	YES
6c	95.612	-0.526	-2.531	NO	YES	NO	NO	NO	0.344	YES	2.602	YES
6d	91.473	-0.097	-1.945	YES	YES	YES	NO	YES	0.149	NO	2.44	YES
6e	92.275	-0.114	-1.751	YES	YES	YES	YES	YES	-0.107	YES	2.586	YES
6f	95.883	-0.498	-2.247	YES	YES	YES	NO	YES	0.265	NO	2.32	YES
6g	93.75	-0.268	-2.186	YES	NO	NO	NO	YES	0.358	NO	2.433	YES
6h	92.88	0.094	-1.605	YES	YES	YES	NO	YES	0.064	YES	2.515	YES
6i	100	-0.398	-1.762	YES	YES	YES	NO	YES	-0.018	YES	2.753	YES
6j	95.735	-0.023	-1.736	YES	YES	YES	NO	YES	0.252	YES	2.325	YES
6k	100	-0.523	-1.761	YES	YES	YES	NO	YES	0.12	NO	2.766	YES
6l	91.009	-0.312	-2.215	YES	YES	YES	NO	YES	0.246	NO	2.796	YES
6m	91.717	-0.487	-2.175	YES	YES	YES	NO	YES	0.027	NO	2.762	YES
6n	91.674	-0.489	-2.168	YES	YES	YES	NO	YES	0.237	YES	2.745	YES
6o	92.031	-0.64	-2.273	YES	YES	NO	NO	NO	0.006	YES	2.969	YES

Table-21: Molecular properties descriptors and lead-likeness of the amino substituted 6-methyl-1-phenyl-1*H*- pyrazolo[3,4-d]pyrimidin-4-ol compounds (7a-7o)

Comp.	**Molecular Formula**	**Molecular weight gm/mol**	**HBA**	**HBD**	**mlogP**	**Synthetic accessibility**	**Bioavailability score**	**Lipinski violation**	**Drug likeness**
7a	$C_{18}H_{14}ClN_5O$	351.79	4	2	3.39	3.02	0.55	0	YES
7b	$C_{18}H_{14}ClN_5O$	351.79	4	2	3.53	2.97	0.55	0	YES
7c	$C_{19}H_{17}N_5O_2$	347.37	5	2	2.59	3.05	0.55	0	YES
7d	$C_{19}H_{17}N_5O$	331.37	4	2	3.26	3.01	0.55	0	YES
7e	$C_{18}H_{14}FN_5O$	335.34	5	2	3.28	2.94	0.55	0	YES
7f	$C_{16}H_{17}N_5O_2$	311.34	5	1	1.97	2.91	0.55	0	YES
7g	$C_{18}H_{13}Cl_2N_5O$	386.23	4	2	4.03	3.02	0.55	0	YES
7h	$C_{20}H_{19}N_5O$	345.40	4	2	3.76	3.17	0.55	0	YES
7i	$C_{18}H_{13}Cl_2N_5O$	386.23	4	2	4.29	3.06	0.55	1	YES
7j	$C_{19}H_{17}N_5O$	331.37	4	2	3.53	3.01	0.55	0	YES
7k	$C_{18}H_{14}ClN_5O$	351.79	4	2	3.80	3.00	0.55	0	YES
7l	$C_{19}H_{17}N_5O_2$	347.37	5	2	3.00	3.08	0.55	0	YES
7m	$C_{17}H_{19}N_5O$	309.37	4	1	3.01	2.88	0.55	0	YES
7n	$C_{18}H_{14}FN_5O$	335.34	5	2	3.68	3.02	0.55	0	YES
7o	$C_{17}H_{20}N_6O$	324.38	5	1	2.22	3.03	0.55	0	YES

Table-22: ADME Properties of Compounds (7a-o)

Comp.	**Absorption**	**Distribution**		**Metabolism Inhibitors CYP**					**Excretion**	**Toxicity**		
	Intestinal absorption (human)	log BB	logPS	CYP 1A2	CYP2 C19	CYP2 C9	CYP2 D6	CYP 3A4	Total Clearance	AMES	LD50	Hepatotoxicity
7a	92.691	0.042	-2.146	YES	YES	YES	NO	NO	0.227	YES	3.282	YES
7b	91.797	0.151	-1.922	YES	YES	YES	NO	YES	-0.026	YES	2.824	YES
7c	95.567	-0.035	-2.475	YES	YES	NO	NO	YES	0.168	NO	3.05	YES
7d	93.256	-0.394	-1.962	YES	YES	NO	NO	YES	0.153	YES	2.828	YES
7e	94.073	-0.019	-2.343	YES	YES	NO	NO	NO	0.022	NO	3.054	YES
7f	96.954	-0.832	-2.661	YES	YES	NO	NO	NO	0.483	NO	2.335	YES
7g	90.956	-0.567	-1.847	YES	YES	YES	NO	YES	0.158	NO	3.07	YES
7h	92.997	-0.26	-1.976	YES	YES	NO	NO	YES	0.173	NO	3.406	YES
7i	90.09	-0.594	-1.895	YES	YES	NO	NO	YES	0.279	YES	3.347	YES
7j	93.433	-0.261	-2.071	YES	YES	NO	NO	NO	0.161	YES	3.461	YES
7k	91.974	-0.437	-2.03	YES	YES	NO	NO	YES	0.014	YES	3.424	YES
7l	93.709	-0.464	-2.349	YES	NO	NO	NO	YES	0.187	NO	3.36	YES
7m	95.215	0.07	-2.297	YES	YES	NO	NO	NO	0.519	YES	2.381	YES
7n	91.96	-0.47	-2.209	YES	NO	NO	NO	YES	-0.073	YES	3.385	YES
7o	94.751	-0.746	-2.6	YES	NO	NO	NO	NO	0.389	YES	2.47	YES

CHAPTER-5

EXPERIMENTAL

CHPTER-5

5. EXPERIMENTAL

General

- Melting points of all synthesized compounds were determined by open capillary tube method. The obtained melting point result was uncorrected.
- TLC (Thin layer chromatography) was used to identify the progress of the reaction.
- KBr utilizing the Shimadzu FT-IR 8400S and Perkin-Elmer LC-MS PE Sciex API/65 were used for IR and mass spectra analysis.
- A Bruker 500 MHz and 125 MHz spectrometer using solvent CDCl3 (Chloroform-d) was used for ^{1}H and ^{13}C NMR spectra analysis. The chemical shift value is represented in ppm.
- Autodock Vina was utilized for docking, while Gromacs YASARA commercial software was utilized for molecular dynamics simulation. Biovia Discovery Studio 2021 software was used for the pose visualization of the structural docked complex.
- Online web software, Swiss ADME and pkCSM, were utilized to check drug likeness and ADMET characteristics.

5.1. Procedure for the synthesis of 2-(bis(methylthio)methylene)malononitrile (S,S acetal) (2)

2-bis(methylthio)methylenemalononitrile(2) was prepared according to the reported procedure (Chavan et al., 2016). 0.2 mol of potassium hydroxide was mixed into 10 mL of water and agitated for 15 minutes. 15ml of dimethylformamide was introduced to this reaction mixture while maintaining cooling and continuously stirred for 20 min. malononitrile**(1)** 0.1 mol was incorporated into the mixture of reaction and stirred for 30 minutes again under cooling conditions. Carbon disulfide (0.1 mol) and dimethyl sulphate (0.2 mol) were added dropwise under continuously stirring and cooling conditions. The progress of the reaction was monitored by TLC using n-hexane and ethyl acetate as the mobile phase. After completion of the reaction, the mixture was transferred into crushed ice. The crude product was filtered and washed with water to obtain a colourless crystalline product **(2)** M.P 60- 64 ^{0}C , Yield-89%.

5.2. Procedure for the synthesis of 2-((methylthio)(amino substituted)methylene) malononitrile (S, N acetal) (3a–o)

Compound **(2)** (0.017) mol was mixed with 20 mL of isopropyl alcohol. Aryl amine (0.017 mol) was incorporated, and it was refluxed for 6 to 7 hours at 50-60 ^{0}C. The progress of reaction was monitored by TLC using n-hexane and ethyl acetate as the mobile phase. After completion of the reaction, it was cooled to ambient temperature and transferred to crushed ice. The crude solid product obtained was filtered and recrystallized from methanol to yield the compounds**(3a–o)**(Baraldi et al., 2003). Yield-70-80%.

5.3. Procedure for the synthesis of 5-amino-3-(amine substituted)-1-phenyl-1*H*-pyrazole-4-carbonitrile (4a-o)

0.01 mol of compounds **(3a-o)** was mixed with phenyl hydrazine (0.01 mol) and heated at 70 to 80 ^{0}C for 1 hrs. After that, ethanol was added and refluxed for 2 to 3 hrs (Sherbiny et al., 2021). The progress of reaction was monitored by TLC using n-hexane and ethyl acetate as the mobile phase. After completion of the reaction, it was cooled to ambient temperature and obtained crude solid product was recrystallized with ethanol, yielding compounds **(4a-o)**. Yield: 75-85%.

5.4. Procedure for the synthesis of N-(4-cyano-1-phenyl-(amino substituted)-1*H*-pyrazol-5-yl)acetamide (5a-o)

Compounds **(5a-o)** were synthesized through the reaction of compounds **(4a-o)** and acetyl chloride. 0.01 mol of compounds (**4a-o)**, 0.02 mol acetyl chloride, pyridine, and ethanol was heated under reflux for 4 to 5 hours at 50 to 60 °C. Reaction progress was monitored by TLC. Solid crude product formed was collected through filtration and recrystallized using ethanol to yield the pure crystalline compounds **(5a-o)**. Yield: 70-85%.

5.5.1. General procedure for the synthesis of acid chloride substituted pyrazole derivatives(6a-d)

Compounds **(6a-o)** were prepared via the reaction of 5-amino-3-(amine substituted)-1-phenyl-1*H*-pyrazole-4-carbonitrile **(5a-d)** with acetyl chloride. Mixture of **5a-d** (0.01mol), pyridine and acetyl chloride (0.02mol) was refluxed in ethanol for 4-5 hrs. at 50-60 ^{0}C. Reaction completion was confirmed by TLC. Reaction mixture was cooled to room temperature. The precipitated solid was filtered and recrystallized from ethanol to obtain pure crystalline product.

5.5.2. General procedure for the synthesis of acid chloride substituted pyrazole derivatives (6e-o)

A mixture of compound **(5e-o)** (0.01 mol), ethanol (15 ml), substituted acid chloride (0,04 mol) and NaOH was stirred and reflux for 6-8 hrs. TLC was used to monitored the progress reaction. Upon completion, the reaction mixture was cooled and poured into crushed ice–water mixture. The resulting solid obtained was collected by filteration, thoroughly washed with water, and dried. The crude product obtained was recrystallized from ethanol to afford the pure crystalline product**.**

5.5.1.1. Synthesis of N-(3-((4-chlorophenyl)amino)-4-cyano-1-phenyl-1*H*-pyrazol-5-yl) acetamide (6a)

Mixture of 5-amino-3-((4-chlorophenyl)amino)-1-phenyl-1*H*-pyrazole-4-carbonitrile (0.01mol), pyridine and acetyl chloride(0.02mol) was refluxed in ethanol for 4-5 hrs. at 50-60 ^{0}C. Reaction completion was confirmed by TLC. Reaction mixture was cooled to room temperature. The precipitated solid was filtered and recrystallized from ethanol to obtain pure crystalline product.

Molecular formula	$C_{18}H_{14}ClN_5O$
Molecular weight	351.79
Colour	Brown
% Yield	80%
Melting point	162-165^{o}C
TLC (mobile phase)	n-Hexane: ethyl acetate 5:5
R_f value	0.70
IR (KBr, cm^{-1})	3240(NH str.), 1656(CO-NH str.), 2225(CN str.
Mass (m/z)	352.2, 353.4(M+2)
^{1}H NMR ($CDCl_3$,δ ppm)	2.19 (s, 3H), 7.81-7.78 (m, 7H), 7.77 - 7.65 (m, 1H), 7.55-7.53 (m, 1H), 7.42-7.37 (m, 2H)
^{13}C NMR ($CDCl_3$,δ ppm)	169.46, 153.17,144.53, 139.67, 137.97, 129.26, 128.87, 127.51, 127.48, 124.06, 122.30, 114.13, 66.17, 24.00
Structure	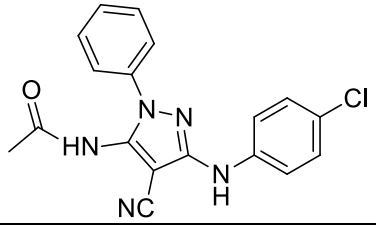

5.5.1.2. Synthesis of N-(4-cyano-3-((4-methoxyphenyl)amino)-1-phenyl-1*H*-pyrazol-5-yl)acetamide (6b)

Mixture of 5-amino-3-((4-methoxyphenyl)amino)-1-phenyl-1*H*-pyrazole-4-carbonitrile (0.01mol), pyridine and acetyl chloride(0.02mol) was refluxed in ethanol for 4-5 hrs. at 50-60 ^{0}C. Reaction completion was confirmed by TLC. Reaction mixture was cooled to room temperature. The precipitated solid was filtered and recrystallized from ethanol to obtain pure crystalline product.

Molecular formula	$C_{19}H_{17}N_5O_2$
Molecular weight	347.37
Colour	Dark brown
% Yield	82%
Melting point	110-112^{o}C
TLC (mobile phase)	n-Hexane: ethyl acetate 5:5
R_f value	0.71
IR (KBr, cm^{-1})	3245(NH str.), 1670 (CO-NH str.), 2220 (CN str.), 1242 (Aromatic-CO)
Mass (m/z)	348.2
^{1}H NMR ($CDCl_3$,δ ppm)	2.19 (s, 3H), 8.12-8.10 (m, 2H), 7.81-7.77 (m, 2H),7.67-7.66 (m, 2H),7.42-7.39 (m, 1H), 7.00-6.96 (m, 2H), 3.80 (s, 3H)
^{13}C NMR ($CDCl_3$,δ ppm)	169.46, 156.01, 153.13, 144.53, 137.97, 135.32, 129.26, 127.51, 124.06, 121.85, 114.80, 114.13, 66.17, 55.35, 24.00
Structure	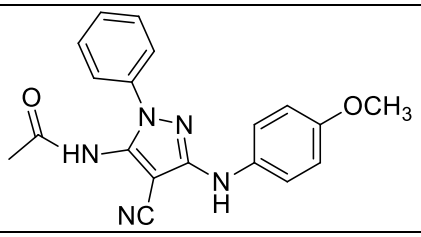

5.5.1.3. Synthesis of N-(4-cyano-3-morpholino-1-phenyl-1*H*-pyrazole-5-yl)acetamide(6c)

Mixture of 5-amino-3-morpholino-1-phenyl-1*H*-pyrazole-4-carbonitrile (0.01mol), pyridine and acetyl chloride(0.02mol) was refluxed in ethanol for 4-5 hrs. at 50-60 ^{0}C. Reaction completion was confirmed by TLC. Reaction mixture was cooled to room temperature. The precipitated solid was filtered and recrystallized from ethanol to obtain pure crystalline product.

Molecular formula	$C_{16}H_{17}N_5O_2$
Molecular weight	311.34
Colour	Brown
% Yield	89%
Melting point	137-139 ^{o}C
TLC (mobile phase)	n-Hexane: ethyl acetate 5:5
R_f value	0.75
IR (KBr, cm^{-1})	3326(NH str.), 1628 (CO-NH str.), 2208 (CN str.)
Mass (m/z)	311.4
^{1}H NMR ($CDCl_3$,δ ppm)	2.27 (3H, s),7.80-7.77 (m, 2H), 7.70-7.68 (m, 2H), 7.42- 7.39 (m, 1H), 3.86-3.74 (m, 8H)
^{13}C NMR ($CDCl_3$, δ ppm)	169.38, 159.79,144.81, 138.29, 129.27, 127.51, 124.00, 113.22, 67.78, 66.36, 48.26, 24.00
Structure	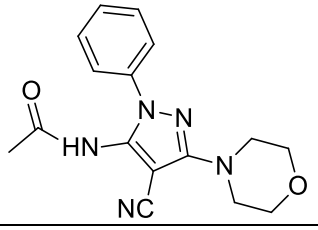

5.5.1.4. Synthesis of N-(4-cyano-1-phenyl-3-(p-tolylamino)-1*H*-pyrazol-5-yl)acetamide(6d)

Mixture of 5-amino-1-phenyl-3-(p-tolylamino)-1*H*-pyrazole-4-carbonitrile(0.01mol), pyridine and acetyl chloride(0.02mol) was refluxed in ethanol for 4-5 hrs. at 50-60 ^{0}C. Reaction completion was confirmed by TLC. Reaction mixture was cooled to room temperature. The precipitated solid was filtered and recrystallized from ethanol to obtain pure crystalline product.

Molecular formula	$C_{19}H_{17}N_5O$
Molecular weight	331.37
Colour	brown
% Yield	83%
Melting point	141-143 ^{o}C
TLC (mobile phase)	n-Hexane: ethyl acetate 5:5
R_f value	0.71
IR (KBr, cm^{-1})	3332(NH str.), 1646 (CO-NH str.), 2209 (CN str.)
Mass (m/z)	332.2
^{1}H NMR ($CDCl_3$,δ ppm)	8.06-8.03 (m, 2H), 7.81-7.77 (m, 2H), 7.67-7.65 (m, 2H), 7.42 (tt, *J* = 7.1, 1.3 Hz, 1H), 7.24-7.22 (m, 2H), 2.35 (d, *J* = 0.9 Hz, 3H)
^{13}C NMR ($CDCl_3$, δ ppm)	169.46, 152.91, 144.53, 138.72, 137.97, 132.01, 129.26, 128.88, 127.51, 124.06, 120.90, 114.13, 66.18, 24.00, 20.73
Structure	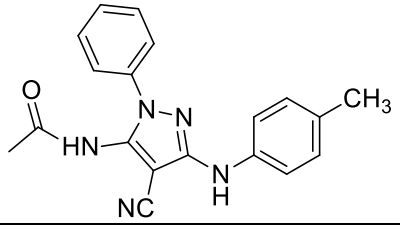

5.5.2.1. Synthesis of N-(4-cyano-3-((4-fluorophenyl)amino)-1-phenyl-1*H*-pyrazol-5-yl)benzamide (6e)

A mixture of 5-amino-3-((4-fluorophenyl)amino)-1-phenyl-1*H*-pyrazole-4-carbonitrile (0.01 mol), ethanol (15 ml), substituted acid chloride(0.04 mol) and NaOH was stirred and reflux for 6-8 hrs. TLC was used to monitored the progress reaction. Upon completion, the reaction mixture was cooled and poured into crushed ice–water mixture. The resulting solid obtained was collected by filteration, thoroughly washed with water, and dried. The crude product obtained was recrystallized from ethanol to afford the pure crystalline product.

Molecular formula	$C_{23}H_{16}FN_5O$
Molecular weight	397.40
Colour	brown
% Yield	90%
Melting point	168-172 ^oC
TLC (mobile phase)	n-Hexane: ethyl acetate 5:5
R_f value	0.76
IR (KBr, cm^{-1})	3340(NH str.), 1650 (CO-NH str.), 2215 (CN str.)
Mass (m/z)	398.14
^1H NMR ($CDCl_3$,δ ppm)	8.21-8.19 (m, 2H), 7.97-7.95 (m, 2H), 7.81-7.77 (m, 2H), 7.70 -7.65 (m, 2H), 7.52-7.46 (m, 1H), 7.46-7.39 (m, 3H), 7.20-7.16 (m, 2H)
^{13}C NMR ($CDCl_3$, δ ppm)	166.42, 158.74, 156.77, 152.64, 145.07, 138.13, 137.88, 137.86, 133.38, 132.19, 129.26, 128.77, 128.49, 127.51, 124.00, 122.04, 121.97, 115.14, 114.96, 114.09, 67.36
Structure	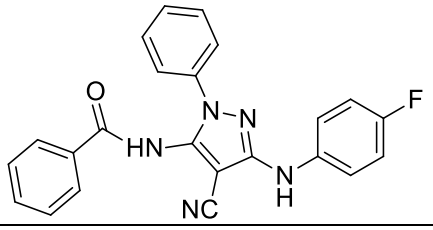

5.5.2.2. Synthesis of N-(4-cyano-3-morpholino-1-phenyl-1*H*-pyrazol-5-yl)benzamide (6f)

A mixture of 0.01 mol of 5-amino-3-morpholino-1-phenyl-1*H*-pyrazole-4-carbonitrile, ethanol (15 ml), substituted acid chloride (0.04 mol) and NaOH was stirred and reflux for 6-8 hrs. TLC was used to monitored the progress reaction. Upon completion, the reaction mixture was cooled and poured into crushed ice–water mixture. The resulting solid obtained was collected by filteration, thoroughly washed with water, and dried. The crude product obtained was recrystallized from ethanol to afford the pure crystalline product.

Molecular formula	$C_{21}H_{19}N_5O_2$
Molecular weight	373.41
Colour	Light brown
% Yield	78%
Melting point	175-180 ^oC
TLC (mobile phase)	n-Hexane: ethyl acetate 5:5
R_f value	0.83
IR (KBr, cm^{-1})	1635 (CO-NH str.), 2218 (CN str.)
Mass (m/z)	374.15
^1H NMR ($CDCl_3$,δ ppm)	7.97-7.96 (m, 1H), 7.81 -7.77 (m, 1H), 7.78(m, 2H) 7.70-7.68 (m, 1H), 7.52-7.39 (m, 5H), 3.85-3.74 (m, 8H)
^{13}C NMR ($CDCl_3$, δ ppm)	(125 MHz, Chloroform-*d*) δ 166.46, 159.84, 144.92, 138.32, 133.38, 132.19, 129.27, 128.77, 128.49, 127.51, 123.97, 113.17, 70.00, 66.36, 48.26
Structure	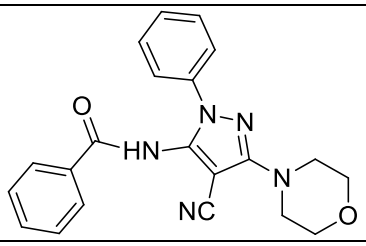

5.5.2.3. Synthesis of N-(4-cyano-3-(4-methylpiperazin-1-yl)-1-phenyl-1*H*-pyrazol-5-yl)benzamide (6g)

A mixture of 0.01 mol of 5-amino-3-(4-methylpiperazin-1-yl)-1-phenyl-1*H*-pyrazole-4-carbonitrile, ethanol (15 ml), substituted acid chloride(0.04 mol) and NaOH was stirred and reflux for 6-8 hrs. TLC was used to monitored the progress reaction. Upon completion, the reaction mixture was cooled and poured into crushed ice–water mixture. The resulting solid obtained was collected by filteration, thoroughly washed with water, and dried. The crude product obtained was recrystallized from ethanol to afford the pure crystalline product.

Molecular formula	$C_{22}H_{22}N_6O$
Molecular weight	386.45
Colour	Reddish brown
% Yield	52%
Melting point	190-195 ^oC
TLC (mobile phase)	n-Hexane: ethyl acetate 5:5
R_f value	0.70
IR (KBr, cm^{-1})	1652(CO-NH str.), 2235 (CN str.)
Mass (m/z)	387.20
^1H NMR ($CDCl_3$,δ ppm)	7.97-7.96 (m, 1H), 7.81-7.77 (m, 2H), 7.70-7.68 (m, 2H), 7.52 -7.39 (m, 5H), 3.67-3.66 (m, 4H), 3.02-3.00 (m, 4H), 2.91 (s, 3H)
^{13}C NMR ($CDCl_3$, δ ppm)	166.46, 159.75, 145.11, 138.34, 133.38, 132.19, 129.27, 128.77, 128.49, 127.51, 123.97, 113.17, 70.00, 54.27, 47.59, 45.01
Structure	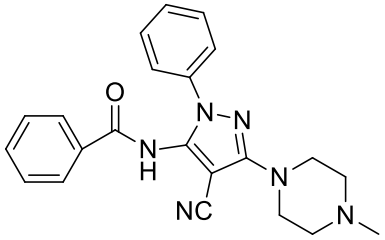

5.5.2.4. Synthesis of N-(4-cyano-1-phenyl-3-(p-tolylamino)-1*H*-pyrazol-5-yl)benzamide (6h)

A mixture of 0.01 mol of 5-amino-1-phenyl-3-(p-tolylamino)-1*H*-pyrazole-4-carbonitrile, ethanol (15 ml), substituted acid chloride(0.04 mol) and NaOH was stirred and reflux for 6-8 hrs. TLC was used to monitored the progress reaction. After completion, the reaction mixture was cooled and poured into crushed ice–water mixture. The resulting solid obtained was collected by filteration, thoroughly washed with water, and dried. The crude product obtained was recrystallized from ethanol to afford the pure crystalline product.

Molecular formula	$C_{24}H_{19}N_5O$
Molecular weight	393.44
Colour	Brownish
% Yield	80%
Melting point	150-152 ^oC
TLC (mobile phase)	n-Hexane: ethyl acetate 5:5
R_f value	0.60
IR (KBr, cm^{-1})	3318(NH str.), 1682 (CO-NH str.), 2208 (CN str.)
Mass (m/z)	393.14
^1H NMR ($CDCl_3$,δ ppm)	8.07-8.01 (m, 2H), 7.97-7.96 (m, 2H), 7.81-7.77 (m, 2H), 7.67-7.66 (m, 1H), 7.52-7.39 (m, 5H), 7.23 (dt, *J* = 7.1, 0.8 Hz, 2H), 2.35 (s, 3H)
^{13}C NMR ($CDCl_3$, δ ppm)	166.42, 152.75, 145.07, 138.72, 138.13, 133.36, 132.19, 132.01, 129.26, 128.88, 128.77, 128.49, 127.51, 124.00, 120.90, 114.09, 67.36, 20.73
Structure	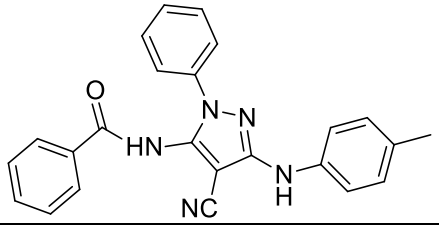

5.5.2.5. Synthesis of N-(4-cyano-3-((3,4-dichlorophenyl)amino)-1-phenyl-1*H*-pyrazol-5-yl)benzenesulfonamide (6i)

A mixture of 0.01 mol of 5-amino-3-((3,4-dichlorophenyl)amino)-1-phenyl-1*H*-pyrazole-4-carbonitrile, ethanol (15 ml), substituted acid chloride(0.04 mol) and NaOH was stirred and reflux for 6-8 hrs. TLC was used to monitored the progress reaction. After completion, the reaction mixture was cooled and poured into crushed ice–water mixture. The resulting solid obtained was collected by filteration, thoroughly washed with water, and dried. The crude product obtained was recrystallized from ethanol to afford the pure crystalline product**.**

Molecular formula	$C_{22}H_{15}Cl_2N_5O_2S$
Molecular weight	484.36
Colour	Dark brown
% Yield	73%
Melting point	140-145 ^oC
TLC (mobile phase)	n-Hexane: ethyl acetate 5:5
R_f value	0.62
IR (KBr, cm^{-1})	3325(NH str.), 1459 (SO_2-NH str.), 2208 (CN str.)
Mass (m/z)	484.4, 486.2 (M+2), 488.8 (M+4).
^1H NMR ($CDCl_3$,δ ppm)	7.79-7.75 (m, 3H), 7.70 (dq, *J* = 7.7, 1.6 Hz, 2H), 7.56 (dq, *J* = 8.8, 1.6 Hz, 2H), 7.43-7.39 (m, 4H), 7.27-7.26 (m, 1H)
^{13}C NMR ($CDCl_3$, δ ppm)	152.51, 142.11, 140.76, 138.38, 137.44, 133.74, 130.74, 129.74, 129.22, 129.20, 127.84, 127.52, 124.93, 124.04, 121.61, 120.20, 113.84, 70.47
Structure	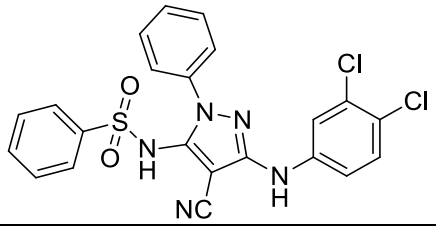

5.5.2.6. Synthesis of N-(4-cyano-3-((2,5-dimethylphenyl)amino)-1-phenyl-1*H*-pyrazol-5-yl)benzenesulfonamide (6j)

A mixture of 0.01 mol of 5-amino-3-((2,5-dimethylphenyl)amino)-1-phenyl-1*H*-pyrazole-4-carbonitrile, ethanol (15 ml), substituted acid chloride(0.04 mol) and NaOH was stirred and reflux for 6-8 hrs. TLC was used to monitored the progress reaction. After completion, the reaction mixture was cooled and poured into crushed ice–water mixture. The resulting solid obtained was collected by filteration, thoroughly washed with water, and dried. The crude product obtained was recrystallized from ethanol to afford the pure crystalline product.

Molecular formula	$C_{24}H_{21}N_5O_2S$
Molecular weight	443.52
Colour	Brown
% Yield	75%
Melting point	148-152 ^oC
TLC (mobile phase)	n-Hexane: ethyl acetate 5:5
R_f value	0.86
IR (KBr, cm^{-1})	3494(NH str.), 1450 (SO_2-NH str.), 2210 (CN str.)
Mass (m/z)	443.2
^1H NMR ($CDCl_3$,δ ppm)	7.95 (tt, *J* = 7.3, 1.3 Hz, 1H), 7.79-7.76 (m, 3H), 7.70 (dq, *J* = 7.7, 1.6 Hz, 2H), 7.56 (dq, *J* = 8.8, 1.6 Hz, 2H), 7.43-7.39 (m, 3H), 7.01 (dq, *J* = 8.2, 1.0 Hz, 2H), 6.80 (ddd, *J* = 7.7, 2.3, 1.1 Hz, 1H), 2.28 (d, *J* = 1.1 Hz, 6H)
^{13}C NMR ($CDCl_3$, δ ppm)	152.53, 142.11, 140.38, 138.38, 137.44, 136.66, 133.74, 130.43, 129.22, 129.20, 127.84, 127.66, 127.52, 124.04, 123.01, 120.97, 113.84, 70.45, 21.62, 17.64
Structure	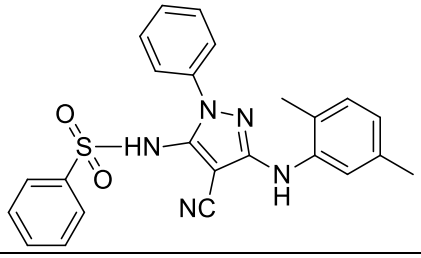

5.5.2.7. Synthesis of N-(4-cyano-3-((2, 3-dichlorophenyl)amino)-1-phenyl-1*H*-pyrazol-5-yl)benzenesulfonamide (6k)

A mixture of 0.01 mol of 5-amino-3-((2,3-dichlorophenyl)amino)-1-phenyl-1*H*-pyrazole-4-carbonitrile, ethanol (15 ml), substituted acid chloride(0.04 mol) and NaOH was stirred and reflux for 6-8 hrs. TLC was used to monitored the progress reaction. After completion, the reaction mixture was cooled and poured into crushed ice–water mixture. The resulting solid obtained was collected by filteration, thoroughly washed with water, and dried. The crude product obtained was recrystallized from ethanol to afford the pure crystalline product.

Molecular formula	$C_{22}H_{15}Cl_2N_5O_2S$
Molecular weight	484.36
Colour	Light brown
% Yield	76%
Melting point	145-150 ^oC
TLC (mobile phase)	n-Hexane: ethyl acetate 5:5
R_f value	0.71
IR (KBr, cm^{-1})	3350(NH str.), 1459 (SO_2-NH str.), 2208 (CN str.)
Mass (m/z)	484.30, 486.2 (M+2), 488.5 (M+4).
^1H NMR ($CDCl_3$,δ ppm)	2.40 (3H, s), 7.83-7.79 (m, 2H), 7.58-7.54 (m, 3H), 7.41 (tt, *J* = 7.2, 1.3 Hz, 1H), 7.27 (d, *J* = 15.8 Hz, 1H), 7.13 (ddd, *J* = 7.7, 2.2, 1.2 Hz, 1H), 6.99 (ddd, *J* = 7.9, 2.1, 1.2 Hz, 1H)
^{13}C NMR ($CDCl_3$, δ ppm)	152.27, 142.17, 139.72, 138.38, 137.44, 134.10, 133.74, 129.22, 129.20, 129.03, 127.84, 127.52, 124.41, 124.04, 123.04, 120.03, 113.81, 70.43
Structure	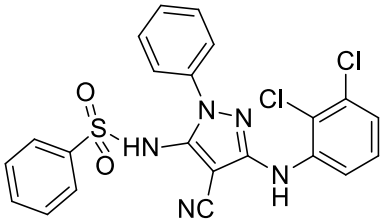

5.5.2.8. Synthesis of N-(4-cyano-1-phenyl-3-(m-tolylamino)-1*H*-pyrazol-5 yl)methanesulfonamide (6l)

A mixture of 0.01 mol of 5-amino-1-phenyl-3-(m-tolylamino)-1*H*-pyrazole-4-carbonitrile, ethanol (15 ml), substituted acid chloride(0.04 mol) and NaOH was stirred and reflux for 6-8 hrs. TLC was used to monitored the progress reaction. After completion, the reaction mixture was cooled and poured into crushed ice–water mixture. The resulting solid obtained was collected by filteration, thoroughly washed with water, and dried. The crude product obtained was recrystallized from ethanol to afford the pure crystalline product**.**

Molecular formula	$C_{18}H_{17}N_5O_2S$
Molecular weight	367.42
Colour	Reddish brown
% Yield	62%
Melting point	168-170 ^oC
TLC (mobile phase)	n-Hexane: ethyl acetate 5:5
R_f value	0.56
IR (KBr, cm^{-1})	3245(NH str.), 1345 (SO_2-NH str.), 2234 (CN str.)
Mass (m/z)	368.12
^1H NMR ($CDCl_3$,δ ppm)	7.79-7.76 (m, 2H), 7.70 (dq, *J* = 7.7, 1.6 Hz, 2H), 7.45-7.39 (m, 3H), 7.14 (d, *J* = 7.6 Hz, 1H), 6.84 (dddd, *J* = 8.2, 2.2, 1.4, 0.7 Hz, 1H), 3.03 (s, 3H), 2.36 (d, *J* = 0.7 Hz, 3H)
^{13}C NMR ($CDCl_3$, δ ppm)	152.37, 141.63, 141.19, 138.63, 137.52, 129.22, 128.85, 127.52, 124.41, 124.07, 121.12, 118.27, 113.84, 68.41, 39.83, 21.45
Structure	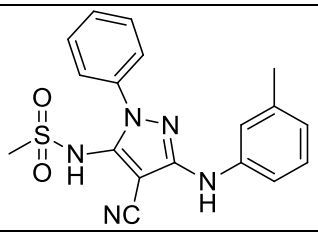

5.5.2.9. Synthesis of N-(3-((3-chlorophenyl)amino)-4-cyano-1-phenyl-1*H*-pyrazol-5-yl)methanesulfonamide (6m)

A mixture of 0.01 mol of 5-amino-3-((3-chlorophenyl)amino)-1-phenyl-1*H*-pyrazole-4-carbonitrile, ethanol (15 ml), substituted acid chloride(0.04 mol) and NaOH was stirred and reflux for 6-8 hrs. TLC was used to monitored the progress reaction. After completion, the reaction mixture was cooled and poured into crushed ice–water mixture. The resulting solid obtained was collected by filteration, thoroughly washed with water, and dried. The crude product obtained was recrystallized from ethanol to afford the pure crystalline product.

Molecular formula	$C_{17}H_{14}ClN_5O_2S$
Molecular weight	387.84
Colour	Brown
% Yield	53%
Melting point	172-174 ^oC
TLC (mobile phase)	n-Hexane: ethyl acetate 5:5
R_f value	0.66
IR (KBr, cm^{-1})	3325(NH str.), 1312(SO_2-NH str.), 2219 (CN str.)
Mass (m/z)	387.7, 389.4(M+2)
^1H NMR ($CDCl_3$,δ ppm)	7.79-7.76 (m, 2H), 7.70 (dq, *J* = 7.7, 1.6 Hz, 2H), 7.55 (t, *J* = 2.2 Hz, 1H), 7.41 (tt, *J* = 7.1, 1.4 Hz, 1H), 7.24 (d, *J* = 7.8 Hz, 1H), 7.13 (ddd, *J* = 7.7, 2.2, 1.2 Hz, 1H), 6.96 (ddd, *J* = 7.9, 2.1, 1.2 Hz, 1H), 3.03 (s, 3H)
^{13}C NMR ($CDCl_3$, δ ppm)	152.68, 142.18, 141.63, 137.52, 133.61, 129.24, 129.22, 127.52, 124.07, 123.37, 119.92, 119.50, 113.84, 68.41, 39.83
Structure	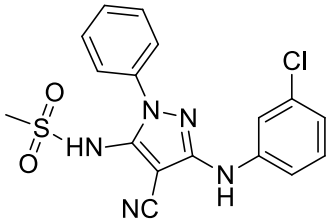

5.5.2.10. Synthesis of N-(3-((2-chlorophenyl)amino)-4-cyano-1-phenyl-1*H*-pyrazol-5-yl)methanesulfonamide (6n)

A mixture of 0.01 mol of 5-amino-3-((2-chlorophenyl)amino)-1-phenyl-1*H*-pyrazole-4-carbonitrile ethanol (15 ml), substituted acid chloride(0.04 mol) and NaOH was stirred and reflux for 6-8 hrs. TLC was used to monitored the progress reaction. After completion, the reaction mixture was cooled and poured into crushed ice–water mixture. The resulting solid obtained was collected by filteration, thoroughly washed with water, and dried. The crude product obtained was recrystallized from ethanol to afford the pure crystalline product.

Molecular formula	$C_{17}H_{14}ClN_5O_2S$
Molecular weight	387.84
Colour	Brown
% Yield	72%
Melting point	152-155 ^oC
TLC (mobile phase)	n-Hexane: ethyl acetate 5:5
R_f value	0.42
IR (KBr, cm^{-1})	3322(NH str.), 1320(SO_2-NH str.), 2213 (CN str.)
Mass (m/z)	387.7, 389.4(M+2)
^1H NMR ($CDCl_3$,δ ppm)	8.19 (dd, *J* = 7.7, 1.4 Hz, 1H), 7.79-7.76 (m, 2H), 7.70 (dq, *J* = 7.7, 1.6 Hz, 2H), 7.54 (dd, *J* = 8.1, 1.4 Hz, 1H), 7.43-7.39 (m, 2H), 7.22-7.19 (m, 1H), 3.03 (s, 3H)
^{13}C NMR ($CDCl_3$, δ ppm)	151.78, 141.63, 138.05, 137.52, 129.38, 129.22, 127.52, 127.38, 125.51, 124.88, 124.07, 123.01, 113.84, 68.37, 39.83; calculated for : 387.84
Structure	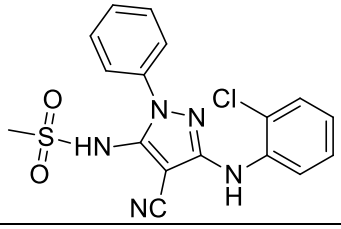

5.5.2.11. Synthesis of (4-cyano-1-phenyl-3-(piperidin-1-yl)-1*H*-pyrazol-5-yl)sulfurous chloride (6o)

A mixture of 0.01 mol of 5-amino-1-phenyl-3-(piperidin-1-yl)-1*H*-pyrazole-4-carbonitrile , ethanol (15 ml), substituted acid chloride(0.04 mol) and NaOH was stirred and reflux for 6-8 hrs. TLC was used to monitored the progress reaction. After completion, the reaction mixture was cooled and poured into crushed ice–water mixture. The resulting solid obtained was collected by filteration, thoroughly washed with water, and dried. The crude product obtained was recrystallized from ethanol to afford the pure crystalline product**.**

Molecular formula	$C_{15}H_{16}ClN_5OS$:
Molecular weight	349.84
Colour	Reddish brown
% Yield	68%
Melting point	95-100 ^oC
TLC (mobile phase)	n-Hexane: ethyl acetate 5:5
R_f value	0.68
IR (KBr, cm^{-1})	1434(SO-NH str.), 2241 (CN str.)
Mass (m/z)	349.6
^1H NMR ($CDCl_3$,δ ppm)	7.79-7.76 (m, 2H), 7.70 (dq, *J* = 7.7, 1.6 Hz, 2H), 3.64-3.62 (m, 4H), 1.73-1.69 (m, 4H), 1.56 (p, *J* = 5.8 Hz, 2H)
^{13}C NMR ($CDCl_3$, δ ppm)	159.27, 147.08, 138.44, 129.23, 127.52, 124.06, 113.07, 68.76, 49.03, 26.26, 24.44
Structure	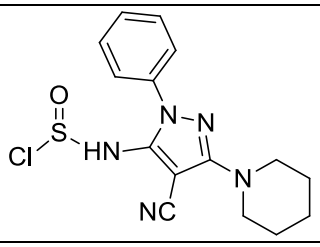

5.6. General Procedure for the synthesis of amino substituted 6-methyl-1-phenyl-1*H*-pyrazolo[3,4-d]pyrimidin-4-ol (7a-o)

Compounds **(5a-o)** (0.5 g.) were dissolved in a solution of potassium hydroxide, hydrogen peroxide (4 ml), and ethanol and refluxed at 70-75 ^{0}C for 2 to 3 hrs. After finishing the reaction, as demonstrated by TLC. After that, it was then acidified with glacial acetic acid to give a precipitate. The crude product was washed with water and recrystallized using ethanol

5.6.1. Synthesis of 3-((2-chlorophenyl)amino)-6-methyl-1-phenyl-1*H*-pyrazolo[3,4-d]pyrimidin-4-ol (7a)

N-(3-((2-chlorophenyl)amino)-4-cyano-1-phenyl-1*H*-pyrazol-5-yl)acetamide **(5a)** was dissolved in a solution of potassium hydroxide, hydrogen peroxide (4 ml), and ethanol and refluxed at 70-75 ^{0}C for 2 to 3 hrs. After finished the reaction, as demonstrated by TLC. After that, it was then acidified with glacial acetic acid to give a precipitate. The crude product was washed with water and recrystallized using ethanol.

Molecular formula	$C_{18}H_{14}ClN_5O$
Molecular weight	351.79
Colour	Brown
% Yield	85%,
Melting point	180-182 ^{0}C
TLC (mobile phase)	n-Hexane: ethyl acetate 5:5
R_f value	0.63
IR (KBr, cm^{-1})	3435(-NH), 3342 (-OH), 2926 (C-H str.)
Mass (m/z)	351.12, 353.3(M+2).
^{1}H NMR ($CDCl_3$,δ ppm)	2.40 (3H, s), 8.20 (dd, *J* = 7.7, 1.4 Hz, 1H), 7.83-7.80 (m, 2H), 7.58 -7.53 (m, 2H), 7.54 (dd, *J* = 8.0, 1.4 Hz, 1H), 7.43-7.39 (m, 2H), 7.22 -7.19 (m, 1H)
^{13}C NMR ($CDCl_3$, δ ppm)	166.23, 162.50, 153.42, 145.93, 138.38, 138.29, 129.38, 128.92, 127.39, 127.01, 125.56, 124.88, 123.01, 121.54, 93.93, 25.06
Structure	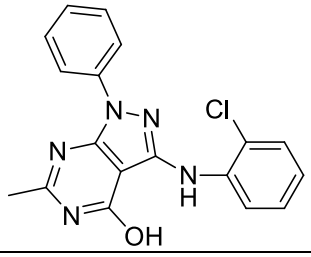

5.6.2. Synthesis of 3-((4-chlorophenyl)amino)-6-methyl-1-phenyl-1*H*-pyrazolo[3,4-d]pyrimidin-4-ol (7b)

N-(3-((4-chlorophenyl)amino)-4-cyano-1-phenyl-1*H*-pyrazol-5-yl)acetamide **(5b)** was dissolved in a solution of potassium hydroxide, hydrogen peroxide (4 ml), and ethanol and refluxed at 70-75 ^{0}C for 2 to 3 hrs. After finished the reaction, as demonstrated by TLC. After that, it was then acidified with glacial acetic acid to give a precipitate. The crude product was washed with water and recrystallized using ethanol.

Molecular formula	$C_{18}H_{14}ClN_5O$
Molecular weight	351.79
Colour	Brown
% Yield	87%
Melting point	160-165 ^{0}C
TLC (mobile phase)	n-Hexane: ethyl acetate 5:5
R_f value	0.52
IR (KBr, cm^{-1})	3438(-NH), 3345 (-OH), 2924 (C-H str.)
Mass (m/z)	351.45, 353.25(M+2)
^{1}H NMR ($CDCl_3$,δ ppm)	δ 2.40 (3H, s), 7.58-7.37 (5H, 7.42 (tdd, *J* = 7.8, 1.6,1.0 Hz), 7.80 (d, *J*= 8.4 Hz, 1H), 7.58-7.54(m, 2H), 7.42-7.37 (m, 2H)
^{13}C NMR ($CDCl_3$, δ ppm)	166.23, 162.49, 153.38, 147.16, 139.95, 138.38, 128.87, 128.92, 127.48, 127.01, 122.29,121.54, 94.05, 25.06
Structure	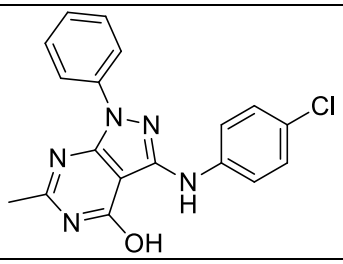

5.6.3. Synthesis of 3-((4-methoxyphenyl)amino)-6-methyl-1-phenyl-1*H*-pyrazolo[3,4-d]pyrimidin-4-ol (7c)

N-(4-cyano-3-((4-methoxyphenyl)amino)-1-phenyl-1*H*-pyrazol-5-yl)acetamide **(5c)** was dissolved in a solution of potassium hydroxide, hydrogen peroxide (4 ml), and ethanol and refluxed at 70-75 ^{0}C for 2 to 3 hrs. After finished the reaction, as demonstrated by TLC. After that, it was then acidified with glacial acetic acid to give a precipitate. The crude product was washed with water and recrystallized using ethanol.

Molecular formula	$C_{19}H_{17}N_5O_2$
Molecular weight	347.37
Colour	Dark brown
% Yield	75%
Melting point	190-192 ^{0}C
TLC (mobile phase)	n-Hexane: ethyl acetate 5:5
R_f value	0.66
IR (KBr, cm^{-1})	3312 (-NH), 3352 (-OH), 2935 (C-H str.)
Mass (m/z)	347.15
^{1}H NMR ($CDCl_3$,δ ppm)	2.40 (3H, s), 3.80 (s, 2H), 6.96 (ddd, 2H), 8.12- 8.10 (m, 2H), 7.83- 7.80 (m, 2H), 7.58- 7.56 (m, 2H), 7.42-7.39 (m, 1H), 7.00- 6.95 (m, 2H)
^{13}C NMR ($CDCl_3$, δ ppm)	166.23, 162.49, 156.01, 153.38, 146.75, 138.38, 135.74, 128.92, 127.01, 121.85, 121.54, 114.81, 94.05, 55.35, 25.06
Structure	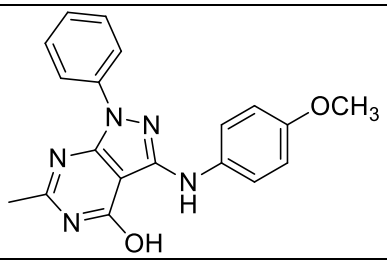

5.6.4. Synthesis of 6-methyl-1-phenyl-3-(p-tolylamino)-1*H*-pyrazolo[3,4-d]pyrimidin-4-ol (7d)

N-(4-cyano-1-phenyl-3-(p-tolylamino)-1*H*-pyrazol-5-yl)acetamide **(5d)** was dissolved in a solution of potassium hydroxide, hydrogen peroxide (4 ml), and ethanol and refluxed at 70-75 ^{0}C for 2 to 3 hrs. After finished the reaction, as demonstrated by TLC. After that, it was then acidified with glacial acetic acid to give a precipitate. The crude product was washed with water and recrystallized using ethanol.

Molecular formula	$C_{19}H_{17}N_5O$
Molecular weight	331.37
Colour	Dark brown
% Yield	90%
Melting point	170-172 ^{0}C
TLC (mobile phase)	n-Hexane: ethyl acetate 5:5
R_f value	0.50
IR (KBr, cm^{-1})	3362 (-NH), 3310 (-OH), 2942 (C-H str.)
Mass (m/z)	331.68
^{1}H NMR ($CDCl_3$,δ ppm)	2.35 (d, *J* = 1.0 Hz, 3H), 2.35(d, *J* = 1.0 Hz, 3H), 8.05- 8.03 (m, 2H), 7.83- 7.79 (m, 2H), 7.58- 7.56 (m, 2H), 7.41 (tt, *J* = 7.2, 1.3 Hz, 1H), 7.24-7.22 (m, 3H)
^{13}C NMR ($CDCl_3$, δ ppm)	166.23, 162.49, 153.38, 147.20, 139.28, 138.38, 132.01, 128.92, 128.89, 127.01, 121.54, 120.91, 94.05, 25.06, 20.73
Structure	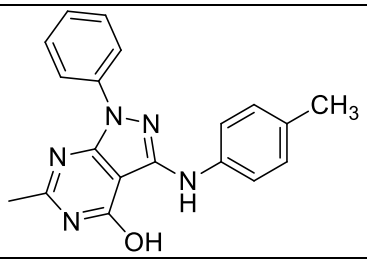

5.6.5. Synthesis of 3-((4-fluorophenyl)amino)-6-methyl-1-phenyl-1*H*-pyrazolo[3,4-d]pyrimidin-4-ol (7e)

N-(4-cyano-3-((4-fluorophenyl)amino)-1-phenyl-1*H*-pyrazol-5-yl)acetamide **(5e)** was dissolved in a solution of potassium hydroxide, hydrogen peroxide (4 ml), and ethanol and refluxed at 70-75 ^{0}C for 2 to 3 hrs. After finished the reaction, as demonstrated by TLC. After that, it was then acidified with glacial acetic acid to give a precipitate. The crude product was washed with water and recrystallized using ethanol.

Molecular formula	$C_{18}H_{14}FN_5O$
Molecular weight	335.34
Colour	Brown
% Yield	86%
Melting point	145-148 ^{0}C
TLC (mobile phase)	n-Hexane: ethyl acetate 5:5
R_f value	0.40
IR (KBr, cm^{-1})	3390 (-NH), 3415 (-OH), 2937 (C-H str.)
Mass (m/z)	335
^{1}H NMR ($CDCl_3$,δ ppm)	2.40 (3H, s), 8.21- 8.19 (m, 2H), 7.83-7.79 (m, 2H), 7.58- 7.56 (m, 3H), 7.41 (tt, *J* = 7.2, 1.3 Hz, 1H), 7.20- 7.16 (m, 2H)
^{13}C NMR ($CDCl_3$, δ ppm)	166.23, 162.49, 158.74, 156.77, 153.38, 146.78, 138.64, 138.62, 138.38, 128.92, 127.01, 122.02, 121.95, 121.54, 115.15, 114.97, 94.05, 25.06
Structure	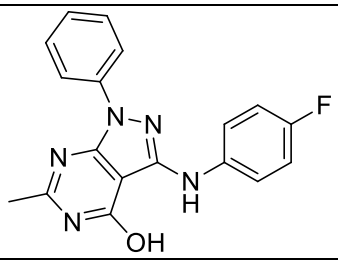

5.6.6. Synthesis of 6-methyl-3-morpholino-1-phenyl-1*H*-pyrazolo[3,4-d]pyrimidin-4-ol (7f)

N-(4-cyano-3-morpholino-1-phenyl-1*H*-pyrazol-5-yl)acetamide **(5f)** was dissolved in a solution of potassium hydroxide, hydrogen peroxide (4 ml), and ethanol and refluxed at 70-75 ^{0}C for 2 to 3 hrs. After finished the reaction, as demonstrated by TLC. After that, it was then acidified with glacial acetic acid to give a precipitate. The crude product was washed with water and recrystallized using ethanol.

Molecular formula	$C_{16}H_{17}N_5O_2$
Molecular weight	311.34
Colour	Brown
% Yield	84%
Melting point	155-160 ^{0}C
TLC (mobile phase)	n-Hexane: ethyl acetate 5:5
R_f value	0.75
IR (KBr, cm^{-1})	3353 (-OH), 2952 (C-H str.)
Mass (m/z)	311.47
^{1}H NMR ($CDCl_3$,δ ppm)	2.40 (3H, s), 7.83-7.79 (m, 2H), 7.58-7.56 (m, 2H), 3.84- 3.80 (m, 4H), 3.77 (dd, *J* = 5.7, 4.5 Hz, 4H)
^{13}C NMR ($CDCl_3$, δ ppm)	164.99, 161.89, 155.38, 149.14, 138.77, 128.92, 127.01, 121.49, 95.96, 66.36, 48.28, 25.06
Structure	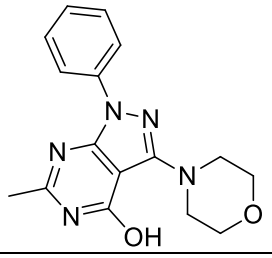

5.6.7. Synthesis of 3-((3, 4-dichlorophenyl)amino)-6-methyl-1-phenyl-1*H*-pyrazolo[3,4-d]pyrimidin-4-ol (7g)

N-(4-cyano-3-((3,4-dichlorophenyl)amino)-1-phenyl-1*H*-pyrazol-5-yl)acetamide **(5g)** was dissolved in a solution of potassium hydroxide, hydrogen peroxide (4 ml), and ethanol and refluxed at 70-75 ^{0}C for 2 to 3 hrs. After finished the reaction, as demonstrated by TLC. After that, it was then acidified with glacial acetic acid to give a precipitate. The crude product was washed with water and recrystallized using ethanol.

Molecular formula	$C_{18}H_{13}Cl_2N_5O$:
Molecular weight	386.23
Colour	Brown
% Yield	74%
Melting point	164-167 ^{0}C
TLC (mobile phase)	n-Hexane: ethyl acetate 5:5
R_f value	0.66
IR (KBr, cm^{-1})	3352 (-NH str.), 3443(O-H str.), 2926 (C-H str.)
Mass (m/z)	386.1, M+2: 388.4, M+4: 390
^{1}H NMR ($CDCl_3$,δ ppm)	2.40 (3H, s), 7.83-7.75 (m, 2H), 7.74 (d, *J* = 2.2 Hz, 1H), 7.58-7.56 (m, 2H), 7.42 - 7.39 (m, 2H), 7.27-7.25 (m, 2H)
^{13}C NMR ($CDCl_3$, δ ppm)	166.23, 162.49, 153.38, 146.47, 140.87, 138.38, 130.76, 129.76, 128.92, 127.01, 124.92, 121.61, 121.54, 120.22, 94.08, 25.06
Structure	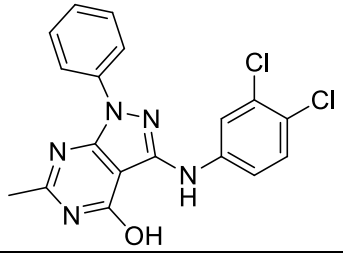

5.6.8. Synthesis of 3-((2, 5-dimethylphenyl)amino)-6-methyl-1-phenyl-1*H*-pyrazolo[3,4-d]pyrimidin-4-ol (7h)

N-(4-cyano-3-((2,5-dimethylphenyl)amino)-1-phenyl-1*H*-pyrazol-5-yl)acetamide **(5h)** was dissolved in a solution of potassium hydroxide, hydrogen peroxide (4 ml), and ethanol and refluxed at 70-75 ^{0}C for 2 to 3 hrs. After finished the reaction, as demonstrated by TLC. After that, it was then acidified with glacial acetic acid to give a precipitate. The crude product was washed with water and recrystallized using ethanol.

Molecular formula	$C_{20}H_{19}N_5O$
Molecular weight	345.40
Colour	Dark brown
% Yield	79%
Melting point	148-150 ^{0}C
TLC (mobile phase)	n-Hexane: ethyl acetate 5:5
R_f value	0.50
IR (KBr, cm^{-1})	3326 (-NH str.), 3264 (O-H str.), 2921(C-H str.)
Mass (m/z)	346.16
^{1}H NMR ($CDCl_3$,δ ppm)	2.40 (s, 3H), 2.28 (d, *J* = 1.1 Hz, 3H), 2.34 (s, 3H), 7.83-7.78 (m, 3H), 7.58-7.56 (m, 2H), 7.42- 7.39 (m, 2H), 7.00 (dq, *J* = 8.3, 0.9 Hz, 1H), 6.81- 6.69 (m, 1H)
^{13}C NMR ($CDCl_3$, δ ppm)	166.23, 162.49, 153.38, 145.76, 140.68, 138.38, 136.77, 130.40, 128.92, 127.64, 127.01, 123.01, 121.54, 120.92, 93.98, 25.06, 21.62, 17.67
Structure	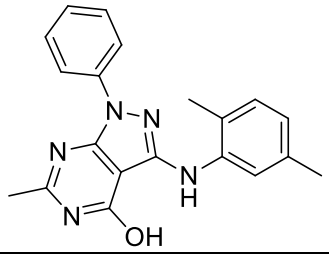

5.6.9. Synthesis of 3-((2,3-dichlorophenyl)amino)-6-methyl-1-phenyl-1*H*-pyrazolo[3,4-d]pyrimidin-4-ol (7i)

N-(4-cyano-3-((2,3-dichlorophenyl)amino)-1-phenyl-1*H*-pyrazol-5-yl)acetamide **(5i)** was dissolved in a solution of potassium hydroxide, hydrogen peroxide (4 ml), and ethanol and refluxed at 70-75 ^{0}C for 2 to 3 hrs. After finished the reaction, as demonstrated by TLC. After that, it was then acidified with glacial acetic acid to give a precipitate. The crude product was washed with water and recrystallized using ethanol.

Molecular formula	$C_{18}H_{13}Cl_2N_5O$
Molecular weight	386.23
Colour	Light brown
% Yield	80%
Melting point	140-142 ^{0}C
TLC (mobile phase)	n-Hexane: ethyl acetate 5:5
R_f value	0.42
IR (KBr, cm^{-1})	3350 (-NH str.), 3410 (O-H str.), 2923 (C-H str.)
Mass (m/z)	386.30, M+2: 388.64, M+4: 390
^{1}H NMR ($CDCl_3$,δ ppm)	2.40 (3H, s), 8.06 (dd, *J* = 7.9, 1.1 Hz, 1H), 7.83-7.79 (m, 2H), 7.58- 7.56 (m, 2H), 7.41 (tt, *J* = 7.2, 1.3 Hz, 1H), 7.20 (d, *J* = 7.9 Hz, 2H), 7.08 (dd, *J* = 7.8, 1.2 Hz, 1H)
^{13}C NMR ($CDCl_3$, δ ppm)	166.23, 162.50, 153.42, 146.09, 140.11, 138.38, 134.14, 129.03, 128.92, 127.01, 124.41, 123.00, 121.54, 120.03, 94.03, 25.06
Structure	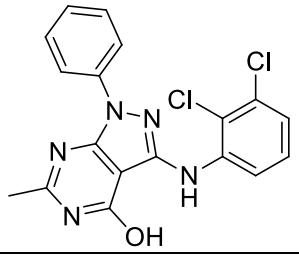

5.6.10. Synthesis of 6-methyl-1-phenyl-3-(m-tolylamino)-1*H*-pyrazolo[3,4-d]pyrimidin-4-ol (7j)

N-(4-cyano-1-phenyl-3-(m-tolylamino)-1*H*-pyrazol-5-yl)acetamide **(5j)** was dissolved in a solution of potassium hydroxide, hydrogen peroxide (4 ml), and ethanol and refluxed at 70-75 ^{0}C for 2 to 3 hrs. After finished the reaction, as demonstrated by TLC. After that, it was then acidified with glacial acetic acid to give a precipitate. The crude product was washed with water and recrystallized using ethanol.

Molecular formula	$C_{19}H_{17}N_5O_3$
Molecular weight	331.37
Colour	Yellowish brown
% Yield	64%
Melting point	97-102 ^{0}C
TLC (mobile phase)	n-Hexane: ethyl acetate 5:5
R_f value	0.67
IR (KBr, cm^{-1})	3359 (-NH str.), 3409 (O-H str.), 2921 (C-H str.)
Mass (m/z)	332. 15.
^{1}H NMR ($CDCl_3$,δ ppm)	2.40 (3H, s), 2.36 (m, 3H), 7.83-7.79 (m, 2H), 7.58- 7.56 (m, 2H), 7.45- 7.39 (m, 3H), 7.14 (d, *J* = 7.6 Hz, 1H), 6.84 (dddd, *J* = 8.2, 2.2, 1.4, 0.7 Hz, 1H)
^{13}C NMR ($CDCl_3$, δ ppm)	166.23, 162.49, 153.38, 146.95, 141.44, 138.71, 138.38, 128.92, 128.88, 127.01, 124.39, 121.54, 121.12, 118.31, 94.05, 25.06, 21.45
Structure	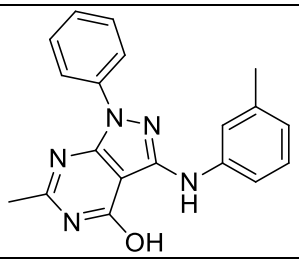

5.6.11. Synthesis of 3-((3-chlorophenyl)amino)-6-methyl-1-phenyl-1*H*-pyrazolo[3,4-d]pyrimidin-4-ol (7k)

N-(3-((3-chlorophenyl)amino)-4-cyano-1-phenyl-1*H*-pyrazol-5-yl)acetamide **(5k)** was dissolved in a solution of potassium hydroxide, hydrogen peroxide (4 ml), and ethanol and refluxed at 70-75 ^{0}C for 2 to 3 hrs. After finished the reaction, as demonstrated by TLC. After that, it was then acidified with glacial acetic acid to give a precipitate. The crude product was washed with water and recrystallized using ethanol.

Molecular formula	$C_{18}H_{14}ClN_5O$
Molecular weight	351.79
Colour	Dark brown
% Yield	56%
Melting point	175-180 ^{0}C
TLC (mobile phase)	n-Hexane: ethyl acetate 5:5
R_f value	0.45
IR (KBr, cm^{-1})	3412(-NH str.), 3323 (-OH str.), 2915(C-H str.)
Mass (m/z)	352, 354 (M+2).
^{1}H NMR ($CDCl_3$,δ ppm)	2.40 (3H, s)7.85-7.77 (m, 2H), 7.60- 7.52 (m, 3H), 7.41 (tt, *J* = 7.2, 1.3 Hz, 1H), 7.25 (d, *J* = 15.8 Hz, 1H), 7.13 (ddd, *J* = 7.7, 2.2, 1.2 Hz, 1H), 6.99 (ddd, *J* = 7.9, 2.1, 1.2 Hz, 1H)
^{13}C NMR ($CDCl_3$, δ ppm)	166.23, 162.49, 153.38, 146.50, 142.27, 138.38, 133.61, 129.22, 128.92, 127.01, 123.34, 121.54, 119.97, 119.51, 94.08, 25.06;: 351.79
Structure	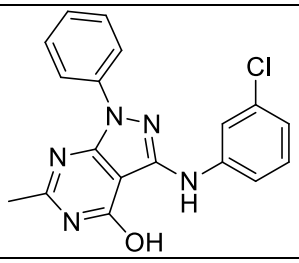

5.6.12. Synthesis of 3-((3-methoxyphenyl)amino)-6-methyl-1-phenyl-1*H*-pyrazolo[3,4-d]pyrimidin-4-ol (7l)

N-(4-cyano-3-((3-methoxyphenyl)amino)-1-phenyl-1*H*-pyrazol-5-yl)acetamide **(5l)** was dissolved in a solution of potassium hydroxide, hydrogen peroxide (4 ml), and ethanol and refluxed at 70-75 ^{0}C for 2 to 3 hrs. After finished the reaction, as demonstrated by TLC. After that, it was then acidified with glacial acetic acid to give a precipitate. The crude product was washed with water and recrystallized using ethanol.

Molecular formula	$C_{19}H_{17}N_5O_2$
Molecular weight	347.37
Colour	Dark brown
% Yield	52%
Melting point	168-172 ^{0}C
TLC (mobile phase)	n-Hexane: ethyl acetate 5:5
R_f value	0.63
IR (KBr, cm^{-1})	3367(-NH), 3417(-OH), 2935 (C-H str.)
Mass (m/z)	348.14
^{1}H NMR ($CDCl_3$,δ ppm)	2.40 (3H, s), 3.82 (s, 3H) 7.83-7.79 (m, 2H), 7.58-7.56 (m, 2H), 7.42-7.38 (m, 2H), 7.22-7.17 (m, 2H), 6.53- 6.50 (m, 1H)
^{13}C NMR ($CDCl_3$, δ ppm)	166.23, 162.49, 160.94, 153.38, 146.51, 142.79, 138.38, 130.03, 128.92, 127.01, 121.54, 114.64, 110.46, 105.96, 94.08, 55.59, 25.06
Structure	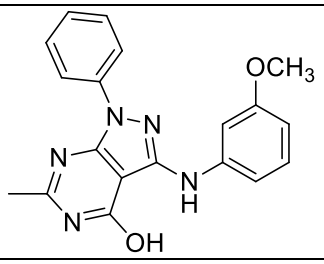

5.6.13. Synthesis of 6-methyl-1-phenyl-3-(piperidin-1-yl)-1*H*-pyrazolo[3,4-d]pyrimidin-4-ol (7m)

N-(4-cyano-1-phenyl-3-(piperidin-1-yl)-1*H*-pyrazol-5-yl)acetamide **(5m)** was dissolved in a solution of potassium hydroxide, hydrogen peroxide (4 ml), and ethanol and refluxed at 70-75 ^{0}C for 2 to 3 hrs. After finished the reaction, as demonstrated by TLC. After that, it was then acidified with glacial acetic acid to give a precipitate. The crude product was washed with water and recrystallized using ethanol.

Molecular formula	$C_{17}H_{19}N_5O$
Molecular weight	309.37
Colour	Cream
% Yield	79%
Melting point	240-245 ^{0}C
TLC (mobile phase)	n-Hexane: ethyl acetate 5:5
R_f value	0.55
IR (KBr, cm^{-1})	3400 (O-H str.), 2922 (C-H str.)
Mass (m/z)	310.23
^{1}H NMR ($CDCl_3$,δ ppm)	2.40 (3H, s), 1.58-1.54 (m, 4H), 1.73 -1.69 (m, 2H), 7.83-7.79 (m, 2H), 7.58-7.56 (m, 3H), 3.63-3.60 (m, 4H)
^{13}C NMR ($CDCl_3$, δ ppm)	164.99, 161.99, 155.36, 148.96, 138.77, 128.92, 127.01, 121.49, 95.87, 49.09, 26.26, 25.06, 24.44
Structure	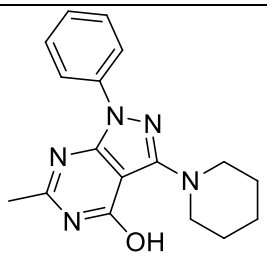

5.6.14. Synthesis of 3-((2-fluorophenyl)amino)-6-methyl-1-phenyl-1*H*-pyrazolo[3,4-d]pyrimidin-4-ol (7n)

N-(4-cyano-3-((2-fluorophenyl)amino)-1-phenyl-1*H*-pyrazol-5-yl)acetamide **(5n)** was dissolved in a solution of potassium hydroxide, hydrogen peroxide (4 ml), and ethanol and refluxed at 70-75 ^{0}C for 2 to 3 hrs. After finished the reaction, as demonstrated by TLC. After that, it was then acidified with glacial acetic acid to give a precipitate. The crude product was washed with water and recrystallized using ethanol.

Molecular formula	$C_{18}H_{14}FN_5O$
Molecular weight	335.34
Colour	Brown
% Yield	72%
Melting point	85-90 ^{0}C
TLC (mobile phase)	n-Hexane: ethyl acetate 5:5
R_f value	0.58
IR (KBr, cm^{-1})	3342 (-NH str.), 3410(-OH str.), 2940 (C-H str.)
Mass (m/z)	336.13
^{1}H NMR ($CDCl_3$,δ ppm)	2.40 (3H, s), 8.20 (ddd, *J* = 8.8, 3.7, 1.4 Hz, 1H), 7.83-7.79 (m, 2H), 7.57 (dq, *J* = 7.5, 1.2 Hz, 2H), 7.41 (tt, *J* = 7.2, 1.3 Hz, 1H), 7.29-7.26 (m, 1H), 7.17-7.08 (m, 2H)
^{13}C NMR ($CDCl_3$, δ ppm)	166.23, 162.50, 155.65, 153.69, 153.42, 146.62, 146.56, 138.38, 129.54, 129.43, 128.92, 127.01, 125.46, 125.44, 123.97, 123.91, 122.33, 122.28, 121.54, 115.29, 115.12, 94.05, 25.06
Structure	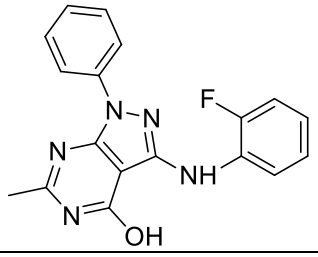

5.6.15. Synthesis of 6-methyl-3-(4-methylpiperazin-1-yl)-1-phenyl-1*H*-pyrazolo[3,4-d]pyrimidin-4-ol (7o)

N-(4-cyano-3-(4-methylpiperazin-1-yl)-1-phenyl-1*H*-pyrazol-5-yl)acetamide **(5o)** was dissolved in a solution of potassium hydroxide, hydrogen peroxide (4 ml), and ethanol and refluxed at 70-75 ^{0}C for 2 to 3 hrs. After finished the reaction, as demonstrated by TLC. After that, it was then acidified with glacial acetic acid to give a precipitate. The crude product was washed with water and recrystallized using ethanol.

Molecular formula	$C_{17}H_{20}N_6O$
Molecular weight	324.38
Colour	Brown
% Yield	75%
Melting point	138-142 ^{0}C
TLC (mobile phase)	n-Hexane: ethyl acetate 5:5
R_f value	0.64
IR (KBr, cm^{-1})	3343(-OH str.), 2910 (C-H str.)
Mass (m/z)	325.02
^{1}H NMR ($CDCl_3$,δ ppm)	2.40 (3H, s), 2.91 (s, 3H), 3.68-3.66 (m, 4H), 3.02-2.91 (m, 4H), 7.83-7.79 (m, 2H), 7.58-7.56 (m, 3H)
^{13}C NMR ($CDCl_3$, δ ppm)	164.99, 161.87, 155.31, 149.26, 138.77, 128.92, 127.01, 121.49, 96.05, 54.24, 47.62, 45.01, 25.06
Structure	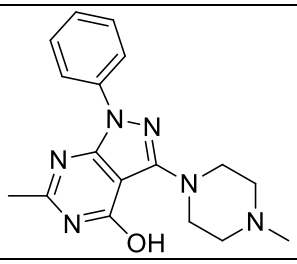

5.7. Methodology

5.7.1. Anti-tubercular activity by Microplate Alamar Blue (MABA) assay

- 200µl of sterile deionzed water was added to all outer perimeter wells of sterile 96 wells plate to minimized evaporation of medium in the test wells during incubation.
- The 96 wells plate received 100 µl of the Middlebrook 7H9 broth and serial dilution of compounds were made directly on plate.
- The final drug concentrations tested were 100 to 0.2 µg/ml.
- Plates were covered and sealed with parafilm and incubated at 37ºC for five days.
- After this time, 25µl of freshly prepared 1:1 mixture of almar blue reagent and 10% tween 80 was added to the plate and incubated for 24 hrs.
- A blue colour in the well was interpreted as no bacterial growth, and pink color was scored as growth.
- The MIC was defined as lowest drug concentration which prevented the colour change from blue to pink (Brien et al., 2000).

5.7.2. Antioxidant activity by DPPH aasay

The DPPH assay method is widely used for the evaluation of antioxidant activity. We have used the DPPH assay for the assessment of the antioxidant activity of compounds **(6a-o)** and **(7a-o)**. This technique reduces DPPH free radicals stability and produces a distinct absorption at 517 nm. DPPH radical is reduced, and the absorbance intensity decreases considerably. For this test, each test compound is prepared in methanol at a final 100 µM concentration. In a 96-well microplate, the DPPH solution (1:1 volume) was combined with the solutions of the test compound, leading to a total volume of 200 µL for each well. 100 µM Ascorbic acid and curcumin were added as standards of antioxidant, and methanol served as the vehicle of the solvent control (Bhardwaj et al., 2025)(S. Kumar & Modi, 2025)(Nayee et al., 2026).

The absorbance result was measured at 517 nm. The DPPH radical scavenging activity (%RSA) of compounds **(6a-o)** and **(7a-o)** were determined by using the following formula:

$$\%RSA = \frac{(A(control) - A(sample))}{(A(control))} * 100$$

Where:

A(control) = absorbance of control

A(sample) = absorbance of test sample

5.7.3. MTT cytotoxicity assay

MTT assay was used for the evaluation of cell viability. It is a laboratory technique for the measurement of cellular growth. We have used this method for the cytotoxicity evaluation of the potent compounds **6m** (MIC: 3.12 µg/mL), **6i** (MIC: 6.25 µg/mL)**, 7g** (6.25 µg/mL) and **7j** (12.5 µg/mL), on HepG2 cell lines. The Cells were incubated in DMEM medium enriched with 10% FBS and 1% antibiotic solution with 5% CO for 24 hrs. On the following day, cells were exposed to various concentrations. Cells were not treated as the control. MTT solution was introduced into culture after 24 hrs. and further incubated for two hrs. The supernatant layer was destroyed after completion of the experiment, 100 µl DMSO was used for the remaining cell layer matrix dissolving, and it was measured at 540 and 660 nm wavelengths by an ELISA plate reader. Minimum inhibitory concentration(IC_{50}) values are identified by Graph Pad Prism-6 software(Morgan, 1998)(Langdon, 2003)(Fotakis & Timbrell, 2006)

5.7.4. Molecular Docking

In this study, Autodock Vina and Autodock tools 1.5.6 were used for the docking study. The crystal structure (PDB:4U0J) and (PDB:4NCR) was downloaded from the Protein Data Bank (RCSB) with 1.62 Å and 1.88 Å resolution. By using the Biovia Discovery Studio 2016, the polar hydrogen atoms were incorporated, and all the water molecules were removed. The grid box was built as x = 20, y = 20, z = 20 in directions within the receptor pocket and 1 Å space between each grid point. The center of the matrix is specified by dimensions x= 43, y= 51, z= -82 for InhA inhibitors and x=32, y= -16, and z=20 for DprE1 inhibitors. Autodock tool 1.5.6 software uses a modified PDB format known as a PDBQT coordinate file, which incorporates partial atomic charges for preparing ligands and receptors. The rotation of selected ligands, which is flexible and non-bonded, is characterized by torsion angles. Subsequently, synthesized InhA **(6a-o)** and DprE1 inhibitors **(7a-o)** were docked with the examined active site of the InhA and DprE1 receptor. Protein-ligand interactions are determined by Biovia Discovery Studio 2021(Mohammed et al., 2024)(Fekadu et al., 2022)(Nayee et al., 2026).

5.7.5. MD simulation

The main reason for the adaptation of MD simulation is to assess the binding stability of protein-ligand complex and understand atomic interactions (Rampogu et al., 2023). In a physiological pH setting, MD simulation of compounds **6m** and **7g** was performed at 100ns.

CHARMM-GUI server was used to prepare the main system files required for simulation, such as .gro, .psf. (Lee et al., 2016). The water box was solvated with the TIP3P water model and neutralized by counter ions. It was minimized by 50,000 steps using the steepest descent algorithm, then underwent equilibration steps: 100 ps in NVT and NPT ensembles, maintaining constant temperature and pressure. The balanced system was subsequently exposed to a 100 ns production run. GROMACS (HPC server Param-Shivaye IIT-BHU Varanasi) was used for the MD simulations (Van Der Spoel et al., 2005). Analysis after the MD run involved computations of RMSD, RMSF, SASA, Rg and H-bond analysis.

5.7.6. ADMET Properties

The synthesis/prediction of molecules is considered an important step in the search for new agents for treating certain diseases. In fact, in order to become a future drug certified and accepted by molecules, it must undergo four stages of absorption, distribution, metabolism, excretion and toxicity (ADMET). Here in this study, target compounds **(6a-o)** and **(7a-o)** were evaluated by using online servers pkCSM and SwissADME. (Al Azzam, 2023)(Mvondo et al., 2021).

CHAPTER-6

SUMMARY

CHAPTER-6

6. SUMMARY

Summary of present work and recommendation

- We have reviewed the recent developments, drug pipeline and reported literature for tuberculosis.
- In the present work we have designed and synthesized series of amine and acid chloride substituted pyrazole derivatives **(6a-o)** and evaluated for their *In-vitro* antitubercular activity against *M. tuberculosis* H37Rv strain. The compounds **(6a-o)** are enoyl acyl carrier protein reductase (InhA) inhibitors.
- Synthesized derivatives **6g**, **6h**, **6i**, **6j** and **6m** possess potent antituberculer activities. Antitubercular activity of compound **6m** was similar to the reference standard drug Pyrazinamide.
- Potent compounds **6i** and **6m** were found to be safe with IC_{50} 125 ± 0.16 µM and 273.8 ± 0.05 µM as indicated by the cytotoxicity studies.
- Molecular docking studies indicated that compounds **6g**, **6h**, **6i**, **6j**, and **6m** demonstrated more efficient interactions with the InhA enzyme.
- Antioxidant potential of synthesized compounds has also been evaluated by DPPH scavenging method. Compounds **6b** and **6d** have displayed good antioxidant activities. Compound **6m** exhibited excellent antioxidant potential.
- The molecular dynamics studies suggested that most potent compound **6m** forms stable interactions with the protein, enhancing its potential as InhA inhibitor. Computational drug-likeness predictions showed that most of the tested compounds were safe, possess druggable features, and exhibit acceptable ADME profiles.
- We have designed and synthesized amino-substituted pyrazolo-pyrimidine compounds**(7a–o)** as DprE1 inhibitors. Antitubercular activities of compounds **(7a-o)** were checked against *M.tuberculosis* H37Rv strain. Compounds **7e**, **7g**, **7j,** and **7k** possess potent antitubercular activities. Cytotoxicity of compounds **7g** and **7j** were found to be IC_{50} 71.63 ± 0.10 µM and 9.281 ± 0.20µM. Compound **7g** was found to be safe.
- Molecular docking studies indicated that compounds **7d**, **7g**, **7h**, **7i**, **7j**, and **7n** exhibited more effective interactions with the DprE1 enzyme.

- ❖ DPPH radical scavenging assay was used for the evaluation of the antioxidant potential of compounds **(7a-o).** Compounds **7b**, **7d**, and **7e** have shown strong antioxidant properties.
- ❖ The molecular dynamics simulation study revealed that the most effective compound, **7g,** establishes stable interactions with the protein, augmenting it as a potential inhibitor of DprE1.
- ❖ Computational predictions of drug-likeness parameters suggested that the majority of examined compounds **(6a-o)** and **(7a-o)** are safe and display suitable ADME characteristics.

Conclusion

- ✓ Synthesized pyrazole containing InhA inhibitors **(6a-o)** and pyrazolo-pyrimidine containing DprE1 inhibitors **(7a-o)** showed good potency against the *M. tuberculosis* H37Rv strain.
- ✓ The results obtained in this research provide an opportunity for additional structure alterations. This compelling justification opens avenues to identify new compounds that act as anti-tubercular drugs.

CHAPTER-7

REFERENCES

CHAPTER-7

7. REFERENCES

References

Ahsan, M. J., Samy, J. G., Dutt, K. R., Agrawal, U. K., Yadav, B. S., Vyas, S., Kaur, R., & Yadav, G. (2011). Design, synthesis and antimycobacterial evaluation of novel 3-substituted-*N*-aryl-6,7-dimethoxy-3a,4-dihydro-3H-indeno[1,2-*c*]pyrazole-2-carboxamide analogues. *Bioorganic & Medicinal Chemistry Letters, 21*(15), 4451–4453. https://doi.org/10.1016/j.bmcl.2011.06.018

Al Azzam, K. M. (2023). SwissADME and pkCSM webservers predictors: An integrated online platform for accurate and comprehensive predictions for in silico ADME/T properties of artemisinin and its derivatives. *Kompleksnoe Ispolzovanie Mineralnogo Syra*, *325*(2), 14–21. https://doi.org/10.31643/2023/6445.13

Alam, J., Alam, O., Alam, P., & Naim, M. J. (2015). A review on pyrazole chemical entity and biological activity. *International Journal of Pharmaceutical Sciences and Research, 6*(12), 1433–1442.

Alegaon, S. G., Alagawadi, K. R., & Dadwe, D. H. (2014). Synthesis and antitubercular activity of novel 3,5-diaryl-4,5-dihydro-1H-pyrazole derivatives. *Drug Research, 64*(10), 553–558. https://doi.org/10.1055/s-0033-1363976

Alegaon, S. G., Hirpara, M. B., Alagawadi, K. R., Jalalpure, S. S., Rasal, V. P., Salve, P. S., & Kumbar, V. M. (2017). Synthesis and biological evaluation of 1,3,4-trisubstituted pyrazole analogues as anti-mycobacterial agents. *Medicinal Chemistry Research, 26*(6), 1127–1138. https://doi.org/10.1007/s00044-017-1821-1

Alex. F. C., Brondani, S., Pizzuti, L., Martins, M. A. P., Zanatta, N., Bonacorso, H. G., & Flores, D. C. (2005). Haloacetylated enol ethers, 19: Synthesis of 3-(2-thienyl)- and 3-(2-furyl)-5-trihalomethyl substituted azoles. *Synthesis, 2005*(16), 2744–2750. https://doi.org/10.1055/s-2005-872140

Alzaidi, A. (2018). The role of cell wall in *Mycobacterium tuberculosis* resistance: Summary review. *International Journal of Life Sciences Research, 6*(4), 100–102.

Aragade, P., Palkar, M., Ronad, P., & Satyanarayana, D. (2013). Coumarinyl pyrazole derivatives of INH: Promising antimycobacterial agents. *Medicinal Chemistry Research, 22*(5), 2279–2283. https://doi.org/10.1007/s00044-012-0222-8

Baraldi, P. G., Fruttarolo, F., Tabrizi, M. A., Preti, D., Romagnoli, R., El-Kashef, H., Moorman, A., Varani, K., Gessi, S., Merighi, S., & Borea, P. A. (2003). Design, synthesis, and biological evaluation of C9- and C2-substituted pyrazolo[4,3-*e*]-1,2,4-triazolo[1,5-*c*]pyrimidines as new A2A and A3 adenosine receptors antagonists. *Journal of Medicinal Chemistry, 46*(7), 1229–1241. https://doi.org/10.1021/jm021023m

Barberis, I., Bragazzi, N. L., Galluzzo, L., & Martini, M. (2017). The history of tuberculosis: From the first historical records to the isolation of Koch's bacillus. *Journal of Preventive Medicine and Hygiene, 58*(1), E9–E12. https://doi.org/10.15167/2421-4248/jpmh2017.58.1.728

Bekhit, A. A., Hymete, A., Asfaw, H., & Bekhit, A. E.-D. A. (2012). Synthesis and biological evaluation of some pyrazole derivatives as anti-malarial agents. *Archiv der Pharmazie, 345*(2), 147–154. https://doi.org/10.1002/ardp.201100078

Bender, M. (2019, October 28). *Tuberculosis: Symptoms, treatment & prevention*. Live Science.

Bhardwaj, B., Vishwakarma, S. K., Singh, A., Kumar, H., Gajendra, T. A., Verma, A., Krishnamurthy, S., Davisson, V. J., & Shrivastava, S. K. (2025). Novel benzothiazole-based cholinesterase inhibitors with amyloid beta disaggregation and antioxidant activity against Alzheimer's disease. *European Journal of Medicinal Chemistry, 298*, 118047. https://doi.org/10.1016/j.ejmech.2025.118047

Bhatt, J. D., Chudasama, C. J., & Patel, K. D. (2015). Pyrazole clubbed triazolo[1,5-*a*]pyrimidine hybrids as anti-tubercular agents: Synthesis, *in vitro* screening and molecular docking study. *Bioorganic & Medicinal Chemistry, 23*(24), 7711–7716. https://doi.org/10.1016/j.bmc.2015.11.018

Bhunia, S. K., Sarkar, M., Banerjee, A., & Giri, B. (2015). An update on pathogenesis and management of tuberculosis with special reference to drug resistance. *Asian*

Pacific Journal of Tropical Disease, 5(9), 673–686. https://doi.org/10.1016/S2222-1808(15)60912-4

Brennan, P. J. (2003). Structure, function, and biogenesis of the cell wall of *Mycobacterium tuberculosis*. *Tuberculosis, 83*(1–3), 91–97. https://doi.org/10.1016/S1472-9792(02)00089-6

Brien, J., Wilson, I., Orton, T., & Pognan, F. (2000). Investigation of the Alamar Blue (resazurin) fluorescent dye for the assessment of mammalian cell cytotoxicity. *European Journal of Biochemistry, 267*(17), 5421–5426. https://doi.org/10.1046/j.1432-1327.2000.01606.x

Burgart, Y. V., Agafonova, N. A., Shchegolkov, E. V., Krasnykh, O. P., Kushch, S. O., Evstigneeva, N. P., Gerasimova, N. A., Maslova, V. V., Triandafilova, G. A., Solodnikov, S. Y., Ulitko, M. V., Makhaeva, G. F., Rudakova, E. V., Borisevich, S. S., Zilberberg, N. V., Kungurov, N. V., Saloutin, V. I., & Chupakhin, O. N. (2020). Multiple biological active 4-aminopyrazoles containing trifluoromethyl and their 4-nitroso-precursors: Synthesis and evaluation. *European Journal of Medicinal Chemistry, 208*, 112768. https://doi.org/10.1016/j.ejmech.2020.112768

Capela, R., Félix, R., Clariano, M., Nunes, D., Perry, M. J., & Lopes, F. (2023). Target identification in anti-tuberculosis drug discovery. *International Journal of Molecular Sciences*, 24(13), 10482. https://doi.org/10.3390/ijms241310482

Castagnolo, D., Manetti, F., Radi, M., Bechi, B., Pagano, M., de Logu, A., Meleddu, R., Saddi, M., & Botta, M. (2009). Synthesis, biological evaluation, and SAR study of novel pyrazole analogues as inhibitors of Mycobacterium tuberculosis: Part 2. Synthesis of rigid pyrazolones. *Bioorganic & Medicinal Chemistry*, 17(15), 5716–5721. https://doi.org/10.1016/j.bmc.2009.05.058

Chakraborty, S., & Rhee, K. Y. (2015). Tuberculosis drug development: History and evolution of the mechanism-based paradigm. *Cold Spring Harbor Perspectives in Medicine*, 5(8), a021147. https://doi.org/10.1101/cshperspect.a021147

Chavan, S. M., Toche, R. B., Patil, V. M., Aware, P. B., & Patil, P. S. (2016). Reactions of ketene dithioacetal for a new versatile synthesis of 4,5-substituted 3-

aminothiophene-2-carboxylate derivatives. *Journal of Sulfur Chemistry*, 37(4), 426–437. https://doi.org/10.1080/17415993.2016.1156117

Chikhale, R. V., Barmade, M. A., Murumkar, P. R., & Yadav, M. R. (2018). Overview of the development of DprE1 inhibitors for combating the menace of tuberculosis. *Journal of Medicinal Chemistry*, 61(19), 8563–8593. https://doi.org/10.1021/acs.jmedchem.8b00281

Cross, G. B. (2025). New drugs for the management of tuberculosis. *Current Opinion in Infectious Diseases*, 38(6), 512–521. https://doi.org/10.1097/QCO.0000000000001156

Dadiboyena, S., Valente, E. J., & Hamme, A. T., II. (2010). Synthesis of novel pyrazoles via [2+3]-dipolar cycloaddition using alkyne surrogates. *Tetrahedron Letters*, 51(9), 1341–1343. https://doi.org/10.1016/j.tetlet.2010.01.017

Dash, S., Rathi, E., Kumar, A., Chawla, K., & Kini, S. G. (2024). Identification of DprE1 inhibitors for tuberculosis through integrated in-silico approaches. *Scientific Reports*, 14, 11315. https://doi.org/10.1038/s41598-024-61901-x

Davies, P. D. O. (2003). The role of DOTS in tuberculosis treatment and control. American *Journal of Respiratory Medicine*, 2(3), 203–209. https://doi.org/10.1007/BF03256649

Dawood, K. M., Eldebss, T. M. A., El-Zahabi, H. S. A., & Yousef, M. H. (2015). Synthesis and antiviral activity of some new bis-1,3-thiazole derivatives. *European Journal of Medicinal Chemistry*, 102, 266–276. https://doi.org/10.1016/j.ejmech.2015.08.005

Dhouib, I., Messaâd, M., HadjKacem, B., Fendri, I., Majdoub, H., & Khemakhem, B. (2023). Pyrazole and pyrazolone derivatives as specific α-glucosidase inhibitors: In vitro combined with in silico, hemolytic and cytotoxicity studies. *Journal of Molecular Structure, 1294*, 136331. https://doi.org/10.1016/j.molstruc.2023.136331

Dixit, S. R., Joshi, S. D., Kulkarni, V. H., Jalalpure, S. S., Kumbar, V. M., Mudaraddi, T. Y., Nadagouda, M. N., & Aminabhavi, T. M. (2017). Pyrrolyl pyrazoline

carbaldehydes as enoyl-ACP reductase inhibitors: Design, synthesis and antitubercular activity. *The Open Medicinal Chemistry Journal, 11*, 92–108. https://doi.org/10.2174/1874104501711010092

Fekadu, M., Zeleke, D., Abdi, B., Guttula, A., Eswaramoorthy, R., & Melaku, Y. (2022). Synthesis, in silico molecular docking analysis, pharmacokinetic properties and evaluation of antibacterial and antioxidant activities of fluoroquinolines. *BMC Chemistry, 16*, 1. https://doi.org/10.1186/s13065-022-00795-0

Fotakis, G., & Timbrell, J. A. (2006). In vitro cytotoxicity assays: Comparison of LDH, neutral red, MTT and protein assay in hepatoma cell lines following exposure to cadmium chloride. *Toxicology Letters, 160*(2), 171–177. https://doi.org/10.1016/j.toxlet.2005.07.001

Fustero, S., Sánchez-Roselló, M., Barrio, P., & Simón-Fuentes, A. (2011). From 2000 to mid-2010: A fruitful decade for the synthesis of pyrazoles. *Chemical Reviews, 111*(11), 6984–7034. https://doi.org/10.1021/cr2000459

Gilmour, B., & Alene, K. A. (2024). Ending tuberculosis: Challenges and opportunities. *Frontiers in Tuberculosis, 2*, 1487518. https://doi.org/10.3389/ftubr.2024.1487518

Grandi, A., Leonelli, C., Rizzuti, A., Rosa, R., Veronesi, P., Grandi, R., Baldassari, S., & Villa, C. (2007). New “green” approaches to the synthesis of pyrazole derivatives. *Molecules, 12*(7), 1482–1495. https://doi.org/10.3390/12071482

Guardia, A., Davie, C. P., Pe, N., Yang, H., Convery, M. A., Centrella, P. A., Daniel, A., Clark, M. A., Huss, S., O'Connor, G. K., McDowell, W., & Castan, P. (2014). Encoded library technology as a source of hits for the discovery and lead optimization of a potent and selective class of bactericidal direct inhibitors of *Mycobacterium tuberculosis* InhA. *Journal of Medicinal Chemistry, 57*(4), 1276–1288. https://doi.org/10.1021/jm401326j

Hassan, G. S., Abou-Seri, S. M., Kamel, G., & Ali, M. M. (2014). Celecoxib analogs bearing benzofuran moiety as cyclooxygenase-2 inhibitors: Design, synthesis and evaluation as potential anti-inflammatory agents. *European Journal of Medicinal Chemistry, 76*, 482–493. https://doi.org/10.1016/j.ejmech.2014.02.033

Insuasty, B., Tigreros, A., Orozco, F., Quiroga, J., Abonía, R., Nogueras, M., Sanchez, A., & Cobo, J. (2010). Synthesis of novel pyrazolic analogues of chalcones and their 3-aryl-4-(3-aryl-4,5-dihydro-1H-pyrazol-5-yl)-1-phenyl-1H-pyrazole derivatives as potential antitumor agents. *Bioorganic & Medicinal Chemistry, 18*(14), 4965–4974. https://doi.org/10.1016/j.bmc.2010.06.013

Ji Ram, V., Sethi, A., Nath, M., & Pratap, R. (2019). Five-membered heterocycles. In V. Ji Ram, A. Sethi, M. Nath, & R. Pratap, *The chemistry of heterocycles: Nomenclature and chemistry of three-to-five-membered heterocycles* (pp. 149–478). Elsevier. https://doi.org/10.1016/B978-0-08-101033-4.00005-x

Nagalingaiah, N. K., Kameshwar, V. H., Nanjundappa, S. H., Ningegowda, S. K., & Kempegowda, M. (2025). Development of novel 3, 5-substituted-1, 2, 4-oxadiazole derivatives: a multidimensional approach with in vitro antibacterial, antioxidant, DFT insights, and molecular dynamics simulations. *Discover Chemistry*, *2*(1), 170.

Khaldan, A., Bouamrane, S., El-Mernissi, R., Maghat, H., Sbai, A., Bouachrine, M., & Lakhlifi, T. (2023). Molecular docking, ADMET prediction, and quantum computational on 2-methoxy benzoyl hydrazone compounds as potential antileishmanial inhibitors. *Biointerface Research in Applied Chemistry, 13*(4), 302. https://doi.org/10.33263/BRIAC134.302

Khan, S., Fakhar, Z., Hussain, A., Ahmad, A., Jairajpuri, D. S., Alajmi, M. F., & Hassan, M. I. (2022). Structure-based identification of potential SARS-CoV-2 main protease inhibitors. *Journal of Biomolecular Structure and Dynamics, 40*(8), 3595–3608. https://doi.org/10.1080/07391102.2020.1848634

Khonde, L. P., Müller, R., Boyle, G. A., Reddy, V., Nchinda, A. T., Eyermann, C. J., Fienberg, S., Singh, V., Myrick, A., Abay, E., Njoroge, M., Lawrence, N., Su, Q., Myers, T. G., Boshoff, H. I. M., Barry, C. E., III, Sirgel, F. A., van Helden, P. D., Massoudi, L. M., Robertson, G. T., Lenaerts, A. J., Basarab, G. S., Ghorpade, S. R., & Chibale, K. (2021). 1,3-Diarylpyrazolyl-acylsulfonamides as potent anti-tuberculosis agents targeting cell wall biosynthesis in *Mycobacterium tuberculosis*. *Journal of Medicinal Chemistry, 64*(17), 12790–12807. https://doi.org/10.1021/acs.jmedchem.1c00837

Kieser, K. J., & Rubin, E. J. (2014). How sisters grow apart: Mycobacterial growth and division. *Nature Reviews Microbiology, 12*(8), 550–562. https://doi.org/10.1038/nrmicro3299

Knechel, N. A. (2009). Tuberculosis: Pathophysiology, clinical features, and diagnosis. *Critical Care Nurse, 29*(2), 34–43. https://doi.org/10.4037/ccn2009968

Kumar, G., Krishna, V. S., Sriram, D., & Jachak, S. M. (2020). Pyrazole–coumarin and pyrazole–quinoline chalcones as potential antitubercular agents. *Archiv der Pharmazie, 353*(8), e2000077. https://doi.org/10.1002/ardp.202000077

Kumar, M., & Panday, S. K. (2022). Pyrazole and its derivatives: An excellent N-heterocycle with wide range of biological applications (A review). *Oriental Journal of Chemistry, 38*(3), 568–592. https://doi.org/10.13005/ojc/380306

Kumar, S., & Modi, G. (2025). Design, synthesis, and biological evaluation of caffeic acid-based novel multifunctional molecules for the management of Alzheimer's disease. *European Journal of Medicinal Chemistry, 296*, 117831. https://doi.org/10.1016/j.ejmech.2025.117831

Laghari, M., Darwis, Y., Memon, A. H., Khan, A. A., Abdulbaqi, I. M. T., & Assi, R. A. (2016). Nanoformulations and clinical trial candidates as probably effective and safe therapy for tuberculosis. *Tropical Journal of Pharmaceutical Research, 15*(1), 201–211. https://doi.org/10.4314/tjpr.v15i1.28

Langdon, S. P. (2003). Cell sensitivity assays: The MTT assay. In S. P. Langdon (Ed.), *Cancer cell culture: Methods and protocols* (Methods in Molecular Medicine, Vol. 731, pp. 237–245). Humana Press. https://doi.org/10.1385/1592594069

Lederer, E. (1971). The mycobacterial cell wall. *Pure and Applied Chemistry, 25*(1), 135–166. https://doi.org/10.1351/pac197125010135

Lee, J., Cheng, X., Jo, S., MacKerell, A. D., Klauda, J. B., & Im, W. (2016). CHARMM-GUI input generator for NAMD, GROMACS, AMBER, OpenMM, and CHARMM/OpenMM simulations using the CHARMM36 additive force field. *Biophysical Journal, 110*(3), 641a. https://doi.org/10.1016/j.bpj.2015.11.3431

Legoabe, L. J., & Beteck, R. M. (2021). Chemical classes presenting novel antituberculosis agents currently in different phases of drug development: A 2010–2020 review. *Pharmaceuticals, 14*(5), 461. https://doi.org/10.3390/ph14050461

Lopes, S. R., Marçal, M., Fernandes, N., Silva, F., Barbosa, P., Vieira, M., Ramos, J. P., & Duarte, R. (2025). Update in tuberculosis treatment: A scoping review of current practices. *Breathe, 21*(1), 240232. https://doi.org/10.1183/20734735.0232-2024

Ly, L. H., & McMurray, D. N. (2008). Tuberculosis: Vaccines in the pipeline. *Expert Review of Vaccines, 7*(5), 635–650. https://doi.org/10.1586/14760584.7.5.635

Manikannan, R., Venkatesan, R., Muthusubramanian, S., Yogeeswari, P., & Sriram, D. (2010). Pyrazole derivatives from azines of substituted phenacyl aryl/cyclohexyl sulfides and their antimycobacterial activity. *Bioorganic & Medicinal Chemistry Letters, 20*(23), 6920–6924. https://doi.org/10.1016/j.bmcl.2010.09.137

Martín, C., Gonzalo-Asensio, J., Aguiló, N., & Arbués, A. (2026). Toward tuberculosis elimination: An update on tuberculosis vaccines in clinical trials. *International Journal of Infectious Diseases, 167*, 108513. https://doi.org/10.1016/j.ijid.2026.108513

Martin, Y. C. (2005). A bioavailability score. *Journal of Medicinal Chemistry, 48*(9), 3164–3170. https://doi.org/10.1021/jm0492002

Martínez-Hoyos, M., Perez-Herran, E., Gulten, G., Encinas, L., Álvarez-Gómez, D., Alvarez, E., Ferrer-Bazaga, S., García-Pérez, A., Ortega, F., Angulo-Barturen, I., Rullas-Trincado, J., Blanco Ruano, D., Torres, P., Castañeda, P., Huss, S., Fernández Menéndez, R., González Del Valle, S., Ballell, L., Barros, D., Modha, S., Dhar, N., Signorino-Gelo, F., McKinney, J. D., García-Bustos, J. F., Lavandera, J. L., Sacchettini, J. C., Jiménez, M. S., Martín-Casabona, N., Castro-Pichel, J., & Mendoza-Losana, A. (2016). Antitubercular drugs for an old target: GSK693 as a promising InhA direct inhibitor. *E Bio Medicine, 8*, 291–301. https://doi.org/10.1016/j.ebiom.2016.05.006

Martínez, L. (2015). Automatic identification of mobile and rigid substructures in molecular dynamics simulations and fractional structural fluctuation analysis. *PLoS ONE, 10*(3), e0119264. https://doi.org/10.1371/journal.pone.0119264

Mohammed, N., Mulugeta, E., Garg, A., & Tadesse, A. (2024). Synthesis, molecular docking studies, and evaluation of antibacterial and antioxidant activities of pyrazoline derivatives. *Results in Chemistry, 8*, 101570. https://doi.org/10.1016/j.rechem.2024.101570

Mohamed-Ezzat, R. A., Omar, M. A., Temirak, A., Abdelsamie, A. S., Abdel-Aziz, M. M., Galal, S. A., Elgemeie, G. H., El Diwani, H. I., Flanagan, K. J., & Senge, M. O. (2024). Synthesis, biological evaluation, and docking studies of pyrazole-linked benzothiazole hybrids as promising anti-TB agents. *Journal of Molecular Structure, 1311*, 138415. https://doi.org/10.1016/j.molstruc.2024.138415

Morgan, D. M. (1998). Tetrazolium (MTT) assay for cellular viability and activity. In *Polyamine protocols (Methods in Molecular Biology*, Vol. 79, pp. 179–183). Humana Press. https://doi.org/10.1385/0-89603-448-8:179

Moulkrere, B. R., Orena, B. S., Mori, G., Saffon-Merceron, N., Rodriguez, F., Lherbet, C., Belkheiri, N., Amari, M., Hoffmann, P., & Fodili, M. (2018). Evaluation of heteroatom-rich derivatives as antitubercular agents with InhA inhibition properties. *Medicinal Chemistry Research, 27*(1), 308–320. https://doi.org/10.1007/s00044-017-2064-x

Mugenyi, N., Ssewante, N., Baruch Baluku, J., Bongomin, F., Mukenya Irene, M., Andama, A., & Byakika-Kibwika, P. (2024). Innovative laboratory methods for improved tuberculosis diagnosis and drug-susceptibility testing. *Frontiers in Tuberculosis, 1*, 1295979. https://doi.org/10.3389/ftubr.2023.1295979

Muluk, M. B., Patil, P. S., Kasare, S. L., Kulkarni, R. S., Dixit, P. P., Choudhari, P. B., & Haval, K. P. (2020). Synthesis and molecular docking studies of novel pyridine-thiazole-hydrazone conjugates as antimicrobial and antioxidant agents. *European Chemical Bulletin, 9*(7), 184–192. https://doi.org/10.17628/ecb.2020.9.184-192

Murphy, K., Habib, S. S., Zaidi, S. M. A., Khowaja, S., Khan, A., Melendez, J., Scholten, E. T., Amad, F., Schalekamp, S., Verhagen, M., Philipsen, R. H. H. M., Meijers, A., & van Ginneken, B. (2020). Computer aided detection of tuberculosis on chest radiographs: An evaluation of the CAD4TB v6 system. *Scientific Reports, 10*, 5492. https://doi.org/10.1038/s41598-020-62148-y

Mvondo, J. G. M., Matondo, A., Mawete, D. T., Bambi, S.-M. N., Mbala, B. M., & Lohohola, P. O. (2021). In silico ADME/T properties of quinine derivatives using SwissADME and pkCSM webservers. *International Journal of TROPICAL DISEASE & Health*, *42*(11), 1–12. https://doi.org/10.9734/ijtdh/2021/v42i1130492

Naik, M., Humnabadkar, V., Tantry, S. J., Panda, M., Narayan, A., Guptha, S., Panduga, V., Manjrekar, P., Jena, L. K., Koushik, K., Shanbhag, G., Jatheendranath, S., Manjunatha, M. R., Gorai, G., Bathula, C., Rudrapatna, S., Achar, V., Sharma, S., Ambady, A., Ghorpade, S. R. (2014). 4-Aminoquinolone piperidine amides: Noncovalent inhibitors of DprE1 with long residence time and potent antimycobacterial activity. *Journal of Medicinal Chemistry, 57*(12), 5419–5434. https://doi.org/10.1021/jm5005978

Nayak, N., Ramprasad, J., & Dalimba, U. (2015). New INH-pyrazole analogs: Design, synthesis and evaluation of antitubercular and antibacterial activity. *Bioorganic & Medicinal Chemistry Letters, 25*(23), 5540–5545. https://doi.org/10.1016/j.bmcl.2015.10.057

Nayee, K. (2017). *Design, synthesis and biological evaluation of some novel pyrazole derivatives as potential antitubercular agents* [Thesis].

Nayee, K., Prajapati, B. K., & Kumar, H. (2026). Design, synthesis, molecular dynamic simulation, ADMET studies, antioxidant and antitubercular screening of amine and acid chloride substituted pyrazole derivatives as an enoyl acyl carrier protein reductase (InhA) inhibitors. *Journal of Molecular Structure, 1354*, 144928. https://doi.org/10.1016/j.molstruc.2025.144928

Nikpour, F., & Beigvand, M. (2008). A facile and convenient approach to the synthesis of 3,5-diaryl-1H-pyrazoles. *Monatshefte für Chemie—Chemical Monthly, 139*(7), 821–824. https://doi.org/10.1007/s00706-007-0829-5

Yahaya, N., & Salleh, N. F. (2020). Prevalence, types and treatment of tuberculosis: A review. *Scientific Inquiry and Review, 4*(4), 41–48.

Oh, S., Trifonov, L., Yadav, V. D., Barry, C. E., III, & Boshoff, H. I. (2021). Tuberculosis drug discovery: A decade of hit assessment for defined targets. *Frontiers in Cellular and Infection Microbiology, 11*, 611304. https://doi.org/10.3389/fcimb.2021.611304

Olson T. (2011). Gabedit - A graphical user interface for computational chemistry softwares. *Journal of Computational Chemistry, 32*(1), 174–182. https://doi.org/10.1002/jcc.21600

Panda, M., Ramachandran, S., Ramachandran, V., Shirude, P. S., Humnabadkar, V., Nagalapur, K., Sharma, S., Kaur, P., Guptha, S., Narayan, A., Mahadevaswamy, J., Ambady, A., Hegde, N., Rudrapatna, S. S., Hosagrahara, V. P., Sambandamurthy, V. K., & Raichurkar, A. (2014). Discovery of pyrazolopyridones as a novel class of noncovalent DprE1 inhibitor with potent anti-mycobacterial activity. *Journal of Medicinal Chemistry, 57*(11), 4761–4771. https://doi.org/10.1021/jm5002937

Pandey, A., Shyamal, S. S., Shrivastava, R., Ekka, S., & Mali, S. N. (2022). Inhibition of *Plasmodium falciparum* fatty acid biosynthesis (FAS-II pathway) by natural flavonoids: A computer-aided drug designing approach. *Chemistry Africa, 5*(5), 1469–1491. https://doi.org/10.1007/s42250-022-00449-7

Paneer, T., Kumar, P.., Saravanan, G., & Prakash, C. R. (2014). Microwave-assisted synthesis, characterization and biological activity of novel pyrazole derivatives. *Journal of Saudi Chemical Society, 18*(6), 1015–1021. https://doi.org/10.1016/j.jscs.2011.12.006

Parmar, K. (2015). *Design, synthesis and biological evaluation of some new chemical entities as antitubercular agents* [Thesis].

Pathak, R. B., Chovatia, P. T., & Parekh, H. H. (2012). Synthesis, antitubercular and antimicrobial evaluation of 3-(4-chlorophenyl)-4-substituted pyrazole derivatives. *Bioorganic & Medicinal Chemistry Letters, 22*(15), 5129–5133. https://doi.org/10.1016/j.bmcl.2012.05.063

Percival, S. L., & Williams, D. W. (2014). Mycobacterium. In S. L. Percival, R. Chalmers, R. M. Embrey, D. W. Williams, R. C. Hunter, J. Gray, & N. J. B. Jones (Eds.), *Microbiology of waterborne diseases: Microbiological aspects and risks* (2nd ed., pp. 177–207). Elsevier. https://doi.org/10.1016/B978-0-12-415846-7.00009-3

Persson, T., & Nielsen, J. (2006). Synthesis of new synthetic precursors for the regioselective synthesis of heterocyclic compounds. *Organic Letters, 8*(15), 3219–3322

Rampogu, S., Shaik, B., Hyun, J., Sung, T., Woo, M., & Woo, K. (2023). Explicit molecular dynamics simulation studies to discover novel natural compound analogues as *Mycobacterium tuberculosis* inhibitors. *Heliyon, 9*(2), e13324. https://doi.org/10.1016/j.heliyon.2023.e13324

Raval, K., & Ganatra, T. (2022). Basics, types and applications of molecular docking: A review. *IP International Journal of Comprehensive and Advanced Pharmacology, 7*(1), 12–16. https://doi.org/10.18231/j.ijcaap.2022.003

Reuter, N., & Martinez, A. (2011). Dynamics, flexibility and ligand-induced conformational changes in biological macromolecules: A computational approach. *Future Medicinal Chemistry, 3*(16), 2079–2100.

Rockefeller, A. (2001). Molecular basis for the peripheral nerve prediction of *Mycobacterium leprae*. *Current Opinion in Microbiology, 4*(1), 21–27.

Rogacki, M. K., Pitta, E., Balabon, O., Huss, S., Lopez-Roman, E. M., Argyrou, A., Blanco-Ruano, D., Cacho, M., Vande Velde, C. M. L., Augustyns, K., Ballell, L., Barros, D., Bates, R. H., Cunningham, F., & Van Der Veken, P. (2018). Identification and profiling of hydantoins—A novel class of potent

antimycobacterial DprE1 inhibitors. *Journal of Medicinal Chemistry, 61*(24), 11221–11249. https://doi.org/10.1021/acs.jmedchem.8b01356

Roshdi, M., & Reza, S. (2025). The growing impact of nontuberculous mycobacteria: A multidisciplinary review of ecology, pathogenesis, diagnosis, and treatment. *Infectious Medicine, 4*, 100203. https://doi.org/10.1016/j.imj.2025.100203

Sabale, P. M., Potey, L. C., & Sabale, V. P. (2018). Synthesis, characterization and docking study of fused benzimidazole and pyrazole derivatives as antitubercular agents. *Journal of Applicable Chemistry, 7*(5), 1189–1195.

Saraswathi, S. G., Bhagavati, V. R., Debata, I., Badiger, S., & R., T. S. (2025). Application of geographic information system (GIS) technology as a tool to identify geospatial distribution of pulmonary tuberculosis cases in Bangalore, South India. *RGUHS National Journal of Public Health, 10*(4), 86–92. https://doi.org/10.26463/rnjph.10_4_12

Shaikh, S. I., Zaheer, Z., Mokale, S. N., & Lokwani, D. K. (2017). Development of new pyrazole hybrids as antitubercular agents: Synthesis, biological evaluation and molecular docking study. *International Journal of Pharmacy and Pharmaceutical Sciences, 9*(11), 50–56.

Shaw, A. Y., Liau, H. H., Lu, P. J., Yang, C. N., Lee, C. H., Chen, J. Y., Xu, Z., & Flynn, G. (2010). 3,5-Diaryl-1H-pyrazole as a molecular scaffold for the synthesis of apoptosis-inducing agents. *Bioorganic & Medicinal Chemistry, 18*(9), 3270–3278. https://doi.org/10.1016/j.bmc.2010.03.016

Shaaban, M. M., Teleb, M., Ragab, H. M., Singh, M., Elwakil, B. H., Heikal, L. A., El-Gendy, A. A., El-Sherbiny, M., & Mahran, M. A. (2024). The first-in-class pyrazole-based dual InhA–VEGFR inhibitors towards integrated antitubercular host-directed therapy. *Bioorganic Chemistry, 145*, 107179.

Sherbiny, F. F., Bayoumi, A. H., El-Morsy, A. M., Sobhy, M., & Hagras, M. (2021). Design, synthesis, biological evaluation, and molecular docking studies of novel pyrazolo[3,4-d]pyrimidine derivative scaffolds as potent EGFR inhibitors and cell

apoptosis inducers. *Bioorganic Chemistry, 116*, 105325. https://doi.org/10.1016/j.bioorg.2021.105325

Shetye, G. S., Franzblau, S. G., & Cho, S. (2020). New tuberculosis drug targets, their inhibitors, and potential therapeutic impact. *Translational Research, 220*, 68–97. https://doi.org/10.1016/j.trsl.2020.03.007

Šink, R., Sosič, I., Živec, M., Fernandez-Menendez, R., Turk, S., Pajk, S., Alvarez-Gomez, D., Lopez-Roman, E. M., Gonzales-Cortez, C., Rullas-Trincado, J., Angulo-Barturen, I., Barros, D., Ballell-Pages, L., Young, R. J., Encinas, L., & Gobec, S. (2015). Design, synthesis, and evaluation of new thiadiazole-based direct inhibitors of enoyl acyl carrier protein reductase (InhA) for the treatment of tuberculosis. *Journal of Medicinal Chemistry, 58*(2), 613–624. https://doi.org/10.1021/jm501029r

Sossen, B., Kubjane, M., & Meintjes, G. (2025). Tuberculosis and HIV coinfection: Progress and challenges towards reducing incidence and mortality. *International Journal of Infectious Diseases, 155*, 107876.

Tallorin, L., Finzel, K., Nguyen, Q. G., Beld, J., La Clair, J. J., & Burkart, M. D. (2016). Trapping of the enoyl-acyl carrier protein reductase–acyl carrier protein interaction. *Journal of the American Chemical Society, 138*(12), 3962–3965. https://doi.org/10.1021/jacs.5b13456

Van Der Spoel, D., Lindahl, E., Hess, B., Groenhof, G., Mark, A. E., & Berendsen, H. J. C. (2005). GROMACS: Fast, flexible, and free. *Journal of Computational Chemistry, 26*(16), 1701–1718. https://doi.org/10.1002/jcc.20291

Vekariya, M. K., Vekariya, R. H., Patel, K. D., Raval, N. P., Shah, P. U., Rajani, D. P., & Shah, N. K. (2018). Pyrimidine-pyrazole hybrids as morpholinopyrimidine-based pyrazole carboxamides: Synthesis, characterisation, docking, ADMET study and biological evaluation. *ChemistrySelect, 3*(24), 6998–7008. https://doi.org/10.1002/slct.201801011

Wan, G., Chen, Y., Zhang, X., Tang, Q., Zhang, Q., Zhou, S., Li, W., Zeng, J., Gao, C., & Yu, L. (2026). Design, synthesis, and antitubercular activity evaluation of novel

nitroimidazole derivatives. *Journal of Medicinal Chemistry, 69*(12), 14213–14235. https://doi.org/10.1021/acs.jmedchem.5c03631

Wan, G., Gao, C., Zhang, X., Qiu, H., Tang, Q., Zeng, J., & Yu, L. (2025). Discovery of 1,3-disubstituted pyrazole derivatives as *Mycobacterium tuberculosis* inhibitors. *Bioorganic & Medicinal Chemistry Letters, 121*, 130156.

Warude, B. J., Wagh, S. N., Chatpalliwar, V. A., Yildirim, M., Celik, I., Rudrapal, M., Khan, J., Chinnam, S., Garud, A. A., & Neharkar, V. S. (2023). Design, docking, MD simulation and in-silico ADMET prediction studies of novel indole-based benzamides targeting estrogen receptor alpha-positive breast cancer therapy. *Pharmacia, 70*(2), 307–316. https://doi.org/10.3897/pharmacia.70.e100356

World Health Organization. (2025). *Global tuberculosis report 2025*. World Health Organization.

Wright, G. D. (2012). Back to the future: A new "old" lead for tuberculosis. *EMBO Molecular Medicine, 4*(10), 1029–1031. https://doi.org/10.1002/emmm.201201711

Xu, Z., Gao, C., Ren, Q., Song, X., Feng, L., & Lv, Z. (2017). Recent advances of pyrazole-containing derivatives as anti-tubercular agents. *European Journal of Medicinal Chemistry, 139*, 429–440. https://doi.org/10.1016/j.ejmech.2017.07.059

Xu, M. X. (2026). Discovery and optimization of phenoxazinone derivatives as potent antitubercular agents targeting FabD protein. *Journal of Medicinal Chemistry, 69*(1), 163–182. https://doi.org/10.1021/acs.jmedchem.5c02148

Yadav, J. S., Reddy, B. V. S., Satheesh, G., Lakshmi, P. N., Kumar, S. K., & Kunwar, A. C. (2004). Rapid and efficient synthesis of optically active pyrazoles under solvent-free conditions. *Tetrahedron Letters, 45*(46), 8587–8590. https://doi.org/10.1016/j.tetlet.2004.09.040

Yokokawa, F., Wang, G., Chan, W. L., Ang, S. H., Wong, J., Ma, I., Rao, S. P. S., Kuhen, K., Glynne, R., Smith, P., Bifani, P., & Jiricek, J. (2013). Discovery of tetrahydropyrazolopyrimidine carboxamide derivatives as potent and orally active

antitubercular agents. *ACS Medicinal Chemistry Letters*, *4*(5), 451–455. https://doi.org/10.1021/ml400071a

Yu, W., Yusuf, B., Wang, S., Tian, X., Hameed, H. M. A., Lu, Z., Chiwala, G., Alam, M. S., Cook, G. M., Maslov, D. A., Zhong, N., & Zhang, T. (2021). Sterilizing effects of novel regimens containing TB47, clofazimine, and linezolid in a murine model of tuberculosis. *Antimicrobial Agents and Chemotherapy*, *65*(10), e00706-21. https://doi.org/10.1128/AAC.00706-21

ANNEXURE

ANNEXURE

1. SSIP grant certificate
2. Anti-tubercular activity certificate
3. Antioxidant activity certificate
4. DPC (Doctoral Progress Committee) review comments
5. List of publications
6. Poster presentation and other seminar participation certificate

1. SSIP grant certificate

L. M. College of Pharmacy
The Lalubhai Motilal College of Pharmacy
Managed by Ahmedabad Education Society
Estd. 1947
NAAC Accredited 'A' Grade

Ref. No.: 2635/2023

Date: 28/03/2023

To,
Ms. Kinjal Nayee,
L. M. College of Pharmacy,
Opp. Gujarat University, Navrangpura, Ahmedabad - 380009.

Subject: Sanction Letter of financial assistance under SSIP 2.0 scheme

Dear **Ms. Kinjal,**
We are pleased to inform you that your project titled **"Design, synthesis, and evaluation of some pyrazole derivatives as antitubercular agents"** has been selected for financial assistance under the SSIP 2.0 (Student Startup and Innovation Policy) scheme. The SSIP Scrutiny Committee of L. M. College of Pharmacy has approved your project for a grant of **INR 40,000/-.**

The purpose of the SSIP 2.0 grant is to provide financial support to students and innovators who have innovative ideas and projects that can benefit society. Your project was selected based on its potential to create a positive impact in the relevant field, as well as its feasibility and potential for success.

As per the guidelines and regulations of the SSIP 2.0 scheme, the grant will be disbursed in three equal installments. The first installment will be disbursed to your account immediately after you submit the duly signed declaration form and other necessary documents.

The next installment will be disbursed only upon satisfactory progress of the project and after submission of the progress report and original copy of bills/receipts related to any expense permitted under the project as proof of expense, duly signed by your mentor. It is important to note that failure to submit the progress report and bills in a timely manner may result in a delay in the next installment.

Once again, we congratulate you on being selected for the SSIP 2.0 grant, and we wish you all the best for the successful completion of your project. We look forward to your progress and contributions to the field.

Copy to:
1. Dr. Beenkumar R. Prajapati, Mentor

Dr. M. T. Chhabria
Principal

Dr. P. D. Bharadia
Coordinator, SSIP Cell

Navrangpura, Ahmedabad 380 009.
Gujarat. India.

Phone : +91 79 2630 2746
Fax : +91 79 2630 4865

principal@lmcp.ac.in
www.lmcp.ac.in

2. Anti-tubercular activity certificate

Maratha Mandal's Central Research Laboratory
Maratha Mandal's NGH Institute of Dental Sciences and Research Centre,
R.S.No. 47A/2, Bauxite Road, Belgaum-590010
Ph. No. 0831-2477682 E-mail: mmnghids@gmail.com/ mmcrl01@gmail.com

Ref No. MMCRL/2023-24/07 *Dated 19/04/2023*

CERTIFICATE

This is to certify that Dr. Kinjal K Nayee from LM College of Pharmacy Ahmedabad has carried out anti-tubercular study work as a part of her thesis titled "Design, synthesis and Evaluation of some Pyrazole Derivatives as anti-tubercular Agents" in Central Research Laboratory of this Institution.

Place: Belgaum

CENTRAL RESEARCH LABORATORY MARATHA MANDAL'S CRL BELGAUM

Dr. Preeti Ingalagi

3. Antioxidant activity certificate

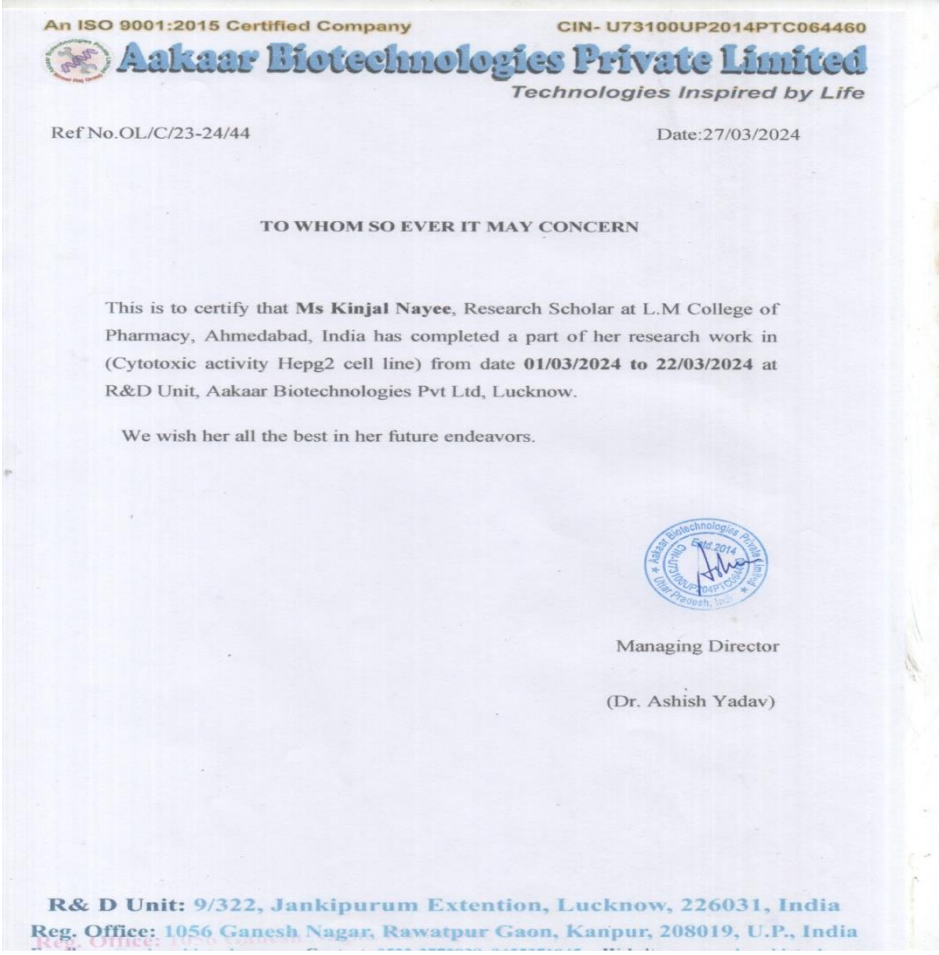

An ISO 9001:2015 Certified Company CIN- U73100UP2014PTC064460

Aakaar Biotechnologies Private Limited

Technologies Inspired by Life

Ref No.OL/C/23-24/44 Date:27/03/2024

TO WHOM SO EVER IT MAY CONCERN

This is to certify that **Ms Kinjal Nayee**, Research Scholar at L.M College of Pharmacy, Ahmedabad, India has completed a part of her research work in (Cytotoxic activity Hepg2 cell line) from date **01/03/2024 to 22/03/2024** at R&D Unit, Aakaar Biotechnologies Pvt Ltd, Lucknow.

We wish her all the best in her future endeavors.

Managing Director

(Dr. Ashish Yadav)

R& D Unit: 9/322, Jankipurum Extention, Lucknow, 226031, India

Reg. Office: 1056 Ganesh Nagar, Rawatpur Gaon, Kanpur, 208019, U.P., India

4. DPC (Doctoral Progress Committee) review comments

DPC	Date	Comments
1.	29/01/2021	• Self study course has been completed successfully. • Preliminary literature survey has been done. The knowledge of disease and target seems to be average; more insight needed. • Title is appropriate. • Literature review should be done intensively specifically for InhA inhibitors. • Presentation skills need improvement. • Reference should be done as per GTU guideline.
2.	04/08/2021	• The student have performed the literature review, designed the molecules and performed the docking studies. • Extensive literature review is further required. • The work done was found to be satisfactory.
3.	31/12/2021	• During this period, the docking studies were performed, and the results were found to be satisfactory. • Some of the intermediates were synthesized, and the synthetic work is in progress. • Spectral studies are yet to be carried out for confirmation of the intermediates synthesized.
4.	12/07/2022	• The docking study of Isoniazid is suggested to perform again taking Isoniazid-NAD adduct. • The mechanisms of reactions involved in the synthesis should be clarified thoroughly. • Spectral analysis of some of the compounds have been shown, it is suggested to be done for other compounds also. • Fundamentals of spectroscopy should be cleared.

		• Machine learning studies are suggested to be completed if possible.
5.	26/12/2022	• The work done during last term is found to be satisfactory. • The presentation has some grammatical mistakes, which needs to be improved. • All the synthesized compounds should be confirmed by appropriate spectral data. • Basics of the reactions should be cleared thoroughly.
6.	28/06/2023	• The Work done during the last semester was found to be satisfactory. • The student has complied to comments mentioned in last DPC. • All the synthesized compounds should be evaluated for biological activity and SAR should be established. • The student has mentioned to perform Molecular dynamic simulation as future plan, which should be completed in next DPC. • All the remaining compounds structure should be established by different spectroscopy methods.
7.	20/12/2023	• All the synthesized compounds should be interpreted. • Fundamentals of spectroscopy should be cleared. • Rest of presentation was good.
8.	10/12/2024	• The work done and presentation was found to be satisfactory. • The experimental work is completed and is recommended for open seminar. • The student need to clear about fundamentals of

		molecular dynamic study. • The student also need to study about the parameters for selection of PDB file.

5. List of Publications

1. Kinjal Nayee, Beenkumar Prajapati, Hansal Kumar."Design, synthesis, molecular dynamic simulation, ADMET studies, antioxidant and antitubercular screening of amine and acid chloride substituted pyrazole derivatives as an enoyl acyl carrier protein reductase (InhA) inhibitors." *Journal of Molecular Structure* (2026), 1354, 144928, 10.1016/j.molstruc.2025.144928. (scopus indexed)
2. Kinjal Nayee, Beenkumar Prajapati, Haribhai Rabari; "Pyrazole derivatives as an enoyl acyl carrier protein reductase(InhA) inhibitors with promising antitubercular activity." *World Journal of Pharmaceutical Research* (2025), Volume 14, Issue 5, 1108-1134.
3. Kinjal Nayee, Beenkumar Prajapati; "Design, synthesis and antitubercular activity of novel pyrazole derivatves as InhA inhibitors" NTP043, pg. No. 102 (Abstract Published- Nirma University)
4. Kinjal Nayee, Beenkumar Prajapati, and Hansal Kumar. "Design, synthesis and antitubercular evaluation of pyrazolo-pyrimidine derivatives as DprE1 inhibitors" (Under communication).

Contents lists available at ScienceDirect

Journal of Molecular Structure

journal homepage: www.elsevier.com/locate/molstr

Design, synthesis, molecular dynamic simulation, ADMET studies, antioxidant and antitubercular screening of amine and acid chloride substituted pyrazole derivatives as an enoyl acyl carrier protein reductase (InhA) inhibitors

Kinjal Nayee [a,*], Been Kumar Prajapati [b], Hansal Kumar [c]

[a] Research Scholar, Gujarat Technological University, Ahmedabad, 382424 Gujarat, India
[b] Department of Pharmaceutical Chemistry, L. M. College of Pharmacy, Navrangpura, Ahmedabad, 380009 Gujarat, India
[c] Department of Pharmaceutical Engineering and Technology, Indian Institute of Technology-Banaras Hindu University, Varanasi 221005, India

ARTICLE INFO

Keywords:
Mycobacterium tuberculosis
Enoyl acyl carrier protein reductase (InhA)
Docking
MD simulation
Cytotoxicity
Antitubercular activity

ABSTRACT

A thorough examination of structure-based drug design offers important insights for developing new, medicinally useful compounds. In this study, we have designed, synthesized, and characterized a series of pyrazole derivatives 5a-o. All the synthesized compounds were characterized by various spectroscopic techniques (such as IR, NMR and mass spectroscopy). Synthesized compounds (5a-o) were subjected to in *vitro* anti-mycobacterial activity against the *M. tuberculosis* (H37Rv) strain via the microplate alamar blue assay method and antioxidant activity using the DPPH assay. The results demonstrated that the synthesized compounds (5a-o) effectively inhibited *M. tuberculosis* H37Rv, displaying promising anti-tubercular potential. Among them, compound 5m was the most potent, with MIC of 3.12 μg/ml., whereas compound 5i exhibited a MIC of 6.25 μg/ml., and comounds 5g, 5h, and 5j demonstrated a MIC of 12.5 μg/ml.. In terms of antioxidant potential, compounds 5b and 5d exhibited good antioxidant activity, with 5m again emerging as the most effective. Cytotoxicity assessments of the most active compounds (5i and 5m) revealed no significant cytotoxic effects. Furthermore, *In-silico* ADME predictions indicated advantageous oral bioavailability and drug-like characteristics across the series. To gain mechanistic insight, molecular docking studies were conducted against the mycobacterial enoyl acyl carrier protein reductase(InhA) enzyme, assisted by molecular dynamics simulations to evaluate the key molecular interaction, conformational changes and stability of docked complexes.

1. Introduction

Mycobacterium tuberculosis is an infectious agent that causes tuberculosis (TB). One of the leading causes of morbidity and mortality worldwide is *M. tuberculosis* (Mtb), transmitted through airborne droplets. Tuberculosis(TB) is largely preventable and curable disease. As per the "Global Tuberculosis Report 2024," there were 10.8 million new tuberculosis cases worldwide in 2023, with an incidence of 134 cases per 100,000 people. In these new cases, 6,62,000(6.1%) were HIV-co-infected and 400,000 (3.7%) were patients with multidrug-resistant tuberculosis(MDR) or rifampicin-resistant tuberculosis[1].

There is continuing interest in the development of new anti-tubercular drugs, particularly against multi-drug resistant(MDR) and extensively drug resistant(EDR) strains of *M. tuberculosis* [2]. To address the growing problem of resistance there is an urgent requirement for a new class of anti-tubercular drugs with unique mechanisms of action to combat *M.tuberculosis*. Mycolic acid is the key component of bacterial cell envelop. Most existing antitubercular drugs inhibiting the synthesis of mycolic acid, which is the long-chain fatty acid composed of 60–90 carbons with α -alkyl β -hydroxy group[3]. InhA is a NADH-dependent 2-trans-enoyl-acyl carrier protein (ACP) reductase, which is an integral part of the FAS-II pathway in *M. tuberculosis*[4]. Fatty acid biosynthesis (FAS) pathway is considered to be an attractive target for developing new antitubercular agents. Mycobacteria contain both fatty acid synthases, FASI and FASII. Moreover, there are differences in the substrate specificity of FAS II enzyme cascades that are unique to mycobacteria, which synthesize mycolic acids, as essential components of their cell envelope[5]. The attractive antimicrobial target, FAS-II

* Corresponding author.
E-mail address: been.prajapati@lmcp.ac.in (K. Nayee).

https://doi.org/10.1016/j.molstruc.2025.144928
Received 11 October 2025; Received in revised form 22 November 2025; Accepted 30 November 2025
Available online 1 December 2025

WORLD JOURNAL OF PHARMACEUTICAL RESEARCH
SJIF Impact Factor 8.453
Volume 14, Issue 5, 1108-1134. Research Article ISSN 2277–7105

PYRAZOLE DERIVATIVES AS AN ENOYL ACYL CARRIER PROTEIN REDUCTASE (INHA) INHIBITORS WITH PROMISING ANTITUBERCULAR ACTIVITY

Kinjal Nayee*[1], Beenkumar Prajapati[2] and Haribhai Rabari[3]

*[1]Research Scholar, Gujarat Technological University, Ahmedabad.
[2,3]L.M. College of Pharmacy, Department of Pharmaceutical Chemistry, Navrangpura, Ahmedabad, India.

Article Received on
23 Jan. 2025,
Revised on 12 Feb. 2025,
Accepted on 04 March 2025
DOI: 10.20959/wjpr20255-35741

***Corresponding Author**
Kinjal Nayee
Research Scholar, Gujarat Technological University, Ahmedabad.
nayeekinjal93@gmail.com

ABSTRACT

Tuberculosis is an infectious disease caused by bacillus Mycobacterium tuberculosis (MTB). New drugs with different mechanisms of action against tuberculosis must be discovered and developed in response to the rising prevalence of multidrug-resistant MTB. Several pyrazole derivatives have been synthesized and tested for anti-tubercular activity in past years. Enoyl acyl carrier protein reductase (InhA), is a clinically proven target for tuberculosis treatment. This review outlines the effectiveness of pyrazole derivatives as an InhA inhibitors and their antitubercular potential.

KEYWORDS: Tuberculosis, Pyrazole, Enoyl Acyl Carrier Protein Reductase (InhA), Antitubercular Activity.

INTRODUCTION

Tuberculosis (TB) disease is usually preventable and curable disease. However, in 2022, tuberculosis accounted for nearly twice as many fatalities globally as HIV/AIDS and was the second most common infectious agent-related cause of death worldwide, after corona virus disease (COVID-19). Each year, more than 10 million people fall ill with tuberculosis. According to the WHO 2023 report, 4,10,000 cases of multidrug-resistant or rifampicin-resistant tuberculosis worldwide.[1] Furthermore, a growing number of MTB strains are becoming resistant to one or more of the widely used anti-TB drugs, which complicates treatment and contributing to the rise in drug-resistant and latent TB infections.

NTP043

Design, Synthesis and Antitubercular Activity of Novel Pyrazole Derivatives as InhA Inhibitors

Nayee Kinjal[1], Prajapati BeenKumar[2]
[1]Research Scholar, Gujarat Technological University, Ahmedabad, India
[2]L.M. College of Pharmacy, Ahmedabad, India
nayeekinjal93@gmail.com

Here, we report the Docking study and antitubercular activity of 15 recently synthesised pyrazole derivatives. The enzyme enoyl ACP reductase (InhA) is a key player in the FAS-II biosynthetic pathway of *M. tuberculosis* and a valuable target for the development of novel anti-TB agents. The binding

NIRMA UNIVERSITY
INSTITUTE OF PHARMACY
NAAC ACCREDITED 'A+' GRADE

NIPiCON 2024
7th Nirma Institute of Pharmacy International Conference
February 7-9, 2024

modes of the synthesized compounds at this active site were studied using Autodock Vina and Schrodinger software. The structures of the synthesized compounds were confirmed by routine spectroscopic techniques ^{1}H and ^{13}C NMR,IR and mass spectrometry.All the synthesized compounds show good docking score.These compounds have shown the same type of interaction as that of 4U0J ligand. The compounds were further evaluated for anti-TB activities against *M. tuberculosis* H37Rv strain by Microplate Alamar Blue Assay.In this study, novel compounds LMN-1 to LMN-15 have been synthesized that were recognized as potent InhA inhibitors.

6. Poster presentation and other seminar participation certificate

NIPiCON 2024

7th Nirma Institute of Pharmacy International Conference

NIRMA UNIVERSITY

INSTITUTE OF PHARMACY

NAAC ACCREDITED A++ GRADE

CERTIFICATE OF APPRECIATION

This is to certify that

Ms Kinjal Nayee

has participated and presented a Scientific Paper in the **Poster session** of

NextGen Therapeutics

in recognition of the valuable contribution to the field of **Session theme** and the dissemination of knowledge during the international conference in the

NIPiCON 2024

NextGen Therapeutics: Multidisciplinary Research Approaches for Drug Development and Delivery

Bridging the Gaps: From Drug Discovery to Patient Care

held on

February 7 - 9, 2024

at

Institute of Pharmacy,

Nirma University, Ahmedabad

DR. NIYATI ACHARYA

Organizing Secretary

NIPiCON 2024

PROF. GOPAL NATESAN

Convener

NIPiCON 2024

Online Workshop on
Multi-Targeted QSAR:
A Novel Approach For Drug Design

25th February, 2021

ORGANIZED BY
Ganpat University
Shree S.K. Patel College of Pharmaceutical Education and Research

Certificate for Particitation

It is our pleasure to certify that Prof./Dr./Mr./Ms. Kinjal Nayee
from L.M. College of Pharmacy has
participated as Delegate in the Online Workshop on "Multi-Targeted QSAR: A Novel Approach For Drug Design" on 25th February 2021 at Ganpat University, Shree S. K. Patel College of Pharmaceutical Education & Research, Gujarat, India.

Dr. Pawan Kumar Gupta
Coordinator

Dr. Paresh U. Patel
Co-Convener

Dr. S. S. Pancholi
Convener & Principal

EXCELON IP™

CERTIFICATE OF PARTICIPATION

This certificate is presented to

Kinjal K Nayee

for participating in the "Idea to IP to Market" webinar organized on the 2nd Anniversary of Excelon IP and World IP Day on 26th April, 2021.

Sanjaykumar Patel
Founder and Principal IP Attorney at Excelon IP

26/04/2021
DATE


L M C P
Estd. 1947
Department of Science & Technology
Government of Gujarat
o2h discovery
CERTIFICATE
This is to certify that
Ms. Kinjal Nayee
has participated as Delegate at
Webinar- 1: Organic Synthesis - Precautions, Set up, Monitoring and Work up
of GUJCOST sponsored Webinar Series on
"Organic Synthesis : Life Line of Pharma API Industry"
Organized by
L. M. College of Pharmacy
in Association with o2h Discovery Pvt. Ltd.
during 25 to 27 February, 2021.
Ms. Diyva Teli
Dr. Anuradha Gajjar
Coordinators
Dr. Mahesh T. Chhabria
Convener
SSIP
AIC-LMCP FOUNDATION
INSTITUTION'S INNOVATION COUNCIL
(Ministry of HRD Initative)
Activate Windows
Go to PC settings to activate Windo